On the Numerical Analysis of Eigenvalue Problems

D I S S E R T A T I O N

zur Erlangung des akademischen Grades

Dr. rer. nat.
im Fach Mathematik

eingereicht an der
Mathematisch-Naturwissenschaftlichen Fakultät II
Humboldt-Universität zu Berlin

von

Dipl.-Math. Joscha Micha Gedicke

Präsident der Humboldt-Universität zu Berlin:
Prof. Dr. Jan-Hendrik Olbertz

Dekan der Mathematisch-Naturwissenschaftlichen Fakultät II:
Prof. Dr. Elmar Kulke

Gutachter:
1. Prof. Dr. Carsten Carstensen
2. Prof. Dr. Volker Mehrmann
3. Prof. Dr. Rolf Rannacher

Tag der Verteidigung: 10. Juni 2013

Vielen Dank an Herrn Prof. C. Carstensen für die Unterstützung dieser Dissertation und die nachdrückliche Förderung meiner wissenschaftlichen Laufbahn.

Vielen Dank an Herrn Prof. V. Mehrmann und Frau Dr. A. Miedlar für die erfolgreiche Zusammenarbeit im MATHEON Forschungsprojekt C22 "Adaptive solutions of parametric eigenvalue problems".

Vielen Dank auch an die gesamte Arbeitsgruppe "Numerical Analysis" von Herrn Prof. C. Carstensen für die sehr angenehme Arbeitsatmosphäre.

Nicht zuletzt vielen Dank an das MATHEON und die BMS für die finanzielle Unterstützung meiner Promotion.

Ich widme diese Arbeit
meinen Eltern und meiner Schwester.

Abstract

This thesis "on the numerical analysis of eigenvalue problems" consists of five major aspects of the numerical analysis of adaptive finite element methods for eigenvalue problems. The first three consider the symmetric Laplace eigenvalue problem while the last two concern a non-symmetric convection-diffusion eigenvalue problem.

The first part presents a combined adaptive finite element method with an iterative algebraic eigenvalue solver for a symmetric eigenvalue problem of asymptotic quasi-optimal computational complexity. The analysis is based on a direct approach for eigenvalue problems and allows the use of higher-order conforming finite element spaces with fixed polynomial degree. The asymptotic quasi-optimal adaptive finite element eigenvalue solver involves a proper termination criterion for the algebraic eigenvalue solver and does not need any coarsening. Numerical evidence illustrates the asymptotic quasi-optimal computational complexity in 2 and 3 dimensions.

The second part introduces fully computable two-sided bounds on the eigenvalues of the Laplace operator on arbitrarily coarse meshes based on some approximation of the corresponding eigenfunction in the nonconforming Crouzeix-Raviart finite element space plus some postprocessing. The efficiency of the guaranteed error bounds involves the global mesh-size and is proven for the large class of graded meshes. Numerical examples demonstrate the reliability of the guaranteed error control even for coarse meshes and inexact solve of the algebraic eigenvalue problem. This motivates an adaptive algorithm which monitors the discretisation error, the maximal mesh-size, and the algebraic eigenvalue error. The accuracy of the guaranteed eigenvalue bounds is surprisingly high with efficiency indices as small as 1.4.

The third part presents an adaptive finite element method (AFEM) based on nodal-patch refinement that leads to an asymptotic error reduction property for the adaptive sequence of simple eigenvalues and eigenfunctions of the Laplace operator. The proven saturation property yields reliability and efficiency for a class of hierarchical a posteriori error estimators. Numerical experiments confirm that the saturation property is present even for very coarse meshes for many examples, but in other cases the smallness assumption on the initial mesh is severe.

The fourth part considers a posteriori error estimators for convection-diffusion eigenvalue problems as discussed by Heuveline and Rannacher (2001) in the context of the dual-weighted residual method (DWR). This presentation directly addresses the variational formulation rather than the non-linear ansatz of Becker and Rannacher. Two different postprocessing techniques attached to the DWR paradigm plus two new dual-weighted a posteriori error estimators are presented. The first new estimator utilises an auxiliary Raviart-Thomas mixed finite element method and the second exploits an averaging technique in combination with ideas of DWR. The six a posteriori error estimators compete in three numerical examples and illustrate reliability and efficiency and the dependence of generic constants on the size of the eigenvalue or the convection coefficient.

The last part presents three adaptive algorithms for eigenvalue problems associated with non-selfadjoint partial differential operators. The basis for the developed algorithms is a homotopy method which departs from a well-understood selfadjoint problem. Apart from the adaptive grid refinement, the progress of the homotopy as well as the solution of the iterative method are adapted to balance the contributions of the different error sources. The first algorithm balances the homotopy, discretisation and approximation errors with respect to a fixed step-size in the homotopy. The second algorithm combines the adaptive step-size control for the homotopy with an adaptation in space that ensures an error below a fixed tolerance. The outcome leads to the third algorithm which allows the complete adaptivity in space, homotopy step-size as well as the iterative algebraic eigenvalue solver. All three algorithms compete in numerical examples.

Zusammenfassung

Die vorliegende Arbeit zum Thema der numerischen Analysis von Eigenwertproblemen befasst sich mit fünf wesentlichen Aspekten der numerischen Analysis von Eigenwertproblemen. Die ersten drei befassen sich mit dem symmetrischen Laplace Eigenwertproblem wohingegen sich die letzten beiden mit einem unsymmetrischen Konvektion-Diffusion Eigenwertproblem beschäftigen.

Der erste Teil präsentiert einen Algorithmus, der die adaptive Finite Elemente Methode mit einem iterativen algebraischen Eigenwertlöser kombiniert. Es wird gezeigt, dass dieser Algorithmus asymptotisch quasi-optimale Rechenlaufzeit besitzt. Die Analysis basiert auf einem direkten Ansatz für das Eigenwertproblem. Sie gilt für konforme Finite Elemente höherer Ordnung mit festem Polynomgrad. Der asymptotisch quasi-optimale adaptive Finite Elemente Eigenwertlöser beinhaltet ein Kriterium zum rechtzeitigen Stoppen der Iterationen und braucht keine Vergröberungen der Gitter. Numerische Experimente demonstrieren die quasi-optimalen Laufzeiten in zwei und drei Raum-Dimensionen.

Der zweite Teil präsentiert explizite beidseitige Schranken für die Eigenwerte des Laplace Operators auf beliebig groben Gittern basierend auf einer Approximation der zugehörigen Eigenfunktion in dem nicht konformen Finite Elemente Raum von Crouzeix und Raviart und einem Postprocessing. Die Effizienz der garantierten Schranke des Eigenwertfehlers hängt von der globalen Gitterweite ab. Trotzdem kann sie hier für die große Klasse von graduierten Gittern bewiesen werden. Numerische Experimente zeigen die Zuverlässigkeit der garantierten Fehlerkontrolle sogar für inexakte algebraische Näherungen der Eigenfunktionen. Dies motiviert einen adaptiven Algorithmus der den Diskretisierungsfehler, die globale Gitterweite und den algebraischen Fehler kontrolliert und ausbalanciert. Die Genauigkeit der garantierten Eigenwert-Schranken ist überraschend sehr gut mit Effizienz-Indizes von 1.4.

Der dritte Teil betrachtet eine adaptive Finite Elemente Methode basierend auf Verfeinerungen von Knoten-Patchen. Dieser Algorithmus zeigt eine asymptotische Fehlerreduktion der adaptiven Sequenz von einfachen Eigenwerten und Eigenfunktionen des Laplace Operators. Die hier erstmals bewiesene Eigenschaft der Saturation des Eigenwertfehlers zeigt Zuverlässigkeit und Effizienz für eine Klasse von hierarchischen a posteriori Fehlerschätzern. Numerische Experimente verifizieren, dass die Saturations-Eigenschaft in vielen Benchmarks selbst auf sehr groben Gittern gilt. In manchen gezeigten Experimenten ist die Annahme, dass die globale Gitterweite hinreichen klein ist, jedoch kritisch.

Der vierte Teil betrachtet a posteriori Fehlerschätzer für Konvektion-Diffusion Eigenwertprobleme, wie sie von Heuveline und Rannacher (2001) im Kontext der dual-gewichteten residualen Methode (DWR) diskutiert wurden. Im Gegensatz zum nicht linearen Ansatz von Becker und Rannacher wird hier ein direkter Ansatz für die Variationsformulierung vorgestellt. Zwei verschiedene Techniken für das Postprocessing im Kontext der DWR Methode und zusätzlich zwei neue dual-gewichtete a posteriori Fehlerschätzer werden vorgestellt. Der erste neue Fehlerschätzer benutzt eine zusätzliche Raviart-Thomas gemischte Finite Elemente Lö-

sung und der zweite kombiniert eine Mittelungstechnik mit den Ideen der DWR Methode. Die sechs a posteriori Fehlerschätzer werden miteinander in drei numerischen Benchmarks verglichen und auf Zuverlässigkeit und Effizienz hin untersucht. Die numerischen Experimente zeigen die Abhängigkeit der Fehlerschranken von generischen Konstanten, der Größe des Eigenwertes oder dem Konvektion-Koeffizienten.

Der letzte Teil beschäftigt sich mit drei adaptiven Algorithmen für Eigenwertprobleme von nicht selbst-adjungierten Operatoren partieller Differentialgleichungen. Alle drei Algorithmen basieren auf einer Homotopie-Methode die vom einfacheren selbst-adjungierten Problem startet. Neben der Gitterverfeinerung wird der Prozess der Homotopie sowie die Anzahl der Iterationen des algebraischen Löser adaptiv gesteuert und die verschiedenen Anteile am gesamten Fehler ausbalanciert. Der erste Algorithmus zeigt Methoden zum Ausbalancieren der Fehler der Homotopie, der Diskretisierung und der algebraischen Approximation für eine feste Schrittweite der Homotopie. Der zweite Algorithmus kombiniert eine adaptive Steuerung der Schrittweiten der Homotopie mit der adaptiven Finiten Elemente Methode im Raum mittels einer festen Fehlertoleranz. Die Kombination beider Algorithmen führt auf den dritten Algorithmus der die Vorteile der ersten beiden kombiniert und damit komplett adaptiv in allen drei Richtungen, dem Raum, der Homotopie, und den algebraischen Iterationen, adaptive arbeitet. Alle drei Algorithmen werden in numerischen Benchmarks miteinander verglichen.

Contents

1 Introduction

The computation of eigenvalues is a fundamental task of numerical mathematics and arises in a large variety of important applications in science and engineering: Eigenvalue problems occur in the dynamics of elastic bodies, the vibrations of membranes, in the separation of variables ansatz for the problems of heat conduction or acoustics, or in the hydrodynamic stability analysis.

1.1 Motivation

For a motivation of this thesis three generally understandable examples for the relevance of eigenvalues/frequencies or eigenfunctions/modes are presented in the following.

The *first* example is the probably most famous example of structural failure of the Tacoma Narrows bridge in 1940 due to too large vibrations of some fundamental mode of the bridge. This mode was some lower torsional twisting vibration mode that had never been observed before. The forces of the wind caused this natural mode of the bridge to vibrate [18] – this physical effect is called aeroelastic fluttering. The enforced vibration of the Tacoma Narrows bridge was a self-exciting vibration that finally caused its failure. Engineers investigated the vibrations of the "Galloping Gerti" and filmed its final damage. Over 6 million people have watched the clip on YouTube (`http://www.youtube.com/watch?gl=DE&hl=de&v=j-zczJXSxnw`). To prevent the new bridge from vibrating in this fatal self-exciting natural mode, the engineers increased the damping of the structure and the torsional stiffness.

The *second* example is some resonance problem of classical string instruments known

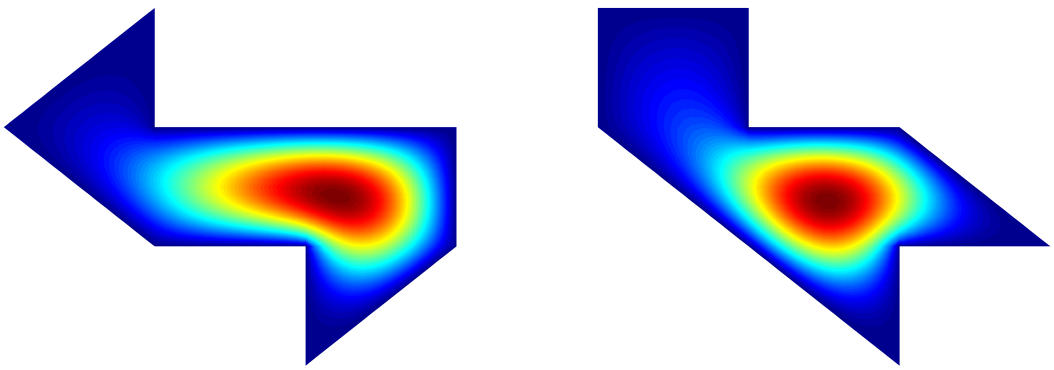

Figure 1.1: The first eigenfunctions of two isospectral domains.

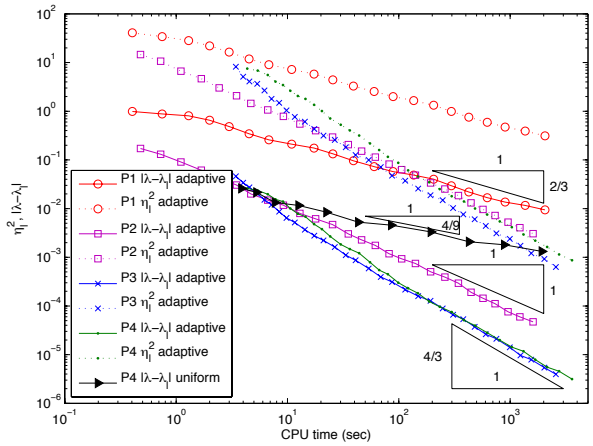

Figure 1.2: State of the art quasi-optimal adaptive finite element method for eigenvalue computations on the 3D L-shaped domain: Eigenvalue errors as function of CPU time from Section 3.8 for various polynomial degrees.

to musicians as *wolf tone*. The problem is that an instrument specific tone that matches some eigenfrequency causes the instrument to sound like the howling of a wolf. Due to [54] this problem is caused by "the beating of two equal forces". The first force is the string vibration while the second one is the body vibration. In this weakly damped coupled string-body system, the body withdraws energy from the string resulting in a lack of sound level. The musician tries to compensate that by putting more energy on the string which then leads to an increase of the sound level. The resulting up and down in the sound level is experienced as the howling of a wolf.

The *third* example of the occurrence of eigenvalue problems is the celebrated article of M. Kac (1966) [72]: "Can one hear the shape of a drum?" The question is whether two different shaped planar drums (of the same area) can have the same spectrum. The answer was published in C. Gordon D. Webb and S. Wolper (1992) [63]: "One cannot hear the shape of a drum". The first eigenfunction for the two isospectral domains from [62] are depicted in Figure 1.1. An interesting empirical observation is that even the discrete eigenvalues coincide (up to round-off errors) when both domains are triangulated with the same number of similar shaped triangles.

1.2 State of the Art

The mathematical studies of eigenvalue problems dates back to the book of Helmholtz, Sensations of Tone (1863), which marks the foundation of acoustics.

The *a priori* error analysis of the finite element method of eigenvalue problems for partial differential equations (PDEs) started with the Laplace eigenvalue model problem [105]. The further development of the a priori error analysis [9, 42] led to the eigenvalue chapter [10] with estimates for general compact operators and their application to general second-order elliptic operators. Further a priori error estimates for self-adjoint

operators can be found in [81, 98]. All those results assume that the global mesh-size is sufficiently small due to the non-linear nature of the eigenvalue problem. The article [100] investigates the convergence behaviour in the pre-asymptotic regime and [79] gives a priori error estimates with explicit constants and without the usual assumption that the mesh-size is sufficiently small.

The *a posteriori* error analysis of the finite element method started with [108] for symmetric second order elliptic eigenvalue problems based on a general non-linear analysis. The duality-based analysis of [80] led to a posteriori error estimates for the L^2 and energy errors but only for sufficiently smooth solutions. In [50] a residual a posteriori error estimator for non-smooth solutions is developed and it is proven that the volumetric part of the residual dominates the jumps for linear finite elements and the smallest eigenvalue. This result has been improved in [33] where it is shown that the volumetric part is not needed for all eigenvalues. Other a posteriori error estimator techniques have been employed for the eigenvalue problem as well. An averaging a posteriori error estimator has been presented in [89] and hierarchical a posteriori error estimators can be found in [65, 91, 92]. The results on symmetric eigenvalue problem have been applied to heterogeneous elastic structures in [109]. For the non-symmetric convection-diffusion eigenvalue problem a posteriori error estimators were presented in [69].

The asymptotic *convergence* analysis of the adaptive finite element method for symmetric eigenvalue problems started with [60] based on a refinement procedure that considers both a standard a posteriori error estimator and the oscillations of eigenfunctions. Asymptotic convergence for a much simpler standard bulk marking strategy and the standard residual type a posteriori error estimator has been presented in [58]. Around the same time the article [33] proved asymptotic convergence for the pure edge-residual a posteriori error estimator.

Based on a coarsening procedure [44] presented the first results on asymptotic *quasi-optimal convergence* of eigenvalue computations. For the adaptive finite element method [45] showed the first result without coarsening. The corresponding result for the Steklov eigenvalue problem can be found in [57]. However, all those results do unrealistically assume the exact knowledge of algebraic eigenpairs.

Assuming a saturation assumption, [91, 92] present *combined* adaptive finite element and linear algebra algorithms. Based on the dual-weighted residual method [96] presented a balanced adaptive finite element and linear algebra algorithm for the non-symmetric convection-diffusion eigenvalue problem.

1.3 Overview and Main Results

This thesis aims at the numerical analysis of eigenvalue problems for the Laplace and the convection-diffusion operators. Fast algorithms (quasi-optimal for the Laplace operator and adaptive homotopy based for the convection-diffusion operator) and sharp error bounds (via lower eigenvalue bounds for the Laplace operator and DWR-based a posteriori error estimators for the convection-diffusion operator) are presented. It is shown by various numerical experiments, or it is even proven for the Laplace operator,

that the adaptive finite element method decreases complexity of the eigenvalue computations and even improves the accuracy of the computed eigenvalues/eigenfunctions in comparison to uniform mesh-refinement. The following gives an overview of the five main parts of this thesis in Chapters 3–7 and presents the main results. The first three parts in Chapters 3–5 consider the symmetric Laplace eigenvalue problem while the last two parts in Chapters 6 and 7 concern a non-symmetric convection-diffusion eigenvalue problem.

The motivation of the *first* part in Chapter 3 is that in practice the computational costs for the iterative algebraic eigenvalue solver dominate the overall computational costs. Hence, it is beneficial to stop the iterations of the algebraic eigenvalue solver at an early stage. In order to preserve the optimal order of convergence, the discretisation and the algebraic errors need to be balanced in the right way. Chapter 3 presents the first adaptive finite element eigenvalue solver (AFEMES) of overall asymptotic quasi-optimal complexity in terms of the CPU time as displayed in Figure 1.2. This is joint work with C. Carstensen and has been published in [34].

The main result is the asymptotic quasi-optimal computational complexity of the proposed AFEMES: Suppose that (λ_ℓ, u_ℓ) is a discrete eigenpair to the continuous eigenpair (λ, u). Let $(\mathcal{T}_\ell)_\ell$ be a sequence of nested regular triangulations and $|||\cdot|||$ denote the energy norm. Suppose that the continuous eigenpair (λ, u) belongs to some approximation class $\mathcal{A}_s$, i.e., there exists some $s > 0$ and some $|u|_{\mathcal{A}_s} < \infty$ such that, for any number N there is an (unknown) optimal mesh $\mathcal{T}_N$ with $|\mathcal{T}_N| \leq |\mathcal{T}_0| + N$ element domains and discrete eigenpair (λ_N, u_N) with

$$\sup_{N\in\mathbb{N}} N^{2s} \left(|||u - u_N|||^2 + |\lambda - \lambda_N| \right) =: |u|^2_{\mathcal{A}_s} < \infty.$$

Then the computational complexity of the AFEMES is quasi-optimal in the sense that

$$|||u - \tilde{u}_\ell|||^2 + |\lambda - \tilde{\lambda}_\ell| \leq \mathcal{O}(t_\ell^{-2s}),$$

where t_ℓ denotes the computational costs in form of the CPU time. The point is that this quasi-optimal complexity holds for any $u \in \mathcal{A}_s$ and all $s > 0$ despite the fact that AFEMES does not require any parameter s. The analysis consists of three steps and does not need any inner node property, coarsening or saturation assumption. Since in the present analysis no oscillations occur, it is not necessary to add additional inner points to reduce some oscillations [60]. In [44] a coarsening of the mesh is needed in some steps to maintain optimality. The present analysis relies only on refinement of some mesh and does not need any coarsening. For hierarchical error estimators [91, 92] reliability is equivalent to the saturation assumption, namely a strict error reduction for uniform refined meshes. For the residual estimator used here the reliability is proven directly. First the asymptotic quasi-optimal convergence is shown for discrete eigenpairs without using the inner node property: Suppose that (λ_ℓ, u_ℓ) is a discrete eigenpair to the continuous eigenpair (λ, u) in some approximation class $\mathcal{A}_s$ for some $s > 0$. Then (λ_ℓ, u_ℓ) converges quasi-optimal, i.e., optimal up to a positive generic multiplicative constant C

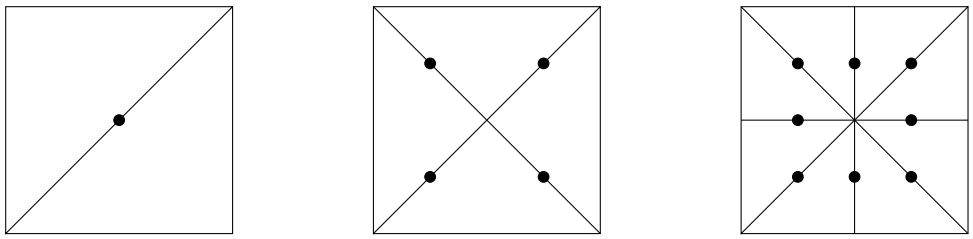

Figure 1.3: Criss (left), criss-cross (middle) and union-jack (right) triangulations of the unit square in 2, 4, and 8 congruent triangles.

with

$$\|\!|u - u_\ell|\!\|^2 + |\lambda - \lambda_\ell| \leq C|u|^2_{\mathcal{A}_s} N_\ell^{-2s}.$$

In contrast to [45] the proofs are based on the eigenvalue formulation and not on a relation to its corresponding source problem. Hence, no additional oscillations arise from the corresponding source problem. The second step extends this result to the case of inexact algebraic eigenvalue solutions: Suppose (λ, u) with $u \in \mathcal{A}_s$ is an eigenpair and (λ_ℓ, u_ℓ) and $(\lambda_{\ell+1}, u_{\ell+1})$ corresponding discrete eigenpairs on levels ℓ and $\ell+1$. Let the iterative approximations $(\tilde{\lambda}_\ell, \tilde{u}_\ell)$ on $\mathcal{T}_\ell$ and $(\tilde{\lambda}_{\ell+1}, \tilde{u}_{\ell+1})$ on $\mathcal{T}_{\ell+1}$ satisfy

$$\begin{aligned} \|\!|u_{\ell+1} - \tilde{u}_{\ell+1}|\!\|^2 + |\lambda_{\ell+1} - \tilde{\lambda}_{\ell+1}| &\leq \omega \eta_\ell^2(\tilde{\lambda}_\ell, \tilde{u}_\ell), \\ \|\!|u_\ell - \tilde{u}_\ell|\!\|^2 + |\lambda_\ell - \tilde{\lambda}_\ell| &\leq \omega \eta_\ell^2(\tilde{\lambda}_\ell, \tilde{u}_\ell), \end{aligned}$$

for sufficiently small $\omega > 0$. Then, the iterative solutions $\tilde{\lambda}_\ell$ and $\tilde{u}_\ell$ converge quasi-optimal, up to some generic constant $C > 0$,

$$\|\!|u - \tilde{u}_\ell|\!\|^2 + |\lambda - \tilde{\lambda}_\ell| \leq C N_\ell^{-2s}.$$

Finally, it is shown that the AFEMES is of linear runtime provided the linear algebra eigenvalue solver satisfies some convergence and complexity assumptions.

Numerical experiments show empirical quasi-optimal computational complexity of the AFEMES for some iterative algebraic eigenvalue solvers and higher-order finite element methods in 2 and 3 dimensions.

The *second* part in Chapter 4 is motivated by the fact that the residual based a posteriori error estimator involves some unknown constant and therefore the accuracy of the computed eigenvalues are much better than the termination criterion of the AFEMES suggests. Hence, sharp eigenvalue error bounds are needed in order to stop the computation at an early stage when the desired accuracy is reached. One way to obtain sharp eigenvalue error bounds is to compute sharp upper and lower eigenvalue bounds. Upper bounds are easily obtained from the Rayleigh-Ritz principle while lower bounds may possibly be obtained by minimising the Rayleigh-quotient on some larger set of non-admissible functions. Chapter 4 presents lower bounds for eigenvalues of the Laplace

operator with the help of nonconforming finite element methods. This is joint work with C. Carstensen and has been accepted for publication [35].

The well-established Rayleigh-Ritz principle for the algebraic as well as for the continuous eigenvalues of the Laplace operator immediately results in *upper* bounds of the eigenvalues by Rayleigh quotients

$$\lambda_1 \leq R(v) := |||v|||^2/\|v\|^2 \quad \text{for any } v \in H^1_0\backslash\{0\}. \tag{1.1}$$

Since *upper* bounds are easily obtained by conforming discretisations via (1.1), the computation of *lower* bounds is of high interest and we solely mention the mile-stones [7, 55, 110] for asymptotic lower bounds in the sense that they provide guaranteed bounds under the assumption that the global mesh-size is sufficiently small. Unfortunately, the minimal mesh-size required to deduce some guaranteed lower eigenvalue bound is *not* quantified in the current literature – so nobody knows whether some mesh allows some guaranteed bound or not. Chapter 4 establishes *guaranteed lower bounds* even for very coarse triangulations like those of Figure 1.3 for the unit square $\Omega = (0,1)^2$ with only very few triangles. For the three meshes of Figure 1.3, clearly in the pre-asymptotic range of convergence, the first main result of Chapter 4 provides the *guaranteed bounds*

$$2.3371 \leq \lambda_1 \leq 32, \quad 4.2594 \leq \lambda_1 \leq 24, \quad \text{and} \quad 6.6182 \leq \lambda_1 \leq 22.0397$$

for the first exact eigenvalue $\lambda_1 = 2\pi^2 = 19.7392$ despite the coarse discretisation with just 1, 4, or 8 degrees of freedom in a Crouzeix-Raviart nonconforming finite element discretisation (CR-NCFEM). To describe the main results of Chapter 3, let $\mathcal{T}$ be an arbitrarily coarse shape-regular triangulation of the polygonal domain Ω into triangles with set $\mathcal{E}$ of edges and let $CR^1_0(\mathcal{T})$ denote the Crouzeix-Raviart nonconforming FEM spaces for the piecewise first-order polynomials. Suppose that $(\tilde\lambda_{CR,1}, \tilde u_{CR,1}) \in \mathbb{R} \times CR^1_0(\mathcal{T})$ is some computed approximation of the smallest exact eigenvalue λ_1 of the associated algebraic eigenvalue problem with the stiffness matrix $\mathbf{A}$, the (diagonal) mass matrix $\mathbf{B}$, and the algebraic residual $\mathbf{r} := \mathbf{A}\tilde{\mathbf{u}}_{CR,1} - \tilde\lambda_{CR,1}\mathbf{B}\tilde{\mathbf{u}}_{CR,1}$ for the algebraic eigenvector $\tilde{\mathbf{u}}_{CR,1}$. Suppose that the first approximated discrete eigenvalue $\tilde\lambda_{CR,1}$ is closer to the first discrete eigenvalue $\lambda_{CR,1}$ than to the second discrete eigenvalue (which has to be guaranteed by algebraic eigenvalue analysis) and that $\|\mathbf{r}\|_{\mathbf{B}^{-1}} < \tilde\lambda_{CR,1}$. Moreover, $H := \max_{T\in\mathcal{T}} \operatorname{diam}(T)$ denotes the maximal mesh-size and $\mathcal{I}_{CM}$ denotes some interpolation operator with $\mathcal{I}_{CM}\tilde u_{CR,1} \not\equiv 0$. The first main result reads

$$\frac{\tilde\lambda_{CR,1} - \|\mathbf{r}\|_{\mathbf{B}^{-1}}}{1 + \kappa^2(\tilde\lambda_{CR,1} - \|\mathbf{r}\|_{\mathbf{B}^{-1}})H^2} \leq \lambda \leq R(\mathcal{I}_{CM}\tilde u_{CR,1}).$$

The explicit constant κ reads $\kappa^2 := (1/8 + j_{1,1}^{-2}) \leq 0.1932$ for the first positive root $j_{1,1} = 3.8317059702$ of the Bessel function of the first kind. Note that the nonconforming eigenvalue for the first two meshes of Figure 1.3 reads $\lambda_0^{CR} = 24$ and is larger than the solution $\lambda = 2\pi^2$. This novel observation shows that the nonconforming eigenvalue by itself does *not* always provide some lower bound for arbitrary coarse meshes in contrast

to the lower bound given in Chapter 4. The asymptotic a posteriori error control of [7] does not provide those error bounds.

The second main result guarantees efficiency in the sense that the difference of the upper and lower bound is bounded by the error for the large class of graded meshes.

The lower bound is generalised to higher eigenvalues under some explicit given mesh-size restriction plus the aforementioned separation condition. Together with a conforming approximation for an upper bound, the bounds for the higher eigenvalues are also efficient.

The efficiency for graded meshes motivates the development of an adaptive algorithm that balances the finite element error and the global mesh size H in order to reduce the difference of the upper and lower eigenvalue bounds. Numerical experiments show convergence of the proposed AFEM and compare conforming and nonconforming discretisations empirically.

For the *third* part in Chapter 5 note that the quasi-optimal algorithm of Chapter 3 is based on a contraction property of the sum of the errors of the eigenfunctions in energy norm plus the residual a posteriori error estimators and this does not imply contraction of the error itself but only proves that either the error or the a posteriori error estimator or both decrease during the adaptive finite element loop. Therefore the question arises whether there exists a refinement strategy that yields contraction of the error on its own. Chapter 5 presents an adaptive finite element method that yields such an asymptotic error reduction. This is joint work with C. Carstensen, V. Mehrmann and A. Miedlar and is submitted for publication [38].

The error reduction (also called saturation) property for the linear second order boundary value problem is reasonably justified in [1, 13, 49, 53, 108]. For the eigenvalue problem, the mathematical justification of the adhoc saturation assumption in [91, 92] is widely open even in the asymptotic range for extreme small mesh-sizes. Chapter 5 appears to be the first contribution to the mathematical foundations of the saturation property

$$\hat{\lambda}_\ell - \lambda \leq \varrho(\lambda_\ell - \lambda) + \mathrm{HOT},$$

for the discrete eigenvalue λ_ℓ to some simple eigenvalue λ, some higher-order and/or fine-grid solution $\widehat{\lambda}_\ell$, and some $0 \leq \varrho < 1$. In [91, 92], the contribution HOT is neglected while this chapter computes the explicit contribution $\mathrm{HOT} := \hat{\lambda}_\ell^3 H_\ell^4$ and therefore justifies that this term can be neglected for very fine meshes. It is true that [33] shows that oscillations can be neglected under certain particular assumptions on the meshes, but the same global arguments do not apply in the present situation where the analysis is based on local estimates.

Chapter 5 presents an adaptive finite element method with asymptotic saturation of a *single* sequence of eigensolutions $(\lambda_\ell, u_\ell)_{\ell \in \mathbb{N}_0}$ in the following sense. There exists some $0 \leq \varrho < 1$ such that for any two subsequent levels ℓ and $\ell+1$ and the maximal mesh-size

H_ℓ it holds that

$$|\lambda - \lambda_{\ell+1}| + |||u - u_{\ell+1}|||^2 \leq \varrho \left(|\lambda - \lambda_\ell| + |||u - u_\ell|||^2 \right) + 2\lambda_{\ell+1}^3 H_\ell^4.$$

The adaptive algorithm utilises a patch-oriented refinement process based on the *red-green-blue* refinement without the interior node property and there is no need to compute any higher-order or fine-grid solutions. Note that the higher-order term $2\lambda_{\ell+1}^3 H_\ell^4$ is explicit even with the multiplicative constant 2 in front of it.

Numerical examples verify the (asymptotic) reliability and efficiency of the hierarchical a posteriori error estimator and therefore confirm the (asymptotic) saturation property. For the first eigenvalue the mesh-size restrictions on H_0 are empirically not visible, but are certainly more severe for larger eigenvalues with much more oscillating eigenfunctions.

The *fourth* part considers the non-symmetric convection-diffusion eigenvalue problem. Since the residual based a posteriori error estimator involves some unknown constant that depends on the convection-coefficient, other techniques that lead to sharp error bounds are of high interest. Chapter 6 presents (empirically) sharp a posteriori error estimators for the convection-diffusion eigenvalue problem based on the dual-weighted residual (DWR) method. This is joint work with C. Carstensen and will be published in [59].

While the numerical approximation of eigenvalues of symmetric second-order elliptic PDEs with real eigenpairs is relatively well understood, much less is known about non-symmetric problems with possibly complex eigenvalues. A posteriori error estimators for some non-symmetric eigenvalue problems can be found in [43, 69, 70]. It is the aim of Chapter 6 to review the results of Heuveline and Rannacher in a direct approach rather than in the non-linear setting of the DWR paradigm after [12, 14, 69]. These results are also applicable to the averaging techniques as for the symmetric eigenvalue problem in [89]. The first two residual and averaging based a posteriori error estimators are based on the residual estimate for the eigenvalue error with dual energy norm $|||\cdot|||_*$, primal and dual residuals Res_ℓ, Res_ℓ^*, and some generic constant $C > 0$,

$$|\lambda - \lambda_\ell| \leq C \left(|||\mathrm{Res}_\ell|||_*^2 + |||\mathrm{Res}_\ell^*|||_*^2 \right).$$

Therefore, the dual norms of the primal and dual residuals can be bounded separately. Numerical experiments indicate that the efficiency indices for the residual-type a posteriori error estimators depend strongly on the convection coefficient β. Therefore, this chapter investigates the dual-weighted residual paradigm from Becker and Rannacher [12, 14, 15]. The DWR based a posteriori error estimators are derived from the asymptotic sharp estimate for simple (non-degenerate) eigenvalues λ with primal and dual eigenfunctions $u, u^* \in H_0^1(\Omega; \mathbb{C})$,

$$|\lambda - \lambda_\ell| \leq C |\mathrm{Res}_\ell(u^* - u_\ell^*) + \mathrm{Res}_\ell^*(u - u_\ell)|,$$

where the constant $C > 0$ tends to $1/(2|b(u, u^*)|)$ as $H_\ell \to 0$. In general the dual-

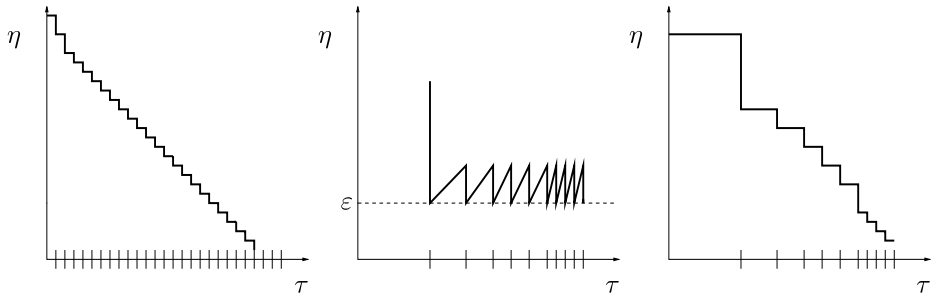

Figure 1.4: Schematic view of three homotopy-based Algorithms.

weighted residual a posteriori error estimators avoid any additional inequality, such as approximation properties with unknown constants. Thus, they are robust with respect to strong convection which is also confirmed by the numerical examples in Section 6.5. One question that arises from the computation of $\mathrm{Res}_\ell(u^* - u_\ell^*)$ or $\mathrm{Res}_\ell^*(u - u_\ell)$ is the calculation of the unknown primal and dual errors $u - u_\ell$ and $u^* - u_\ell^*$. The rather heuristic approach of [12] states that it is numerically reliable and efficient to approximate these quantities which occur only in the weights. The idea is that one does not need to approximate the weights with higher accuracy than the size of the residual terms. In practice the unknown primal and dual solutions u, u^* are replaced by solutions of a higher-order method or by some higher-order interpolation. Benchmark experiments provide numerical evidence that the DWR methodology in combination with the L^2 interpolation scheme of [111] is empirical reliable and efficient for unstructured triangular meshes while [69] is restricted to structured meshes because of the approximation of the weights by second-order difference quotients. In addition, two new dual-weighted a posteriori error estimators are presented. The first new estimator is based on the Raviart-Thomas mixed finite element method (MFEM) of first-order and the second one on averaging techniques. Hence, they are named by dual-weighted mixed (DWM) and dual-weighted averaging (DWA) a posteriori error estimators.

The *fifth* part contributes to the fact that the eigenvalues for the non-symmetric convection-diffusion eigenvalue problem may be ill-conditioned and the (symmetric) Rayleigh-Ritz principle does not hold. Therefore, it is harder to guarantee convergence of some iterative algebraic eigenvalue solver towards some specific eigenvalue. The idea is now to first compute the eigenvalues for the simpler symmetric eigenvalue problem where the eigenvalues converge safely and then bring in the non-symmetric part via a homotopy method. Chapter 7 presents three versions of adaptive homotopy algorithms for the convection-diffusion eigenvalue problem. This is joint work with C. Carstensen, V. Mehrmann and A. Miedlar and has been published in [37].

The difficulty with non-selfadjoint PDE eigenvalue problems is multifold, eigenvalues may be complex, or may have different algebraic and geometric multiplicity. The latter property is a particular difficulty because this property is destroyed in the finite dimensional approximation. The computed eigenvalues and eigenfunctions may have

large errors due to the ill-conditioning of the problem although the approximation error is small. Even when the discretisation retains the multiplicities of the eigenvalues, the algebraic eigensolvers have difficulties with the ill-conditioning of multiple eigenvalues.

Chapter 7 studies the restricted class of convection-diffusion eigenvalue problems and simple eigenvalues, where for the pure diffusion problem the discussed adaptive methods work nicely. To design a robust adaptive algorithm for the convection-diffusion problem a homotopy method is applied. Homotopy methods are well established for non-symmetric matrix eigenvalue problems [84, 85, 86, 88]. Here, the homotopy approach is used not only on the matrix level but on the level of the differential operator as well. The continuation method uses a 'time'-stepping procedure with nodes $t_0 = 0 < t_1 < \ldots < t_N = 1$ to compute the eigenvalues and eigenvectors of

$$-\Delta u + t_i \beta \cdot \nabla u = \lambda u \quad \text{in} \quad \Omega.$$

The final homotopy value 1 results in the desired problem

$$-\Delta u + \beta \cdot \nabla u = \lambda u \quad \text{in} \quad \Omega.$$

The combination of the adaptive homotopy with mesh adaptivity and iterative matrix eigenvalue solvers involves three different types of errors: the *discretisation error* η that arises when the infinite dimensional variational problems is considered in a finite dimensional subspace [69] and Chapter 6, the *homotopy error* ν that arises because the diffusion problem is slowly transferred to the convection-diffusion problem [22] and the *approximation error* μ that arises from the iterative matrix eigensolver in finite precision arithmetic [11, 68, 94, 104]. To develop adaptive algorithms that are adaptive with respect to all three types of errors, three different algorithms are proposed as depicted in Figure 1.4. The *first* algorithm balances the homotopy, the discretisation and the approximation errors with respect to a fixed step-size in the homotopy. The *second* algorithm combines the adaptive step-size control for the homotopy with an adaptation in space that ensures an error below a fixed tolerance. The outcome leads to the *third* algorithm which allows the complete adaptivity in space, homotopy step-size as well as the iterative algebraic eigenvalue solver. The overall eigenvalue error is shown to be bounded by the a posteriori eigenvalue error bound

$$|\lambda(1) - \tilde{\lambda}_\ell(t)| \leq C\Big(\nu(\tilde{\lambda}_\ell(t), \tilde{u}_\ell(t), \tilde{u}^*_\ell(t)) + \eta^2(\tilde{\lambda}_\ell(t), \tilde{u}_\ell(t), \tilde{u}^*_\ell(t)) + \mu^2(\tilde{\lambda}_\ell(t), \tilde{u}_\ell(t), \tilde{u}^*_\ell(t))\Big),$$

in terms of the homotopy a posteriori error estimator $\nu(\tilde{\lambda}_\ell(t), \tilde{u}_\ell(t), \tilde{u}^*_\ell(t))$, the discretisation a posteriori error estimator $\eta^2(\lambda_\ell(t), u_\ell(t), u^*_\ell(t))$, the algebraic a posteriori error estimator $\mu^2(\tilde{\lambda}_\ell(t), \tilde{u}_\ell(t), \tilde{u}^*_\ell(t))$, and some generic constant $C > 0$.

1.4 Outlook and Open Questions

For an *outlook* and *open questions* note that, despite the guaranteed lower eigenvalue bounds of Chapter 4, this work restricts to simple eigenvalues. For the symmetric prob-

lem a convergence result of the adaptive finite element method for multiple or clustered eigenvalues has been proven in [33]. This convergence result is based on a refinement strategy that refines the mesh accordingly to the sum of the a posteriori error estimators of all the discrete eigenfunctions to some multiple eigenvalue. The open question is whether this leads to optimal convergence of one particular eigenfunction. The fact that different eigenfunctions of the eigenspace to some multiple eigenvalue may have different regularity rises the question whether for larger eigenspaces adaptive mesh-refinement is better than just uniform refinement. In the case of non-symmetric eigenvalue problems the possible blow up of the condition number of clustered/multiple eigenvalues makes efficient error control impossible. Besides the question of multiple or clustered eigenvalues there is a number of open questions for simple eigenvalues that result from this thesis as well. Open questions include the quasi-optimal convergence of the adaptive nonconforming finite element method for the eigenvalue problem as it is shown for the conforming finite elements in Chapter 3. Nonconforming methods, that provide lower eigenvalue bounds for the Laplace operator as shown in Chapter 4, play an important role in the stabilisation of numerical schemes such as the locking-free Kouhia-Stenberg finite element for linear elasticity. Does the Kouhia-Stenberg finite element provide lower eigenvalue bounds for linear elasticity? The techniques of Chapter 4 inspired [32] for lower eigenvalue bounds for fourth-order problems such as the Kirchhoff-Plate. Other possible future research activities may lead to lower eigenvalue bounds in the context of the stability analysis of time-evolution problems. Concerning the non-symmetric eigenvalue problems, future work will extend the homotopy algorithms of Chapter 7 to more complex eigenvalue problems such as the quadratic eigenvalue problems arising in dissipative acoustics [16]. The homotopy method enables the computation of some non-zero complex eigenvalues with certain features of interest of the indefinite quadratic eigenvalue problem without the need of full matrix decompositions.

2 Preliminaries

The summary of the functional analysis background in Section 2.1 is derived from [27, 52]. The presentation of the finite elements in Section 2.2 is based on [23, 27]. The a priori results for the model PDE eigenvalue problems in Section 2.3 and Section 2.4 have been taken from [10, 20, 105]. Adaptive mesh-refinement algorithms are described in Section 2.5 following [1, 8, 108].

Throughout this thesis, the notation $x \lesssim y$ abbreviates the inequality $x \leq Cy$ and $x \approx y$ the inequalities $Dy \leq x \leq Cy$ with constants $C > 0$ and $D > 0$ which do not depend on the mesh-size.

2.1 Functional Analysis Background

Let Ω be a connected open subset of $\mathbb{R}^n$ that is Lebesgue-measurable. The Lebesgue integral over Ω for real valued functions f that are Lebesgue measurable is $\int_\Omega f\,dx$. The Lebesgue spaces are defined for $1 \leq p < \infty$,

$$L^p(\Omega) := \{f : \|f\|_{L^p(\Omega)} < \infty\}$$

with the Lebesgue norms

$$\|f\|^p_{L^p(\Omega)} := \int_\Omega |f|^p\,dx.$$

The norm for $p = \infty$ is defined as

$$\|f\|_{L^\infty(\Omega)} := \operatorname{ess\,sup}\{|f(x)| : x \in \Omega\}.$$

The Lebesgue spaces are Banach spaces. Moreover, in this thesis $p = 2$ and $L^2(\Omega)$ is a Hilbert space with L^2-scalar product

$$\int_\Omega fg\,dx \quad \text{for any } f, g \in L^2(\Omega).$$

The following inequalities are frequently used in this thesis.

Lemma 2.1.1 (Minkowski's inequality)**.** *For $1 \leq p \leq \infty$ and $f, g \in L^p(\Omega)$, it holds that*

$$\|f + g\|_{L^p(\Omega)} \leq \|f\|_{L^p(\Omega)} + \|g\|_{L^p(\Omega)}. \quad \square$$

Lemma 2.1.2 (Hölder's inequality)**.** *For $1 \leq p, q \leq \infty$ such that $1 = 1/p + 1/q$,*

$f \in L^p(\Omega)$ and $g \in L^q(\Omega)$, it holds that $fg \in L^1(\Omega)$ and

$$\|fg\|_{L^1(\Omega)} \leq \|f\|_{L^p(\Omega)} \|g\|_{L^q(\Omega)}. \quad \square$$

In the special case $p = q = 2$ this inequality is called Cauchy-Schwarz inequality.

Lemma 2.1.3 (Cauchy-Schwarz inequality)**.** *For $f, g \in L^2(\Omega)$ it holds that $fg \in L^1(\Omega)$ and*

$$\int_\Omega fg \, dx \leq \|f\|_{L^2(\Omega)} \|g\|_{L^2(\Omega)}. \quad \square$$

Let $C^m(\Omega)$, $m \in \mathbb{N}$, denote the space of m-times continuously differentiable functions and the subset $C_0^m(\Omega)$ those functions with compact support.

The function $f \in L^2(\Omega)$ has a weak derivative (in $L^2(\Omega)$) if there exists a function $g = \partial^\alpha u$ such that

$$\int_\Omega g\varphi \, dx = (-1)^{|\alpha|} \int_\Omega f \partial^\alpha \varphi \, dx \quad \text{for all } \varphi \in C_0^\infty(\Omega).$$

Let $m \in \mathbb{N}$ and $f \in L^2(\Omega)$ such that all weak derivatives $\partial^\alpha f$ with $|\alpha| \leq m$ exist. Then

$$\|f\|^2_{H^m(\Omega)} := \sum_{|\alpha| \leq m} \|\partial^\alpha f\|^2_{L^2(\Omega)}$$

is a norm and

$$|f|^2_{H^m(\Omega)} := \sum_{|\alpha| = m} \|\partial^\alpha f\|^2_{L^2(\Omega)}$$

a semi-norm. The Sobolev spaces to $L^2(\Omega)$ are defined as

$$H^m(\Omega) := \{f \in L^2(\Omega) : \|f\|_{H^m(\Omega)} < \infty\}.$$

Sobolev spaces $H^m(\Omega)$ are Hilbert spaces. For domains Ω with Lipschitz boundary, the Sobolev spaces have boundary values in the sense of traces.

Theorem 2.1.4 (Trace theorem)**.** *Suppose that Ω has a Lipschitz boundary $\partial\Omega$, then there exists a constant $C > 0$ such that*

$$\|f\|_{L^2(\partial\Omega)} \leq C \|f\|^{1/2}_{L^2(\Omega)} \|f\|^{1/2}_{H^1(\Omega)} \quad \textit{for all } f \in H^1(\Omega). \quad \square$$

The subset of $H^1(\Omega)$ with zero trace on the boundary $\partial\Omega$ defines

$$H_0^1(\Omega) := \{f \in H^1(\Omega) : f|_{\partial\Omega} = 0 \text{ in } L^2(\partial\Omega)\}.$$

For the space $H_0^1(\Omega)$, the semi-norm $|.|_{H^1(\Omega)}$ is actually a norm.

The domain $\Omega \subseteq \mathbb{R}^n$ is star-shaped with respect to a ball B if the convex hull of $\{x\} \cup B$ is a subset of Ω for all $x \in \Omega$.

Lemma 2.1.5 (Poincaré's inequality)**.** *Suppose that Ω is the finite union of star-shaped domains with respect to a ball. Then there exists a constant $C_P < \infty$ such that*

$$\|f\|_{L^2(\Omega)} \leq C_P |f|_{H^1(\Omega)} \quad \textit{for all } f \in H_0^1(\Omega). \quad \square$$

Let $\fint_\Omega f\,dx$ denote the integral mean value $\frac{1}{|\Omega|}\int_\Omega f\,dx$.

Lemma 2.1.6 (Friedrichs' inequality)**.** *Suppose that Ω is the finite union of star-shaped domains with respect to a ball. Then there exists a constant $C_F < \infty$ such that*

$$\left\| f - \fint_\Omega f\,dx \right\|_{L^2(\Omega)} \leq C_F |f|_{H^1(\Omega)} \quad \textit{for all } f \in H^1(\Omega). \quad \square$$

Suppose that Ω is a bounded Lipschitz domain, then the Gauss-divergence theorem and the integration by parts formula hold.

Theorem 2.1.7 (Gauss-divergence theorem)**.** *Suppose that $f \in C^1(\Omega) \cap C(\overline{\Omega})$, then it holds that*

$$\int_\Omega \mathit{div}(f)\,dx = \int_{\partial\Omega} f\nu\,ds. \quad \square$$

Theorem 2.1.8 (Integration by parts formula)**.** *Suppose that $f, g \in C^1(\Omega) \cap C(\overline{\Omega})$, then it holds that*

$$\int_\Omega \left(\frac{\partial f}{\partial x_j} g + f \frac{\partial g}{\partial x_j} \right) dx = \int_{\partial\Omega} f g \nu_j\,ds. \quad \textit{for } 1 \leq j \leq n. \quad \square$$

2.2 Finite Elements

According to the definition due to Ciarlet, a finite element is a triple (T, P_T, N_T) [27] where

1. $T \subseteq \mathbb{R}^n$ is a bounded closed set with non-empty interior and piecewise smooth boundary,
2. P_T is a finite-dimensional space of functions on T and
3. $N_T = \{N_1, \ldots, N_m\}$ is a basis for the dual space P_T'.

The finite element function space P_T is the space of shape functions and N_T the set of nodal variables.

The nodal basis $\{\varphi_1, \ldots, \varphi_m\}$ of P_T for some finite element (T, P_T, N_T) is the basis that is dual to N_T, that is $N_i(\varphi_j) = \delta_{i,j}$ for Kronecker's $\delta_{i,j} = 0$ for $i \neq j$ and $\delta_{i,j} = 1$ for $i = j$, $1 \leq i, j \leq m$.

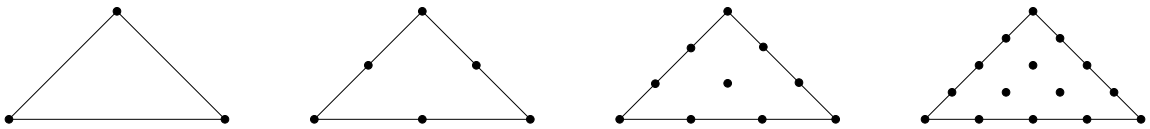

Figure 2.1: P_k, $k = 1, 2, 3, 4$, finite element.

2.2.1 Conforming Finite Element

As an example of a H^1-conforming finite element consider the triangular Lagrange finite elements. Let P_T be the space of polynomials of degree $\leq k$ and N_T be the shape functions that consist of the point evaluation in the barycentric coordinates as depicted in Figure 2.1 for $k = 1, 2, 3, 4$.

As a consequence of the Bramble-Hilbert lemma [27, (4.3.8)], the nodal interpolation operator $\mathcal{I}$ satisfies the following approximation property.

Lemma 2.2.1 ([27, (4.4.4)])**.** *For all $v \in H^2(T)$ there exists a constant $C < \infty$ such that for the diameter $diam(T) := \sup_{x,y\in T}|x - y|$*

$$|v - \mathcal{I}v|_{H^1(T)} \leq C\, diam(T)|v|_{H^2(T)}. \quad \square$$

For the linear triangular Lagrange finite element the constant C is explicitly bounded by

$$C(\alpha) := \sqrt{\frac{1/4 + 2/j_{1,1}^2}{1 - |\cos(\alpha)|}},$$

for the maximal angle $0 < \alpha < \pi$ of the triangle T and the first positive root of the Bessel function J_1 [39].

2.2.2 Nonconforming Finite Element

The H^1-nonconforming Crouzeix-Raviart finite element consists of the affine functions P_T and the shape functions N_T that consist of the point evaluation in the midpoints of the three edges as depicted in Figure 2.2.

The nonconforming interpolant $\mathcal{I}_{NC}$ specifies the values for the edge degrees of freedom as

$$\mathcal{I}_{NC}v(\text{mid}(E)) := \frac{1}{|E|}\int_E v\, ds \quad \text{for all edges } E \text{ of } T.$$

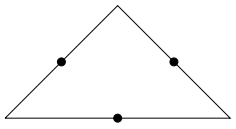

Figure 2.2: Crouzeix-Raviart finite element.

The following approximation estimate with explicit constant holds [39], cf. Theorem 4.2.1,

$$\|v - \mathcal{I}_{NC} v\|_{L^2(T)} \leq \sqrt{\operatorname{diam}(T)^2/8 + \operatorname{diam}(T)^2/j_{1,1}^2}\ |v - \mathcal{I}_{NC} v|_{H^1(T)}.$$

2.3 The Symmetric Model Eigenvalue Problem

As a simple model problem for a symmetric, elliptic eigenvalue problem consider the following eigenvalue problem of the Laplace operator: Seek a non-trivial eigenpair $(\lambda, u) \in \mathbb{R} \times \{H^1(\Omega;\mathbb{R}) \cap H^2_{loc}(\Omega;\mathbb{R})\}$ such that

$$-\Delta u = \lambda u \quad \text{in } \Omega \qquad \text{and} \qquad u = 0 \quad \text{on } \partial\Omega \tag{2.1}$$

in a bounded Lipschitz domain $\Omega \subset \mathbb{R}^n$, $n = 2, 3$. It is well known, that problem (2.1) has countably many solutions with positive eigenvalues that can be ordered increasingly

$$0 < \lambda_1 \leq \lambda_2 \leq \lambda_3 \leq \dots$$

and there exist some orthonormal basis $(u_1, u_2, u_3, ...)$ of corresponding eigenvectors.

The weak problem seeks for a non-trivial eigenpair $(\lambda, u) \in \mathbb{R} \times \{V := H^1_0(\Omega;\mathbb{R})\}$ with $b(u,u) = 1$ and

$$a(u,v) = \lambda b(u,v) \quad \text{for all } v \in V.$$

The bilinear forms $a(\cdot,\cdot)$ and $b(\cdot,\cdot)$ are defined by

$$a(u,v) := \int_\Omega \nabla u \cdot \nabla v \, dx \qquad \text{and} \qquad b(u,v) := \int_\Omega uv \, dx$$

and induce the norms $|||.||| := |.|_{H^1(\Omega;\mathbb{R})}$ on V and $\|.\| := \|.\|_{L^2(\Omega;\mathbb{R})}$ on $L^2(\Omega;\mathbb{R})$.

2.3.1 Conforming Discrete Eigenvalue Problem

The conforming finite element space of order $k \in \mathbb{N}$ for the shape-regular triangulation of the polygonal domain Ω into triangles $\mathcal{T}$ is defined by

$$P_k(\mathcal{T}) := \left\{ v \in L^2(\Omega;\mathbb{R}) : \forall T \in \mathcal{T},\ v|_T \text{ is polynomial of degree} \leq k \right\}.$$

Let $V_C := P_k(\mathcal{T}) \cap H^1_0(\Omega;\mathbb{R})$ denote the finite-dimensional subspace of fixed order $k > 0$. The corresponding discrete eigenvalue problem reads: Seek a non-trivial eigenpair $(\lambda_C, u_C) \in \mathbb{R} \times V_C$ with $b(u_C, u_C) = 1$ and

$$a(u_C, v_C) = \lambda_C b(u_C, v_C) \quad \text{for all } v_C \in V_C.$$

The following a priori error estimate [105] holds.

Lemma 2.3.1. *Let V_C be the conforming finite element space of order k and λ_C a simple eigenvalue. For sufficiently small global mesh-size H_ℓ it holds that*

$$|\lambda - \lambda_C| + |||u - u_C|||^2 \lesssim H_\ell^{\max(s,2k)} \lambda^{k+1},$$

where $s > 0$ depends on the regularity of the solution. □

For multiple eigenvalues similar a priori estimates hold [10].

2.3.2 Nonconforming Discrete Eigenvalue Problem

Let $\mathcal{T}$ be an arbitrarily shape-regular triangulation of the polygonal domain Ω into triangles with set $\mathcal{E}$ of edges and let

$$CR_0^1(\mathcal{T}) := \{v \in P_1(\mathcal{T}) \mid v \text{ is continuous at } \mathrm{mid}(\mathcal{E}) \text{ and } v = 0 \text{ at } \mathrm{mid}(\mathcal{E}(\partial\Omega))\}$$

denote the Crouzeix-Raviart nonconforming FEM spaces for the piecewise first-order polynomials $P_1(\mathcal{T})$. For all interior edges $E \in \mathcal{E}(\Omega)$, the edge-oriented basis function ψ_E is defined by

$$\psi_E(\mathrm{mid}(E)) = 1 \quad \text{and} \quad \psi_E(\mathrm{mid}(F)) = 0 \text{ for all } F \in \mathcal{E}\backslash E.$$

Then $CR_0^1(\mathcal{T}) = \mathrm{span}\{\psi_E \,|\, E \in \mathcal{E}(\Omega)\} \nsubseteq V$ and the nonconforming discrete eigenvalue problem reads: Seek an eigenpair $(\lambda_{CR}, u_{CR}) \in \mathbb{R} \times CR_0^1(\mathcal{T})$ with $b(u_{CR}, u_{CR}) = 1$ and

$$a_{NC}(u_{CR}, v_{CR}) = \lambda_{CR} b(u_{CR}, v_{CR}) \quad \text{for all } v_{CR} \in CR_0^1(\mathcal{T}).$$

The nonconforming bilinear form a_{NC},

$$a_{NC}(u_{CR}, v_{CR}) := \sum_{T\in\mathcal{T}} \int_T \nabla u_{CR} \cdot \nabla v_{CR}\, dx \quad \text{for all } u_{CR}, v_{CR} \in CR_0^1(\mathcal{T}),$$

induces the mesh-dependent norm $|||.|||_{NC} := a_{NC}(\cdot,\cdot)^{1/2}$. For the nonconforming finite element solutions the following a priori error estimates [7] holds.

Lemma 2.3.2. *For the Crouzeix-Raviart nonconforming finite element space, simple eigenvalues and sufficiently small global mesh-size H_ℓ, it holds that*

$$|\lambda - \lambda_{CR}| + |||u - u_{CR}|||_{NC}^2 \lesssim H_\ell^{\max(s,2)},$$

where $s > 0$ depends on the regularity of the solution. □

2.4 The Non-Symmetric Model Eigenvalue Problem

The convection-diffusion model eigenvalue problem reads: Seek an eigenpair $(\lambda, u) \in \mathbb{C} \times \{H^1_0(\Omega;\mathbb{C}) \cap H^2_{loc}(\Omega;\mathbb{C})\}$ with

$$-\Delta u + \beta \cdot \nabla u = \lambda u \quad \text{in } \Omega.$$

The given data $\beta \in H(div, \Omega; \mathbb{R}^2)$ is supposed to be divergence free in the bounded Lipschitz domain $\Omega \subseteq \mathbb{R}^2$, i.e., $\int_\Omega v \operatorname{div} \beta \, dx = 0$ for all $v \in V := H^1_0(\Omega;\mathbb{C})$.

The weak problem considers the two complex Hilbert spaces V with energy norm $|||\cdot||| = |\cdot|_{H^1(\Omega;\mathbb{C})}$ (which is a norm on V) and $W := L^2(\Omega;\mathbb{C})$ with norm $\|\cdot\|_{L^2(\Omega;\mathbb{C})}$. The weak form reads: Seek an eigenpair $(\lambda, u) \in \mathbb{C} \times V$ with $\|u\| = 1$ such that

$$a(u, v) = \lambda b(u, v) \quad \text{for all } v \in V. \tag{2.2}$$

The bilinear form $a(\cdot,\cdot)$ is elliptic and continuous in V and the bilinear form $b(\cdot,\cdot)$ is continuous, symmetric and positive definite, and hence induces a norm $\|\cdot\| := b(\cdot,\cdot)^{1/2}$ on W. For the above model problem, $\|\cdot\| = \|\cdot\|_{L^2(\Omega;\mathbb{C})}$ and the bilinear forms (where $\overline{(\cdot)}$ denotes complex conjugation) read

$$a(u, v) = \int_\Omega (\nabla u \cdot \nabla \overline{v} + (\beta \cdot \nabla u)\overline{v}) \, dx \qquad \text{and} \qquad b(u, v) = \int_\Omega u\overline{v} \, dx.$$

Since β is assumed to be divergence free, an integration by parts yields

$$\int_\Omega (\beta \cdot \nabla v)\overline{v} \, dx = -\int_\Omega (\beta \cdot \nabla \overline{v}) v \, dx.$$

Hence, for all $v \in V$, it holds that

$$|||v|||^2 = \operatorname{Re} a(v, v).$$

Thus, the ellipticity constant (which is one) of the bilinear form $a(\cdot,\cdot)$ is independent of the convection-coefficient β.

The analysis of the non-symmetric eigenvalue problem requires the dual eigenvalue problem: Seek a (dual) eigenpair $(\lambda^*, u^*) \in \mathbb{C} \times V$ with $\|u^*\| = 1$ such that

$$a(v, u^*) = \overline{\lambda^*} b(v, u^*) \quad \text{for all } v \in V.$$

Since the embedding of V in W is continuous and compact, the spectral theory for compact operators [10, 73] is applicable. The Riesz-Schauder theorem shows that the primal and dual spectra consist of finite or countably many eigenvalues with no finite accumulation point. In particular, the algebraic multiplicities are finite.

Given any conforming finite-dimensional subspace $V_\ell \subset V$, the discrete problems read: Seek primal and dual (discrete) eigenpairs (λ_ℓ, u_ℓ) and $(\lambda^*_\ell, u^*_\ell)$ with $\|u_\ell\| = 1 = \|u^*_\ell\|$

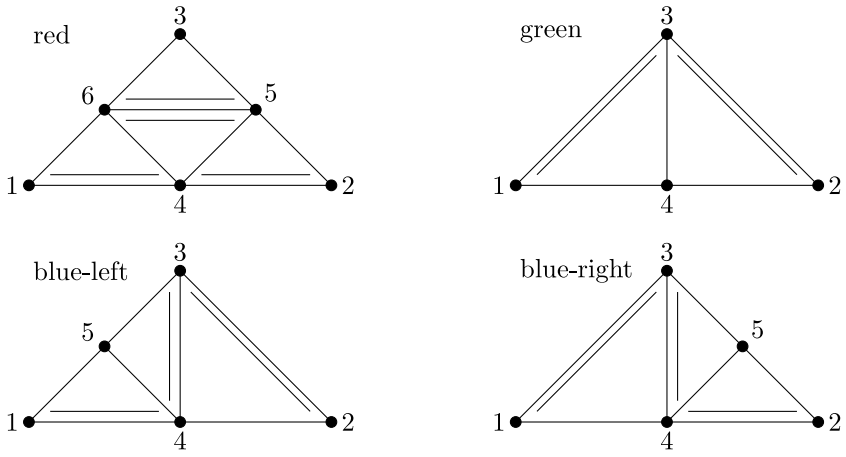

Figure 2.3: *Red*, *green* and *blue* refinement. The new reference edge is marked through a second line in parallel opposite the new vertices new_1, new_2 or new_3.

such that

$$a(u_\ell, v_\ell) = \lambda_\ell b(u_\ell, v_\ell) \quad \text{for all } v_\ell \in V_\ell;$$
$$a(v_\ell, u_\ell^*) = \overline{\lambda_\ell^*} b(v_\ell, u_\ell^*) \quad \text{for all } v_\ell \in V_\ell.$$

The primal and dual eigenvalues λ_j and λ_j^* as well as the primal and dual discrete eigenvalues $\lambda_{\ell,j}$ and $\lambda_{\ell,j}^*$ are connected by

$$\lambda_j = \overline{\lambda_j^*} \qquad \text{for } j = 1, 2, 3, \ldots \quad \text{and} \quad \lambda_{\ell,j} = \overline{\lambda_{\ell,j}^*} \quad \text{for all } j = 1, \ldots, \dim(V_\ell).$$

The abstract a priori theory yields the following upper bounds in terms of the maximal mesh-size H_ℓ for the linear conforming finite element approximations,

$$|\lambda - \lambda_\ell| \lesssim H_\ell^{s_1+s_2}, \qquad |\!|\!| u - u_\ell |\!|\!| \lesssim H_\ell^{s_1}, \qquad |\!|\!| u^* - u_\ell^* |\!|\!| \lesssim H_\ell^{s_2},$$

where $0 < s_1 \leq 1$ and $0 < s_2 \leq 1$ depend on the regularity of the primal and dual eigenfunctions [10, Chapter 10.3].

2.5 Adaptive Mesh-Refinement Algorithms

Let $\mathcal{T}_\ell$ be a sequence of *regular triangulations* in the sense of Ciarlet of the bounded Lipschitz domain Ω into at least two triangles such that all $T \in \mathcal{T}_\ell$ are closed triangles with positive area $|T|$ and two distinct intersecting triangles $T_1, T_2 \in \mathcal{T}_\ell$ share either one common edge or one common node. Let $\mathcal{E}_\ell$ denote the set of all edges of the triangulation $\mathcal{T}_\ell$.

2.5.1 Closure Algorithm

Given a triangulation $\mathcal{T}_\ell$ on the level ℓ, let $E(T)$ denote the reference edge for a given triangle T. To preserve the quality of the mesh, the closure algorithm computes the smallest subset $\widehat{\mathcal{M}}_\ell$ of $\mathcal{E}_\ell$ which includes all marked edges of the subset $\mathcal{M}_\ell \subseteq \mathcal{E}_\ell$ of selected edges for refinement such that

$$\Big\{E(T) : T \in \mathcal{T}_\ell \quad \text{with} \quad \mathcal{E}_\ell(T) \cap \widehat{\mathcal{M}}_\ell \neq \emptyset\Big\} \subseteq \widehat{\mathcal{M}}_\ell.$$

In other words, once an edge E of an element T is marked for refinement, the reference edge $E(T)$ of T is marked as well.

An important result for the proof of optimality of the mesh-refinement is that the closure algorithm marks only a constant number of additional edges over all levels.

Proposition 2.5.1 (Boundedness of closure, [19, 103])**.** *Let $\mathcal{T}_{\ell+1}$ be a refinement of $\mathcal{T}_\ell$, obtained using one of the refinement algorithms below and the closure algorithm. Suppose $\mathcal{T}_0$ is the initial coarse triangulation. Then it holds that*

$$|\mathcal{T}_L| - |\mathcal{T}_0| \lesssim \sum_{\ell=0}^{L-1} |\mathcal{M}_\ell|,$$

where $|\mathcal{T}_\ell|$ denotes the cardinality of all triangles in $\mathcal{T}_\ell$. □

2.5.2 Red-Green-Blue Refinement

Given a triangulation $\mathcal{T}_\ell$ on the level ℓ, let $E(T)$ denote the reference edge for a given triangle $T \in \mathcal{T}_\ell$. Note that the reference edge $E(T)$ will be the same edge of T in all triangulations $\mathcal{T}_\ell$ which include T. However, once T in $\mathcal{T}_\ell$ is refined, the reference edges will be specified for the different sub-triangles as indicated in Figure 2.3.

The *red-green-blue* mesh-refinement algorithm consists of the following five different refinements. Elements with no marked edge are *not* refined, elements with one marked edge are refined *green*, elements with two marked edges are refined *blue-left* or *blue-right*, and elements with three marked edges are refined *red* as depicted in Figure 2.3.

2.5.3 Newest-Vertex Bisection

The *newest-vertex* algorithm consists of successive bisections of triangles until no hanging node remains. Thereby, always the edge opposite to the newest vertex is bisected. Hence, in the notion of reference edges, $E(T)$ is always opposite to the newest vertex of each triangle $T \in \mathcal{T}_\ell$.

Therefore, after the closure algorithm is applied, one of the following refinement rules is applicable, namely *no* refinement, *green* refinement, *blue left* or *blue right* refinement and *bisec3* refinement as depicted in Figure 2.4. Note that the case of three marked edges is refined differently for the *newest-vertex* refinement and the *red-green-blue* algorithm.

A corresponding *newest-vertex* bisection refinement algorithm for $n = 3$ based on the concept of reference edges can be found in [8].

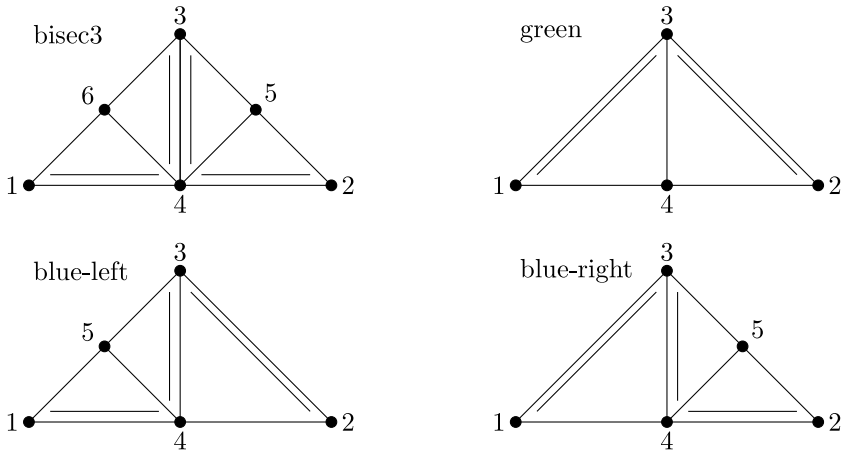

Figure 2.4: *Bisec3*, *green* and *blue* refinement. The new reference edge is marked through a second line in parallel opposite the new vertices new_1, new_2 or new_3.

The *newest-vertex* bisection algorithm allows for an overlay estimate that is one of the key arguments in the proof of quasi-optimality. For two arbitrary refinements $\mathcal{T}_\ell$ and $\mathcal{T}_m$ of the initial triangulation $\mathcal{T}_0$ define the overlay $\mathcal{T}_\ell \oplus \mathcal{T}_m$ as the smallest common refinement such that all triangles of $\mathcal{T}_\ell$ and $\mathcal{T}_m$ are either contained or further refined in $\mathcal{T}_\ell \oplus \mathcal{T}_m$.

Proposition 2.5.2 (Overlay, [41, 102])**.** *The smallest common refinement of $\mathcal{T}_m$ and $\mathcal{T}_\ell$, $\mathcal{T}_m \oplus \mathcal{T}_\ell$, satisfies*

$$|\mathcal{T}_m \oplus \mathcal{T}_\ell| - |\mathcal{T}_\ell| \leq |\mathcal{T}_m| - |\mathcal{T}_0|. \quad \square$$

3 An Adaptive Finite Element Eigenvalue Solver of Asymptotic Quasi-Optimal Computational Complexity

This chapter presents a combined adaptive finite element method with an iterative algebraic eigenvalue solver for a symmetric eigenvalue problem of asymptotic quasi-optimal computational complexity. The analysis is based on a direct approach for eigenvalue problems and allows the use of higher-order conforming finite element spaces with fixed polynomial degree. The asymptotic quasi-optimal adaptive finite element eigenvalue solver (AFEMES) involves a proper termination criterion for the algebraic eigenvalue solver and does not need any coarsening. Numerical evidence illustrates the asymptotic quasi-optimal computational complexity in 2 and 3 dimensions.

This chapter is joint work with C. Carstensen and has been published in [34].

3.1 Introduction

The eigenvalue problems for symmetric second-order elliptic boundary value problems can be discretised with some adaptive finite element method (AFEM). In practice, the resulting finite-dimensional generalised eigenvalue problems are solved iteratively. Thus, the computation involves the discretisation error of some AFEM as well as the error left from the termination of some iterative algebraic eigenvalue solver. This chapter presents the first adaptive finite element eigenvalue solver (AFEMES) of overall asymptotic quasi-optimal complexity, i.e., for sufficiently small mesh-sizes the error is optimal up to a generic multiplicative constant. AFEMES is shown in the pseudocode below.

AFEMES

Input: Coarse triangulation $\mathcal{T}_0$, initial guess $(\tilde\lambda_0, \tilde u_0)$,
parameters $0 < \theta \leq 1$, $0 < \omega$.
$\delta_0 := 2\sqrt{\omega}\eta_0(\tilde\lambda_0, \tilde u_0)$;
for $\ell = 0, 1, \ldots$ (until termination)
  while ($\delta_\ell > \sqrt{\omega}\eta_\ell(\tilde\lambda_\ell, \tilde u_\ell)$)
    $\delta_\ell := \delta_\ell/2$;
    $[\tilde\lambda_\ell, \tilde u_\ell]$:= LAES$(\mathcal{T}_\ell, \tilde\lambda_\ell, \tilde u_\ell, \delta_\ell)$;
  end
  $\mathcal{T}_{\ell+1}$:= Refine$(\mathcal{T}_\ell$,Mark$(\mathcal{T}_\ell, \theta, \eta_\ell(\tilde\lambda_\ell, \tilde u_\ell)))$;
  $\delta_{\ell+1} := 2\sqrt{\omega}\eta_\ell(\tilde\lambda_\ell, \tilde u_\ell)$; $\tilde\lambda_{\ell+1} := \tilde\lambda_\ell$; $\tilde u_{\ell+1} := P_\ell^{\ell+1}\tilde u_\ell$;
end
Output: Sequence of triangulations $\mathcal{T}_\ell$ and approximations $(\tilde\lambda_\ell, \tilde u_\ell)$.

The algorithm computes one fixed simple eigenvalue. The adaptive mesh refinement via subroutines `Mark` and `Refine` is well-established in the finite element community [19, 41, 48, 102] while `LAES` represents any state-of-the-art iterative eigenvalue solver well-established in the numerical linear algebra community that satisfies the convergence and

complexity assumptions of Section 3.2. The parameters θ and ω depend on the regularity of the solution and η_ℓ denotes the error estimator from Section 3.4. The prolongation operator from triangulation $\mathcal{T}_\ell$ onto $\mathcal{T}_{\ell+1}$ is denoted by $P_\ell^{\ell+1}$. The pseudocode gives one possible error balance of the two error sources of asymptotic quasi-optimal complexity.

The works on asymptotic convergence [33, 58, 60, 100] as well as on asymptotic quasi-optimal convergence [45, 57] of adaptive mesh refinement for the eigenvalue problem do assume unrealistically the exact knowledge of algebraic eigenpairs. Another optimality result for linear symmetric operator eigenvalue problems [44] is based on coarsening. Assuming a saturation assumption, [91, 92] present combined adaptive finite element and linear algebra algorithms.

As a simple model problem for a symmetric, elliptic eigenvalue problem consider the eigenvalue problem of the Laplace operator of Section 2.3: Seek a non-trivial eigenpair $(\lambda, u) \in \mathbb{R} \times \{H_0^1(\Omega) \cap H_{loc}^2(\Omega)\}$ such that

$$-\Delta u = \lambda u \quad \text{in } \Omega \qquad \text{and} \qquad u = 0 \quad \text{on } \partial\Omega \tag{3.1}$$

in a bounded Lipschitz domain $\Omega \subset \mathbb{R}^n$, $n = 2, 3$. For simplicity, this chapter restricts to the case that the eigenvalue of interest λ is a simple eigenvalue, hence its algebraic and geometric multiplicity equals one.

Consider the weak formulation of the eigenvalue problem given in Section 2.3 with bilinear forms $a(\cdot,\cdot)$ and $b(\cdot,\cdot)$ that induce the norms $|\!|\!|.|\!|\!| := |.|_{H^1(\Omega)}$ on $V := H_0^1(\Omega)$ and $\|.\| := \|.\|_{L^2(\Omega)}$ on $L^2(\Omega)$.

Let $V_\ell := P_k(\mathcal{T}_\ell) \cap V$ denote the finite-dimensional subspace of fixed order $k > 0$, for the conforming finite element space $P_k(\mathcal{T}_\ell)$ defined in Subsection 2.2.1, and $N_\ell := \dim(V_\ell)$. The corresponding discrete eigenvalue problem reads: Seek a non-trivial eigenpair $(\lambda_\ell, u_\ell) \in \mathbb{R} \times V_\ell$ with $b(u_\ell, u_\ell) = 1$ and

$$a(u_\ell, v_\ell) = \lambda_\ell b(u_\ell, v_\ell) \quad \text{for all } v_\ell \in V_\ell.$$

This chapter proves asymptotic quasi-optimal computational complexity of the proposed AFEMES: Suppose that (λ_ℓ, u_ℓ) is a discrete eigenpair to the continuous eigenpair (λ, u). Let $(\mathcal{T}_\ell)_\ell$ be a sequence of nested regular triangulations. Suppose that the continuous eigenpair (λ, u) belongs to some approximation class $\mathcal{A}_s$, i.e., there exists some $s > 0$ and some $|u|_{\mathcal{A}_s} < \infty$ such that, for any number N there is an (unknown) optimal mesh $\mathcal{T}_N$ with $|\mathcal{T}_N| \leq |\mathcal{T}_0| + N$ element domains and discrete eigenpair (λ_N, u_N) with

$$\sup_{N\in\mathbb{N}} N^{2s} \left(|\!|\!| u - u_N |\!|\!|^2 + |\lambda - \lambda_N| \right) =: |u|_{\mathcal{A}_s}^2 < \infty.$$

Then the computational complexity of the AFEMES is quasi-optimal in the sense that

$$|\!|\!| u - \tilde{u}_\ell |\!|\!|^2 + |\lambda - \tilde{\lambda}_\ell| \leq \mathcal{O}(t_\ell^{-2s}),$$

where t_ℓ denotes the computational costs, i.e., the CPU time. The point is that this quasi-optimal complexity holds for any $u \in \mathcal{A}_s$ and all $s > 0$ despite the fact that

AFEMES does not require any parameter s. The analysis consists of three steps and does not need any inner node property, coarsening or saturation assumption. Since in the present analysis no oscillations occur, it is not necessary to add additional inner points to reduce some oscillations [60]. In [44] a coarsening of the mesh is needed in some steps to maintain optimality. The present analysis relies only on refinement of some mesh and does not need any coarsening. For hierarchical error estimators [91, 92] reliability is equivalent to the saturation assumption, namely a strict error reduction for uniform refined meshes. For the residual estimator used here the reliability is proven directly in Section 3.4. First the asymptotic quasi-optimal convergence for the model problem (3.1) is shown for discrete eigenpairs without using the inner node property: Suppose that (λ_ℓ, u_ℓ) is a discrete eigenpair to the continuous eigenpair (λ, u) in some approximation class $\mathcal{A}_s$ for some $s > 0$. Then (λ_ℓ, u_ℓ) converges quasi-optimal, i.e., optimal up to a positive generic multiplicative constant C with

$$|||u - u_\ell|||^2 + |\lambda - \lambda_\ell| \leq C|u|^2_{\mathcal{A}_s} N_\ell^{-2s}.$$

In contrast to [45] the proofs are based on the eigenvalue formulation and not on a relation to its corresponding source problem. Hence, no additional oscillations arising from the corresponding source problem have to be treated. In a second step this result is extended to the case of inexact algebraic eigenvalue solutions: Suppose (λ, u) with $u \in \mathcal{A}_s$ is an eigenpair and (λ_ℓ, u_ℓ) and $(\lambda_{\ell+1}, u_{\ell+1})$ corresponding discrete eigenpairs on levels ℓ and $\ell + 1$. Let the iterative approximations $(\tilde{\lambda}_\ell, \tilde{u}_\ell)$ on $\mathcal{T}_\ell$ and $(\tilde{\lambda}_{\ell+1}, \tilde{u}_{\ell+1})$ on $\mathcal{T}_{\ell+1}$ satisfy

$$\begin{aligned} |||u_{\ell+1} - \tilde{u}_{\ell+1}|||^2 + |\lambda_{\ell+1} - \tilde{\lambda}_{\ell+1}| &\leq \omega \eta_\ell^2(\tilde{\lambda}_\ell, \tilde{u}_\ell), \\ |||u_\ell - \tilde{u}_\ell|||^2 + |\lambda_\ell - \tilde{\lambda}_\ell| &\leq \omega \eta_\ell^2(\tilde{\lambda}_\ell, \tilde{u}_\ell), \end{aligned}$$

for sufficiently small $\omega > 0$. Then, the iterative solutions $\tilde{\lambda}_\ell$ and $\tilde{u}_\ell$ converge quasi-optimal,

$$|||u - \tilde{u}_\ell|||^2 + |\lambda - \tilde{\lambda}_\ell| \lesssim N_\ell^{-2s}.$$

Finally, it is shown that the AFEMES is of linear runtime $t_\ell \approx N_\ell$ provided the linear algebra eigenvalue solver satisfies some convergence and complexity assumptions of Section 3.2.

The outline of this chapter is as follows. Section 3.2 concerns the basic structure of the standard adaptive finite element method (AFEM) for eigenvalue problems. Section 3.3 presents some algebraic and analytic properties for the model problem (3.1). The discrete reliability of a residual type error estimator is shown in Section 3.4 together with the standard reliability and efficiency. In Section 3.5 a contraction property for the quasi-error up to higher-order terms leads to quasi-optimal convergence of the AFEM under the usual assumption that the mesh-size is sufficiently small and that the algebraic subproblems are solved exactly. Relaxing this last assumption in Section 3.6, the results for quasi-optimal convergence are extended to the case of approximated discrete eigenpairs.

These relaxed results are in Section 3.7 combined with some iterative eigenvalue solver and thus lead to the combined AFEM and iterative algebraic eigenvalue solver AFEMES with asymptotic quasi-optimal computational complexity. The numerical experiments of Section 3.8 show empirical quasi-optimal computational complexity of the AFEMES for some iterative algebraic eigenvalue solvers and higher-order finite element methods in 2 and 3 dimensions.

3.2 Adaptive Finite Element Eigenvalue Solver

The adaptive finite element method computes a sequence of discrete subspaces

$$V_0 \subsetneq V_1 \subsetneq V_2 \subsetneq \ldots \subsetneq V_\ell \subset V$$

using local refinement of the underlying mesh of the domain Ω. The corresponding sequence of meshes $\mathcal{T}_0, \mathcal{T}_1, \mathcal{T}_2, \ldots$ consists of nested regular triangulations. The AFEM consists of the following loop

$$\text{Solve} \to \text{Estimate} \to \text{Mark} \to \text{Refine}.$$

3.2.1 Solve

Given a mesh $\mathcal{T}_\ell$ on level ℓ the step Solve computes the stiffness matrix A_ℓ and the mass matrix B_ℓ and solves the finite-dimensional generalised algebraic eigenvalue problem

$$A_\ell x_\ell = \lambda_\ell B_\ell x_\ell$$

with $N_\ell := \dim(V_\ell)$ and

$$u_\ell = \sum_{k=1}^{N_\ell} x_{\ell,k}\varphi_k, \qquad V_\ell = \operatorname{span}\{\varphi_1, \ldots, \varphi_{N_\ell}\}.$$

Practically, these discrete eigenvalue problems are solved inexactly using iterative algebraic eigenvalue solvers. In this chapter the linear algebraic eigenvalue solver (LAES), used as a 'black box' iterative solver in the quasi-optimal algorithm AFEMES, is assumed to be any iterative eigenvalue solver of quasi-optimal computational complexity in the sense that for any given tolerance $\varepsilon > 0$, the LAES computes some approximation $(\tilde{\lambda}_{\ell,m}, \tilde{u}_{\ell,m})$ of the generalised algebraic eigenvalue problem from a close enough initial guess $(\tilde{\lambda}_{\ell,0}, \tilde{u}_{\ell,0})$ such that

$$|||u_\ell - \tilde{u}_{\ell,m}|||^2 + |\lambda_\ell - \tilde{\lambda}_{\ell,m}| \leq \varepsilon^2$$

in at most, up to a generic multiplicative constant,

$$\max\left\{1, \log(\varepsilon^{-1}|||u_\ell - \tilde{u}_{\ell,0}|||)\right\} \times N_\ell$$

arithmetic operations. That is, each iteration of the solver requires at most $\mathcal{O}(N_\ell)$ operations and the convergence depends only on $\tilde{u}_{\ell,0}$ and not on N_ℓ.

The eigenvalue error of the preconditioned inverse iteration converges independently of H_ℓ for preconditioners that are spectrally equivalent to A_ℓ [78, Theorem 5]. The complexity depends on the sparsity of the preconditioner. The geometric multigrid V-cycle is known to converge independently of H_ℓ and the number of levels ℓ for a fixed number of smoothing steps for Richardson [25] or Jacobi smoothers [26]. The preconditioned inverse iteration (PINVIT) and the locally optimal block preconditioned conjugate gradient (LOBPCG) algorithms with the V-cycle geometric multigrid preconditioner have been shown numerically to be of quasi-optimal computational complexity for uniform meshes [77]. Since in this chapter the mesh is refined adaptively, global smoothing might be inefficient and local smoothing needs to be applied. However, the numerical examples of Section 3.8 show that empirically global smoothing is efficient for those examples. The numerical examples of Subsection 3.8 compare the V-cycle geometric multigrid preconditioned PINVIT and LOBPCG algorithms with a standard solve of the Arnoldi method as implemented in ARPACK [83] where the linear systems are solved using a LU factorisation. The stopping criteria for PINVIT [92] and LOBPCG [77] are based on the scalar product of the algebraic residual and the preconditioned algebraic residual.

3.2.2 Estimate

The error in the eigenfunction or eigenvalue of interest is estimated based on the solution (λ_ℓ, u_ℓ) of the underlying algebraic eigenvalue problem

$$\eta_\ell^2(\lambda_\ell, u_\ell) := \sum_{T\in\mathcal{T}_\ell} \eta_\ell(\lambda_\ell, u_\ell; T)^2 + \sum_{E\in\mathcal{E}_\ell} \eta_\ell(\lambda_\ell, u_\ell; E)^2.$$

3.2.3 Mark

Based on the refinement indicators, edges and elements are marked for refinement in a bulk criterion [48] such that $\mathcal{M}_\ell \subseteq \mathcal{T}_\ell \cup \mathcal{E}_\ell$ is an (almost) minimal set of marked edges with

$$\begin{aligned} \theta\eta_\ell^2(\lambda_\ell, u_\ell) &\leq \eta_\ell^2(\lambda_\ell, u_\ell; \mathcal{M}_\ell), \\ \eta_\ell^2(\lambda_\ell, u_\ell; \mathcal{M}_\ell) &:= \sum_{T\in\mathcal{M}_\ell\cap\mathcal{T}_\ell} \eta_\ell^2(\lambda_\ell, u_\ell; T) + \sum_{E\in\mathcal{M}_\ell\cap\mathcal{E}_\ell} \eta_\ell^2(\lambda_\ell, u_\ell; E) \end{aligned}$$

for a bulk parameter $0 < \theta \leq 1$. This is done in a greedy algorithm which marks edges and elements with larger contributions. In [102] a quasi-optimal algorithm of complexity $\mathcal{O}(|\mathcal{T}_\ell \cup \mathcal{E}_\ell|)$ is proposed, where $|\mathcal{T}_\ell \cup \mathcal{E}_\ell|$ denotes the cardinality of all edges in $\mathcal{E}_\ell$ and all elements in $\mathcal{T}_\ell$. Since sorting the refinement indicators in $\mathcal{O}(|\mathcal{T}_\ell \cup \mathcal{E}_\ell| \log|\mathcal{T}_\ell \cup \mathcal{E}_\ell|)$ does not dominate the overall computational costs in practise, this simple approach is used in the numerical examples of Section 3.8.

3.2.4 Refine

In this step of the AFEM loop, the mesh is refined locally corresponding to the set $\mathcal{M}_\ell$ of marked edges and elements. The mesh is refined by the closure algorithm of Section 2.5.1 and the newest-vertex refinement algorithm of Section 2.5.3.

3.3 Algebraic Properties

This section summarises some known and some new algebraic properties of the model problem (3.1), such as the relation between the eigenvalue error and the error with respect to the norms $|||.|||$ and $\|.\|$ [105]

$$|||u - u_\ell|||^2 = \lambda\|u - u_\ell\|^2 + \lambda_\ell - \lambda. \tag{3.2}$$

Throughout this section suppose that $(\lambda_\ell, u_\ell) \in \mathbb{R} \times V_\ell$ and $(\lambda_{\ell+m}, u_{\ell+m}) \in \mathbb{R} \times V_{\ell+m}$ are discrete eigenpairs to the continuous eigenpair $(\lambda, u) \in \mathbb{R} \times V$ on the levels ℓ and $\ell + m$.

Lemma 3.3.1 (Quasi-orthogonality)**.** *Let $\mathcal{T}_{\ell+m}$ be a refinement of the triangulation $\mathcal{T}_\ell$ for some level ℓ such that $V_\ell \subset V_{\ell+m}$. Then, for $e_\ell := u - u_\ell$ and $e_{\ell+m} := u - u_{\ell+m}$, the quasi-orthogonality holds, i.e.*

$$|||u_{\ell+m} - u_\ell|||^2 = |||e_\ell|||^2 - |||e_{\ell+m}|||^2 - \lambda\|e_\ell\|^2 + \lambda\|e_{\ell+m}\|^2 + \lambda_{\ell+m}\|u_{\ell+m} - u_\ell\|^2.$$

Proof. Since $\mathcal{T}_{\ell+m}$ is a refinement of $\mathcal{T}_\ell$, (3.2) implies

$$|||u_{\ell+m} - u_\ell|||^2 = \lambda_{\ell+m}\|u_{\ell+m} - u_\ell\|^2 + \lambda_\ell - \lambda_{\ell+m}.$$

Hence,

$$\begin{aligned} |||u_{\ell+m} - u_\ell|||^2 &= \lambda_{\ell+m}\|u_{\ell+m} - u_\ell\|^2 + \lambda_\ell - \lambda - (\lambda_{\ell+m} - \lambda) \\ &= |||e_\ell|||^2 - |||e_{\ell+m}|||^2 - \lambda\|e_\ell\|^2 + \lambda\|e_{\ell+m}\|^2 + \lambda_{\ell+m}\|u_{\ell+m} - u_\ell\|^2. \end{aligned}$$ □

Let the residual $\mathrm{Res}_\ell \in V^*$ be defined by

$$\mathrm{Res}_\ell(v) := \lambda_\ell b(u_\ell, v) - a(u_\ell, v) \quad \text{for all } v \in V.$$

Notice that $V_\ell \subset \ker(\mathrm{Res}_\ell)$.

Lemma 3.3.2. *Let $\mathcal{T}_{\ell+m}$ be a refinement of $\mathcal{T}_\ell$ such that $V_\ell \subset V_{\ell+m} \subseteq V$. Then it holds that*

$$|||u_{\ell+m} - u_\ell||| \leq |||Res_\ell|||_{V^*_{\ell+m}} + \frac{(\lambda_{\ell+m} + \lambda_\ell)}{2}\frac{\|u_{\ell+m} - u_\ell\|^2}{|||u_{\ell+m} - u_\ell|||}.$$

Proof. Elementary algebraic manipulations, together with the assumption that $V_\ell \subset$

$V_{\ell+m}$, show

$$\begin{aligned}\|\!|u_{\ell+m}-u_\ell|\!\|^2 &= \lambda_\ell b(u_\ell, u_{\ell+m}-u_\ell) - a(u_\ell, u_{\ell+m}-u_\ell)\\ &\qquad + a(u_{\ell+m}, u_{\ell+m}-u_\ell) - \lambda_\ell b(u_\ell, u_{\ell+m}-u_\ell)\\ &= \mathrm{Res}_\ell(u_{\ell+m}-u_\ell) + (\lambda_{\ell+m}+\lambda_\ell)(1-b(u_{\ell+m},u_\ell))\\ &\le \|\!|\mathrm{Res}_\ell|\!\|_{V_{\ell+m}^*}\|\!|u_{\ell+m}-u_\ell|\!\| + \frac{(\lambda_{\ell+m}+\lambda_\ell)}{2}\|u_{\ell+m}-u_\ell\|^2. \qquad \square\end{aligned}$$

The remaining part of this section is devoted to show that the second term on the right hand side in Lemma 3.3.2 is of higher-order, namely

$$\|u_{\ell+m}-u_\ell\| \lesssim H_\ell^r \|\!|u_{\ell+m}-u_\ell|\!\|.$$

Here and throughout this chapter, $H_\ell := \max_{T\in\mathcal{T}_\ell}\mathrm{diam}(T)$ is the maximal mesh-size and $0<r\le 1$ depends on the regularity of the solution of the corresponding boundary value problem. The first part follows the argumentation as in [105] for the case $u_{\ell+m}\equiv u$. The second part exploits regularity of the corresponding boundary value problem together with the Aubin-Nitsche technique. Let $G_\ell : V\to V_\ell$ denote the Galerkin projection onto V_ℓ such that for any $v\in V$ it holds that

$$a(v-G_\ell v, v_\ell) = 0 \quad \text{for all } v_\ell\in V_\ell.$$

Suppose the i-th eigenvalue $\lambda=\lambda_{\infty,i}$ is simple. Let the initial mesh-size H_0 be sufficiently small such that there exist two separation bounds M and $M_{\ell+m}$, independent of H_ℓ, which satisfy for the index set $I_\ell := \{1,\dots,i-1,i+1,\dots,\dim(V_\ell)\}$

$$0<M := \sup_{\ell\in\mathbb{N}_0}\max_{j\in I_\ell}\frac{\lambda_{\infty,i}}{|\lambda_{\ell,j}-\lambda_{\infty,i}|}<\infty \;\text{ and }\; 0<M_{\ell+m}:=\max_{j\in I_\ell}\frac{\lambda_{\ell+m,i}}{|\lambda_{\ell,j}-\lambda_{\ell+m,i}|}<\infty.$$

Lemma 3.3.3. *Let $\mathcal{T}_{\ell+m}$ be a refinement of $\mathcal{T}_\ell$ such that $V_\ell\subset V_{\ell+m}\subseteq V$, then for the Galerkin projection $G_\ell : V\to V_\ell$ it holds that*

$$\begin{aligned}\|u_{\ell+m}-u_\ell\| &\le 2(1+M_{\ell+m})\|u_{\ell+m}-G_\ell u_{\ell+m}\|,\\ \|u-u_\ell\| &\le 2(1+M)\|u-G_\ell u\|.\end{aligned}$$

Proof. Note that for the Galerkin projection it holds that

$$(\lambda_{\ell,j}-\lambda_{\ell+m,i})b(G_\ell u_{\ell+m,i}, u_{\ell,j}) = \lambda_{\ell+m,i}b(u_{\ell+m,i}-G_\ell u_{\ell+m,i}, u_{\ell,j}).$$

Since $u_{\ell,1},\dots,u_{\ell,N_\ell}$, for $N_\ell=\dim(V_\ell)$, forms an orthogonal basis for V_ℓ, the Galerkin projection of $u_{\ell+m,i}$ can be written as

$$G_\ell u_{\ell+m,i} = \sum_{j=1}^{N_\ell} b(G_\ell u_{\ell+m,i}, u_{\ell,j})u_{\ell,j}.$$

Let $\gamma := b(G_\ell u_{\ell+m,i}, u_{\ell,i})$ be the coefficient for $j = i$ in the previous formula. The orthogonality of the discrete eigenfunctions $u_{\ell,1}, \dots, u_{\ell,N_\ell}$ yield

$$\begin{aligned}
\|G_\ell u_{\ell+m,i} - \gamma u_{\ell,i}\|^2 &= \sum_{\substack{j=1\\ j\neq i}}^{N_\ell} b(G_\ell u_{\ell+m,i}, u_{\ell,j})^2 \\
&= \sum_{\substack{j=1\\ j\neq i}}^{N_\ell} \left(\frac{\lambda_{\ell+m,i}}{|\lambda_{\ell,j} - \lambda_{\ell+m,i}|}\right)^2 b(u_{\ell+m,i} - G_\ell u_{\ell+m,i}, u_{\ell,j})^2 \\
&\leq M_{\ell+m}^2 \sum_{\substack{j=1\\ j\neq i}}^{N_\ell} b(u_{\ell+m,i} - G_\ell u_{\ell+m,i}, u_{\ell,j})^2 \\
&\leq M_{\ell+m}^2 \|u_{\ell+m,i} - G_\ell u_{\ell+m,i}\|^2.
\end{aligned}$$

The triangle inequality shows that

$$\|u_{\ell+m,i}\| - \|u_{\ell+m,i} - \gamma u_{\ell,i}\| \leq \|\gamma u_{\ell,i}\| \leq \|u_{\ell+m,i}\| + \|u_{\ell+m,i} - \gamma u_{\ell,i}\|.$$

Since the eigenfunctions are normalized to one this implies

$$|\gamma - 1| \leq \|u_{\ell+m,i} - \gamma u_{\ell,i}\|.$$

Hence,

$$\|u_{\ell+m,i} - u_{\ell,i}\| \leq \|u_{\ell+m,i} - \gamma u_{\ell,i}\| + \|(\gamma - 1)u_{\ell,i}\| \leq 2\|u_{\ell+m,i} - \gamma u_{\ell,i}\|.$$

Thus,

$$\begin{aligned}
\|u_{\ell+m,i} - u_{\ell,i}\| &\leq 2\|u_{\ell+m,i} - G_\ell u_{\ell+m,i}\| + 2\|G_\ell u_{\ell+m,i} - \gamma u_{\ell,i}\| \\
&\leq 2(1 + M_{\ell+m})\|u_{\ell+m,i} - G_\ell u_{\ell+m,i}\|.
\end{aligned}$$

The second inequality follows analogously since $V_\ell \subset V$. □

Lemma 3.3.4. *Let $\mathcal{T}_{\ell+m}$ be a refinement of $\mathcal{T}_\ell$ such that $V_\ell \subset V_{\ell+m} \subseteq V$. Suppose that the solution of the corresponding boundary value problem to* (3.1)*, seek $z \in V$ such that*

$$a(z, v) = \int_\Omega f v \, dx \quad \text{for all } v \in V,$$

is H^{1+r}-regular for all $f \in L^2(\Omega)$ and some $0 < r \leq 1$, i.e., $z \in H^{1+r}(\Omega) \cap V$ and $\|z\|_{H^{1+r}(\Omega)} \leq C_{reg}\|f\|_{L^2(\Omega)}$. Then it holds that

$$\begin{aligned}
\|u_{\ell+m} - G_\ell u_{\ell+m}\| &\leq C_{apx} C_{reg} H_\ell^r |\!|\!| u_{\ell+m} - u_\ell |\!|\!|, \\
\|u - G_\ell u\| &\leq C_{apx} C_{reg} H_\ell^r |\!|\!| u - u_\ell |\!|\!|.
\end{aligned}$$

Proof. The following convergence estimate holds for the Galerkin projection $G_\ell z \in V_\ell$

of $z \in V$

$$\|z - G_\ell z\|_{H^1(\Omega)} \leq C_{\mathrm{apx}} H_\ell^r \|z\|_{H^{1+r}(\Omega)}$$

for some $0 < r \leq 1$ [27, Theorem 14.3.3]. The Aubin-Nitzsche duality technique for the dual boundary value problem, seek $z \in V$ such that

$$a(z, v) = b(u_{\ell+m} - G_\ell u_{\ell+m}, v) \quad \text{for all } v \in V,$$

and the regularity assumption $z \in H^{1+r}(\Omega) \cap V$,

$$\|z\|_{H^{1+r}(\Omega)} \leq C_{reg} \|u_{\ell+m} - G_\ell u_{\ell+m}\|,$$

lead to

$$\begin{aligned} \|u_{\ell+m} - G_\ell u_{\ell+m}\| &\leq C_{\mathrm{apx}} C_{\mathrm{reg}} H_\ell^r \|\!| u_{\ell+m} - G_\ell u_{\ell+m} |\!\| \\ &\leq C_{\mathrm{apx}} C_{\mathrm{reg}} H_\ell^r \|\!| u_{\ell+m} - u_\ell |\!\|. \end{aligned}$$

The second inequality follows from formally taking $m \to \infty$. □

Lemma 3.3.5. *Let $\mathcal{T}_{\ell+m}$ be a refinement of $\mathcal{T}_\ell$ such that $V_\ell \subset V_{\ell+m} \subseteq V$. For sufficiently small initial mesh-size H_0 there exists a constant $C_0 > 0$ depending only on $\mathcal{T}_0$ such that $1 \leq \kappa(H_\ell) < C_0$ with*

$$\|\!| u_{\ell+m} - u_\ell |\!\| \leq \kappa(H_\ell) \|\!| Res_\ell |\!\|_{V_{\ell+m}^*}, \qquad \|\!| u - u_\ell |\!\| \leq \kappa(H_\ell) \|\!| Res_\ell |\!\|_{V^*}$$

and $\lim_{H_\ell \to 0} \kappa(H_\ell) = 1$.

Proof. Suppose that H_ℓ is sufficiently small such that

$$\delta_\ell := 2C_{\mathrm{apx}}^2 C_{\mathrm{reg}}^2 (\lambda_{\ell+m} + \lambda_\ell)(1 + \max\{M, M_{\ell+m}\})^2 H_\ell^{2r} \ll 1.$$

Then Lemma 3.3.2, Lemma 3.3.3 together with Lemma 3.3.4 lead to

$$\|\!| u_{\ell+m} - u_\ell |\!\| \leq (1 - \delta_\ell)^{-1} \|\!| \mathrm{Res}_\ell |\!\|_{V_{\ell+m}^*} \quad \text{and} \quad \|\!| u - u_\ell |\!\| \leq (1 - \delta_\ell)^{-1} \|\!| \mathrm{Res}_\ell |\!\|_{V^*}.$$

Notice that $\kappa(H_\ell) := (1 - \delta_\ell)^{-1} \to 1$ as the maximal mesh-size tends to zero and $C_0 := (1 - \delta_0)^{-1}$. □

3.4 A Posteriori Error Estimator

This section establishes the discrete reliability and recalls the reliability and efficiency of the standard residual-based error estimator [45, 50, 58, 60]. Let $p_\ell := \nabla u_\ell$ denote the discrete gradient and $\mathcal{E}_\ell$ the set of inner edges ($n = 2$) or inner faces ($n = 3$) of $\mathcal{T}_\ell$. For $E \in \mathcal{E}_\ell$ let $T_+, T_- \in \mathcal{T}_\ell$ be the two neighbouring triangles such that $E = T_+ \cap T_-$. The jump of the discrete gradient p_ℓ along an inner edge $E \in \mathcal{E}_\ell$ in normal direction ν_E,

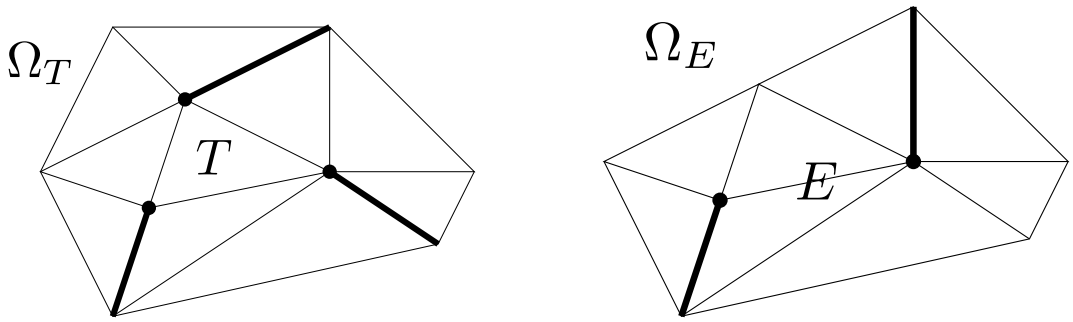

Figure 3.1: Patches for the Scott-Zhang interpolation operator.

pointing from T_+ to T_-, is defined by $[p_\ell] \cdot \nu_E := \left(p_\ell|_{T_+} - p_\ell|_{T_-}\right) \cdot \nu_E$. Then the residual error estimator is defined by

$$\eta_\ell^2(\lambda_\ell, u_\ell) := \sum_{T \in \mathcal{T}_\ell} \eta_\ell(\lambda_\ell, u_\ell; T)^2 + \sum_{E \in \mathcal{E}_\ell} \eta_\ell(\lambda_\ell, u_\ell; E)^2$$

with $n = 2, 3$ and

$$\eta_\ell(\lambda_\ell, u_\ell; T)^2 := |T|^{2/n} \|\lambda_\ell u_\ell + \operatorname{div}(p_\ell)\|_{L^2(T)}^2,$$
$$\eta_\ell(\lambda_\ell, u_\ell; E)^2 := |E|^{1/(n-1)} \|[p_\ell] \cdot \nu_E\|_{L^2(E)}^2.$$

Note that the Scott-Zhang quasi-interpolation operator $J : V \to V_\ell$ [101] is a projection $J(v_\ell) = v_\ell$ for all $v_\ell \in V_\ell$. In addition, it is locally a L^2-projection onto $(n-1)$-dimensional edges or faces. Therefore, each node is assigned any edge or face which contains it. Edge-basis functions are interpolated on their edge and element-basis functions are interpolated over the interior of their element. The element and edge patches Ω_T and Ω_E are displayed in Figure 3.1. In the following, the Scott-Zhang quasi-interpolation operator is restricted to $V_{\ell+m}$ for a refined triangulation $\mathcal{T}_{\ell+m}$ of $\mathcal{T}_\ell$. If it is possible, each nodal-basis function is assigned an edge of the boundary or an edge which is not refined. Thus, the homogeneous boundary values are preserved. Let v_ℓ denote the Scott-Zhang interpolant of $v_{\ell+m}$ in V_ℓ. Then for all elements $T \in \mathcal{T}_\ell$ and all edges $E \in \mathcal{E}_\ell$ that are not refined, $v_{\ell+m}|_T = v_\ell|_T$ and $v_{\ell+m}|_E = v_\ell|_E$ holds. The finite overlap of all the patches Ω_T and Ω_E implies the approximation property [101]

$$\sum_{T \in \mathcal{T}_\ell} |T|^{-1/n} \|v_{\ell+m} - v_\ell\|_{L^2(T)} + \sum_{E \in \mathcal{E}_\ell} |E|^{-1/(2n-2)} \|v_{\ell+m} - v_\ell\|_{L^2(E)} \lesssim |\!|\!| v_{\ell+m} |\!|\!|.$$

Lemma 3.4.1 (Discrete Reliability)**.** *For sufficiently small H_0 let (λ_ℓ, u_ℓ) be a discrete eigenpair on level ℓ and $\mathcal{M}_\ell \subseteq \mathcal{T}_\ell \cup \mathcal{E}_\ell$ be any set of edges and elements. Suppose that the refinement algorithm of Section 3.2 computes the refined mesh $\mathcal{T}_{\ell+m}$. Then it holds that*

$$|\!|\!| Res_\ell |\!|\!|_{V_{\ell+m}^*} \lesssim \eta_\ell(\lambda_\ell, u_\ell; \mathcal{M}_\ell).$$

Proof. Let v_ℓ denote the Scott-Zhang interpolant of $v_{\ell+m} \in V_{\ell+m}$ in V_ℓ. For all common elements $T \in \mathcal{T}_\ell \cap \mathcal{T}_{\ell+m}$ and all common edges $E \in \mathcal{E}_\ell \cap \mathcal{E}_{\ell+m}$ it holds that $v_\ell|_T = v_{\ell+m}|_T$ and $v_\ell|_E = v_{\ell+m}|_E$. Hence,

$$\begin{aligned}\mathrm{Res}_\ell(v_{\ell+m}) &= \mathrm{Res}_\ell(v_{\ell+m} - v_\ell) = \lambda_\ell b(u_\ell, v_{\ell+m} - v_\ell) - a(u_\ell, v_{\ell+m} - v_\ell)\\ &\lesssim \sum_{T\in\mathcal{T}_\ell\setminus\mathcal{T}_{\ell+m}} |T|^{1/n}\|\lambda_\ell u_\ell + \mathrm{div}(p_\ell)\|_{L^2(T)}\||T|^{-1/n}(v_{\ell+m} - v_\ell)\|_{L^2(T)}\\ &\quad + \sum_{E\in\mathcal{E}_\ell\setminus\mathcal{E}_{\ell+m}} |E|^{1/(2n-2)}\|[p_\ell]\cdot\nu_E\|_{L^2(E)}\||E|^{-1/(2n-2)}(v_{\ell+m} - v_\ell)\|_{L^2(E)}\\ &\lesssim \eta_\ell(\lambda_\ell, u_\ell; \mathcal{M}_\ell)|\!|\!|v_{\ell+m}|\!|\!|.\end{aligned}$$

□

Lemma 3.4.2. *For sufficiently small H_0 it holds that*

$$|\!|\!|\mathrm{Res}_\ell|\!|\!|_{V^*} \lesssim \eta_\ell(\lambda_\ell, u_\ell) \lesssim |\!|\!|e_\ell|\!|\!|.$$

Proof. The first inequality can be proved as Lemma 3.4.1. For the second inequality, Durán et al. [50] showed the local lower bound for piecewise linear finite element functions using the bubble-function technique. In the case of higher-order finite elements the arguments of the proof remain the same as in the linear case except that $\mathrm{div}(p_\ell)$ can be non-zero. Thus the local discrete inverse inequality $|\omega_E|^{1/n}\|\mathrm{div}(p_\ell)\|_{L^2(\omega_E)} \lesssim \|\nabla e_\ell\|_{L^2(\omega_E)}$ has to be applied additionally. Therefore, the local lower bound

$$\begin{aligned}|\omega_E|^{1/n}\|\lambda_\ell u_\ell + \mathrm{div}(p_\ell)\|_{L^2(\omega_E)} + |E|^{1/(2n-2)}\|[p_\ell]\cdot\nu_E\|_{L^2(E)}&\\ \lesssim \|\nabla e_\ell\|_{L^2(\omega_E)} + |\omega_E|^{1/n}\|\lambda u - \lambda_\ell u_\ell\|_{L^2(\omega_E)}&\end{aligned}$$

holds for the edge patch $\omega_E := T_+ \cup T_-$, for $T_\pm \in \mathcal{T}_\ell$ with $E = T_+ \cap T_-$. The global version reads

$$\eta_\ell^2(\lambda_\ell, u_\ell) \lesssim |\!|\!|e_\ell|\!|\!|^2 + H_\ell^2\|\lambda u - \lambda_\ell u_\ell\|^2.$$

As shown in [33], some elementary algebra in the spirit of Lemma 3.3.1 shows that

$$\|\lambda u - \lambda_\ell u_\ell\|^2 = (\lambda_\ell - \lambda)^2 + \lambda\lambda_\ell\|e_\ell\|^2.$$

Equation (3.2) yields $(\lambda_\ell - \lambda)^2 \le |\!|\!|e_\ell|\!|\!|^4$ and $\lambda\lambda_\ell\|e_\ell\|^2 \le \lambda_\ell|\!|\!|e_\ell|\!|\!|^2$. Since λ_ℓ is bounded by λ_0 it follows that

$$\eta_\ell(\lambda_\ell, u_\ell) \lesssim |\!|\!|e_\ell|\!|\!|$$

even for large mesh-sizes $H_\ell \lesssim 1$. □

Remark 3.4.3. Lemma 3.3.5, Lemma 3.4.1 and Lemma 3.4.2 show that for sufficiently small H_ℓ there exist two constants $0 < C_{\mathrm{rel}}$ and $0 < C_{\mathrm{eff}}$ such that

$$\eta_\ell(\lambda_\ell, u_\ell)/C_{\mathrm{eff}} \le |\!|\!|e_\ell|\!|\!| \le C_{\mathrm{rel}}\eta_\ell(\lambda_\ell, u_\ell) \quad\text{and}\quad |\!|\!|u_{\ell+m} - u_\ell|\!|\!| \le C_{\mathrm{rel}}\eta_\ell(\lambda_\ell, u_\ell; \mathcal{M}_\ell).$$

Similar results as in Lemma 3.4.1 and 3.4.2 for general bilinear forms $a(\cdot,\cdot)$ with jumping coefficients include additional terms that represent data oscillations, cf. [1, 58, 108].

3.5 Quasi-Optimal Convergence

This section is devoted to the asymptotic quasi-optimal convergence analysis of the adaptive eigenvalue computation based on exact solutions of the algebraic eigenvalue problems. At first the approximation class $\mathcal{A}_s$ is defined and its properties are described. Lemma 3.5.2 shows an estimator reduction which is used in the proof of the contraction property in Lemma 3.5.3. The contraction property and the bulk criterion are key arguments in the proof of the quasi-optimality in Theorem 3.5.4.

Definition 3.5.1 (Approximation class)**.** *For an initial triangulation $\mathcal{T}_0$ and for $s > 0$ let the approximation class be defined by*

$$\mathcal{A}_s := \left\{ v \in V : |v|_{\mathcal{A}_s} := \sup_{\varepsilon>0} \varepsilon \inf_{\mathcal{T}_\varepsilon : |\!|\!| v - v_\varepsilon |\!|\!| \le \varepsilon} (|\mathcal{T}_\varepsilon| - |\mathcal{T}_0|)^s < \infty \right\}.$$

The infimum is taken over all refinements $\mathcal{T}_\varepsilon$ of $\mathcal{T}_0$ computed by the refinement algorithm of Section 3.2 with $|\!|\!| v - v_\varepsilon |\!|\!| \le \varepsilon$ and $v_\varepsilon \in V_\varepsilon$.

Notice that $\mathcal{A}_s$ contains all functions that can be approximated within pre-described tolerance $\varepsilon > 0$ in a finite element space V_ε, $|\!|\!| v - v_\varepsilon |\!|\!| \le \varepsilon$ for some $v_\varepsilon \in V_\varepsilon$, based on the triangulation $\mathcal{T}_\varepsilon$ with $|\mathcal{T}_\varepsilon| - |\mathcal{T}_0| \le \varepsilon^{-1/s} |v|_{\mathcal{A}_s}^{1/s}$. For uniform refinement classical a priori estimates show that for $0 < r \le 1$, $H^{1+r}(\Omega) \cap V \subset \mathcal{A}_{r/n}$, but the class contains much more functions which motivates the use of adaptivity. Due to [102] an equivalent formulation, similar to that of [41], reads

$$\mathcal{A}_s := \left\{ v \in V : \sup_{N\in\mathbb{N}} N^s \inf_{\mathcal{T}_\varepsilon : |\mathcal{T}_\varepsilon| - |\mathcal{T}_0| \le N} |\!|\!| v - v_\varepsilon |\!|\!| < \infty \right\}.$$

In the following the marking strategy of Section 3.2 is a key argument in the proofs.

Lemma 3.5.2. *Let (λ_ℓ, u_ℓ) and $(\lambda_{\ell+1}, u_{\ell+1})$ be discrete eigenpairs on the levels ℓ and $\ell+1$ to the continuous eigenpair (λ, u), then there exists some $\Lambda > 0$, such that, for all levels $\ell \ge 0$ and $0 < \theta \le 1$, it holds that*

$$\eta_{\ell+1}(\lambda_{\ell+1}, u_{\ell+1}) \le \sqrt{(1 - \theta(1 - 2^{-2/n}))}\, \eta_\ell(\lambda_\ell, u_\ell) + \Lambda |\!|\!| u_{\ell+1} - u_\ell |\!|\!|.$$

Proof. As in the proof of [33, Lemma 5.1], Young's inequality [52], some discrete inverse inequalities and the bulk criterion of Section 3.2 lead to

$$\eta_{\ell+1}^2(\lambda_{\ell+1}, u_{\ell+1}) \le (1+\delta)(1 - \theta(1 - 2^{-2/n}))\eta_\ell^2(\lambda_\ell, u_\ell) + \Lambda^2(1 + 1/\delta) |\!|\!| u_{\ell+1} - u_\ell |\!|\!|^2$$

for any $0 < \delta$ from Young's inequality, $0 < \theta \leq 1$ bulk parameter and $0 < \Lambda$ from application of various discrete inverse inequalities. Thereby, the factor $2^{-2/n}$ results from at least one bisection of refined elements or edges. The choice

$$\delta = \frac{\Lambda |\!|\!| u_{\ell+1} - u_\ell |\!|\!|}{\sqrt{(1-\theta(1-2^{-2/n}))}\eta_\ell(\lambda_\ell, u_\ell)}$$

proves the assertion. □

Lemma 3.5.3 (Contraction property)**.** *Let (λ_ℓ, u_ℓ) and $(\lambda_{\ell+1}, u_{\ell+1})$ be discrete eigenpairs on the levels ℓ and $\ell+1$ to the same continuous eigenpair (λ, u) and let the mesh-size H_ℓ be sufficiently small, then there exist constants $0 < \varrho < 1$ and $\gamma > 0$, such that, for all $\ell = 0, 1, 2, \ldots$, it holds that*

$$\gamma\eta_{\ell+1}^2(\lambda_{\ell+1}, u_{\ell+1}) + |\!|\!| u - u_{\ell+1} |\!|\!|^2 \leq \varrho \left(\gamma\eta_\ell^2(\lambda_\ell, u_\ell) + |\!|\!| u - u_\ell |\!|\!|^2 \right). \tag{3.3}$$

Proof. Theorem 5.3 of [33] shows for $0 < \rho < 1$ that

$$\gamma\eta_{\ell+1}^2(\lambda_{\ell+1}, u_{\ell+1}) + |\!|\!| e_{\ell+1} |\!|\!|^2 \leq \rho \left(\gamma\eta_\ell^2(\lambda_\ell, u_\ell) + |\!|\!| e_\ell |\!|\!|^2 \right) + 3\lambda_{\ell+1}\|e_{\ell+1}\|^2 + 3\lambda_\ell\|e_\ell\|^2.$$

Lemma 3.3.3 and 3.3.4 show

$$\|u - u_\ell\|^2 \leq \sigma(H_\ell)^2 |\!|\!| u - u_\ell |\!|\!|^2, \tag{3.4}$$

where $\sigma(H_\ell) := 2(1+M)C_{\text{apx}}C_{\text{reg}}H_\ell^r$.
Hence, for sufficiently small mesh-size H_0, (3.3) follows with the constant

$$0 < \varrho := \frac{\rho + 3\lambda_0\sigma(H_\ell)^2}{1 - 3\lambda_0\sigma(H_\ell)^2} < 1.$$ □

Theorem 3.5.4. *Suppose that (λ_ℓ, u_ℓ) is a discrete eigenpair to the continuous eigenpair (λ, u) with $u \in \mathcal{A}_s$ and that the initial mesh-size H_0 is sufficiently small. Then λ_ℓ and u_ℓ from the AFEM converge quasi-optimal in the sense that*

$$|\!|\!| e_\ell |\!|\!|^2 + |\lambda - \lambda_\ell| \lesssim (|\mathcal{T}_\ell| - |\mathcal{T}_0|)^{-2s} \lesssim N_\ell^{-2s}.$$

Proof. First it is shown that for a set $\mathcal{M}_\ell$ of marked edges and elements from the marking strategy of Section 3.2, based on the bulk criterion, $\eta_\ell(\lambda_\ell, u_\ell)$ and a bulk parameter $\theta > 0$, it holds that

$$|\mathcal{M}_\ell| \lesssim |\!|\!| e_\ell |\!|\!|^{-1/s} |u|_{\mathcal{A}_s}^{1/s}.$$

Note that it is sufficient that $\mathcal{M}_\ell$ is a set with almost minimal cardinality, i.e. minimal cardinality up to a uniform multiplicative constant which is independent of the level ℓ,

that fulfils the bulk criterion. Suppose $\mathcal{T}_{\ell+\varepsilon}$ is any refinement of $\mathcal{T}_\ell$ such that

$$|||e_{\ell+\varepsilon}||| \leq \rho |||e_\ell|||$$

for some $0 < \rho < 1$. Suppose that H_ℓ and θ are sufficiently small, such that

$$0 < \theta \leq \frac{(1-\rho^2)}{C_{\mathrm{rel}}^2 C_{\mathrm{eff}}^2} - \lambda\sigma(H_\ell)^2,$$

where $\sigma(H_\ell)$ from Lemma 3.5.3 tends to zero as $H_\ell \to 0$. Using the efficiency estimates of Remark 3.4.3 together with the quasi-orthogonality of Lemma 3.3.1 yields

$$\begin{aligned}(1-\rho^2)\eta_\ell^2(\lambda_\ell, u_\ell)/C_{\mathrm{eff}}^2 &\leq (1-\rho^2)|||e_\ell|||^2 \leq |||e_\ell|||^2 - |||e_{\ell+\varepsilon}|||^2 \\ &= |||u_{\ell+\varepsilon} - u_\ell|||^2 + \lambda\|e_\ell\|^2 - \lambda\|e_{\ell+\varepsilon}\|^2 - \lambda_{\ell+\varepsilon}\|u_{\ell+\varepsilon} - u_\ell\|^2.\end{aligned}$$

Let $\mathcal{M}_\varepsilon := (\mathcal{T}_\ell \backslash \mathcal{T}_{\ell+\varepsilon}) \cup (\mathcal{E}_\ell \backslash \mathcal{E}_{\ell+\varepsilon})$, then the reliability of Remark 3.4.3 and (3.4) yield

$$\begin{aligned}(1-\rho^2)\eta_\ell^2(\lambda_\ell, u_\ell)/C_{\mathrm{eff}}^2 &\leq C_{\mathrm{rel}}^2\eta_\ell^2(\lambda_\ell, u_\ell; \mathcal{M}_\varepsilon) + \lambda\|e_\ell\|^2 \\ &\leq C_{\mathrm{rel}}^2\eta_\ell^2(\lambda_\ell, u_\ell; \mathcal{M}_\varepsilon) + \lambda\sigma(H_\ell)^2 C_{\mathrm{rel}}^2\eta_\ell^2(\lambda_\ell, u_\ell).\end{aligned}$$

Therefore $\mathcal{M}_\varepsilon$ satisfies the bulk criterion. Since $\mathcal{M}_\ell$ is the set with almost minimal cardinality that fulfils the bulk criterion, it holds that

$$|\mathcal{M}_\ell| \lesssim |\mathcal{M}_\varepsilon| \lesssim |\mathcal{T}_{\ell+\varepsilon}| - |\mathcal{T}_\ell|.$$

Let $\mathcal{T}_\varepsilon$ be an optimal mesh with smallest cardinality such that

$$|||e_\varepsilon||| \leq \rho |||e_\ell|||.$$

The definition of the approximation space $\mathcal{A}_s$ shows that

$$|\mathcal{T}_\varepsilon| - |\mathcal{T}_0| \leq \rho^{-1/s}|||e_\ell|||^{-1/s}|u|_{\mathcal{A}_s}^{1/s}.$$

Let $\mathcal{T}_{\ell+\varepsilon}$ be the smallest common refinement of $\mathcal{T}_\varepsilon$ and $\mathcal{T}_\ell$. The overlay estimate of Lemma 2.5.2 yields

$$|\mathcal{M}_\ell| \lesssim |\mathcal{T}_{\ell+\varepsilon}| - |\mathcal{T}_\ell| = |\mathcal{T}_\varepsilon \oplus \mathcal{T}_\ell| - |\mathcal{T}_\ell| \leq |\mathcal{T}_\varepsilon| - |\mathcal{T}_0| \lesssim |||e_\ell|||^{-1/s}|u|_{\mathcal{A}_s}^{1/s}.$$

This and the boundedness of closure in Lemma 2.5.1 yield

$$|\mathcal{T}_L| - |\mathcal{T}_0| \lesssim \sum_{\ell=0}^{L-1}|\mathcal{M}_\ell| \lesssim |u|_{\mathcal{A}_s}^{1/s}\sum_{\ell=0}^{L-1}|||e_\ell|||^{-1/s}.$$

The efficiency estimate of Remark 3.4.3 yields

$$\gamma\eta_\ell^2(\lambda_\ell, u_\ell) + |||u - u_\ell|||^2 \leq \left(1 + \gamma C_{\mathrm{eff}}^2\right)|||u - u_\ell|||^2.$$

Thus,

$$\|\!|u-u_\ell|\!\|^{-1/s} \leq \left(1+\gamma C_{\text{eff}}^2\right)^{1/(2s)} \left(\gamma\eta_\ell^2(\lambda_\ell,u_\ell)+\|\!|u-u_\ell|\!\|^2\right)^{-1/(2s)}.$$

Lemma 3.5.3 leads to

$$\left(\gamma\eta_\ell^2(\lambda_\ell,u_\ell)+\|\!|u-u_\ell|\!\|^2\right)^{-1/(2s)} \leq \varrho^{1/(2s)} \left(\gamma\eta_{\ell+1}^2(\lambda_{\ell+1},u_{\ell+1})+\|\!|u-u_{\ell+1}|\!\|^2\right)^{-1/(2s)}.$$

Exploiting the reliability of the estimator and a geometric series argument yields that $|\mathcal{T}_L|-|\mathcal{T}_0|$ is, up to a generic multiplicative constant, bounded by

$$\begin{aligned}
&|u|_{\mathcal{A}_s}^{1/s} \left(1+\gamma C_{\text{eff}}^2\right)^{1/(2s)} \left(\gamma\eta_L^2(\lambda_L,u_L)+\|\!|u-u_L|\!\|^2\right)^{-1/(2s)} \sum_{\ell=1}^{L} \varrho^{\ell/(2s)} \\
&\quad\lesssim |u|_{\mathcal{A}_s}^{1/s} \left(\frac{1+\gamma C_{\text{eff}}^2}{1+\gamma/C_{\text{rel}}^2}\right)^{1/(2s)} (1-\varrho^{1/(2s)})^{-1} \|\!|u-u_L|\!\|^{-1/s}.
\end{aligned}$$

Note that Euler's formula [51] shows $(|\mathcal{T}_\ell|-|\mathcal{T}_0|)\approx N_\ell$. Finally equation (3.2) proves $|\lambda-\lambda_\ell|\lesssim(|\mathcal{T}_\ell|-|\mathcal{T}_0|)^{-2s}$. □

3.6 Quasi-Optimal Convergence for Inexact Algebraic Solutions

This section contributes to the fact that in practise the underlying algebraic eigenvalue problems are solved inexactly using iterative algebraic eigenvalue solvers. A relationship between the error estimator in the discrete solution and any approximation to it is established in Lemma 3.6.1. As in the case of discrete solutions, the contraction property in Lemma 3.6.2 and the local quasi-optimality in Lemma 3.6.3 lead to the global asymptotic quasi-optimality in Theorem 3.6.4.

Lemma 3.6.1. *Let $v_\ell,\tilde{v}_\ell\in V_\ell$ be normalised discrete functions, $\|v_\ell\|=\|\tilde{v}_\ell\|=1$, and $\mu,\tilde{\mu}\in\mathbb{R}^+$ arbitrary positive real numbers bounded from above by $\tilde{\lambda}_0$. Then it holds that*

$$|\eta_\ell(\mu,v_\ell)-\eta_\ell(\tilde{\mu},\tilde{v}_\ell)|^2 \leq C\left(\|\!|v_\ell-\tilde{v}_\ell|\!\|^2+|\mu-\tilde{\mu}|\right)$$

for a constant $0<C$ independent of the mesh-size H_ℓ.

Proof. Using twice the triangle inequality first for vectors and then for functions yields

$$\begin{aligned}
|\eta_\ell(\mu,v_\ell)-\eta_\ell(\tilde{\mu},\tilde{v}_\ell)|^2 \leq{}& \sum_{T\in\mathcal{T}_\ell} |T|^{2/n}\|\mu v_\ell-\tilde{\mu}\tilde{v}_\ell+\operatorname{div}(\nabla v_\ell-\nabla\tilde{v}_\ell)\|_{L^2(T)}^2 \\
&+\sum_{E\in\mathcal{E}_\ell} |E|^{1/(n-1)}\|[\nabla v_\ell-\nabla\tilde{v}_\ell]\cdot\nu_E\|_{L^2(E)}^2.
\end{aligned}$$

The local discrete inverse inequality

$$|T|^{2/n}\|\operatorname{div}(\nabla v_\ell)\|_{L^2(T)}^2 \lesssim \|\nabla v_\ell\|_{L^2(T)}^2,$$

together with the trace inequality

$$\|v\|^2_{L^2(E)} \lesssim |E|^{-1/(n-1)}\|v\|^2_{L^2(\omega_E)} + |E|^{1/(n-1)}\|\nabla v\|^2_{L^2(\omega_E)},$$

the Poincaré inequality and the finite overlay of the patches lead to

$$\begin{aligned}
&|\eta_\ell(\mu, v_\ell) - \eta_\ell(\tilde{\mu}, \tilde{v}_\ell)|^2 \\
&\lesssim \sum_{T\in\mathcal{T}_\ell} |T|^{2/n}\|\mu v_\ell - \tilde{\mu}\tilde{v}_\ell\|^2_{L^2(T)} + \sum_{T\in\mathcal{T}_\ell}\|\nabla v_\ell - \nabla\tilde{v}_\ell\|^2_{L^2(T)} + \sum_{E\in\mathcal{E}_\ell}\|\nabla v_\ell - \nabla\tilde{v}_\ell\|^2_{L^2(\omega_E)} \\
&\lesssim H_\ell^2\|\mu v_\ell - \tilde{\mu}\tilde{v}_\ell\|^2 + |\!|\!| v_\ell - \tilde{v}_\ell |\!|\!|^2 \\
&\lesssim (1 + \tilde{\lambda}_0^2 H_0^2)|\!|\!| v_\ell - \tilde{v}_\ell |\!|\!|^2 + 2\tilde{\lambda}_0 H_0^2|\mu - \tilde{\mu}|.
\end{aligned}$$

□

Lemma 3.6.2 (Contraction property for inexact algebraic solutions)**.** *Suppose that* (λ_ℓ, u_ℓ) *and* $(\lambda_{\ell+1}, u_{\ell+1})$ *are discrete (exact) eigenpairs to the continuous eigenpair* (λ, u) *with* $u \in \mathcal{A}_s$ *on levels* ℓ *and* $\ell+1$*. Let* $(\tilde{\lambda}_\ell, \tilde{u}_\ell)$ *and* $(\tilde{\lambda}_{\ell+1}, \tilde{u}_{\ell+1})$ *be the corresponding approximations to the discrete eigenpairs, which satisfy*

$$\begin{aligned}
|\!|\!| u_{\ell+1} - \tilde{u}_{\ell+1} |\!|\!|^2 + |\lambda_{\ell+1} - \tilde{\lambda}_{\ell+1}| &\leq \omega\eta_\ell^2(\tilde{\lambda}_\ell, \tilde{u}_\ell), \\
|\!|\!| u_\ell - \tilde{u}_\ell |\!|\!|^2 + |\lambda_\ell - \tilde{\lambda}_\ell| &\leq \omega\eta_\ell^2(\tilde{\lambda}_\ell, \tilde{u}_\ell),
\end{aligned}$$

for sufficiently small $\omega > 0$*. Then, for sufficiently small mesh-size* H_ℓ*, there exists some* $0 < \nu < 1$*, such that the contraction property*

$$\gamma\eta_\ell^2(\tilde{\lambda}_{\ell+1}, \tilde{u}_{\ell+1}) + |\!|\!| u - \tilde{u}_{\ell+1} |\!|\!|^2 \leq \nu\left(\gamma\eta_\ell^2(\tilde{\lambda}_\ell, \tilde{u}_\ell) + |\!|\!| u - \tilde{u}_\ell |\!|\!|^2\right)$$

holds.

Proof. The assumptions, Lemma 3.6.1 and Young's inequality [52] show that for any $\delta > 0$

$$\begin{aligned}
&\gamma\eta_\ell^2(\tilde{\lambda}_{\ell+1}, \tilde{u}_{\ell+1}) + |\!|\!| u - \tilde{u}_{\ell+1} |\!|\!|^2 \\
&\quad\leq (1+\delta)\left(\gamma\eta_\ell^2(\lambda_{\ell+1}, u_{\ell+1}) + |\!|\!| u - u_{\ell+1} |\!|\!|^2\right) \\
&\qquad + (1 + 1/\delta)\left(\gamma|\eta_\ell(\tilde{\lambda}_{\ell+1}, \tilde{u}_{\ell+1}) - \eta_\ell(\lambda_{\ell+1}, u_{\ell+1})|^2 + |\!|\!| u_{\ell+1} - \tilde{u}_{\ell+1} |\!|\!|^2\right) \\
&\quad\leq (1+\delta)\left(\gamma\eta_\ell^2(\lambda_{\ell+1}, u_{\ell+1}) + |\!|\!| u - u_{\ell+1} |\!|\!|^2\right) \\
&\qquad + (1 + 1/\delta)\left(\gamma C|\lambda_{\ell+1} - \tilde{\lambda}_{\ell+1}| + (1+\gamma C)|\!|\!| u_{\ell+1} - \tilde{u}_{\ell+1} |\!|\!|^2\right) \\
&\quad\leq (1+\delta)\left(\gamma\eta_\ell^2(\lambda_{\ell+1}, u_{\ell+1}) + |\!|\!| u - u_{\ell+1} |\!|\!|^2\right) + (1+1/\delta)(1+\gamma C)\omega\eta_\ell^2(\tilde{\lambda}_\ell, \tilde{u}_\ell).
\end{aligned}$$

The contraction property Lemma 3.5.3 and another application of Young's inequality [52] yield

$$\begin{aligned}
&\gamma\eta_\ell^2(\tilde{\lambda}_{\ell+1}, \tilde{u}_{\ell+1}) + |\!|\!| u - \tilde{u}_{\ell+1} |\!|\!|^2 \\
&\quad\leq (1+\delta)\varrho\left(\gamma\eta_\ell^2(\lambda_\ell, u_\ell) + |\!|\!| u - u_\ell |\!|\!|^2\right) + (1+1/\delta)(1+\gamma C)\omega\eta_\ell^2(\tilde{\lambda}_\ell, \tilde{u}_\ell)
\end{aligned}$$

This leads to

$$\gamma\eta_\ell^2(\tilde\lambda_{\ell+1},\tilde u_{\ell+1})+\|\!|u-\tilde u_{\ell+1}|\!\|^2\le(1+\delta)^2\varrho\left(\gamma\eta_\ell^2(\tilde\lambda_\ell,\tilde u_\ell)+\|\!|u-\tilde u_\ell|\!\|^2\right)\\+(1+(1+\delta)\varrho)(1+1/\delta)(1+\gamma C)\omega\eta_\ell^2(\tilde\lambda_\ell,\tilde u_\ell).$$

Any choice of $0<\delta<\varrho^{-1/2}-1$ results in

$$0<\omega<\frac{\gamma-(1+\delta)^2\varrho\gamma}{(1+(1+\delta)\varrho)(1+1/\delta)(1+\gamma C)}.$$

The choice

$$0<\nu:=(1+\delta)^2\varrho+(1+(1+\delta)\varrho)(1+1/\delta)(1+\gamma C)\omega/\gamma<1$$

concludes the proof. □

Lemma 3.6.3. *Let (λ,u) with $u\in\mathcal{A}_s$ be an eigenpair and let (λ_ℓ,u_ℓ) be the corresponding discrete eigenpair with approximation $(\tilde\lambda_\ell,\tilde u_\ell)$ which satisfies*

$$\|\!|u_\ell-\tilde u_\ell|\!\|^2+|\lambda_\ell-\tilde\lambda_\ell|\le\omega\eta_\ell^2(\tilde\lambda_\ell,\tilde u_\ell)$$

for a sufficient small $\omega>0$. Suppose that $\mathcal{M}_{\tilde\lambda_\ell,\tilde u_\ell}$ is the set of marked edges and elements using the marking strategy of Section 3.2 based on the bulk criterion and $\eta_\ell(\tilde\lambda_\ell,\tilde u_\ell)$, then for sufficiently small H_ℓ and bulk parameter $\theta>0$ it holds that

$$|\mathcal{M}_{\tilde\lambda_\ell,\tilde u_\ell}|\lesssim\|\!|u-\tilde u_\ell|\!\|^{-1/s}|u|_{\mathcal{A}_s}^{1/s}.$$

Proof. Let $\mathcal{T}_\varepsilon$ be the smallest partition of $\mathcal{T}_0$ such that

$$\|\!|u-u_\varepsilon|\!\|\le\rho\|\!|u-\tilde u_\ell|\!\|$$

for $0<\rho<1/2$. Thus, the definition of $|u|_{\mathcal{A}_s}$ yields

$$|\mathcal{T}_\varepsilon|-|\mathcal{T}_0|\le\rho^{-1/s}\|\!|u-\tilde u_\ell|\!\|^{-1/s}|u|_{\mathcal{A}_s}^{1/s}.$$

Let $\mathcal{T}_{\ell+\varepsilon}:=\mathcal{T}_\ell\oplus\mathcal{T}_\varepsilon$ be the smallest common refinement of $\mathcal{T}_\ell$ and $\mathcal{T}_\varepsilon$, this leads to

$$\|\!|u-u_{\ell+\varepsilon}|\!\|\le\rho\|\!|u-\tilde u_\ell|\!\|\le\rho\|\!|u-u_\ell|\!\|+\rho\|\!|u_\ell-\tilde u_\ell|\!\|\le\rho\|\!|u-u_\ell|\!\|+\rho\sqrt{\omega}\eta_\ell(\tilde\lambda_\ell,\tilde u_\ell)\\\le\left(2\rho^2\|\!|u-u_\ell|\!\|^2+2\rho^2\omega\eta_\ell^2(\tilde\lambda_\ell,\tilde u_\ell)\right)^{1/2}.$$

This estimate proves the inequality

$$(1-2\rho^2)C_{\mathrm{eff}}^{-2}\eta_\ell^2(\lambda_\ell,u_\ell)-2\rho^2\omega\eta_\ell^2(\tilde\lambda_\ell,\tilde u_\ell)\le(1-2\rho^2)\|\!|u-u_\ell|\!\|^2-2\rho^2\omega\eta_\ell^2(\tilde\lambda_\ell,\tilde u_\ell)\\\le\|\!|u-u_\ell|\!\|^2-\|\!|u-u_{\ell+\varepsilon}|\!\|^2.$$

Let $\mathcal{M}_\varepsilon:=(\mathcal{T}_\ell\backslash\mathcal{T}_{\ell+\varepsilon})\cup(\mathcal{E}_\ell\backslash\mathcal{E}_{\ell+\varepsilon})$, then the quasi-orthogonality from Lemma 3.3.1 and

the discrete reliability of Lemma 3.4.1 yield

$$\begin{aligned}(1-2\rho^2)C_{\mathrm{eff}}^{-2}\eta_\ell^2(\lambda_\ell,u_\ell)-2\rho^2\omega\eta_\ell^2(\tilde\lambda_\ell,\tilde u_\ell)&\le |\!|\!| u_{\ell+\varepsilon}-u_\ell|\!|\!|^2+\lambda\|e_\ell\|^2\\ &\le C_{\mathrm{rel}}^2\eta_\ell^2(\lambda_\ell,u_\ell;\mathcal{M}_\varepsilon)+\lambda\sigma(H_\ell)^2C_{\mathrm{rel}}^2\eta_\ell^2(\lambda_\ell,u_\ell),\end{aligned}$$

where $\sigma(H_\ell)$ from Lemma 3.5.3 tends to zero as $H_\ell\to 0$. Thus,

$$((1-2\rho^2)C_{\mathrm{eff}}^{-2}-\lambda\sigma(H_\ell)^2C_{\mathrm{rel}}^2)\eta_\ell^2(\lambda_\ell,u_\ell)\le C_{rel}^2\eta_\ell^2(\lambda_\ell,u_\ell;\mathcal{M}_\varepsilon)+2\rho^2\omega\eta_\ell^2(\tilde\lambda_\ell,\tilde u_\ell).$$

Lemma 3.6.1 together with the assumption yields

$$|\eta_\ell(\lambda_\ell,u_\ell)-\eta_\ell(\tilde\lambda_\ell,\tilde u_\ell)|^2\le C\left(|\!|\!| u_\ell-\tilde u_\ell|\!|\!|^2+|\lambda_\ell-\tilde\lambda_\ell|\right)\le C\omega\eta_\ell^2(\tilde\lambda_\ell,\tilde u_\ell).$$

Therefore,

$$\begin{aligned}&((1-2\rho^2)C_{\mathrm{eff}}^{-2}-\lambda\sigma(H_\ell)^2C_{\mathrm{rel}}^2)2^{-1}\eta_\ell^2(\tilde\lambda_\ell,\tilde u_\ell)\\ &\quad\le((1-2\rho^2)C_{\mathrm{eff}}^{-2}-\lambda\sigma(H_\ell)^2C_{\mathrm{rel}}^2)\eta_\ell^2(\lambda_\ell,u_\ell)\\ &\qquad+((1-2\rho^2)C_{\mathrm{eff}}^{-2}-\lambda\sigma(H_\ell)^2C_{\mathrm{rel}}^2)C\omega\eta_\ell^2(\tilde\lambda_\ell,\tilde u_\ell)\\ &\quad\le C_{\mathrm{rel}}^2\eta_\ell^2(\lambda_\ell,u_\ell;\mathcal{M}_\varepsilon)+2\rho^2\omega\eta_\ell^2(\tilde\lambda_\ell,\tilde u_\ell)\\ &\qquad+((1-2\rho^2)C_{\mathrm{eff}}^{-2}-\lambda\sigma(H_\ell)^2C_{\mathrm{rel}}^2)C\omega\eta_\ell^2(\tilde\lambda_\ell,\tilde u_\ell)\\ &\quad\le 2C_{\mathrm{rel}}^2\eta_\ell^2(\tilde\lambda_\ell,\tilde u_\ell;\mathcal{M}_\varepsilon)+2\rho^2\omega\eta_\ell^2(\tilde\lambda_\ell,\tilde u_\ell)\\ &\qquad+(2C_{\mathrm{rel}}^2+(1-2\rho^2)C_{\mathrm{eff}}^{-2}-\lambda\sigma(H_\ell)^2C_{\mathrm{rel}}^2)C\omega\eta_\ell^2(\tilde\lambda_\ell,\tilde u_\ell).\end{aligned}$$

The choice $\sigma(H_\ell)\ll 1$ and $0<\omega\ll 1$ shows $0<\theta\le\Theta\le 1$ with

$$\Theta:=\frac{((1-2\rho^2)C_{\mathrm{eff}}^{-2}-\lambda\sigma(H_\ell)^2C_{\mathrm{rel}}^2)(2^{-1}-C\omega)-2(C_{\mathrm{rel}}^2C+\rho^2)\omega}{2C_{\mathrm{rel}}^2}$$

and hence the bulk criterion for the set $\mathcal{M}_\varepsilon$ based on $\eta_\ell(\tilde\lambda_\ell,\tilde u_\ell)$ is satisfied. Since the set $\mathcal{M}_{\tilde\lambda_\ell,\tilde u_\ell}$ has been chosen with almost minimal cardinality, the overlay estimate leads to

$$|\mathcal{M}_{\tilde\lambda_\ell,\tilde u_\ell}|\lesssim|\mathcal{M}_\varepsilon|\lesssim|\mathcal{T}_{\ell+\varepsilon}|-|\mathcal{T}_\ell|\le|\mathcal{T}_\varepsilon|-|\mathcal{T}_0|\lesssim|\!|\!| u-\tilde u_\ell|\!|\!|^{-1/s}|u|_{\mathcal{A}_s}^{1/s}.\qquad\square$$

Theorem 3.6.4. *Suppose that (λ,u) with $u\in\mathcal{A}_s$ is an eigenpair and let (λ_ℓ,u_ℓ) and $(\lambda_{\ell+1},u_{\ell+1})$ be the corresponding discrete eigenpairs on levels ℓ and $\ell+1$. Let the iterative approximations $(\tilde\lambda_\ell,\tilde u_\ell)$ on $\mathcal{T}_\ell$ and $(\tilde\lambda_{\ell+1},\tilde u_{\ell+1})$ on $\mathcal{T}_{\ell+1}$ satisfy*

$$\begin{aligned}|\!|\!| u_{\ell+1}-\tilde u_{\ell+1}|\!|\!|^2+|\lambda_{\ell+1}-\tilde\lambda_{\ell+1}|&\le\omega\eta_\ell^2(\tilde\lambda_\ell,\tilde u_\ell),\\ |\!|\!| u_\ell-\tilde u_\ell|\!|\!|^2+|\lambda_\ell-\tilde\lambda_\ell|&\le\omega\eta_\ell^2(\tilde\lambda_\ell,\tilde u_\ell)\end{aligned}$$

for sufficiently small $\omega>0$. Then, for sufficiently small initial mesh-size H_0, the itera-

tive solutions $\tilde{\lambda}_\ell$ and $\tilde{u}_\ell$ converge quasi-optimally, i.e.

$$|||u - \tilde{u}_\ell|||^2 + |\lambda - \tilde{\lambda}_\ell| \lesssim (|\mathcal{T}_\ell| - |\mathcal{T}_0|)^{-2s} \lesssim N_\ell^{-2s}.$$

Proof. Lemma 3.6.3 and Proposition 2.5.1 yield

$$|\mathcal{T}_L| - |\mathcal{T}_0| \lesssim \sum_{\ell=0}^{L-1} |\mathcal{M}_{\tilde{\lambda}_\ell, \tilde{u}_\ell}| \lesssim |u|_{\mathcal{A}_s}^{1/s} \sum_{\ell=0}^{L-1} |||u - \tilde{u}_\ell|||^{-1/s}.$$

The efficiency estimate of Remark 3.4.3 and Lemma 3.6.1 show

$$\begin{aligned}
\eta_\ell^2(\tilde{\lambda}_\ell, \tilde{u}_\ell) &\leq 2\eta_\ell^2(\lambda_\ell, u_\ell) + 2C \left(|||u_\ell - \tilde{u}_\ell|||^2 + |\lambda_\ell - \tilde{\lambda}_\ell| \right) \\
&\leq 4C_{\mathrm{eff}}^2 |||u - \tilde{u}_\ell|||^2 + (2C + 4C_{\mathrm{eff}}^2) \left(|||u_\ell - \tilde{u}_\ell|||^2 + |\lambda_\ell - \tilde{\lambda}_\ell| \right) \\
&\leq 4C_{\mathrm{eff}}^2 |||u - \tilde{u}_\ell|||^2 + (2C + 4C_{\mathrm{eff}}^2) \omega \eta_\ell^2(\tilde{\lambda}_\ell, \tilde{u}_\ell).
\end{aligned}$$

Hence, for $0 < \omega < (2C + 4C_{\mathrm{eff}}^2)^{-1}$, it holds that

$$\eta_\ell(\tilde{\lambda}_\ell, \tilde{u}_\ell) \lesssim |||u - \tilde{u}_\ell|||.$$

For the other direction, notice that

$$|||u - \tilde{u}_\ell||| \leq |||u - u_\ell||| + |||u_\ell - \tilde{u}_\ell||| \leq C_{\mathrm{rel}} \eta_\ell(\lambda_\ell, u_\ell) + \sqrt{\omega} \eta_\ell(\tilde{\lambda}_\ell, \tilde{u}_\ell),$$

implies

$$|||u - \tilde{u}_\ell|||^2 \leq 2C_{\mathrm{rel}}^2 \eta_\ell^2(\lambda_\ell, u_\ell) + 2\omega \eta_\ell^2(\tilde{\lambda}_\ell, \tilde{u}_\ell) \leq \left(4C_{\mathrm{rel}}^2 + 4C_{\mathrm{rel}}^2 C\omega + 2\omega \right) \eta_\ell^2(\tilde{\lambda}_\ell, \tilde{u}_\ell).$$

Thus,

$$|||u - \tilde{u}_\ell|||^{-1/s} \lesssim \left(\gamma \eta_\ell^2(\tilde{\lambda}_\ell, \tilde{u}_\ell) + |||u - \tilde{u}_\ell|||^2 \right)^{-1/(2s)}.$$

Lemma 3.6.2 leads to

$$\left(\gamma \eta_\ell^2(\tilde{\lambda}_\ell, \tilde{u}_\ell) + |||u - \tilde{u}_\ell|||^2 \right)^{-1/(2s)} \leq \nu^{1/(2s)} \left(\gamma \eta_{\ell+1}^2(\tilde{\lambda}_{\ell+1}, \tilde{u}_{\ell+1}) + |||u - \tilde{u}_{\ell+1}|||^2 \right)^{-1/(2s)}.$$

A geometric series argument yields

$$\begin{aligned}
|\mathcal{T}_L| - |\mathcal{T}_0| &\lesssim |u|_{\mathcal{A}_s}^{1/s} \left(\gamma \eta_L^2(\tilde{\lambda}_L, \tilde{u}_L) + |||u - \tilde{u}_L|||^2 \right)^{-1/(2s)} \sum_{\ell=1}^{L} \nu^{\ell/(2s)} \\
&\lesssim |u|_{\mathcal{A}_s}^{1/s} (1 - \nu^{1/(2s)})^{-1} |||u - \tilde{u}_L|||^{-1/s}.
\end{aligned}$$

Since

$$|\lambda - \tilde{\lambda}_\ell| \leq |\lambda - \lambda_\ell| + |\lambda_\ell - \tilde{\lambda}_\ell| \leq |\lambda - \lambda_\ell| + \omega \eta_\ell^2(\tilde{\lambda}_\ell, \tilde{u}_\ell)$$

it holds that

$$|\lambda - \tilde{\lambda}_\ell| \leq |\lambda - \lambda_\ell| + 2\omega C_{\text{eff}}^2 |||u - u_\ell|||^2 + 2\omega C \left(|||u_\ell - \tilde{u}_\ell|||^2 + |\lambda_\ell - \tilde{\lambda}_\ell| \right).$$

This leads to

$$|\lambda - \tilde{\lambda}_\ell| \lesssim |\lambda - \lambda_\ell| + |||u - u_\ell|||^2 + |||u - \tilde{u}_\ell|||^2$$

for sufficiently small $\omega > 0$. Thus, Theorem 3.5.4 proves $|\lambda - \tilde{\lambda}_\ell| \lesssim (|\mathcal{T}_\ell| - |\mathcal{T}_0|)^{-2s}$ and Euler's formula [51] shows $(|\mathcal{T}_\ell| - |\mathcal{T}_0|) \approx N_\ell$. □

The choice of the bulk parameter θ is asymptotically independent of λ and depends on the reliability and efficiency constants as well as on ω. The choice of the parameter ω in particular depends on the constant of Lemma 3.6.1 and therefore on the initial mesh-size H_0 and the initial guess $\tilde{\lambda}_0$. Empirical choices of these parameters for some numerical examples are discussed in Section 3.8.

3.7 Quasi-Optimal Complexity

This section presents the proof of the quasi-optimal computational complexity of the AFEMES which combines the AFEM with some iterative algebraic eigenvalue solver. In order to prove overall asymptotic quasi-optimal complexity, the iterative solver needs to have a constant contraction factor independent of the size of the discrete problem and to be of linear complexity. In other words for any $\varepsilon > 0$ the algorithm LAES has to compute an iterative solution of the algebraic eigenvalue problem $(\tilde{\lambda}_{\ell,m}, \tilde{u}_{\ell,m})$ from an initial guess $(\tilde{\lambda}_{\ell,0}, \tilde{u}_{\ell,0})$ such that

$$|||u_\ell - \tilde{u}_{\ell,m}|||^2 + |\lambda_\ell - \tilde{\lambda}_{\ell,m}| \leq \varepsilon^2$$

in $\lesssim \max\{1, \log(\varepsilon^{-1} |||u_\ell - \tilde{u}_{\ell,0}|||)\} \times N_\ell$ arithmetic operations.

Theorem 3.7.1. *Let (λ, u) with $u \in \mathcal{A}_s$ be an eigenpair. Then for sufficiently small H_0, $0 < \theta \ll 1$ and $0 < \omega \ll 1$, the algorithm AFEMES computes from a coarse triangulation $\mathcal{T}_0$ and an initial guess $(\tilde{\lambda}_0, \tilde{u}_0)$ sufficiently close to (λ, u), a sequence of triangulations $(\mathcal{T}_\ell)_\ell$ and corresponding approximated eigenpairs $(\tilde{\lambda}_\ell, \tilde{u}_\ell)$ such that*

$$|||u - \tilde{u}_\ell|||^2 + |\lambda - \tilde{\lambda}_\ell| \lesssim \eta_\ell^2(\tilde{\lambda}_\ell, \tilde{u}_\ell) \lesssim t_\ell^{-2s}$$

where t_ℓ denotes the computational costs in form of the CPU-time.

Proof. First it is shown that the while-loop is terminating after a finite number of iterations on each level. Remark, that the while-loop is executed at least once and that in further runs it holds that

$$|||u_\ell - \tilde{u}_\ell|||^2 + |\lambda_\ell - \tilde{\lambda}_\ell| \leq \delta_\ell^2$$

because of the previous calls of LAES. Using Lemma 3.6.1 yields

$$\begin{aligned}\sqrt{\omega}\eta_\ell(\tilde{\lambda}_\ell,\tilde{u}_\ell) &\geq \sqrt{\omega}\eta_\ell(\lambda_\ell,u_\ell) - \sqrt{\omega}|\eta_\ell(\tilde{\lambda}_\ell,\tilde{u}_\ell) - \eta_\ell(\lambda_\ell,u_\ell)| \\ &\geq \sqrt{\omega}\eta_\ell(\lambda_\ell,u_\ell) - \sqrt{\omega C}\left(|||u_\ell-\tilde{u}_\ell|||^2 + |\lambda_\ell-\tilde{\lambda}_\ell|\right)^{1/2} \\ &\geq \sqrt{\omega}\eta_\ell(\lambda_\ell,u_\ell) - \delta_\ell\sqrt{\omega C}.\end{aligned}$$

Therefore, the while-loop is at least terminated on the level ℓ if

$$\delta_\ell \leq \frac{\sqrt{\omega}\eta_\ell(\lambda_\ell,u_\ell)}{1+\sqrt{\omega C}}.$$

Due to the geometric decrease of δ_ℓ this is achieved in a bounded constant number of steps for all levels ℓ. The choice of the initial value for δ_ℓ on each level ℓ and the fact that after the while-loop terminates $\delta_\ell \leq \sqrt{\omega}\eta_\ell(\tilde{\lambda}_\ell,\tilde{u}_\ell)$ shows that the conditions of Theorem 3.6.4 are satisfied. Thus, the convergence of

$$|||u-\tilde{u}_\ell||| \lesssim N_\ell^{-s}$$

is quasi-optimal. Moreover the proof of Theorem 3.6.4 shows

$$|||u-\tilde{u}_\ell||| \lesssim \eta_\ell(\tilde{\lambda}_\ell,\tilde{u}_\ell) \lesssim |||u-\tilde{u}_\ell||| \tag{3.5}$$

for sufficiently small $\omega > 0$. For the eigenvalue error it holds that

$$\begin{aligned}|\lambda-\tilde{\lambda}_\ell| &\leq |\lambda-\lambda_\ell| + |\lambda_\ell-\tilde{\lambda}_\ell| \leq C_{\mathrm{rel}}^2\eta_\ell^2(\lambda_\ell,u_\ell) + \delta_\ell^2 \\ &\leq 2C_{\mathrm{rel}}^2\eta_\ell^2(\tilde{\lambda}_\ell,\tilde{u}_\ell) + (2C_{\mathrm{rel}}^2C+1)\delta_\ell^2 \leq (2C_{\mathrm{rel}}^2 + (2C_{\mathrm{rel}}^2C+1)\omega)\eta_\ell^2(\tilde{\lambda}_\ell,\tilde{u}_\ell).\end{aligned}$$

Hence,

$$|||u-\tilde{u}_\ell|||^2 + |\lambda-\tilde{\lambda}_\ell| \lesssim \eta_\ell^2(\tilde{\lambda}_\ell,\tilde{u}_\ell) \lesssim N_\ell^{-2s}.$$

Because of the quasi-optimal convergence and the finite number of iterations of the while-loop, it remains to show that Mark, Refine and LAES are of linear computational complexity. A quasi-optimal algorithm for Mark and Refine can be found in [102]. In the first execution of the while-loop, except for the first level for which the costs can be bounded by a constant separately, before LAES is executed, it holds that

$$|||u_\ell-\tilde{u}_\ell||| = |||u_\ell-\tilde{u}_{\ell-1}||| \leq |||u-u_\ell||| + |||u-\tilde{u}_{\ell-1}|||.$$

Lemma 3.5.3 reads

$$|||u-u_\ell|||^2 \leq 2\varrho\left(\gamma C_{\mathrm{eff}}^2+1\right)\left(|||u-\tilde{u}_{\ell-1}|||^2 + |||u_{\ell-1}-\tilde{u}_{\ell-1}|||^2\right).$$

Thus, (3.5), the termination of the while-loop on the previous level $\ell-1$ and the initial-

isation of δ_ℓ yield

$$\|\!|u_\ell - \tilde{u}_\ell|\!\| \lesssim \eta_{\ell-1}(\tilde{\lambda}_{\ell-1}, \tilde{u}_{\ell-1}) + \delta_{\ell-1} \lesssim \eta_{\ell-1}(\tilde{\lambda}_{\ell-1}, \tilde{u}_{\ell-1}) \lesssim \delta_\ell.$$

If it is not the first evaluation of the while-loop, then $\|\!|u_\ell - \tilde{u}_\ell|\!\| \leq 2\delta_\ell$ because of the previous call of LAES. Thus, before any call of LAES for $\ell > 0$, it holds that $\|\!|u_\ell - \tilde{u}_\ell|\!\| \lesssim \delta_\ell$ which shows that LAES can be executed in linear time $t_\ell \approx N_\ell$. □

3.8 Numerical Experiments

The numerical experiments for $n = 2, 3$ show asymptotic quasi-optimal computational complexity of the AFEMES for linear P_1 up to fourth order P_4 finite elements. The AFEMES is implemented in Matlab for $n = 2, 3$. The aim of the implementation is not to be the fastest one but to verify the asymptotic quasi-optimal complexity of the AFEMES in numerical experiments. The implementation of the AFEM follows the ideas of [3] and in an enhanced way of [56]. The mesh refinement for $n = 3$ is based on a bisection type strategy [8]. The quasi-optimal complexity is measured by plotting the number of seconds a computation needs to finish on a single CPU-core of an AMD-Opteron processor 8378 at 2,4 GHz and with 128GB ram versus the eigenvalue error or the a posteriori error estimator. The numerical experiments compare the computational performance of different algebraic eigenvalue solvers in combination with the asymptotic quasi-optimal AFEMES. These are the ARPACK solver as implemented in the Matlab function "eigs", the preconditioned inverse iteration (PINVIT) with one multigrid V-cycle as preconditioner, and the LOBPCG implementation in Matlab [74] using also one multigrid V-cycle as preconditioner. The reference algorithm to solve the eigenvalue problem only once on an arbitrary uniform refined mesh with ARPACK (eigs) will be denoted by "ARPACK uniform" and the measured time involves the assembly of the matrices, the time to solve the algebraic eigenvalue problem and the calculation of the a posteriori error estimator. The standard AFEM algorithm with the ARPACK solver for default tolerance in the range of the machine precision is denoted by "ARPACK AFEM". For the V-cycle geometric multigrid preconditioner global Richardson smoothing (n=2) and Jacobi smoothing (n=3) with empirical optimal scaling factors independently of H_ℓ are used. All eigensolvers start from the same initial guess $x_0 = (1, \ldots, 1)^t$ on $\mathcal{T}_0$.

3.8.1 Slit Domain

Consider the two-dimensional model eigenvalue problem (3.1) on the slit domain $\Omega = ((-1,1)\times(-1,1))\backslash([0,1]\times\{0\})$ with tip at the origin. An approximation of the smallest eigenvalue with high accuracy is computed with higher-order finite elements on fine meshes

$$\lambda = 8.3713297112,$$

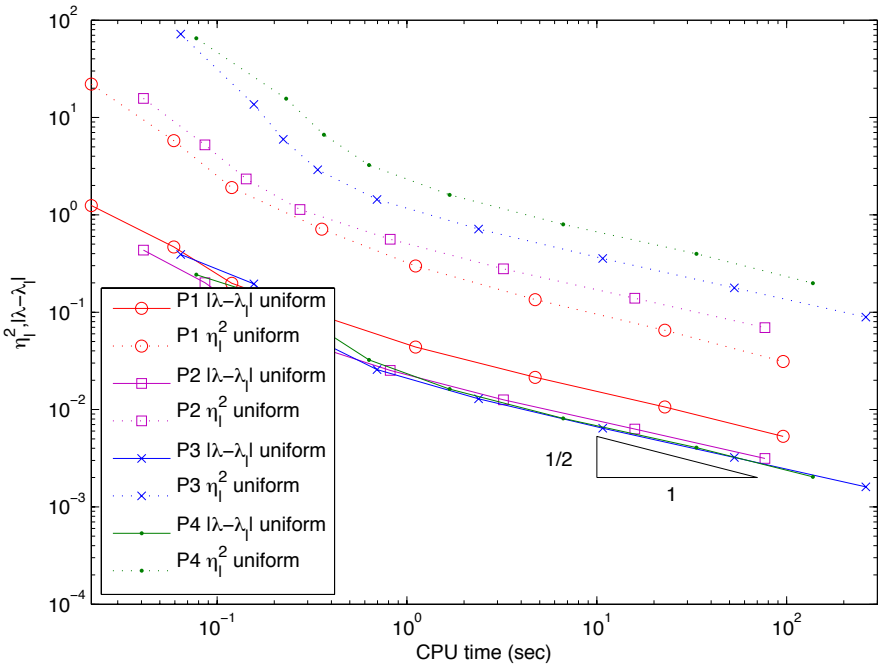

Figure 3.2: Eigenvalue errors and estimated errors on the slit domain for uniform meshes for $\theta = 1$ and $\omega = 10^{-3}$.

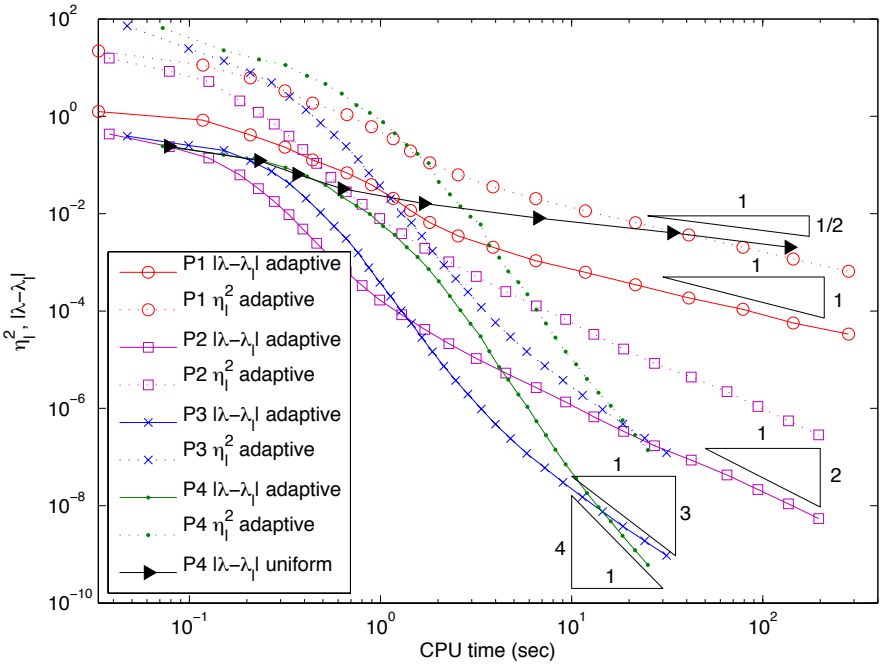

Figure 3.3: Eigenvalue errors and estimated errors on the slit domain for adaptive meshes for $\theta = 0.5$ and $\omega = 10^{-3}$.

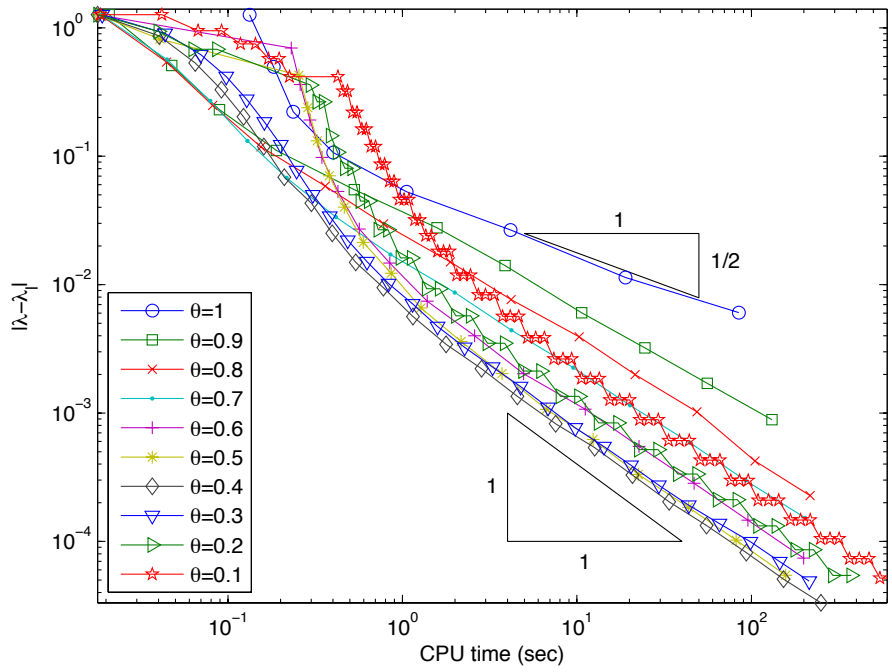

Figure 3.4: Eigenvalue errors for different values of $\theta = 0.1, \ldots, 1$ on the slit domain for P_1 and $\omega = 10^{-1}$.

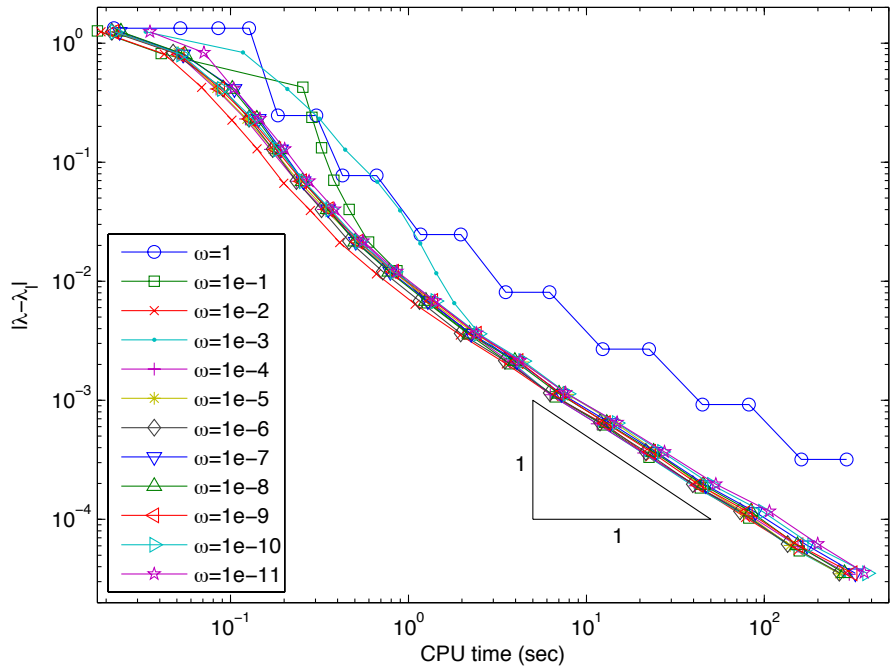

Figure 3.5: Eigenvalue errors for different orders of magnitude of ω on the slit domain for P_1 and $\theta = 0.5$.

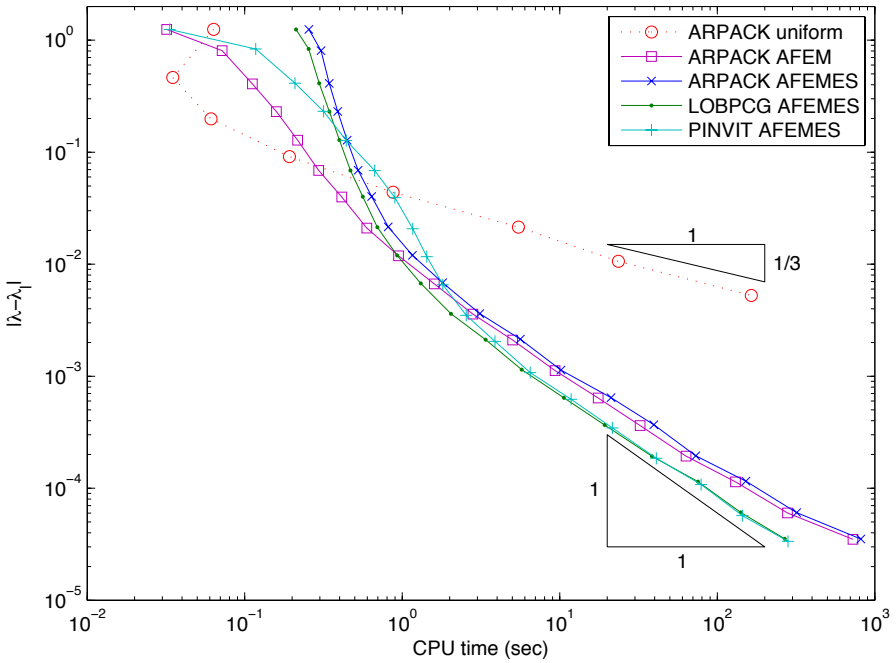

Figure 3.6: Eigenvalue errors for different algebraic solvers on the slit domain for P_1, $\theta = 0.5$ and $\omega = 10^{-3}$.

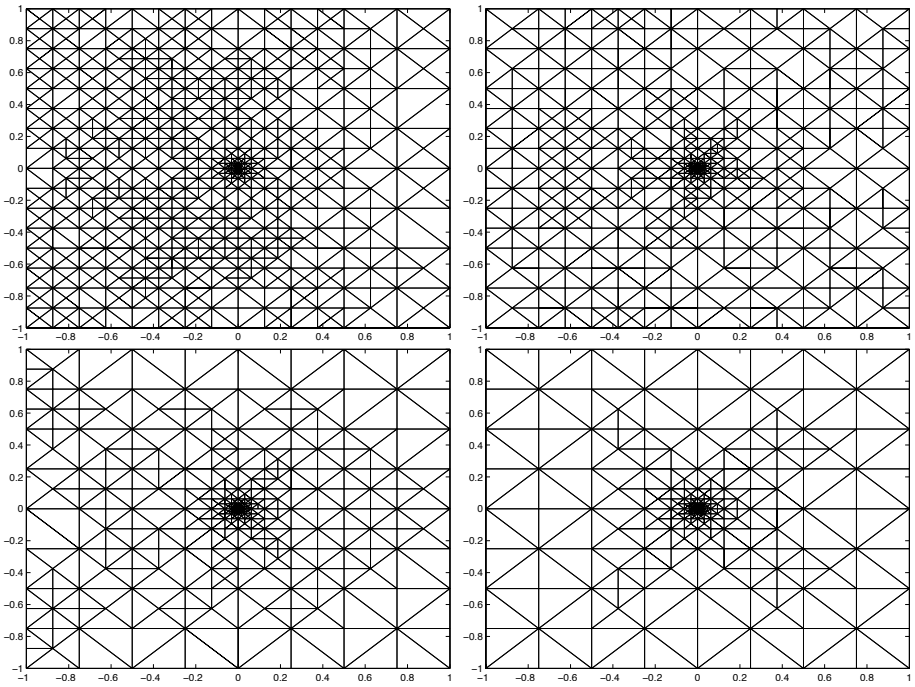

Figure 3.7: Adaptive refined meshes for P_k, $k = 1, 2, 3, 4$ (top left to bottom right), with about 500 nodes.

where all digits except the last one are exact. Note that $N_\ell^{-1/2} \approx H_\ell$ holds for uniform meshes and $n = 2$. Thus, for P_k, $k = 1, \dots, 4$, convergence rates of $\mathcal{O}(t_\ell^{-k})$ are optimal for the eigenvalue error of the AFEMES. For the following experiments the PINVIT algebraic eigenvalue solver is used and the parameters are $\theta = 0.5$ and $\omega = 10^{-3}$. The algorithm stops when a tolerance of 10^{-9} in the eigenvalue error is reached due to the accuracy of the reference eigenvalue or the number of degrees of freedom exceeds 10^6. In Figure 3.2 it is shown that the error estimator is numerically reliable and efficient for uniform meshes but these meshes result in suboptimal convergence rates of about $\mathcal{O}(t_\ell^{-1/2})$ due to the singularity at the origin. Note that the same rates are obtained for N_ℓ instead of t_ℓ. Thus the computational costs are quasi-optimal for uniform meshes. In contrast using adaptive refinement results in experimental optimal convergence rates of $\mathcal{O}(t_\ell^{-k})$, $k = 1, \dots, 4$, as shown in Figure 3.3 and the error estimator shows to be numerically reliable and efficient.

The asymptotic quasi-optimal AFEMES involves two parameters $\omega > 0$ and $0 < \theta \leq 1$ which have to be sufficiently small. Figure 3.4 shows a numerical strong dependency of the size of the eigenvalue error on θ for $\omega = 0.1$. For $\theta = 1$ uniform refinement results in suboptimal convergence rates. Smaller values lead to optimal convergence rates and down to $\theta = 0.4$ the error decreases. Then for even smaller values for θ, the convergence rates are numerically optimal, but $\theta \ll 1$ leads to more iterations of the algebraic eigenvalue solver and thus to more computational work. Note that for values $\theta \leq 0.2$ the algorithm marks too few elements such that the algorithm accepts the value of the previous level as approximation for the next one from time to time. This results in the effect that those convergence plots look like a stair. Different values for ω lead almost all (asymptotically) to optimal convergence rates as depicted in Figure 3.5. Only the value $\omega = 1$ is not small enough. The computational costs for smaller values only moderately increases.

The asymptotic quasi-optimal complexity of AFEMES depends on the choice of the algebraic eigenvalue solver. Figure 3.6 shows that the AFEMES is in the long term faster than one solve of ARPACK on an uniform mesh for linear P_1 finite elements ("ARPACK uniform"). The results obtained with the multigrid preconditioned PINVIT and LOBPCG solver show asymptotic quasi-optimal computational complexity. The AFEMES shows larger computational time for ARPACK than for PINVIT and LOBPCG due to the use of matrix factorisations instead of multigrid and the convergence rate deteriorates for larger number of unknowns because the time for the matrix factorisations dominates the computational costs. PINVIT and LOBPCG with matrix factorisations would lead to similar large computational costs.

Different adaptive refined meshes for P_k, $k = 1, 2, 3, 4$, with about 500 nodes are displayed in Figure 3.7. Note that the meshes are strongly refined towards the corner singularity at the origin.

3.8.2 Unit Cube

Consider the three-dimensional model eigenvalue problem (3.1) on the unit cube $\Omega = (0, 1) \times (0, 1) \times (0, 1)$ for the 11th eigenvalue $\lambda_{11} = 12\pi^2$ which is simple. Note that

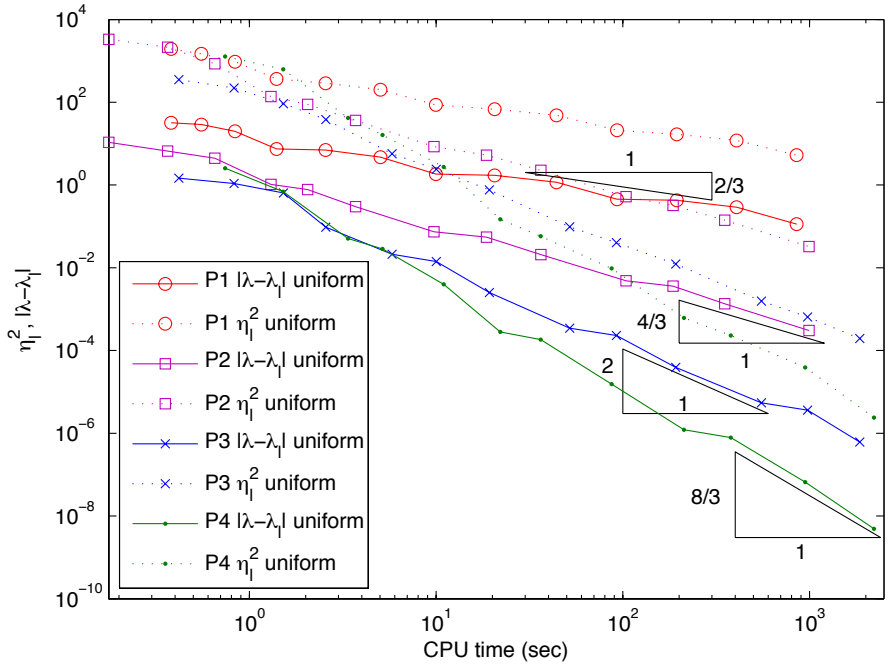

Figure 3.8: Eigenvalue errors and estimated errors for the 11th eigenvalue on the cube for uniform meshes with $\theta = 1$ and $\omega = 10^{-4}$.

$N_\ell^{-1/3} \approx H_\ell$ holds for uniform meshes and $n = 3$. Thus, for P_k, $k = 1, \dots, 4$, convergence rates of $\mathcal{O}(t_\ell^{-2k/3})$ for the eigenvalue error are optimal. The asymptotic quasi-optimal AFEMES is stopped when 10^6 degrees of freedom are reached because of hardware limitations. Figure 3.8 shows optimal convergence rates for uniform meshes of $\mathcal{O}(t_\ell^{-2k/3})$, $k = 1, \dots, 4$, computing the 11th eigenvalue with the AFEMES using the LOBPCG solver. The 11th eigenvalue is computed without any shift but from a subspace iteration.

3.8.3 3D L-Shaped Domain

Consider the model eigenvalue problem (3.1) on the three-dimensional L-shaped domain $\Omega = ((-1,1)^3)\backslash([0,1]^2 \times [-1,1])$. The first eigenvalue is the sum of π^2 and the first eigenvalue of the two-dimensional L-shaped domain with approximation 9.6397238440219 [17],

$$\lambda = 19.509328245111$$

(all displayed digits are correct). The asymptotic quasi-optimal AFEMES is stopped when 10^6 degrees of freedom are reached. In this non-convex three-dimensional example uniform refinement results in suboptimal convergence rates $\mathcal{O}(t_\ell^{-4/9})$ as shown in Figure 3.9. Note that the same rates are obtained for N_ℓ and that the AFEMES is based on isotropic refinement and therefore cannot create anisotropic meshes. Thus, we do not expect similar optimal rates for adaptive refined meshes as for the two-dimensional case due to the edge singularity. This is no contradiction to the theory because the defini-

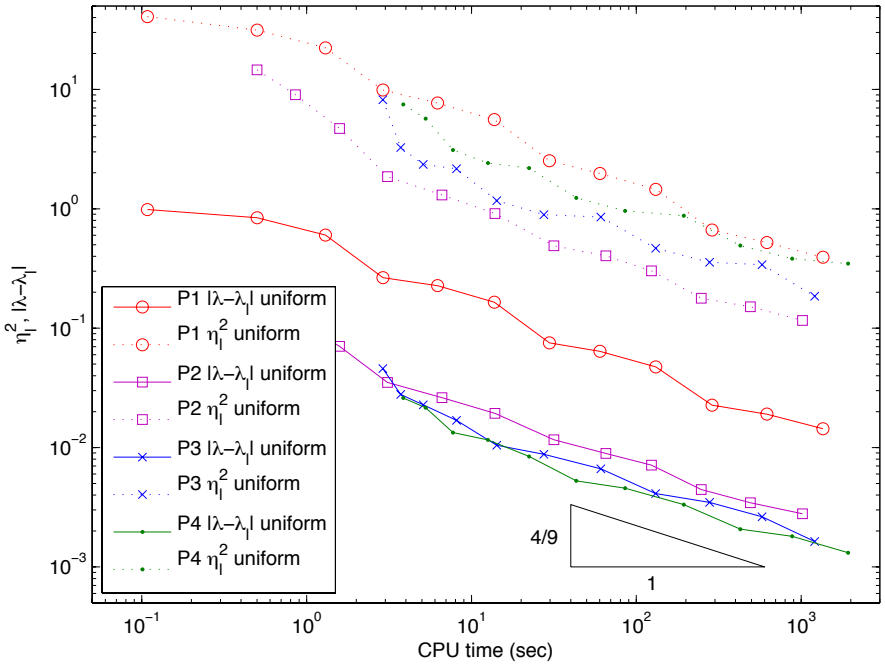

Figure 3.9: Eigenvalue errors and estimated errors on the three-dimensional L-shaped domain for uniform meshes with $\theta = 1$ and $\omega = 10^{-3}$.

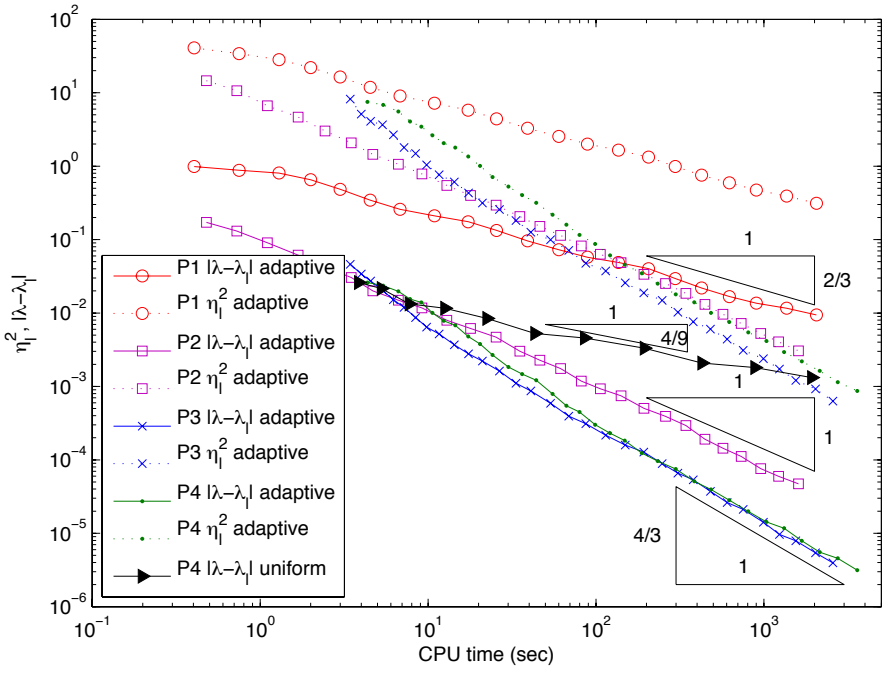

Figure 3.10: Eigenvalue errors and estimated errors on the three-dimensional L-shaped domain for adaptive meshes with $\theta = 0.5$ and $\omega = 10^{-3}$.

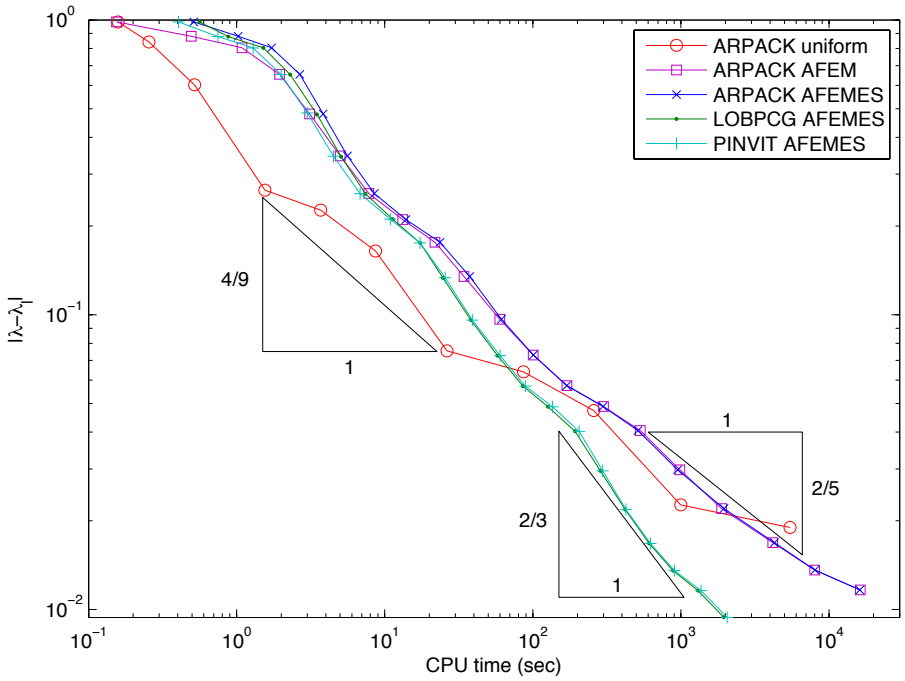

Figure 3.11: Eigenvalue errors for the first eigenvalue and different algebraic solvers on the L-shaped domain for P_1, $\theta = 0.5$ and $\omega = 10^{-3}$.

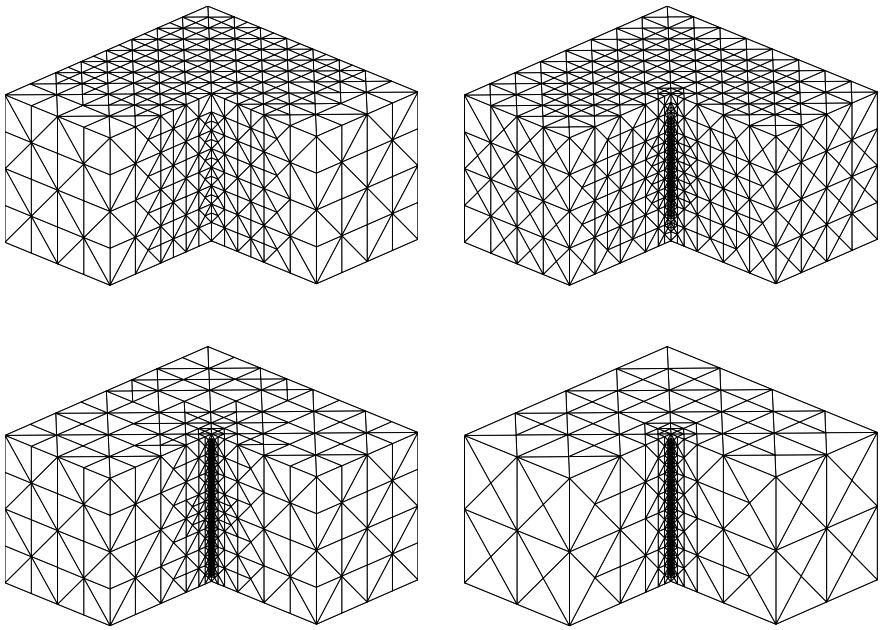

Figure 3.12: Adaptive refined meshes for P_k, $k = 1, 2, 3, 4$ (top left to bottom right), with about 3000 nodes.

tion of the approximation spaces involves only all possible isotropic and no anisotropic refinements. For isotropic refinement for domains with edges [5, Section 4.2] states the optimal relation $N_\ell \approx H_\ell^{-3}$ for linear P_1 and the suboptimal relations $N_\ell \approx H_\ell^{-3}|\ln H_\ell|$ for P_2, $N_\ell \approx H_\ell^{-2/9}$ for P_3 and $N_\ell \approx H_\ell^{-1/6}$ for P_4 finite elements. Therefore, isotropic meshes are not optimal for P_k, $k \geq 2$ and convergence rates of $\mathcal{O}(t_\ell^{-2/3})$ for P_1, rates slightly less that than $\mathcal{O}(t_\ell^{-4/3})$ for P_2 and rates of $\mathcal{O}(t_\ell^{-4/3})$ for P_3 and P_4 are the best possible for isotropic refinements. Figure 3.10 shows that the asymptotic quasi-optimal algorithm AFEMES with the PINVIT solver, $\theta = 0.5$ and $\omega = 10^{-3}$ leads to these rates and that the error estimator is reliable and efficient for P_k, $k = 1, \ldots, 4$.

The computational time for the complete AFEMES with linear finite elements is faster compared to one uniform solve with ARPACK as shown in Figure 3.11 for larger degrees of freedom. For smaller numbers of unknowns the computational costs for the assembly of the matrices and the calculation of the error estimator dominates and the convergence rate of ARPACK uniform is the best possible for uniform meshes but deteriorates for larger systems because of the computation of the matrix factorisations. Since the computational costs for the matrix factorisations get more severe for $n = 3$ and larger number of degrees of freedom, this example shows that ARPACK with matrix factorisations leads to suboptimal computational complexity even for adaptive refined meshes. The PINVIT and the LOBPCG solver with multigrid preconditioner lead to almost the same quasi-optimal complexity. Note that both graphs almost cover each other.

Different adaptive refined meshes for P_k, $k = 1, 2, 3, 4$, with about 3000 nodes are displayed in Figure 3.12. The meshes are strongly refined towards the edge singularity for the higher-order methods.

3.9 Software Implementation

The software implementation for the numerical experiments in MATLAB [90] follows the ideas of [3, 36] and in an enhanced way those of [56]. The basic data structures and refinement routines are described in [36, 56]. The present implementation makes use of the object oriented features introduced in MATLAB in the year 2008. The software directory with the software files used for the numerical experiments of this chapter is listed in Table 3.1.

`afemPkEllipticEigenvalue.m` is the main script that implements the AFEM loop and calls subroutines that execute the steps `Solve`, `Estimate`, `Mark` and `Refine`.

`estimatePkEigenvalue.m` computes the a posteriori error estimator

$$\eta_\ell^2(\lambda_\ell, u_\ell) := \sum_{T \in \mathcal{T}_\ell} |T| \|\lambda_\ell u_\ell + \operatorname{div}(p_\ell)\|_{L^2(T)}^2 + \sum_{E \in \mathcal{E}_\ell} |E|^{1/2} \|[p_\ell] \cdot \nu_E\|_{L^2(E)}^2.$$

`Mesh.m` is a class object that encapsulates all the data structures as described in [36, 56] and provides methods for marking-strategies, the closure algorithm and the mesh-refinement algorithms of Section 2.5.

```
|-- afemPkEllipticEigenvalue.m (main script)
|-- estimatePkEigenvalue.m
|-- Mesh.m
|-- solvePkLaplaceEigenvalue.m
|-- extern
|   |-- license.txt (GNU LGPL ver 2.1)
|   `-- lobpcg.m (Author: A. Knyazev)
|-- Geometries
|   `-- ... (several geometric data)
|-- Pk
|   |-- Pk.m
|   |-- PkEvaluate.m
|   |-- PkFunctionHandles.m
|   |-- PkInterpolation.m
|   `-- PkMatrix.m
`-- Tools
    |-- integrate.m
    |-- localDoFtoGlobalDoF.m
    |-- matMul.m
    |-- Multigrid.m
    `-- plotConvergence.m
```

Table 3.1: The software directory of Chapter 3.

`solvePkLaplaceEigenvalue.m` contains the software implementation of several algebraic eigenvalue solvers and the call of the MATLAB routine `eigs` that implements the ARPACK iterative eigenvalue solver [83]. The implementation of the PINVIT [78, 92] algorithm with the iteration formula for the Rayleigh-quotient $R(x) := \frac{x'Ax}{x'Bx}$, $x \in \mathbb{R}^N$,

$$x_\ell^{k+1} = x_\ell^k - T^{-1}(Ax_\ell^k - R(x_\ell^k)Bx_\ell^k),$$

is displayed in the following.

```
function [x,lambda,iter] = pinvit(x,A,B,tol,mg,dampMG)
  iter = 0;
  z = 0;
  e = 2*tol;
  while (e > tol)
    x = x - z;
    Ax = A*x;
    Bx = B*x;
    lambda = (x'*Ax)/(x'*Bx);
    r = Ax - lambda*Bx;
    z = mg.solve(r,0,[],dampMG,1,false);
    e = sqrt(2*r'*z);
    iter = iter + 1;
  end
end
```

The input consists in a initial non-zero coefficient vector `x`, the stiffness matrix `A`, the

mass matrix `B`, the desired tolerance `tol`, a multigrid preconditioner object `mg` and a damping factor for the Richardson iteration of the pre- and post-smoothing steps of the multigrid algorithm. The output is the coefficient vector `x`, the eigenvalue `lambda` and the number of iterations `iter`. Lines 2-4 are for initialisation of the iteration loop. The while-loop in lines 5-14 starts with the correction step with the correction `z` of the previous step. Lines 7-9 compute the Rayleigh-quotient. The residual is computed in line 10 and the multigrid preconditioner is applied to the residual vector in line 11. The error is estimated in line 12. The last step increments the iteration count in line 13.

The folder *extern* contains the MATLAB implementation of the LOBPCG eigenvalue solver by A. Knyazev [74].

The folder *Geometries* contains the geometric data for the initial coarse triangulations of the unit square, the L-shaped domain, the slit domain and the isospectral domains.

The folder *Pk* contains the implementation of the triangular Lagrange finite element of arbitrary degree $k > 0$. The finite element itself is encapsulated in the class object `Pk`. The file `PkEvaluate.m` implements methods for the evaluation of L^2 values or values of the gradient. More complicated functions like the evaluation of the volume residual and the edge jumps are contained in `PkFunctionHandles.m`. `PkInterpolation.m` provides methods to compute the prolongation matrix from one refinement level to the next one and `PkMatrix.m` provides methods for the fast assembly of the stiffness and mass matrices.

`integrate.m` implements an interface for numerical quadrature for 1-D and 2-D integrals based on Gauss-Legendre integration formulas of arbitrary degree. The 2-D version is based on a cross-product of the 1-D formulas and the Duffy-transformation [106]. For more detailed information on the implementation cf. [36].

`localDoFtoGlobalDoF.m` provides the mapping of the local degrees of freedom to the global enumeration of the degrees of freedom that is used for the global assembly from the local stiffness and/or mass matrices.

`matMul.m` is a function that expands the idea of the build in element-wise multiplication `.*` to an element-wise matrix-matrix multiplication. The first dimension is thereby the element number and the second and third the dimensions of the element-matrices. The key point is that for performance issues the implementation does not need any loop. Instead it uses one call of the build in function `bsxfun`. Altogether only four lines of code are necessary as displayed below.

```
16 permA = permute(A,[1 2 4 3]);
   permB = permute(B,[1 4 3 2]);
   val = bsxfun(@times,permA,permB);
   val = sum(val,4);
```

`Multigrid.m` is a class object that provides methods to solve linear systems of equations via the geometric V-cycle multigrid algorithm. In particular it stores the necessary matrices for all the levels. The key multigrid function is displayed below.

```
20 function x = MG(x,A,T,b,prolong,level,damp,L,U)
     if level == 1
       x = U\(L\b);
     else
       for k = 1:3
25       x = x - damp*T{level}*(A{level}*x - b);
       end
       defect = prolong{level-1}'*(b - A{level}*x);
       x0 = zeros(length(defect),1);
       correction = Multigrid.MG(x0,A,T,defect,prolong,level-1,damp,L,U);
30     x = x + prolong{level-1}*correction;
       for k = 1:3
         x = x - damp*T{level}*(A{level}*x - b);
       end
     end
35 end
```

The input is the initial vector `x`, the stiffness matrices for all levels `A`, the preconditioners `T`, which are the identity matrices for the Richardson iteration or the diagonal matrices with the inverse diagonal entries of `A` for the Jacobi iteration, the right hand side `b`, the prolongation matrices `prolong`, the current level `level`, the damping parameter `damp` and the LU-factorisation of the coarse level stiffness matrix A_1 into lower and upper triangular matrices `L` and `U`. On the coarsest level the system is solved via the LU-factorisation in lines 21-22. On higher levels an approximation of the solution of the linear system $Ax = b$ is obtained in three steps [23, 27].

1. The pre-smoothing step in lines 24-26 does three iterations of the Richardson or Jacobi iteration,
$$x_{k+1} = x_k - \omega T_\ell^{-1}(A_\ell x_k - b_\ell)$$
where ω is chosen such that $1/\omega$ provides an upper bound for the spectral radius of A for all levels ℓ.

2. The error correction step in lines 27-30 restricts the residual onto the coarser level, computes a correction via a recursive call of the multigrid function with zero initial guess and then adds the prolongated correction onto the pre-smoothed vector `x`.

3. The post-smooting step in lines 31-33 does again three iterations of the Richardson or Jacobi iteration.

`plotConvergence.m` is a function that helps plotting convergence graphs in a log-log scale.

4 Guaranteed Lower Bounds for Eigenvalues

This chapter introduces fully computable two-sided bounds on the eigenvalues of the Laplace operator on arbitrarily coarse meshes based on some approximation of the corresponding eigenfunction in the nonconforming Crouzeix-Raviart finite element space plus some postprocessing. The efficiency of the guaranteed error bounds involves the global mesh-size and is proven for the large class of graded meshes. Numerical examples demonstrate the reliability of the guaranteed error control even with inexact solve of the algebraic eigenvalue problem. This motivates an adaptive algorithm which monitors the discretisation error, the maximal mesh-size, and the algebraic eigenvalue error. The accuracy of the guaranteed eigenvalue bounds is surprisingly high with efficiency indices as small as 1.4.

This chapter is joint work with C. Carstensen and has been accepted for publication in [35].

4.1 Introduction

The well-established Rayleigh-Ritz principle for the algebraic as well as for the continuous eigenvalues of the Laplacian on a bounded polygonal Lipschitz domain Ω,

$$-\Delta u = \lambda u \quad \text{for } u \in V\backslash\{0\} := H^1_0(\Omega)\backslash\{0\}, \tag{4.1}$$

immediately results in *upper* bounds of the eigenvalues by Rayleigh quotients

$$\lambda_1 \leq R(v) := |||v|||^2/\|v\|^2 \quad \text{for any } v \in V\backslash\{0\}. \tag{4.2}$$

Although λ_1 in (4.2) denotes the first exact eigenvalue of (4.1), the well-established min-max principle [105, Section 6.1:(13)] applies to the higher eigenvalues $0 < \lambda_1 < \lambda_2 \leq \lambda_3 \leq \ldots$ Since *upper* bounds are easily obtained by conforming discretisations via (4.2), the computation of *lower* bounds is of high interest and we solely mention the mile-stones [7, 55, 110] for asymptotic lower bounds in the sense that they provide guaranteed bounds under the assumption that the global mesh-size is *sufficiently* small. Unfortunately, the minimal mesh-size required to deduce some guaranteed lower eigenvalue bound is *not* quantified in the current literature – so nobody knows whether some mesh allows some guaranteed bound or not. This chapter establishes *guaranteed lower bounds* even for very coarse triangulations like those of Figure 4.1 for the unit square $\Omega = (0,1)^2$ with only two triangles. For the three meshes of Figure 4.1, clearly in the pre-asymptotic range of convergence, Theorem 4.3.1 of this chapter provides the *guaranteed bounds*

$$2.3371 \leq \lambda_1 \leq 32, \quad 4.2594 \leq \lambda_1 \leq 24, \quad \text{and} \quad 6.6182 \leq \lambda_1 \leq 22.0397 \tag{4.3}$$

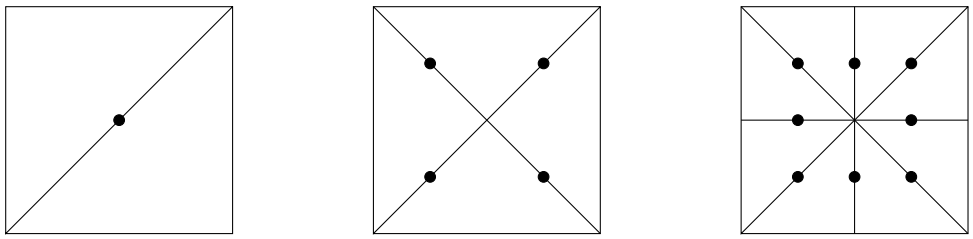

Figure 4.1: Criss (left), criss-cross (middle) and union-jack (right) triangulations of the unit square in 2, 4, and 8 congruent triangles.

for the first exact eigenvalue $\lambda_1 = 2\pi^2 = 19.7392$ despite the coarse discretisation with just 1, 4, or 8 degrees of freedom in a Crouzeix-Raviart nonconforming finite element discretisation (CR-NCFEM); cf. Example 4.3.7 and 4.3.10 below for more details.

To the best knowledge of the authors, any other a posteriori error control requires some (unquantified) sufficiently small global mesh size [33, 47, 50]; for an a priori error analysis see [10, 105]. The asymptotic convergence of the conforming FEM is presented in [33, 58, 60] and the asymptotic quasi-optimal convergence and complexity in Chapter 3 and [44, 45]. Recently, [71] proves asymptotic lower bounds of several nonconforming FEM and higher order elliptic operators. The main results of this chapter are by no means restricted to the present case and work for 3D as well as for biharmonic eigenvalue problems [32].

To describe the main results of this chapter, let $\mathcal{T}$ be an arbitrarily coarse shape-regular triangulation of the polygonal domain Ω into triangles with set $\mathcal{E}$ of edges and let

$$CR_0^1(\mathcal{T}) := \{v \in P_1(\mathcal{T}) \mid v \text{ is continuous at } \mathrm{mid}(\mathcal{E}) \text{ and } v = 0 \text{ at } \mathrm{mid}(\mathcal{E}(\partial\Omega))\}$$

denote the Crouzeix-Raviart nonconforming FEM spaces for the piecewise first-order polynomials $P_1(\mathcal{T}) := \{v \in L^2(\Omega) \mid \forall T \in \mathcal{T},\ v|_T \text{ is affine}\}$. The degrees of freedom for a triangle are depicted in Figure 2.2. Suppose that $(\tilde{\lambda}_{CR,1}, \tilde{u}_{CR,1}) \in \mathbb{R} \times CR_0^1(\mathcal{T})$ is some computed approximation of the smallest exact eigenvalue λ_1 of the associated algebraic eigenvalue problem with the stiffness matrix $\mathbf{A}$, the (diagonal) mass matrix $\mathbf{B}$, and the algebraic residual $\mathbf{r} := \mathbf{A}\tilde{\mathbf{u}}_{CR,1} - \tilde{\lambda}_{CR,1}\mathbf{B}\tilde{\mathbf{u}}_{CR,1}$ for the algebraic eigenvector $\tilde{\mathbf{u}}_{CR,1}$. Suppose that the first approximated discrete eigenvalue $\tilde{\lambda}_{CR,1}$ is closer to the first discrete eigenvalue $\lambda_{CR,1}$ than to the second discrete eigenvalue (which has to be guaranteed by algebraic eigenvalue analysis) and that $\|\mathbf{r}\|_{\mathbf{B}^{-1}} < \tilde{\lambda}_{CR,1}$. The numerical experiments of Section 4.6 show that for the simple first eigenvalue the algebraic separation condition is not critical, but cluster of eigenvalues may lead to difficulties with this separation condition on the level of the algebraic eigensolve. The first main result, in Theorem 4.3.1 below, implies

$$\frac{\tilde{\lambda}_{CR,1} - \|\mathbf{r}\|_{\mathbf{B}^{-1}}}{1 + \kappa^2(\tilde{\lambda}_{CR,1} - \|\mathbf{r}\|_{\mathbf{B}^{-1}})H^2} \leq \lambda_1 \leq R(\mathcal{I}_{CM}\tilde{u}_{CR,1}).$$

Since $\tilde{\lambda}_{CR,1}$ is the nearest approximation to $\lambda_{CR,1}$, the algebraic residual $\mathbf{r}$ yields an upper bound for the discrete eigenvalue error in Lemma 4.3.8. Moreover, $\mathcal{I}_{CM}$ denotes the interpolation operator of Section 4.3 which ensures $\mathcal{I}_{CM}\tilde{u}_{CR,1} \not\equiv 0$ to define the Rayleigh quotient and $H := \max_{T\in\mathcal{T}} \operatorname{diam}(T)$ denotes the maximal mesh-size. The explicit constant κ reads $\kappa^2 := (1/8 + j_{1,1}^{-2}) \leq 0.1932$ for the first positive root $j_{1,1}$ of the Bessel function of the first kind.

Note that the nonconforming eigenvalue for the first two meshes of Figure 4.1 reads $\lambda_{CR,1} = 24$ and is larger than the solution $\lambda = 2\pi^2$. This novel observation shows that the nonconforming eigenvalue by itself does *not* always provide some lower bound for arbitrary coarse meshes in contrast to the lower bound given in this chapter. The asymptotic a posteriori error control of [7] does not provide those error bounds.

The second main result, Theorem 4.4.1, guarantees efficiency in the sense that the difference of the upper and lower bound is bounded by the error for the large class of graded meshes.

The lower bound is generalised to higher eigenvalues under some explicit given mesh-size restriction plus the aforementioned separation condition. Together with a conforming approximation for an upper bound, the bounds for the higher eigenvalues are also efficient.

The efficiency for graded meshes motivates the development of an adaptive algorithm that balances the finite element error and the global mesh size H in order to reduce the difference of the upper and lower eigenvalue bounds.

The remaining parts of this chapter are organised as follows. Section 4.2 presents the model problem (4.1) and the necessary notation. Section 4.3 proves the explicit lower and upper bounds for the smallest eigenvalue based on the nonconforming discrete eigenvalue as well as on its approximation. The efficiency of the resulting a posteriori error estimator follows in Section 4.4. Section 4.5 establishes some bounds for higher eigenvalues and their efficiency. Section 4.6 presents some adaptive algorithm which monitors the discretisation error, the maximal mesh-size, and the algebraic eigenvalue error and verifies the theoretical results in some numerical experiments. An empirical comparison of conforming and nonconforming discretisations is included as well. Since the consistent mass matrix is diagonal, nonconforming discretisations are of particular attraction in practise.

4.2 Notation and Preliminaries

Consider the weak formulation of the eigenvalue problem given in Section 2.3 with bilinear forms $a(\cdot,\cdot)$ and $b(\cdot,\cdot)$ that induce the norms $|||.||| := |.|_{H^1(\Omega)}$ on $V := H_0^1(\Omega)$ and $\|.\| := \|.\|_{L^2(\Omega)}$ on $L^2(\Omega)$. Section 4.3 focuses on the computation of the first eigenvalue λ_1 which is simple [52, Section 6.5, Theorem 2]. The min-max principle [105, Section 6.1:(13)] reduces for the smallest eigenvalue to

$$\lambda_1 = \min_{v\in V\setminus\{0\}} R(v) \quad \text{with the Rayleigh quotient} \quad R(v) := a(v,v)/b(v,v).$$

Let $\mathcal{T}$ be a *regular triangulation* as in Section 2.5. Let $\mathcal{E}$ denote the set of all edges ($\mathcal{E}(\Omega)$ of interior edges) of the triangulation $\mathcal{T}$, let $\mathrm{mid}(E)$ be the midpoint and h_E the length of an edge $E \in \mathcal{E}$. Let $h_T := \mathrm{diam}(T)$, $H := \max_{T\in\mathcal{T}} h_T$ and $h_{\mathcal{T}} \in P_0(\mathcal{T})$ piecewise defined as $h_{\mathcal{T}}|_T = h_T$. Let $[\cdot]_E := (\cdot)|_{T_+} - (\cdot)|_{T_-}$ denote the jump across an interior edge $E \in \mathcal{E}(\Omega)$ with $E = T_+ \cap T_-$, $T_\pm \in \mathcal{T}$, and $[\cdot]_E := (\cdot)$ for $E \subset \partial\Omega$. Let $\mathcal{N}$ denote the set of all nodes ($\mathcal{N}(\Omega)$ of interior nodes) in the triangulation $\mathcal{T}$.

The conforming finite element space is defined by $V_C(\mathcal{T}) := H^1_0(\Omega) \cap P_1(\mathcal{T})$. In the following let Π_0 denote the L^2 projection onto piecewise constants $P_0(\mathcal{T})$ as well as $P_0(\mathcal{T};\mathbb{R}^n)$.

Consider the discrete nonconforming eigenvalue problem of Subsection 2.3.2 with the Crouzeix-Raviart nonconforming finite element space $CR^1_0(\mathcal{T})$.

The nonconforming bilinear form a_{NC},

$$a_{NC}(u_{CR}, v_{CR}) := \sum_{T\in\mathcal{T}} \int_T \nabla u_{CR} \cdot \nabla v_{CR}\, dx \quad \text{for all } u_{CR}, v_{CR} \in CR^1_0(\mathcal{T}),$$

induces the mesh-dependent norm $|||.|||_{NC} := a_{NC}(\cdot,\cdot)^{1/2}$ and the Rayleigh-quotient

$$R_{NC}(v_{CR}) := a_{NC}(v_{CR}, v_{CR})/\|v_{CR}\|^2 \quad \text{for all } v_{CR} \in CR^1_0(\mathcal{T})\backslash\{0\}.$$

The nonconforming interpolant $\mathcal{I}_{NC} : V \to CR^1_0(\mathcal{T})$ is defined for any $v \in V$ by

$$\mathcal{I}_{NC} v(\mathrm{mid}(E)) := \frac{1}{|E|}\int_E v\, ds \quad \text{for all } E \in \mathcal{E}.$$

The proof of the L^2 error estimate below is essentially contained in [39]; we present the main arguments of the proof for completeness.

Theorem 4.2.1 (L^2 interpolation error estimate [39])**.** *Any $v \in H^1_0(\Omega)$ satisfies for $\kappa^2 = (1/8 + j_{1,1}^{-2})$*

$$\|v - \mathcal{I}_{NC} v\| \le \kappa H |||v - \mathcal{I}_{NC} v|||_{NC}.$$

Proof. The proof reduces to the corresponding estimate on a single triangle T. Let $f \in H^1(T)$ satisfy $\int_E f\mathrm{ds} = 0$ on the triangle $T = \mathrm{conv}(\{P\}\cup E)$ with an edge E opposite to the vertex P. Then it remains to prove for the first positive root $j_{1,1} = 3.8317059702$ of the Bessel function J_1 of the first kind that

$$\|f\|_{L^2(T)} \le \sqrt{\max_{x\in E} |P-x|^2/8 + h_T^2/j_{1,1}^2}\; |f|_{H^1(T)}. \tag{4.4}$$

The theorem of Pythagoras for $a := f - \fint_T f(x)dx$ and $b := \fint_T f(x)dx$ reads

$$\|f\|^2_{L^2(T)} = \|a+b\|^2_{L^2(T)} = \|a\|^2_{L^2(T)} + \|b\|^2_{L^2(T)}.$$

The Poincaré inequality [82] gives

$$\|a\|_{L^2(T)} = \Big\|f - \fint_T f(x)dx\Big\|_{L^2(T)} \leq h_T/j_{1,1}\,|f|_{H^1(T)}.$$

The trace identity [39, Lemma 2.1] (from an integration by parts) reads

$$\fint_E f\,ds - \fint_T f\,dx = \frac{1}{2}\fint_T (x-P)\cdot\nabla f(x)\,dx.$$

Since $\fint_E f\,ds = 0$ this leads to ($\bullet$ abbreviates identity)

$$|T||b| = \Big|\int_T f(x)\,dx\Big| = \frac{1}{2}\Big|\int_T (x-P)\cdot\nabla f(x)\,dx\Big| \leq \frac{1}{2}\|\bullet - P\|_{L^2(T)}|f|_{H^1(T)}.$$

With polar coordinates (r,φ) and the notation for $|x-P| =: r$ and $\alpha < \varphi < \beta$ with some distance $0 < \delta(\varphi) \leq \max_{x\in E}|P-x|$ of P to E elementary calculations yield

$$\begin{aligned}\|x-P\|^2_{L^2(T)} &= \int_\alpha^\beta \int_0^{\delta(\varphi)} r^2 r\,dr d\varphi = \int_\alpha^\beta \delta(\varphi)^4/4\,d\varphi \\ &\leq \max_{x\in E}|P-x|^2/2 \int_\alpha^\beta \int_0^{\delta(\varphi)} r\,dr d\varphi = |T|\max_{x\in E}|P-x|^2/2\,.\end{aligned}$$

This results in the bound

$$|b| = \Big|\fint_T f(x)\,dx\Big| \leq 2^{-3/2}|T|^{-1/2}\max_{x\in E}|P-x||f|_{H^1(T)}.$$

The preceding two estimates control the two terms a and b of the above Pythagoras identity and so conclude the proof of (4.4); indeed,

$$\begin{aligned}||f||^2_{L^2(T)} &\leq h_T^2/j_{1,1}^2\,|f|^2_{H^1(T)} + \max_{x\in E}|P-x|^2/8\,|f|^2_{H^1(T)} \\ &= \left(\max_{x\in E}|P-x|^2/8 + h_T^2/j_{1,1}^2\right)\,|f|^2_{H^1(T)}.\end{aligned}$$ □

4.3 Explicit Bounds for the Smallest Eigenvalue

This section is devoted to the proof of the explicit bounds for the first eigenvalue λ_1. Recall that H is the maximal diameter in the triangulation $\mathcal{T}$ and that $\kappa^2 = (1/8 + j_{1,1}^{-2})$ is the constant from Theorem 4.2.1.

Theorem 4.3.1. *Let $(\tilde\lambda_{CR,1}, \tilde u_{CR,1}) \in \mathbb{R}\times CR^1_0(\mathcal{T})$ be an approximation of the eigenpair (λ_1, u_1) of the smallest eigenvalue with $\|\tilde u_{CR,1}\|_{L^2(\Omega)} = 1$ and with algebraic residual $\mathbf{r} := \mathbf{A}\tilde{\mathbf{u}}_{CR,1} - \tilde\lambda_{CR,1}\mathbf{B}\tilde{\mathbf{u}}_{CR,1}$ and let $\mathcal{I}_{CM}\tilde u_{CR,1}$ be the quasi-interpolant of $\tilde u_{CR,1}$ from Definition 4.3.3 below. Suppose separation of $\tilde\lambda_{CR,1}$ from the remaining discrete spectrum in the sense that $\tilde\lambda_{CR,1}$ is closer to the smallest discrete eigenvalue $\lambda_{CR,1}$ than to any*

other discrete eigenvalue and suppose that $\|\mathbf{r}\|_{\mathbf{B}^{-1}} < \tilde{\lambda}_{CR,1}$. *Then it holds that*

$$\frac{\tilde{\lambda}_{CR,1} - \|\mathbf{r}\|_{\mathbf{B}^{-1}}}{1 + \kappa^2(\tilde{\lambda}_{CR,1} - \|\mathbf{r}\|_{\mathbf{B}^{-1}})H^2} \leq \lambda_1 \leq R(\mathcal{I}_{CM}\tilde{u}_{CR,1}).$$

The remaining part of this section is devoted to the proof of Theorem 4.3.1. The point of departure is the particular case of exact solve.

Theorem 4.3.2 (Lower bound for exact solve)**.** *The first exact eigenvalue* λ_1 *and the first discrete eigenvalue* $\lambda_{CR,1}$ *satisfy*

$$\frac{\lambda_{CR,1}}{1 + \kappa^2\lambda_{CR,1}H^2} \leq \lambda_1.$$

Proof. The Pythagoras theorem in $L^2(\Omega;\mathbb{R}^2)$ reads

$$\lambda_1 = a(u_1,u_1) = \|\nabla u_1\|^2 = \|\nabla u_1 - \Pi_0\nabla u_1\|^2 + \|\Pi_0\nabla u_1\|^2.$$

An integration by parts on one triangle $T \in \mathcal{T}$ and $\int_E (v - \mathcal{I}_{NC}v)\,ds = 0$, for all $v \in V$ and $E \in \mathcal{E}$, show

$$\begin{aligned}|T|\Pi_0\nabla v|_T &= \int_T \nabla v\,dx = \int_{\partial T} v\nu_T\,ds \\ &= \int_{\partial T} (\mathcal{I}_{NC}v)\nu_T\,ds = \int_T \nabla(\mathcal{I}_{NC}v)\,dx = |T|\nabla(\mathcal{I}_{NC}v|_T).\end{aligned}$$

This proves the known identity for the piecewise defined gradient $(\nabla_{NC}\cdot)|_T := \nabla(\cdot|_T)$

$$\Pi_0\nabla v = \nabla_{NC}(\mathcal{I}_{NC}v). \tag{4.5}$$

The combination with the aforementioned Pythagoras identity reads

$$\lambda_1 = |\!|\!| u_1 - \mathcal{I}_{NC}u_1 |\!|\!|_{NC}^2 + |\!|\!| \mathcal{I}_{NC}u_1 |\!|\!|_{NC}^2.$$

The min-max principle [105, Section 6.1:(13)] on the discrete eigenvalue problem allows the estimate

$$\lambda_{CR,1}\|\mathcal{I}_{NC}u_1\|^2 \leq |\!|\!| \mathcal{I}_{NC}u_1 |\!|\!|_{NC}^2.$$

The combination of the previous results leads to

$$|\!|\!| u_1 - \mathcal{I}_{NC}u_1 |\!|\!|_{NC}^2 + \lambda_{CR,1}\|\mathcal{I}_{NC}u_1\|^2 \leq \lambda_1. \tag{4.6}$$

Some elementary algebra based on $\|u_1\| = 1$ and the binomial expansion yield

$$\begin{aligned}1 + \|u_1 - \mathcal{I}_{NC}u_1\|^2 - 2\|u_1 - \mathcal{I}_{NC}u_1\| \\ \leq 1 + \|u_1 - \mathcal{I}_{NC}u_1\|^2 - 2b(u_1 - \mathcal{I}_{NC}u_1, u_1) = \|\mathcal{I}_{NC}u_1\|^2.\end{aligned}$$

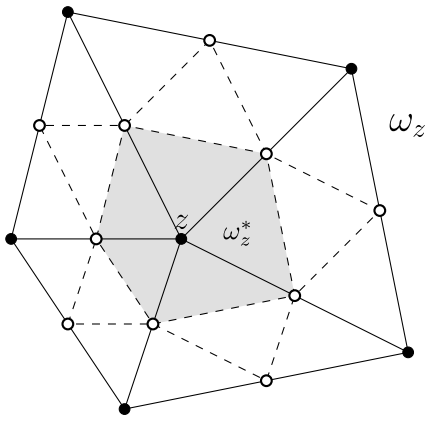

Figure 4.2: Patch ω_z of $\mathcal{T}$ (solid lines) with refined patch ω_z^* (grey) of the sub-triangulation $\mathcal{T}^* := \mathrm{red}(\mathcal{T})$ (solid and dashed lines).

Set $s = \alpha/(1+\alpha)$ with $\alpha := \kappa^2 H^2 \lambda_{CR,1}$. This results in

$$1 + \|u_1 - \mathcal{I}_{NC}u_1\|^2 - 2s\|u_1 - \mathcal{I}_{NC}u_1\| - 2(1-s)\|u_1 - \mathcal{I}_{NC}u_1\| \leq \|\mathcal{I}_{NC}u_1\|^2.$$

The Young inequality $2s\|u_1 - \mathcal{I}_{NC}u_1\| \leq s^2 + \|u_1 - \mathcal{I}_{NC}u_1\|^2$ leads to

$$1 - s^2 - 2(1-s)\|u_1 - \mathcal{I}_{NC}u_1\| \leq \|\mathcal{I}_{NC}u_1\|^2.$$

The a priori estimate of Theorem 4.2.1 plus another Young inequality [52]

$$2\|\!|u_1 - \mathcal{I}_{NC}u_1|\!\|_{NC} \leq t + \|\!|u_1 - \mathcal{I}_{NC}u_1|\!\|_{NC}^2/t$$

for $t := (1-s)\kappa H \lambda_{CR,1} > 0$ result in

$$1 - s^2 - (1-s)^2 H^2 \kappa^2 \lambda_{CR,1} - \|\!|u_1 - \mathcal{I}_{NC}u_1|\!\|_{NC}^2/\lambda_{CR,1} \leq \|\mathcal{I}_{NC}u_1\|^2. \tag{4.7}$$

The combination of (4.6)-(4.7) proves

$$\lambda_{CR,1}\left((1-s^2) - \left((1-s)\kappa H\right)^2 \lambda_{CR,1}\right) \leq \lambda_1.$$

This and the definition of s lead to

$$\frac{\lambda_{CR,1}}{1 + \kappa^2 H^2 \lambda_{CR,1}} \leq \lambda_1. \qquad \square$$

For the analysis of an upper bound, notice that the min-max principle [105, Section 6.1:(13)] for the smallest eigenvalue shows

$$\lambda_1 = \min_{v \in V\backslash\{0\}} R(v) \leq R(w) \quad \text{for any } w \in V_C(\mathcal{T})\backslash\{0\}.$$

Thus, any conforming approximation close to the nonconforming eigenfunction provides

a guaranteed upper bound. The post-processing of [40] provides such a sufficiently accurate conforming interpolation $\mathcal{I}_{CM} : CR_0^1(\mathcal{T}) \to V_C(\mathcal{T}^*)$ for the red-refined triangulation $\mathcal{T}^* := \mathrm{red}(\mathcal{T})$ of $\mathcal{T}$ into triangles depicted in Figure 4.2. (The red-refined triangulation $\mathrm{red}(\mathcal{T})$ results from dividing each triangle in $\mathcal{T}$ into 4 congruent sub-triangles by connecting the midpoints of the edges by straight lines.)

Definition 4.3.3. *For all nodes z in the red-refined triangulation $\mathcal{T}^* = red(\mathcal{T})$ and $v_{CR} \in CR_0^1(\mathcal{T})$, set*

$$\mathcal{I}_{CM} v_{CR}(z) := \begin{cases} 0 & \text{if } z \text{ lies on the boundary } \partial\Omega, \\ v_{CR}(z) & \text{if } z \text{ is the midpoint of an edge } E \in \mathcal{E}(\Omega), \\ v_{min}(z) & \text{if } z \in \mathcal{N}(\Omega), \end{cases}$$

where the average $v_{min}(z)$ in the interior node $z \in \mathcal{N}(\Omega)$ in the coarse triangulation $\mathcal{T}$ is determined locally on nodal patches ω_z^* covered by the triangles $\mathcal{T}^*(z) := \{T \in \mathcal{T}^* \mid z \in \mathcal{N}(T)\}$ of the red-refined triangulation $\mathcal{T}^*$ of Figure 4.2. Let

$$W_z := \{w \in P_1(\mathcal{T}^*(z)) \cap C(\overline{\omega}_z^*) \mid w = v_{CR} \text{ on } \partial\omega_z^*\}$$

denote the one-dimensional piecewise affine space of continuous functions on ω_z^* with prescribed boundary values on $\partial\omega_z^*$. The function v_{min} in W_z is the unique minimizer of

$$\min_{w \in W_z} \sum_{T \in \mathcal{T}^*(z)} \|\nabla(v_{CR} - w)\|^2_{L^2(T)}. \tag{4.8}$$

Lemma 4.3.4. *Any Crouzeix-Raviart function $v_{CR} \in CR_0^1(\mathcal{T})$ with its jump of the tangential derivative $[\partial v_{CR}/\partial s]_E$ across an edge E satisfies*

$$|||v_{CR} - \mathcal{I}_{CM} v_{CR}|||^2_{NC} \lesssim \sum_{E \in \mathcal{E}} h_E \|[\partial v_{CR}/\partial s]_E\|^2_{L^2(E)} \lesssim \min_{v \in V} |||v_{CR} - v|||^2_{NC}.$$

Proof. The design of the interpolant $\mathcal{I}_{CM}$ shows that $\|\nabla(v_{CR} - \mathcal{I}_{CM} v_{CR})\|^2_{L^2(T_4)} = 0$ for those centred triangles $T_4 \in \mathcal{T}^*$ with all three nodes of T_4 as midpoints of edges in the coarse triangulation $\mathcal{T}$. Let $z \in N$ denote some node of $\mathcal{T}$ and set $\mathcal{E}^*(z) := \{F \in \mathcal{E}^* \mid z \in N^*(F)\}$ for the smaller edges in the patch ω_z^* which share z in the red-refined triangulation $\mathcal{T}^*$ of Figure 4.2. Consider the two semi-norms ρ_1 and ρ_2 defined, for all $v_{CR} \in CR_0^1(\mathcal{T})|_{\omega_z^*} := \{v_{CR}|_{\omega_z^*} : v_{CR} \in CR_0^1(\mathcal{T})\}$, by

$$\rho_1(v_{CR}) := \|\nabla(v_{CR} - \mathcal{I}_{CM} v_{CR})\|_{L^2(\omega_z^*)} \quad \text{and} \quad \rho_2(v_{CR})^2 := \sum_{F \in \mathcal{E}^*(z)} h_F \|[\partial v_{CR}/\partial s]_F\|^2_{L^2(F)}.$$

In the first step one shows for some constant $C(z)$ that

$$\rho_1(v_{CR}) \le C(z) \rho_2(v_{CR}) \quad \text{for all } v_{CR} \in CR_0^1(\mathcal{T})|_{\omega_z^*}. \tag{4.9}$$

To do so, suppose that $\rho_2(v_{CR}) = 0$. Then it holds that $v_{CR}|_{\omega_z^*} \in C(\omega_z^*) \cap P_1(\omega_z^*)$. For an interior node z, it follows $(\mathcal{I}_{CM} v_{CR})(z) = v_{CR}(z)$ and so $\rho_1(v_{CR}) = 0$. For a

boundary node z, $\rho_2(v_{CR}) = 0$ implies $h_F \|\partial v_{CR}/\partial s\|^2_{L^2(F)} = 0$ and so v_{CR} vanishes along $F \in \mathcal{E}^*(z)$ with $F \subset \partial\Omega$. This implies $\mathcal{I}_{CM} v_{CR}(z) = 0$ and so $\rho_1(v_{CR}) = 0$. Hence, in either case $\rho_2(v_{CR}) = 0$ implies $\rho_1(v_{CR}) = 0$. The equivalence-of-norms argument on the finite-dimensional vector space $CR^1_0(\mathcal{T})|_{\omega_z^*}$ proves (4.9) with some constant $C(z)$.

The second step verifies that $C(z) \lesssim 1$ with a scaling argument for the finite element basis functions [108], $\nabla\varphi \approx 1/h$.

In step three, the sum of all estimates (4.9) and the fact that v_{CR} equals $\mathcal{I}_{CM} v_{CR}$ on all centred triangles in the red-refinement $\mathcal{T}^*$, show

$$\begin{aligned}\|\!| v_{CR} - \mathcal{I}_{CM} v_{CR} |\!\|^2_{NC} &= \sum_{z\in N} \|\nabla(v_{CR} - \mathcal{I}_{CM} v_{CR})\|^2_{L^2(\omega_z^*)} \\ &\leq \Big(\max_{z\in N} C(z)\Big) \sum_{E\in\mathcal{E}} h_E \|[\partial v_{CR}/\partial s]_E\|^2_{L^2(E)}.\end{aligned}$$

This concludes the proof of the first inequality.

The second inequality

$$\sum_{E\in\mathcal{E}} h_E \|[\partial v_{CR}/\partial s]_E\|^2_{L^2(E)} \lesssim \min_{v\in V} \|\!| v_{CR} - v |\!\|^2_{NC}$$

can be found in the context of efficiency of a posteriori error estimates for nonconforming schemes [31, 46]. □

Lemma 4.3.5. *$\mathcal{I}_{CM} : CR^1_0(\mathcal{T}) \to P_1(\mathcal{T}^*) \cap C_0(\Omega)$ is linear and uniformly bounded in the sense that*

$$\|\mathcal{I}_{CM}\| := \sup_{v_{CR}\in CR^1_0(\mathcal{T})\setminus\{0\}} \|\!| \mathcal{I}_{CM} v_{CR} |\!\| / \|\!| v_{CR} |\!\|_{NC} \lesssim 1.$$

Proof. The critical value $v_{min}(z)$ of the minimising function $v_{min} \in P_1(\mathcal{T}^*(z))$ of (4.8) for an interior node $z \in \mathcal{N}(\Omega)$ is computed from the one-dimensional linear equation

$$\sum_{T\in\mathcal{T}^*(z)} \int_T \nabla\varphi_z^* \cdot \nabla(v_{min} - v_{CR}) dx = 0$$

for the piecewise affine nodal basis function φ_z^* associated with the node $z \in \mathcal{N}^*$ in the refined triangulation $\mathcal{T}^*$, obtained from the optimality condition for the minimising function (4.8) with respect to the variable $v_{min}(z)$. (This follows from the implementation of the boundary values on $\partial\omega_z^*$ and the ansatz of the remaining $v_{min}(z)\varphi_z^*$.) This design shows that $\mathcal{I}_{CM} : CR^1_0(\mathcal{T}) \to P_1(\mathcal{T}^*) \cap C_0(\Omega)$ is a linear operator. Lemma 4.3.4 plus some triangle inequality shows the boundedness of $\mathcal{I}_{CM}$: Indeed, any $v_{CR} \in CR^1_0(\mathcal{T})$ satisfies

$$\begin{aligned}\|\!| \mathcal{I}_{CM} v_{CR} |\!\| &\leq \|\!| v_{CR} - \mathcal{I}_{CM} v_{CR} |\!\|_{NC} + \|\!| v_{CR} |\!\|_{NC} \\ &\lesssim \min_{v\in V} \|\!| v_{CR} - v |\!\|_{NC} + \|\!| v_{CR} |\!\|_{NC} \lesssim \|\!| v_{CR} |\!\|_{NC}.\end{aligned}$$ □

Lemma 4.3.6 (Upper bound)**.** *The conforming interpolation $\mathcal{I}_{CM}v_{CR} \in V_C(\mathcal{T}^*)$ of any nonconforming function $v_{CR} \in CR_0^1(\mathcal{T})$, which is normalised by $\|v_{CR}\| = 1$, satisfies*

$$\lambda_1 \leq R(\mathcal{I}_{CM}v_{CR}).$$

Proof. Since $\|v_{CR}\| = 1$, $(\mathcal{I}_{CM}v_{CR})(\mathrm{mid}(E)) = v_{CR}(\mathrm{mid}(E)) \neq 0$ for at least one edge $E \in \mathcal{E}$. Hence, $\mathcal{I}_{CM}v_{CR} \not\equiv 0$. Therefore, the assertion follows immediately from the continuous Rayleigh-Ritz principle [105, Section 6.1:(13)] without any extra condition. □

Example 4.3.7. For the three triangulations of the unit square $\Omega = (0,1)^2$ depicted in Figure 4.1, the first exact eigenvalue reads $\lambda_1 = 2\pi^2 = 19.7392$ and is smaller than the first discrete conforming eigenvalue $\lambda_{C,1} = 24$ from the related one-dimensional algebraic eigenvalue problem for the criss-cross and the union-jack triangulations. The criss and the criss-cross triangulations of Figure 4.1 lead to the discrete nonconforming eigenvalue $\lambda_{CR,1} = 24$. The nonconforming eigenvalue approximation of the smallest eigenvalue for the union-jack triangulation reads $\lambda_{CR,1} = 18.3344$ up to some truncation error of finite machine precision from the iterative algebraic eigenvalue solver and is empirically below the exact eigenvalue. Theorem 4.3.1 leads to the guaranteed error bounds (4.3). Note that for the union-jack pattern, the proposed conforming interpolation on the red-refined triangulation $\mathcal{T}^*$ provides an upper bound which is strictly smaller than the conforming eigenvalue $\lambda_{C,1} = 24$ for the coarse mesh $\mathcal{T}$.

Since the algebraic eigenvalue problems are solved iteratively, the algebraic eigenvalue error has to be considered as well. The algebraic eigenvalue problem reads

$$\mathbf{A}\mathbf{u}_{CR} = \lambda_{CR}\mathbf{B}\mathbf{u}_{CR}$$

for the coefficient vector $\mathbf{u}_{CR} \equiv (u_{CR}(\mathrm{mid}(E)) : E \in \mathcal{E}(\Omega))$ of the discrete solution

$$u_{CR} = \sum_{E \in \mathcal{E}(\Omega)} \mathbf{u}_{CR}(E)\psi_E$$

for the edge-oriented basis $(\psi_E \,|\, E \in \mathcal{E}(\Omega))$ of $CR_0^1(\mathcal{T})$. Set $\|\mathbf{x}\|_M := \sqrt{\mathbf{x}^T M \mathbf{x}}$ for some SPD matrix M.

Lemma 4.3.8 ([94, Theorem 15.9.1])**.** *Let $(\tilde{\lambda}_{CR}, \tilde{\mathbf{u}}_{CR})$ be an approximated algebraic eigenpair such that $\tilde{\lambda}_{CR}$ is closer to some λ_{CR} than to any other discrete eigenvalue. Suppose that the coefficient vector $\tilde{\mathbf{u}}_{CR}$ is normalised with respect to $\mathbf{B}$, $\|\mathbf{B}\tilde{\mathbf{u}}_{CR}\|_{\mathbf{B}^{-1}} = \|\tilde{\mathbf{u}}_{CR}\|_{\mathbf{B}} = 1$. Then the algebraic residual $\mathbf{r} := \mathbf{A}\tilde{\mathbf{u}}_{CR} - \tilde{\lambda}_{CR}\mathbf{B}\tilde{\mathbf{u}}_{CR}$ satisfies*

$$|\lambda_{CR} - \tilde{\lambda}_{CR}| \leq \|\mathbf{r}\|_{\mathbf{B}^{-1}}. \quad \square$$

Remark 4.3.9. The local mass matrix of the CR-NCFEM for some $T \in \mathcal{T}$ equals $|T|/3$ times the 3×3 identity matrix $I_{3\times 3}$. Hence, the global mass matrix $\mathbf{B}$ is diagonal and the residual norm $\|\mathbf{r}\|_{\mathbf{B}^{-1}}$ of the error bound is directly computable.

Proof of Theorem 4.3.1. Lemma 4.3.8 and the monotonicity of $t/(1+\kappa^2 H^2 t)$ in $t > 0$ allows to formally replace $\lambda_{CR,1}$ in Theorem 4.3.2 with $\tilde{\lambda}_{CR,1} - \|\mathbf{r}\|_{\mathbf{B}^{-1}}$ for $\tilde{\lambda}_{CR,1} > \|\mathbf{r}\|_{\mathbf{B}^{-1}}$ which proves the lower bound. The upper bound is proven in Lemma 4.3.6. □

Example 4.3.10. Since the iterative solution of the underlying discrete algebraic eigenvalue problem dominates the overall computational costs in general, the truncation error in the iterative solution may be much larger than machine precision. For example, the Rayleigh-quotient for the starting vector $(1,\dots,1) \in \mathbb{R}^8$ of the union-jack triangulation of Figure 4.1 (discussed also in Example 4.3.7) yields the nonconforming eigenvalue approximation $\tilde{\lambda}_{CR,1} = 24$ and the corresponding guaranteed bounds

$$6.9360 \leq \lambda_1 \leq 24.$$

This is competitive with the bounds (4.3) from much more expensive eigenvalue computations.

4.4 Efficiency for Graded Meshes

This section is devoted to the efficiency of the eigenvalue estimate of Theorem 4.3.1 with the difference of its upper and lower bounds

$$\eta := R(\mathcal{I}_{CM}\tilde{u}_{CR,1}) - \frac{\tilde{\lambda}_{CR,1} - \|\mathbf{r}\|_{\mathbf{B}^{-1}}}{1+\kappa^2(\tilde{\lambda}_{CR,1} - \|\mathbf{r}\|_{\mathbf{B}^{-1}})H^2}. \tag{4.10}$$

Efficiency means that this length η of the interval is bounded in terms of the error and will be proven in the following for the class of graded meshes. (Graded meshes will be defined in the second half of this section.)

Theorem 4.4.1. *For all graded meshes the estimate of Theorem 4.3.1 is efficient in the sense that the difference η of the upper and lower bounds satisfies*

$$\begin{aligned}\eta \lesssim{}& (1+H^2\tilde{\lambda}_{CR,1})|||u_1 - \tilde{u}_{CR,1}|||_{NC}^2 + H^2\left((\lambda_1 - \lambda_{CR,1})^2 + \lambda_1\lambda_{CR,1}\|u_1 - u_{CR,1}\|^2\right)\\ &+ |\lambda_1 - \tilde{\lambda}_{CR,1}| + \|\mathbf{A}(\mathbf{u}_{CR,1} - \tilde{\mathbf{u}}_{CR,1})\|_{\mathbf{B}^{-1}} + \lambda_{CR,1}\|u_{CR,1} - \tilde{u}_{CR,1}\| + |\lambda_{CR,1} - \tilde{\lambda}_{CR,1}|.\end{aligned}$$

The remaining parts of this section are devoted to the proof of Theorem 4.4.1. The first results hold on arbitrary shape-regular meshes.

Lemma 4.4.2. *The difference η from* (4.10) *of the lower and upper eigenvalue bounds satisfies*

$$\begin{aligned}\eta \lesssim{}& (1+H^2\tilde{\lambda}_{CR,1})|||u_1 - \tilde{u}_{CR,1}|||_{NC}^2 + |\lambda_1 - \tilde{\lambda}_{CR,1}| + \tilde{\lambda}_{CR,1}^2 H^2\\ &+ \|\mathbf{A}(\mathbf{u}_{CR,1} - \tilde{\mathbf{u}}_{CR,1})\|_{\mathbf{B}^{-1}} + \lambda_{CR,1}\|u_{CR,1} - \tilde{u}_{CR,1}\| + |\lambda_{CR,1} - \tilde{\lambda}_{CR,1}|.\end{aligned}$$

Proof. Some preliminary manipulations in step one of this proof show

$$\begin{aligned}\eta &= R(\mathcal{I}_{CM}\tilde{u}_{CR,1}) - \lambda_1 + \lambda_1 - \frac{\tilde{\lambda}_{CR,1}}{1+\kappa^2(\tilde{\lambda}_{CR,1} - \|\mathbf{r}\|_{\mathbf{B}^{-1}})H^2} + \frac{\|\mathbf{r}\|_{\mathbf{B}^{-1}}}{1+\kappa^2(\tilde{\lambda}_{CR,1} - \|\mathbf{r}\|_{\mathbf{B}^{-1}})H^2} \\ &\leq R(\mathcal{I}_{CM}\tilde{u}_{CR,1}) - \lambda_1 + |\lambda_1 - \tilde{\lambda}_{CR,1}| + \tilde{\lambda}_{CR,1}\frac{\kappa^2(\tilde{\lambda}_{CR,1} - \|\mathbf{r}\|_{\mathbf{B}^{-1}})H^2}{1+\kappa^2(\tilde{\lambda}_{CR,1} - \|\mathbf{r}\|_{\mathbf{B}^{-1}})H^2} + \|\mathbf{r}\|_{\mathbf{B}^{-1}} \\ &\leq R(\mathcal{I}_{CM}\tilde{u}_{CR,1}) - \lambda_1 + |\lambda_1 - \tilde{\lambda}_{CR,1}| + \tilde{\lambda}_{CR,1}^2\kappa^2 H^2 + \|\mathbf{r}\|_{\mathbf{B}^{-1}}.\end{aligned} \tag{4.11}$$

Step two will be the proof of

$$R(\mathcal{I}_{CM}\tilde{u}_{CR,1}) - \lambda_1 \lesssim (1 + H^2\tilde{\lambda}_{CR,1})|||u_1 - \tilde{u}_{CR,1}|||_{NC}^2. \tag{4.12}$$

Elementary algebra reveals for $\tilde{v}_C := \mathcal{I}_{CM}\tilde{u}_{CR,1}/\|\mathcal{I}_{CM}\tilde{u}_{CR,1}\|$ that

$$R(\mathcal{I}_{CM}\tilde{u}_{CR,1}) - \lambda_1 = |||\tilde{v}_C|||^2 - |||u_1|||^2 = |||u_1 - \tilde{v}_C|||^2 + 2a(u_1, \tilde{v}_C - u_1).$$

Since $V_C(\mathcal{T}^*) \subset V$ and $\|u_1\| = 1 = \|\tilde{v}_C\|$ it follows that

$$2a(u_1, \tilde{v}_C - u_1) = -2\lambda_1 + 2\lambda_1 b(u_1, \tilde{v}_C) = -\lambda_1\|u_1 - \tilde{v}_C\|^2 \leq 0.$$

This shows that

$$R(\mathcal{I}_{CM}\tilde{u}_{CR,1}) - \lambda_1 \leq 2|||\tilde{u}_{CR,1} - \tilde{v}_C|||_{NC}^2 + 2|||u_1 - \tilde{u}_{CR,1}|||_{NC}^2.$$

The Young inequality [52] leads to

$$\begin{aligned}|||\tilde{u}_{CR,1} - \tilde{v}_C|||_{NC}^2 &= |||\tilde{u}_{CR,1} - \mathcal{I}_{CM}\tilde{u}_{CR,1} + \mathcal{I}_{CM}\tilde{u}_{CR,1}(1 - 1/\|\mathcal{I}_{CM}\tilde{u}_{CR,1}\|)|||_{NC}^2 \\ &\leq 2|||\tilde{u}_{CR,1} - \mathcal{I}_{CM}\tilde{u}_{CR,1}|||_{NC}^2 + 2(\|\mathcal{I}_{CM}\tilde{u}_{CR,1}\| - 1)^2 R(\mathcal{I}_{CM}\tilde{u}_{CR,1}).\end{aligned}$$

Since $\|\tilde{u}_{CR,1}\| = 1$, an inverse triangle inequality shows

$$(\|\mathcal{I}_{CM}\tilde{u}_{CR,1}\| - 1)^2 = (\|\mathcal{I}_{CM}\tilde{u}_{CR,1}\| - \|\tilde{u}_{CR,1}\|)^2 \leq \|\tilde{u}_{CR,1} - \mathcal{I}_{CM}\tilde{u}_{CR,1}\|^2.$$

Note that $(\tilde{u}_{CR,1} - \mathcal{I}_{CM}\tilde{u}_{CR,1})|_{T_4} \equiv 0$ on each centred triangle T_4 in $\mathcal{T}^*$. For the remaining triangles $T \in \mathcal{T}^*$ of the patches ω_z^* for nodes $z \in \mathcal{N}(\Omega)$, it holds that $(\tilde{u}_{CR,1} - \mathcal{I}_{CM}\tilde{u}_{CR,1})|_E \equiv 0$ on the edges E with $E \subset \partial\omega_z^*$. Hence, the Friedrich's inequality shows for those triangles

$$\|\tilde{u}_{CR,1} - \mathcal{I}_{CM}\tilde{u}_{CR,1}\|_{L^2(T)} \leq h_T\|\nabla(\tilde{u}_{CR,1} - \mathcal{I}_{CM}\tilde{u}_{CR,1})\|_{L^2(T)}.$$

The summation over all triangles yields

$$\|\tilde{u}_{CR,1} - \mathcal{I}_{CM}\tilde{u}_{CR,1}\| \lesssim H|||\tilde{u}_{CR,1} - \mathcal{I}_{CM}\tilde{u}_{CR,1}|||_{NC}. \tag{4.13}$$

The remaining term $H^2R(\mathcal{I}_{CM}\tilde{u}_{CR,1})$ is bounded by $16H^2\tilde{\lambda}_{CR,1}$ because of the uniform boundedness of $\mathcal{I}_{CM}$ in Lemma 4.3.5 and the inequality of the discrete norms $\|\tilde{u}_{CR,1}\|^2 \leq 16\|\mathcal{I}_{CM}\tilde{u}_{CR,1}\|^2$. The proof of the latter estimate considers the centred triangle T_4 of the fine triangulation $\mathcal{T}^*$ with $(\mathcal{I}_{CM}\tilde{u}_{CR,1})|_{T_4} = \tilde{u}_{CR,1}|_{T_4}$. Set $x := (\tilde{u}_{CR,1}(\mathrm{mid}(E_j)))_{j=1,2,3} \in \mathbb{R}^3$ of the three edges E_1, E_2, E_3 of T and compute (with the Rayleigh quotient ≥ 1 of the displayed 3x3 matrix)

$$\|\mathcal{I}_{CM}\tilde{u}_{CR,1}\|^2_{L^2(T_4)} = \frac{|T|}{48}x^T \begin{pmatrix} 2 & 1 & 1 \\ 1 & 2 & 1 \\ 1 & 1 & 2 \end{pmatrix} x \geq \frac{|T|}{48}x \cdot x = \|\tilde{u}_{CR,1}\|^2_{L^2(T)}/16.$$

Finally, the estimate

$$|||\tilde{u}_{CR,1} - \mathcal{I}_{CM}\tilde{u}_{CR,1}|||^2_{NC} \lesssim \sum_{E\in\mathcal{E}} h_E\|[\partial\tilde{u}_{CR,1}/\partial s]_E\|^2_{L^2(E)} \lesssim \min_{v\in V}|||\tilde{u}_{CR,1} - v|||^2_{NC}$$

from Lemma 4.3.4 concludes the proof of (4.12) in step two.

Step three will be the proof of

$$\|\mathbf{r}\|_{\mathbf{B}^{-1}} \leq \|\mathbf{A}(\mathbf{u}_{CR,1} - \tilde{\mathbf{u}}_{CR,1})\|_{\mathbf{B}^{-1}} + \lambda_{CR,1}\|u_{CR,1} - \tilde{u}_{CR,1}\| + |\lambda_{CR,1} - \tilde{\lambda}_{CR,1}|. \tag{4.14}$$

The definition of the algebraic residual $\mathbf{r} := \mathbf{A}\tilde{\mathbf{u}}_{CR,1} - \tilde{\lambda}_{CR,1}\mathbf{B}\tilde{\mathbf{u}}_{CR,1}$ plus the triangle inequality yield

$$\begin{aligned}\|\mathbf{r}\|_{\mathbf{B}^{-1}} = \|&\mathbf{A}\tilde{\mathbf{u}}_{CR,1} - \mathbf{A}\mathbf{u}_{CR,1} + \lambda_{CR,1}\mathbf{B}\mathbf{u}_{CR,1} - \lambda_{CR,1}\mathbf{B}\tilde{\mathbf{u}}_{CR,1} \\ &+ \lambda_{CR,1}\mathbf{B}\tilde{\mathbf{u}}_{CR,1} - \tilde{\lambda}_{CR,1}\mathbf{B}\tilde{\mathbf{u}}_{CR,1}\|_{\mathbf{B}^{-1}}.\end{aligned}$$

This and the triangle inequality prove (4.14) in step three.

Step four is the finish of the proof. Indeed, the combination of (4.11)–(4.14) concludes the proof of Lemma 4.4.2. □

The following estimate is proved with the same arguments as in the conforming case and is reported in [47] for the nonconforming CR-NCFEM.

Lemma 4.4.3 ([47])**.** *Let $(\lambda_{CR}, u_{CR}) \in \mathbb{R} \times CR^1_0(\mathcal{T})$ be a discrete eigenpair of the eigenpair (λ, u). Then it holds that*

$$\|h_{\mathcal{T}}\lambda_{CR}u_{CR}\|^2 \lesssim |||u - u_{CR}|||^2_{NC} + H^2\left((\lambda - \lambda_{CR})^2 + \lambda\lambda_{CR}\|u - u_{CR}\|^2\right). \quad \square$$

The second half of this section concerns the somehow surprising result of Theorem 4.4.4 for graded meshes which are described in the following.

Given a polygonal domain with a coarse triangulation $\mathcal{T}_0$ into triangles called *macro elements* (which specify the geometry), the domain Ω will be covered by piecewise affine images of the graded mesh on the reference triangle T_{ref} with vertices $(0,0)$, $(1,0)$, and $(0,1)$. Provided the coarse triangulation satisfies the condition that each triangle has

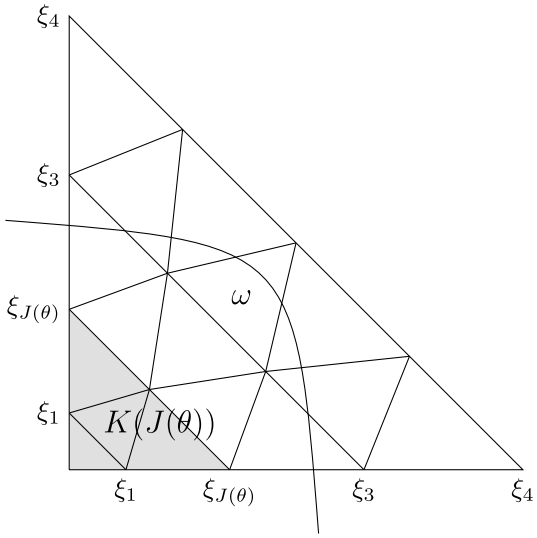

Figure 4.3: Reference triangle T_{ref} with 3/2-graded sub-triangles for $N = 4$.

at most one vertex as a corner of $\partial\Omega$, then the grading parameter α can be different for each such corner of $\partial\Omega$ and $\alpha := 1$ for all those macro triangles without a vertex at a corner of $\partial\Omega$. One verifies directly that the structured mesh is a (shape) regular triangulation. On each element $K \in \mathcal{T}_0$, the mesh of the reference triangle is obtained by an affine transformation. The graded mesh on the macro element T_{ref} of Figure 4.3 is generated as follows: Given some grading parameter $\alpha > 0$ and given an integer $N \geq 2$, set $\xi_j := (j/N)^\alpha$ and draw line segments aligned to the anti-diagonal through $(0, \xi_j)$ and $(\xi_j, 0)$ for $j = 0, 1, \ldots, N$. Each of these line segments is divided into j uniform edges and so define the set of nodes $(0, 0)$ and $(j - k, k)\xi_j/j$ for $k = 0, \ldots, j$ and $j = 1, \ldots, N$. The triangles are then given by the vertices $\xi_j/j(j - k, k)$ and $\xi_j/j(j - k - 1, k + 1)$ aligned with anti-diagonal and the vertex $\xi_{j-1}/(j - 1)(j - k - 1, k)$ on the finer and $\xi_{j+1}/(j + 1)(j - k, k + 1)$ on the coarser neighbouring segment. The smallest triangle reads $\mathrm{conv}\{(0, 0), (0, \xi_1), (\xi_1, 0)\}$ with diameter $\sqrt{2}\xi_1 \approx N^{-\alpha}$. The largest triangles have diameter $H \approx N^{-1}$.

Theorem 4.4.4. *Any function $f \in L^2(\Omega)\backslash\{0\}$ and any graded triangulation $\mathcal{T}$ of Ω satisfy*

$$\|h_{\mathcal{T}} f\| \approx 1/N.$$

The equivalence constant $C(f)$ in the assertion $1/N \leq C(f)\|h_{\mathcal{T}} f\|$ depends on f.

Proof. The first inequality follows from

$$\|h_{\mathcal{T}} f\| \leq H\|f\| \approx \|f\|/N.$$

To verify the reverse inequality, consider one triangle $K \in \mathcal{T}_0$. Some affine diffeomorphism (which depends only on $\mathcal{T}_0$) maps K onto T_{ref} and some transformation shows that

it suffices to verify the assertion on T_{ref}. Without loss of generality, let $f \in L^2(T_{ref})\backslash\{0\}$ satisfy $|f| \geq \varepsilon > 0$ on a set ω of measure $|\omega| > 0$. Let the volume fraction $\theta := |\omega|/|T_{ref}|$ of ω in T_{ref} be fixed and consider the question where $\omega \subset T_{ref}$ of fixed area $|\omega| = \theta/2$ may be located to minimise the term $\int_{T_{ref}\cap\omega} h_{\mathcal{T}}^2\, dx$. Figure 4.3 illustrates the situation where ω is placed where h_T is small. In the end, one deduces that for some index $J(\theta)$ (which is maximal with $\xi_{J(\theta)}^2 \leq \theta$), the minimising set ω includes the sub-triangle $K(J(\theta)) := \mathrm{conv}\{(0,0),(\xi_{J(\theta)},0),(0,\xi_{J(\theta)})\}$ and the induced sub-triangulation $\mathcal{T}(K(J(\theta)))$. Hence,

$$\|h_{\mathcal{T}}\|_{L^2(K(J(\theta))} \leq \|h_{\mathcal{T}}\|_{L^2(\omega)} \leq \frac{1}{\varepsilon}\|h_{\mathcal{T}} f\|_{L^2(\omega)} \leq \frac{1}{\varepsilon}\|h_{\mathcal{T}} f\|_{L^2(\Omega)}.$$

Thus it remains to prove that

$$N^{-1} \lesssim \|h_{\mathcal{T}}\|_{L^2(K(J(\theta))}.$$

Since the j-th diagonal layer consists of $2j-1$ triangles, it holds that

$$\sum_{j=1}^{J(\theta)} (2j-1)\left(\frac{j^\alpha - (j-1)^\alpha}{N^\alpha}\right)^4 \lesssim \sum_{T\in\mathcal{T}(K(J(\theta)))} \int_T h_T^2\, dx.$$

The binomial expansion shows

$$\sum_{j=1}^{J(\theta)} \left(\frac{j^\alpha - (j-1)^\alpha}{N^\alpha}\right)^4 \approx \sum_{j=1}^{J(\theta)} \left(\frac{j^{\alpha-1}\alpha}{N^\alpha}\right)^4.$$

This leads to

$$\frac{\alpha^4}{N^2}\sum_{j=1}^{J(\theta)} \left(\frac{j}{N}\right)^{4\alpha-3} N^{-1} = \sum_{j=1}^{J(\theta)} j\left(\frac{j^{\alpha-1}\alpha}{N^\alpha}\right)^4 \lesssim \sum_{j=1}^{J(\theta)} (2j-1)\left(\frac{j^\alpha-(j-1)^\alpha}{N^\alpha}\right)^4.$$

Since $J(\theta) = N\sqrt[2\alpha]{2|K(J(\theta))|}$, the sum on the right hand side is a Riemann sum over the interval $[0, \sqrt[2\alpha]{2|K(J(\theta))|}]$. Since $\alpha \geq 1$,

$$\frac{\alpha^4}{N^2}\sum_{j=1}^{J(\theta)} \left(\frac{j}{N}\right)^{4\alpha-3} N^{-1} \approx \frac{\alpha^4}{N^2}\int_0^{\sqrt[2\alpha]{2|K(J(\theta))|}} x^{4\alpha-3} dx = \frac{\alpha^4 (2|K(J(\theta))|)^{(2\alpha-1)/\alpha}}{N^2(4\alpha-2)} \approx \frac{1}{N^2}.$$

This proves the assertion for $N \geq N_0$ and sufficiently large N_0 so that $J(\theta) \geq 1$. For $1 \leq N \leq N_0$, $N\|h_{\mathcal{T}} f\| \geq N^{1-\alpha}\|f\|$ is bounded from below in terms of N_0. This concludes the proof for all $N \in \mathbb{N}$. □

Proof of Theorem 4.4.1. The assertion follows from Lemma 4.4.2, Theorem 4.4.4, and Lemma 4.4.3. □

4.5 Error Bounds for Higher Eigenvalues

This section is devoted to some computable lower bounds of higher eigenvalues. It is emphasised that λ_J could be a multiple eigenvalue and λ_J could even be a part of a cluster without any separation (on the continuous level), cf. Example 4.5.3 below. However, any clustering of discrete eigenvalues may have some disastrous effect on the smallness of the discrete residual $\mathbf{r}$ in the algebraic eigenvalue problem.

Theorem 4.5.1. *Suppose that the separation condition* $H < \left(\sqrt{1+1/J}-1\right)/(\kappa\lambda_J^{1/2})$ *holds for the J-th exact eigenvalue* λ_J. *Let* $(\tilde\lambda_{CR,J}, \tilde u_{CR,J}) \in \mathbb{R}\times CR_0^1(\mathcal{T})$ *with normalised* $\tilde u_{CR,J}$, $\|\tilde u_{CR,J}\|_{L^2(\Omega)} = 1$, *and algebraic residual* $\mathbf{r} := \mathbf{A}\tilde{\mathbf{u}}_{CR,J} - \tilde\lambda_{CR,J}\mathbf{B}\tilde{\mathbf{u}}_{CR,J}$ *approximate the J-th eigenpair* (λ_J, u_J). *Suppose separation of* $\tilde\lambda_{CR,J}$ *from the remaining discrete spectrum in the sense that* $\tilde\lambda_{CR,J}$ *is closer to the discrete eigenvalue* $\lambda_{CR,J}$ *than to any other discrete eigenvalues and that* $\|\mathbf{r}\|_{\mathbf{B}^{-1}} < \tilde\lambda_{CR,J}$. *Then it holds that*

$$\frac{\tilde\lambda_{CR,J} - \|\mathbf{r}\|_{\mathbf{B}^{-1}}}{1+\kappa^2(\tilde\lambda_{CR,J}-\|\mathbf{r}\|_{\mathbf{B}^{-1}})H^2} \le \lambda_J \le \max_{\xi\in\mathbb{R}^J\setminus\{0\}} R\left(\sum_{j=1}^J \xi_j \mathcal{I}_{CM}\tilde u_{CR,j}\right).$$

The difference of the upper and lower bounds

$$\eta_J := \max_{\xi\in\mathbb{R}^J\setminus\{0\}} R\left(\sum_{j=1}^J \xi_j \mathcal{I}_{CM}\tilde u_{CR,j}\right) - \frac{\tilde\lambda_{CR,J} - \|\mathbf{r}\|_{\mathbf{B}^{-1}}}{1+\kappa^2(\tilde\lambda_{CR,J}-\|\mathbf{r}\|_{\mathbf{B}^{-1}})H^2} \tag{4.15}$$

is efficient in the sense that

$$\begin{aligned}\eta_J \lesssim{}& \left(1+H^2\max_{\xi\in\mathbb{R}^J\setminus\{0\}} R\left(\sum_{j=1}^J \xi_j\mathcal{I}_{CM}\tilde u_{CR,j}\right)\right)\max_{\xi\in\mathbb{R}^J\setminus\{0\}}\left|\!\left|\!\left| u_J - \sum_{j=1}^J \xi_j\tilde u_{CR,j}\right|\!\right|\!\right|_{NC}\\ &+ |\lambda_J-\tilde\lambda_{CR,J}| + H^2\left((\lambda_J-\lambda_{CR,J})^2 + \lambda_J\lambda_{CR,J}\|u_J-u_{CR,J}\|^2\right)\\ &+ \|\mathbf{A}(\mathbf{u}_{CR,J}-\tilde{\mathbf{u}}_{CR,J})\|_{\mathbf{B}^{-1}} + \lambda_{CR,J}\|u_{CR,J}-\tilde u_{CR,J}\| + |\lambda_{CR,J}-\tilde\lambda_{CR,J}|.\end{aligned}$$

The proofs start with the linear independence of nonconforming interpolants.

Lemma 4.5.2. *Let* $(u_1,\dots,u_J)$ *be some b-orthonormal basis of exact eigenvectors in* V *for the exact first* J *eigenvalues* $0<\lambda_1<\lambda_2\le\ldots\le\lambda_J$ *on the continuous level. For any global mesh-size* $H < \left(\sqrt{1+1/J}-1\right)/(\kappa\lambda_J^{1/2})$, *the nonconforming interpolants* $\mathcal{I}_{NC}u_1,\dots,\mathcal{I}_{NC}u_J$ *are linear independent.*

Proof. For any $j=1,\dots,J$, Theorem 4.2.1 shows

$$\|u_j - \mathcal{I}_{NC}u_j\| \le \kappa H\left|\!\left|\!\left| u_j-\mathcal{I}_{NC}u_j\right|\!\right|\!\right|_{NC} \le \kappa H\left|\!\left|\!\left| u_j\right|\!\right|\!\right|_{NC} \le \kappa H\lambda_j^{1/2} =: d_j. \tag{4.16}$$

With the Kronecker $\delta_{jk} = 1$ for $j = k$ and $\delta_{jk} = 0$ for $j \neq k$, this implies

$$\begin{aligned}
&|b(\mathcal{I}_{NC}u_j, \mathcal{I}_{NC}u_k) - \delta_{jk}| = |b(\mathcal{I}_{NC}u_j, \mathcal{I}_{NC}u_k) - b(u_j, u_k)| \\
&= |-b(u_j - \mathcal{I}_{NC}u_j, \mathcal{I}_{NC}u_k) - b(u_j, u_k - \mathcal{I}_{NC}u_k)| \\
&= |b(u_j - \mathcal{I}_{NC}u_j, u_k - \mathcal{I}_{NC}u_k) - b(u_j - \mathcal{I}_{NC}u_j, u_k) - b(u_j, u_k - \mathcal{I}_{NC}u_k)| \\
&\leq \|u_j - \mathcal{I}_{NC}u_j\|\|u_k - \mathcal{I}_{NC}u_k\| + \|u_j - \mathcal{I}_{NC}u_j\| + \|u_k - \mathcal{I}_{NC}u_k\| \\
&\leq d_j d_k + d_j + d_k.
\end{aligned}$$

Direct calculations show that $H < \left(\sqrt{1 + 1/J} - 1\right) / (\kappa \lambda_J^{1/2})$ leads to

$$\max_{j=1}^{J} \left(\sum_{k=1}^{J} (d_j d_k + d_j + d_k) \right) < 1.$$

The Gershgorin theorem [61, Theorem 7.2.1] shows that the eigenvalues of

$$(b(\mathcal{I}_{NC}u_j, \mathcal{I}_{NC}u_k))_{j,k=1,\ldots,J}$$

are all positive. □

Proof of the lower bound in Theorem 4.5.1 for $\mathbf{r} \equiv 0$. Lemma 4.5.2 guarantees that

$$\mathcal{I}_{NC}u_1, \ldots, \mathcal{I}_{NC}u_J$$

are linearly independent. The Rayleigh-Ritz principle [105, Section 6.1:(13)] on the discrete level states that the discrete eigenvalue $\lambda_{CR,J}$ of number J equals

$$\lambda_{CR,J} = \min_{V_J \subset CR_0^1(\mathcal{T}), \dim(V_J) = J} \max_{v \in V_J \setminus \{0\}} R_{NC}(v).$$

Therein, the notation $\dim(V_J) = J$ abbreviates that the minimum is taken over all subspaces of $CR_0^1(\mathcal{T})$ of dimension J. Since $\mathcal{I}_{NC}u_1, \ldots, \mathcal{I}_{NC}u_J$ are linear independent, there exist some real coefficients $\xi_1, \ldots, \xi_J$ such that the Rayleigh quotient is maximised in $V_J := \operatorname{span}\{\mathcal{I}_{NC}u_1, \ldots, \mathcal{I}_{NC}u_J\}$. This leads to

$$\lambda_{CR,J} \leq R_{NC}\left(\sum_{j=1}^{J} \xi_j \mathcal{I}_{NC}u_j \right). \tag{4.17}$$

One may assume without loss of generality that

$$\sum_{j=1}^{J} \xi_j^2 = 1.$$

Let $v := \sum_{j=1}^{J} \xi_j u_j$ and observe that $\|v\|^2 = \sum_{j=1}^{J} \xi_j^2 = 1$. Since $\nabla_{NC}(v - \mathcal{I}_{NC}v)$ is L^2

orthogonal to $\nabla_{NC}\mathcal{I}_{NC}v$, the Pythagoras theorem reads

$$|||v - \mathcal{I}_{NC}v|||_{NC}^2 + |||\mathcal{I}_{NC}v|||_{NC}^2 = |||v|||^2.$$

The orthogonality of the eigenfunctions shows

$$|||v|||^2 = |||\sum_{j=1}^{J} \xi_j u_j|||^2 = \sum_{j=1}^{J} \xi_j^2 |||u_j|||^2 = \sum_{j=1}^{J} \xi_j^2 \lambda_j.$$

The combination of the aforementioned equalities results in

$$|||v - \mathcal{I}_{NC}v|||_{NC}^2 + |||\mathcal{I}_{NC}v|||_{NC}^2 = \sum_{j=1}^{J} \xi_j^2 \lambda_j \leq \lambda_J.$$

Together with (4.17) in the form of

$$\lambda_{CR,J}\|\mathcal{I}_{NC}v\|^2 \leq |||\mathcal{I}_{NC}v|||_{NC}^2,$$

the previous estimate yields

$$|||v - \mathcal{I}_{NC}v|||_{NC}^2 + \lambda_{CR,J}\|\mathcal{I}_{NC}v\|^2 \leq \lambda_J.$$

Since $\|v\|^2 = 1$, the Cauchy-Schwarz inequality followed by the binomial expansion implies

$$1 + \|v - \mathcal{I}_{NC}v\|^2 - 2\|v - \mathcal{I}_{NC}v\| \leq 1 + \|v - \mathcal{I}_{NC}v\|^2 - 2b(v - \mathcal{I}_{NC}v, v) = \|\mathcal{I}_{NC}v\|^2.$$

Following the proof of Theorem 4.3.1 with the substitution of u_1 by v eventually results in

$$\frac{\lambda_{CR,J}}{1 + \kappa^2 \lambda_{CR,J} H^2} \leq \lambda_J. \qquad \square$$

Proof of the lower bound in Theorem 4.5.1 for $\mathbf{r} \not\equiv 0$. Lemma 4.3.8 and the monotonicity of $t/(1 + \kappa^2 H^2 t)$ in $t > 0$ allows the substitution of λ_{CR} by $\tilde{\lambda}_{CR,J} - \|\mathbf{r}\|_{B^{-1}}$ for $\tilde{\lambda}_{CR,J} > \|\mathbf{r}\|_{B^{-1}}$. $\square$

Proof of the upper bound in Theorem 4.5.1. Let $\tilde{u}_{CR,1}, \ldots, \tilde{u}_{CR,J}$ be the first J approximated discrete orthonormal eigenvectors. Since $\mathcal{I}_{CM}\tilde{u}_{CR,1} \equiv \tilde{u}_{CR,1}$ on each centred triangle of $\mathcal{T}^*$ with all vertices as midpoints of edges in $\mathcal{E}(\mathcal{T})$, the functions

$$\mathcal{I}_{CM}\tilde{u}_{CR,1}, \ldots, \mathcal{I}_{CM}\tilde{u}_{CR,J}$$

are linear independent. Thus, there exist maximising coefficients ξ_j with $\sum_{j=1}^{J} \xi_j^2 = 1$

such that

$$\lambda_J = \min_{V_J \subset V, \dim(V_J)=J} \max_{v \in V_J \setminus \{0\}} R(v) \leq R\left(\sum_{j=1}^{J} \xi_j \mathcal{I}_{CM} \tilde{u}_{CR,j}\right). \qquad \square$$

Proof of efficiency in Theorem 4.5.1. The proof of efficiency of the difference of the upper and lower bounds in (4.15) follows from some modifications of the arguments of Lemma 4.4.2–4.4.3 and Theorem 4.4.4. Therefore the remaining parts of this proof only sketch the main steps. The arguments in (4.11) lead to

$$\eta_J \leq \max_{\xi \in \mathbb{R}^J \setminus \{0\}} R\left(\sum_{j=1}^{J} \xi_j \mathcal{I}_{CM} \tilde{u}_{CR,j}\right) - \lambda_J + |\lambda_J - \tilde{\lambda}_{CR,J}| + \tilde{\lambda}_{CR,J}^2 \kappa^2 H^2 + \|\mathbf{r}\|_{\mathbf{B}^{-1}}. \quad (4.18)$$

Suppose that $\xi_1, \ldots, \xi_J$ denote some coefficients of a maximiser $\tilde{v}_C := \sum_{j=1}^{J} \xi_j \mathcal{I}_{CM} \tilde{u}_{CR,j}$ in the Rayleigh quotient of (4.18) and set $\tilde{v}_{CR} := \sum_{j=1}^{J} \xi_j \tilde{u}_{CR,j}$. The arguments of step two in the proof of Lemma 4.4.2 leads here to

$$R(\tilde{v}_C) - \lambda_J \lesssim |\!|\!| u_J - \tilde{v}_{CR} |\!|\!|_{NC} + |\!|\!| \tilde{v}_{CR} - \tilde{v}_C |\!|\!|_{NC} + (\|\tilde{v}_C\| - 1)^2 R(\tilde{v}_C).$$

Since $\tilde{u}_{CR,1}, \ldots, \tilde{u}_{CR,J}$ is orthonormal and, without loss of generality, $\xi_1^2 + \ldots + \xi_J^2 = 1$, it holds that $\|\tilde{v}_{CR}\| = 1$ and

$$(\|\tilde{v}_C\| - 1)^2 \leq \|\tilde{v}_{CR} - \tilde{v}_C\|^2.$$

The discrete scaling argument of (4.13) implies

$$\|\tilde{v}_{CR} - \tilde{v}_C\| \lesssim H |\!|\!| \tilde{v}_{CR} - \tilde{v}_C |\!|\!|_{NC}.$$

The linearity of $\mathcal{I}_{CM}$ from Lemma 4.3.5, $\tilde{v}_{CR} - \tilde{v}_C = \tilde{v}_{CR} - \mathcal{I}_{CM} \tilde{v}_{CR}$, plus Lemma 4.3.4 show

$$|\!|\!| \tilde{v}_{CR} - \tilde{v}_C |\!|\!|_{NC} \lesssim |\!|\!| u_J - \tilde{v}_{CR} |\!|\!|_{NC}.$$

The arguments of steps three and four in the proof of Lemma 4.4.2 plus Lemma 4.4.3 and Theorem 4.4.4 conclude the proof of the efficiency. $\square$

Example 4.5.3. The criss-cross triangulation of Figure 4.1 leads to the matrices $\mathbf{A} = 4\, I_{4\times 4} = \mathbf{B}/24$ for the 4×4-dimensional identity matrix $I_{4\times 4}$. Any vector $\mathbf{u}_{CR} \in \mathbb{R}^4$ is eigenvector with $\mathbf{r} \equiv 0$ to the eigenvalue $\lambda_{CR} = 24$ of multiplicity four. For $J = 2$ one may choose the basis $(u_{CR,1}, u_{CR,2})$ proportional to $(1,1,1,1)$ and $(1,1,1,0)$ that leads to the bounds $4.2594 \leq \lambda_2 \leq 72$. Note that the exact second and third eigenvalues $\lambda_2 = \lambda_3 = 5\pi^2 = 49.348$ coincide. The condition $H < \left(\sqrt{3/2} - 1\right)/(\kappa\pi\sqrt{5})$ is violated, but some elementary direct considerations with u_2 and u_3 on the continuous level show that $\mathcal{I}_{NC} u_2$ and $\mathcal{I}_{NC} u_3$ obtain positive and negative values in Ω. Thus the positivity of u_1 implies that $\mathcal{I}_{NC} u_1$ and $\mathcal{I}_{NC} u_2$ are linearly independent. Therefore, the aforementioned

eigenvalue bounds for λ_2 are guaranteed. The eigenvalue bounds are remarkable in that $J = 2$ cuts a cluster of eigenvalues on the continuous level ($\lambda_2 = \lambda_3$) as well as on the discrete level ($\lambda_{CR,1} = \ldots = \lambda_{CR,4}$).

Remark 4.5.4. Note that Lemma 4.5.2 provides an explicit bound for the global mesh-size that leads to the separation condition in Theorem 4.5.1 but does not need any regularity assumption of the eigenfunctions. Elliptic regularity for some convex domain Ω [64, Theorem 4.3.1.4] shows

$$\|D^2 u_J\| = \|\Delta u_J\| = \lambda_J \|u_J\| = \lambda_J.$$

Since (4.5), the Poincaré inequality on a triangle $T \in \mathcal{T}$ [82] reads

$$\|\nabla(u_J - \mathcal{I}_{NC} u_J)\|^2_{L^2(T)} \leq h_T^2 / j_{1,1}^2 \|D^2 u_J\|^2_{L^2(T)}.$$

The square roots of the sum of all those inequalities reads

$$|||u_J - \mathcal{I}_{NC} u_J|||_{NC} \leq H / j_{1,1} \|D^2 u_J\|_{L^2(\Omega)}.$$

This and Theorem 4.2.1 plus the aforementioned elliptic regularity estimate shows

$$\|u_J - \mathcal{I}_{NC} u_J\| \leq \kappa H |||u_J - \mathcal{I}_{NC} u_J|||_{NC} \leq \kappa H^2 / j_{1,1} \|D^2 u_J\| \leq \kappa H^2 \lambda_J / j_{1,1}.$$

This leads to the improved separation condition

$$H^2 < j_{1,1} \left(\sqrt{1 + 1/J} - 1 \right) / (\kappa \lambda_J)$$

for higher eigenvalues on convex domains in Theorem 4.5.1. The reduced elliptic regularity allows a similar proof with rather unknown constants from $\|u_J\|_{H^s(\Omega)} \leq C(s) \|\lambda_J u_J\|$.

4.6 Numerical Experiments

This section presents an adaptive algorithm and provides some numerical examples for the unit square, the L-shaped domain, and two isospectral domains.

4.6.1 Adaptive Finite Element Algorithm

The basic adaptive finite element method (AFEM) starts from an initial coarse triangulation $\mathcal{T}_0$ and generates a sequence of nested triangulations $\mathcal{T}_0, \mathcal{T}_1, \ldots$ with corresponding non-nested nonconforming spaces $(CR_0^1(\mathcal{T}_\ell))_\ell$ in successive loops of the form

$$\texttt{Solve} \longrightarrow \texttt{Estimate} \longrightarrow \texttt{Mark} \longrightarrow \texttt{Refine}.$$

Input

$\mathcal{T}_0$, $0 < \theta \leq 1$, $\tau > 0$.

Solve

Given an approximation $(\tilde{\lambda}_{1,\ell}, \tilde{u}_{1,\ell}) \in \mathbb{R} \times CR_0^1(\mathcal{T}_\ell)$ on the triangulation $\mathcal{T}_\ell$, do

Repeat

Run one iteration step of the preconditioned inverse iteration (PINVIT) [78] with one V-cycle multigrid iteration with Richardson smoother [24] as a preconditioner

until

$\|\mathbf{r}_\ell\|_{\mathbf{B}_\ell^{-1}} \leq \min\{\tilde{\lambda}_{1,\ell}, \tau\}$, $\mathbf{r}_\ell := \mathbf{A}_\ell \tilde{\mathbf{u}}_{1,\ell} - \tilde{\lambda}_{1,\ell} \mathbf{B}_\ell \tilde{\mathbf{u}}_{1,\ell}$,
and if $1 > \kappa^4(\tilde{\lambda}_{1,\ell} - \|\mathbf{r}_\ell\|_{\mathbf{B}_\ell^{-1}})^2 H_\ell^4$ until $\eta_2 \leq \max\{\eta_1, \eta_3\}$.

Estimate

The error estimate of Theorem 4.3.1 reads

$$|\lambda_1 - \tilde{\lambda}_{1,\ell}| \leq \eta_1 + \eta_2 + \eta_3$$

with

$$\eta_1 := \frac{\tilde{\lambda}_{1,\ell} \kappa^2 (\tilde{\lambda}_{1,\ell} - \|\mathbf{r}_\ell\|_{\mathbf{B}_\ell^{-1}}) H_\ell^2}{1 - \kappa^4 (\tilde{\lambda}_{1,\ell} - \|\mathbf{r}_\ell\|_{\mathbf{B}_\ell^{-1}})^2 H_\ell^4},$$

$$\eta_2 := \frac{\|\mathbf{r}_\ell\|_{\mathbf{B}_\ell^{-1}}}{1 + \kappa^2 (\tilde{\lambda}_{1,\ell} - \|\mathbf{r}_\ell\|_{\mathbf{B}_\ell^{-1}}) H_\ell^2},$$

$$\eta_3 := R(\mathcal{I}_{CM} \tilde{u}_{1,\ell}) - \frac{\tilde{\lambda}_{1,\ell}}{1 - \kappa^4 (\tilde{\lambda}_{1,\ell} - \|\mathbf{r}_\ell\|_{\mathbf{B}_\ell^{-1}})^2 H_\ell^4}.$$

Mark

The mesh-refinement selects a set of edges $\mathcal{M}_\ell \subseteq \mathcal{E}_\ell$ with the goal to balance the contributions $\eta_1 + \eta_2 + \eta_3$ as follows
(a) **If** $1 \leq \kappa^4 (\tilde{\lambda}_{1,\ell} - \|\mathbf{r}_\ell\|_{\mathbf{B}_\ell^{-1}})^2 H_\ell^4$ or $\eta_1 > \max\{\eta_2, \eta_3\}$ then $\mathcal{M}_\ell := \cup\{E \in \mathcal{E}_\ell : |E| = H_\ell\}$.
(b) **Else if** $\eta_3 \geq \max\{\eta_1, \eta_2\}$ then the set of marked edges $\mathcal{M}_\ell \subseteq \mathcal{E}_\ell$ is of minimal cardinality that fulfils the bulk criterion [48]

$$\theta \sum_{E \in \mathcal{E}_\ell} \eta_\ell^2(E) \leq \sum_{E \in \mathcal{M}_\ell} \eta_\ell^2(E) \quad \text{for} \quad \eta_\ell^2(E) := h_E \|[\partial \tilde{u}_{1,\ell} / \partial s]\|_{L^2(E)}^2.$$

Refine

Given the set $\mathcal{M}_\ell \subseteq \mathcal{E}_\ell$ of marked edges, the refinement $\mathcal{T}_{\ell+1}$ is computed as a minimal regular triangulation such that $\mathcal{M}_\ell \subseteq \mathcal{E}_\ell \backslash \mathcal{E}_{\ell+1}$ and each triangle is refined by one of the red-gree-blue refinement-rules of Subsection 2.5.2.

N	16	56	208	800
$\lambda_{2,\ell} - \lambda_{1,\ell}$	12.0964	25.4691	28.5894	29.3549
N	3136	12416	49408	197120
$\lambda_{2,\ell} - \lambda_{1,\ell}$	29.5454	29.5930	29.6048	29.6078

Table 4.1: Spectral gap for the smallest eigenvalue of the unit square for different meshes with $N = |\mathcal{E}_\ell(\Omega)|$ degrees of freedom.

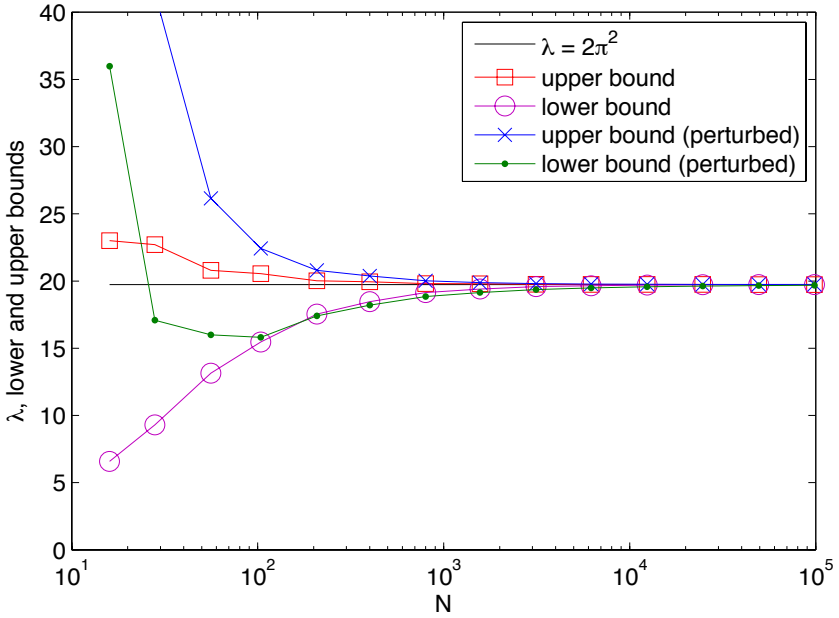

Figure 4.4: Computed and randomly perturbed upper and lower bounds on the smallest eigenvalue of the unit square.

4.6.2 Unit Square

Consider the model problem (4.1) on the unit square $\Omega = (0,1)^2$ with the smallest eigenvalue $\lambda_1 = 2\pi^2$.

The first experiment in Table 4.1 investigates the critical algebraic condition on the spectral gap $\lambda_{2,\ell} - \lambda_{1,\ell}$. The results are computed for a sequence of red-refined meshes and the ARPACK [83] solver (implemented in the Matlab function 'eigs') with tolerance up to machine precision. The spectral gap is relatively large even for coarse meshes and motivates the choice $\tau = 1$.

Figure 4.4 verifies that the lower and upper bounds of Theorem 4.3.1 are empirically lower and upper eigenvalue bounds and presents some perturbed bounds as well. The perturbed bounds are obtained from a perturbed eigenvector

$$\tilde{\mathbf{u}}_{1,\ell} = \mathbf{u}_{1,\ell} + \mathrm{rand}(0,1)/(\dim(CR_0^1(\mathcal{T}_\ell))\lambda_{1,\ell}),$$

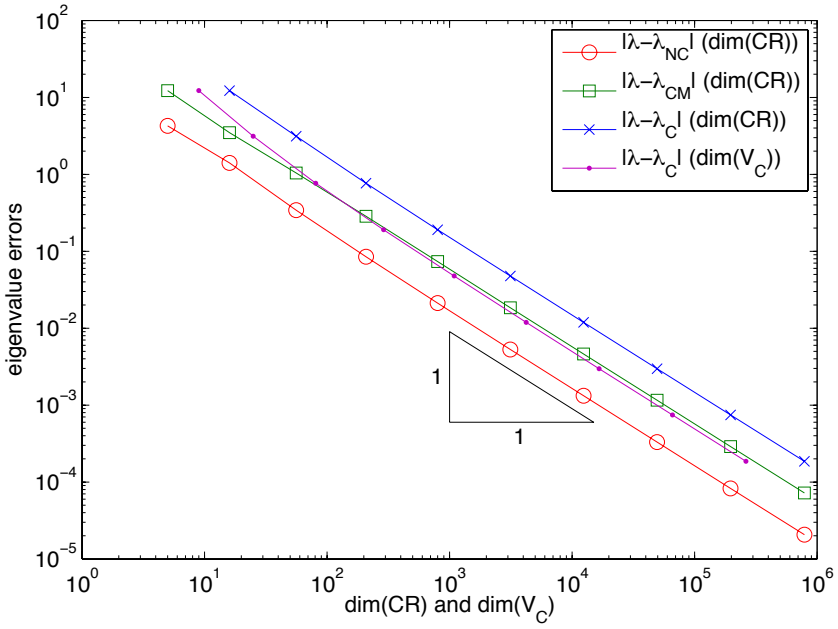

Figure 4.5: Convergence history for the unit square for different eigenvalue errors.

where $\mathbf{u}_{1,\ell}$ is computed with ARPACK up to machine precision. The perturbed eigenvalue is the Rayleigh quotient of the perturbed eigenvector. Note that the numerical results show that for the first mesh the perturbation is too large such that a different eigenvalue is approximated and the lower bound does *not* hold.

Figure 4.5 compares the accuracy of the nonconforming and the conforming FEMs on uniform red-refined meshes. The first observation is that the nonconforming eigenvalue error $|\lambda_1 - \lambda_{CR,1}|$ is smaller than the conforming eigenvalue error $|\lambda_1 - \lambda_{C,1}|$ displayed versus its degrees of freedoms $N := \dim(V_C)$. The comparison of the conforming eigenvalue error $|\lambda_1 - \lambda_{C,1}|$ and the error for the post-processing $\lambda_{CM,1} := R(\mathcal{I}_{CM} u_{CR,1})$, $|\lambda_1 - \lambda_{CM,1}|$, both plotted versus $N = \dim(CR_0^1(\mathcal{T}))$, shows that the proposed interpolation on the red-refined mesh leads to better upper bounds than a conforming approximation on the coarse mesh.

4.6.3 L-Shaped Domain

Consider the model problem (4.1) on the L-shaped domain $\Omega = (-1,1)^2 \backslash ([0,1] \times [-1,0])$ with $\lambda_1 = 9.6397238440219$ [17].

Figure 4.6 compares the eigenvalue error for the mean value μ of the upper and lower eigenvalue bounds in Theorem 4.3.1 to its upper bound $\eta/2$. Uniform red-refined meshes with ARPACK result in suboptimal convergence of the estimator $\eta/2$ as expected for the first eigenfunction with singularity at the origin but lead to a surprising super-convergence of the error $|\lambda_1 - \mu|$. The surprising super-convergence of $|\lambda_1 - \mu|$ might result from some super-convergence phenomena on this highly structured grid, cf. [112] for super-convergence phenomena of eigenvalues. For graded meshes with ARPACK

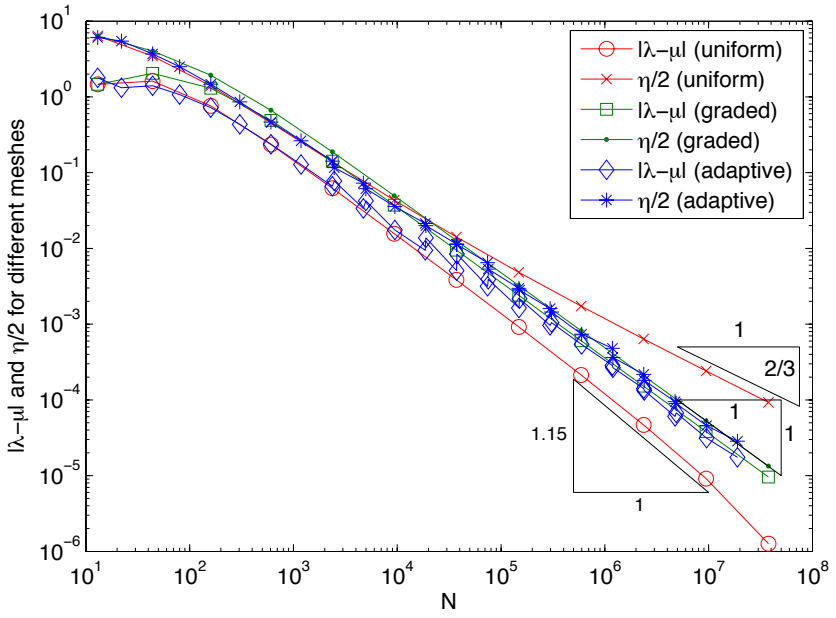

Figure 4.6: Convergence history for the L-shaped domain.

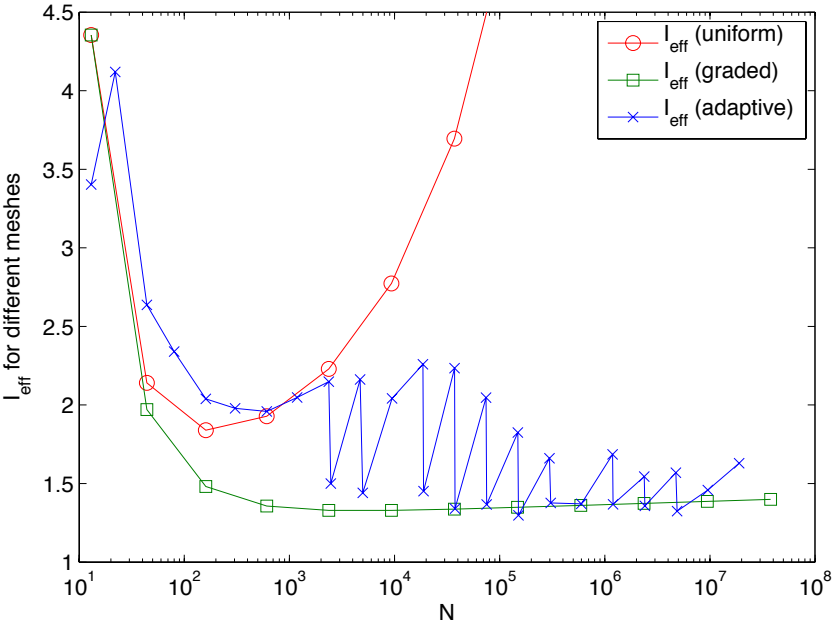

Figure 4.7: Efficiency indices for the L-shaped domain.

the empirical convergence rate is optimal and for the proposed adaptive algorithm it is asymptotically optimal. The eigenvalue error of the adaptive algorithm is not monotone which results from the fact that the algorithm starts with uniform refinements at the beginning an therefore the error matches the super-convergent error. Afterwards one step of uniform refinement is followed by one step of adaptive refinement that destroys the mesh-symmetry and therefore the super-convergence. As a result the error gets closer and closer to the quasi-optimal error for graded meshes. In contrast to that the error bound $\eta/2$ is monotonically decreasing. This illustrates the mixed adaptive strategy with respect to the algebraic eigenvalue error, the global mesh-size, and the approximation error and provides numerical evidence for the superiority of adaptive mesh-refinement.

Figure 4.7 displays the efficiency indices $I_{\mathit{eff}} := (\eta/2)/|\lambda_1 - \mu|$. Clearly, for uniform meshes one observes the mentioned efficiency gap. The values for graded and adaptive meshes are between 1 and 2 and tend to 1.4. Since $\eta/2$ is a guaranteed upper bound, all values are greater or equal to one.

4.6.4 Isospectral Domains

Consider the model problem (4.1) on the two isospectral domains of Figure 4.8 with the approximation of the 50-th eigenvalue $\lambda_{50} = 54.187936$ [17]. For the numerical experiments, both domains are triangulated similarly with the same number of triangles. The experiments show for uniform red-refinements and ARPACK that both domains lead to the same eigenvalue approximations up to machine precision. Table 4.2 verifies empirically the theoretical upper and lower bounds of Theorem 4.5.1 and shows that also the computed upper and lower bounds are equal up to machine precision for both domains. An interesting observation on the maximising Rayleigh quotient in Theorem 4.5.1 is that the maximum of $R(\xi_1 \mathcal{I}_{CM}\tilde{u}_{CR,1} + \ldots + \xi_{50}\mathcal{I}_{CM}\tilde{u}_{CR,50})$ is obtained for $\xi_1 = \ldots = \xi_{45} = 0$ and $\xi_{50} = 1$ in all displayed numerical experiments. The separation condition of Theorem 4.5.1 leads in this example with $J = 50$ to $H < 0.007$ which is satisfied for the triangulations in the last and second last entry of Table 4.2. Remark 4.5.4 illustrates that this condition is coarse but explicit constants for the non-convex domain at hand require more insight which is compensated by this strong separation condition in this chapter.

4.7 Software Implementation

The software directory with the software files used for the numerical experiments of this chapter is listed in Table 4.3. In the following the files that were not mentioned in the previous chapter and the details of the previously mentioned local to global enumeration are described.

`afemCRLaplaceEVP.m` is the main script that implements the proposed AFEM loop based on the eigenvalue bounds.

The folder *CR* contains the implementation of the Crouzeix-Raviart nonconforming finite element space of first (and of third) order in the class object `CRk`. The file

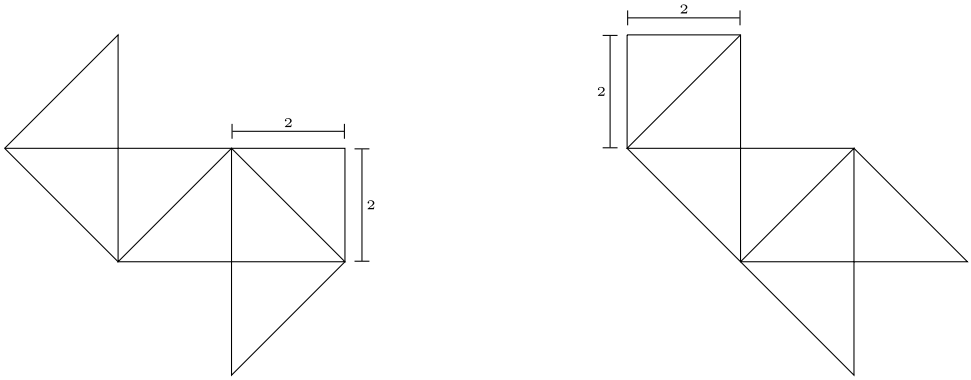

Figure 4.8: Two isospectral domains.

	lower bounds	
N	left domain	right domain
186	8.484029241600**799**	8.484029241600**801**
708	22.079541883464980	22.079541883464987
2760	40.139305042643208	40.139305042643237
10896	49.823736249152233	49.823736249152240
43296	53.022275017108896	53.022275017108903
172608	53.889870459421545	53.889870459421537
689280	54.112360562895724	54.112360562895560
2754816	54.168723796821510	54.168723796821538
11014656	54.183012990240513	54.183012990240186
	upper bounds	
N	left domain	right domain
186	114.265331199149**0**	114.265331199148**8**
708	64.39713286238**6258**	64.39713286238**7565**
2760	56.619351329573**185**	56.619351329573**249**
10896	54.818424684560**334**	54.818424684560**306**
43296	54.352753736838**082**	54.352753736838**132**
172608	54.231273697990**432**	54.231273697990**602**
689280	54.199573365120**656**	54.199573365121**147**
2754816	54.191162363149**061**	54.191162363147**861**
11014656	54.188868310**30701**	54.188868310**29948**

Table 4.2: Bounds for $\lambda_{50} = 54.187936$ for the isospectral domains of Figure 4.8.

```
|-- afemCRLaplaceEVP.m (main script)
|-- Mesh.m
|-- solvePkLaplaceEigenvalue.m
|-- CR
|   |-- CRInterpolation.m
|   |-- CRk.m
|-- Geometries
|   `-- ... (several geometric data)
|-- Pk
|   |-- Pk.m
|   |-- PkEvaluate.m
|   |-- PkFunctionHandles.m
|   |-- PkInterpolation.m
|   `-- PkMatrix.m
`-- Tools
    |-- integrate.m
    |-- localDoFtoGlobalDoF.m
    |-- matMul.m
    |-- Multigrid.m
    |-- ncPostProc.m
    `-- plotConvergence.m
```

Table 4.3: The software directory of Chapter 4.

`CRInterpolation.m` contains functions to compute the prolongation matrix. A special property of the nonconforming Crouzeix-Raviart finite element is its diagonal mass matrix. The assembly of the mass matrix is displayed below.

```
1 o = zeros(mesh.nrElems,1);
  a = mesh.area4e/3;
  localMama = reshape([a,o,o,o,a,o,o,o,a]',[3 3 mesh.nrElems]);
  [I,J] = localDoFtoGlobalDoF(dofU4e);
5 B = sparse(I(:),J(:),localMama(:));
```

Lines 1-3 create the local mass matrices

$$\frac{|T|}{3}\begin{pmatrix} 1 & & \\ & 1 & \\ & & 1 \end{pmatrix},$$

with entries $B_{j,k} = \int_\Omega \varphi_j \varphi_k \, dx$. Line 4 maps the local degrees of freedom to the global enumeration and line 5 assemblies the global mass matrix with only one `sparse` command.

The advantage of the diagonal mass matrix is that the algebraic residual estimate $\|\mathbf{r}\|_{\mathbf{B}^{-1}}$ can be explicitly computed as shown below.

```
6 r = A*x-eigenvalue*(B*x);
  BInv = spdiags(1./spdiags(A,0),0,size(B,1),size(B,2));
  rNorm = sqrt(r'*BInv*r);
```

`localDoFtoGlobalDoF.m` implements the local to global numbering as displayed below.

```
9  function [I,J] = localDoFtoGlobalDoF(dof4e1,dof4e2)
10    if nargin < 2
         dof4e2 = dof4e1;
      end
      nrDoF1 = size(dof4e1,2);
      nrDoF2 = size(dof4e2,2);
15    dof4e1 = dof4e1';
      I = repmat(dof4e1,nrDoF2,1);
      I = I(:);
      dof4e2 = dof4e2';
      J = (dof4e2(:)*ones(1,nrDoF1))';
20    J = J(:);
   end
```

The input are two matrices where the rows contain the global enumeration for the degrees of freedom on each triangle. The first input contains the enumeration for the columns and the second for the rows of the global matrix. The output are two arrays that contain the global enumeration for the local matrices with respect to linear indexing. If the first and the second argument of the underlying bilinear form is discretised in the same finite element space only one input is needed and the second will be a copy of the first one (lines 10-12). Lines 15-17 copy the global enumeration for the columns the number of rows times. Finally lines 18-20 copy the global enumeration for the rows the number of columns times.

`ncPostProc.m` computes the interpolation $\mathcal{I}_{CM}u_{CR} \in V_C(\mathcal{T})$ of $u \in CR_0^1(\mathcal{T})$.

5 An Adaptive Finite Element Method with Asymptotic Saturation for Eigenvalue Problems

This chapter discusses adaptive finite element methods (AFEMs) for the solution of elliptic eigenvalue problems associated with partial differential operators. An adaptive method based on nodal-patch refinement leads to an asymptotic error reduction property for the computed sequence of simple eigenvalues and eigenfunctions. This justifies the use of the proven saturation property for a class of reliable and efficient hierarchical a posteriori error estimators. Numerical experiments confirm that the saturation property is present even for very coarse meshes for many examples; in other cases the smallness assumption on the initial mesh may be severe.

This chapter is joint work with C. Carstensen, V. Mehrmann and A. Miedlar and is submitted for publication [38].

5.1 Introduction

We discuss the error reduction (also called saturation) property in adaptive finite element (AFEM) methods. This property is a frequent assumption that a mesh refinement procedure will eventually lead to convergence of the approximate finite element solution to the exact solution. For boundary value problems associated with linear second order elliptic partial differential equations (PDEs), this assumption has been reasonably justified in [49], and is used in a number of publications, [1, 13, 53, 108].

For the eigenvalue problem associated with partial differential equations, the mathematical justification of the ad hoc saturation assumption, see e.g. [91, 92], is widely open even in the asymptotic range for extremely small mesh-sizes.

This chapter lays the mathematical justification of the saturation property for the simplest model problem of an elliptic PDE eigenvalue problem of Section 2.3, i.e., for the Laplace operator on a bounded Lipschitz domain $\Omega \subset \mathbb{R}^2$, which is the problem of determining an eigenvalue/eigenfunction pair $(\lambda, u) \in \mathbb{R} \times \{H_0^1(\Omega) \cap H_{loc}^2(\Omega)\}$ such that

$$-\Delta u = \lambda u \quad \text{in } \Omega \qquad \text{and} \qquad u = 0 \quad \text{on } \partial\Omega. \tag{5.1}$$

It is well known, that problem (5.1) has a countable number of eigenvalue/eigenfunction pairs with positive eigenvalues that can be ordered increasingly [10].

We will discuss the case of determining one single and simple eigenvalue λ, i.e., we assume that there is no other eigenvalue in a small neighbourhood of λ, and we present an adaptive finite element method for a *single* sequence of eigenvalue/eigenfunction pairs $(\lambda_\ell, u_\ell)_{\ell \in \mathbb{N}_0}$ of the discretised problem. For this method we will prove the *asymptotic saturation condition*, that there exists a constant $0 \leq \varrho < 1$ such that any two subsequent

mesh refinement levels ℓ and $\ell+1$ with maximal mesh-sizes H_ℓ, $H_{\ell+1}$ satisfy

$$|\lambda - \lambda_{\ell+1}| + |||u - u_{\ell+1}|||^2 \leq \varrho \left(|\lambda - \lambda_\ell| + |||u - u_\ell|||^2 \right) + 2\lambda_{\ell+1}^3 H_\ell^4. \tag{5.2}$$

The adaptive algorithm utilizes a patch-oriented refinement process based on the newest-vertex bisection without interior node property and there is no need to compute any higher-order or fine-grid solutions.

Note that the remainder term of *oscillations* $\lambda_{\ell+1}^3 H_\ell^4$ in (5.2) is explicit even with the multiplicative constant 2 in front of it. This justifies the assumption of [91, 92] that this remainder may be neglected for sufficiently small mesh-sizes.

Our results complement those of [33] where it is shown that oscillations can be neglected under certain particular assumptions on the meshes; however the same global arguments do not apply in the present situation.

The numerical examples of Section 5.5 verify the (asymptotic) reliability and efficiency of the hierarchical error estimator and therefore confirm the (asymptotic) saturation property. For the smallest eigenvalue, the mesh-size restrictions on H_0 are empirically not visible, but they are certainly more severe for larger eigenvalues with much more oscillatory eigenfunctions.

The saturation property has to be considered in comparison to the error estimator reduction in the convergence analysis of adaptive finite element eigenvalue solvers [33, 34, 45]. In explicit residual-based error estimators, the mesh-size enters as a weight and hence reduces under refinement. This implies a reduction property of such error estimators and eventually leads to linear convergence of some total error which is a convex combination of the error estimator and the error; cf. e.g. [33, Thm 5.2], [34, Lemma 5.3], [45, Thm 5.2]. In contrast to this, the saturation property describes the reduction (5.2) of the error terms without involving any error estimator contribution, but with immediate important applications in the context of the solution of the algebraic eigenvalue problems that have to be solved at each level of refinement [91, 92]. The proofs are rather independent, e.g., the saturation property (5.2) cannot be proved by simply reducing the mesh-size.

The outline of the remaining part of this chapter is as follows. Section 5.2 describes the adaptive finite element method (AFEM) based on patch refinement. The discrete efficiency of the edge residual a posteriori error estimator is introduced in Section 5.3. The proof of the saturation property and its equivalence to the reliability and the efficiency of the hierarchical error estimator follow in Section 5.4. Section 5.5 verifies the theoretical results for some numerical benchmark problems on the unit square, the L-shaped domain, and two isospectral domains.

5.2 Adaptive Finite Element Method

Consider the elliptic eigenvalue problem (5.1) and let $\mathcal{T}_\ell$ denote a shape-regular triangulation of Ω into triangles as in Subsection 2.5. The linear conforming finite element

space for the triangulation $\mathcal{T}_\ell$ is defined by

$$V_\ell := \left\{ v \in H_0^1(\Omega) : \text{ for all } \ T \in \mathcal{T}_\ell,\, v|_T \text{ is affine} \right\}.$$

The adaptive finite element method computes a sequence of discrete subspaces

$$V_0 \subsetneq V_1 \subsetneq V_2 \subsetneq \ldots \subsetneq V_\ell \subset V$$

via successive local refinement of the underlying mesh $\mathcal{T}_0, \mathcal{T}_1, \mathcal{T}_2, \ldots$ of the domain Ω through a loop of the form

$$\text{Solve} \rightarrow \text{Estimate} \rightarrow \text{Mark} \rightarrow \text{Refine}.$$

In the following we briefly summarize these components, for details see [27, 33]. The input consists of a shape-regular triangulation $\mathcal{T}_0$ (with some initialization of the reference edges) and some bulk parameter $0 < \theta \leq 1$.

5.2.1 Solve

Consider the weak formulation of the eigenvalue problem given in Section 2.3 with bilinear forms $a(\cdot,\cdot)$ and $b(\cdot,\cdot)$ that induce the norms $|\!|\!|.|\!|\!| := |.|_{H^1(\Omega)}$ on $V := H_0^1(\Omega)$ and $\|.\| := \|.\|_{L^2(\Omega)}$ on $L^2(\Omega)$.

The corresponding discrete eigenvalue problem consists of determining an eigenvalue/eigenfunction pair $(\lambda_\ell, u_\ell) \in \mathbb{R} \times V_\ell$ with $b(u_\ell, u_\ell) = 1$ and

$$a(u_\ell, v_\ell) = \lambda_\ell b(u_\ell, v_\ell) \quad \text{for all } v_\ell \in V_\ell.$$

Using the coordinate representation, the discrete eigenvalue problem leads to the finite-dimensional generalized algebraic eigenvalue problem

$$A_\ell x_\ell = \lambda_\ell B_\ell x_\ell$$

for the stiffness and mass matrices

$$A_\ell = [a(\varphi_i, \varphi_j)]_{j,k=1,\ldots,N_\ell} \qquad \text{and} \qquad B_\ell = [b(\varphi_i, \varphi_j)]_{j,k=1,\ldots,N_\ell}$$

associated with the nodal basis functions $\varphi_1, \ldots, \varphi_{N_\ell}$ of $V_\ell = \{\varphi_1, \ldots, \varphi_{N_\ell}\}$, with the discrete eigenvector $x_\ell =: [x_{\ell,1}, \ldots, x_{\ell,N_\ell}]^T$. The approximated eigenfunction is then expressed as

$$u_\ell = \sum_{k=1}^{N_\ell} x_{\ell,k} \varphi_k \in V_\ell.$$

5.2.2 Estimate

The error in the eigenvalue/eigenfunction pair can be estimated a posteriori via

$$|\lambda - \lambda_\ell| + \|\!|u - u_\ell|\!\|^2 \lesssim \mu_\ell^2 := \|\!|u_{\ell-1} - u_\ell|\!\|^2.$$

Recall that $\lesssim$ denotes an inequality that holds up to a multiplicative constant.

Such an a posteriori error estimator for the discussed Laplace eigenvalue problem has been presented in [91]. Hierarchical a posteriori error estimators based on edge bubble-functions were considered in [65, 92] for the eigenvalues and eigenfunctions.

5.2.3 Mark

For the triangulation $\mathcal{T}_\ell$ let N_ℓ (resp. $N_\ell(\Omega)$) denote the set of nodes (resp. interior nodes) and let $\mathcal{E}_\ell$ (resp. $\mathcal{E}_\ell(\Omega)$) denote the set of edges (resp. interior edges). For a node $z \in N_\ell$, we denote by $\mathcal{E}_\ell(z) \subseteq \mathcal{E}_\ell$ the subset of edges that share the node z and by ω_z the union of triangles in $\mathcal{T}_\ell$ that share the node z. The maximal mesh-size is denoted by $H_\ell := \max_{T\in\mathcal{T}_\ell} \operatorname{diam}(T)$. For $E \in \mathcal{E}_\ell(\Omega)$ let $T_+, T_- \in \mathcal{T}_\ell$ be the two neighbouring triangles such that $E = T_+ \cap T_-$. The jump of the discrete gradient ∇u_ℓ along an inner edge $E \in \mathcal{E}_\ell(\Omega)$ in normal direction ν_E, pointing from T_+ to T_-, is defined by $[\nabla u_\ell] \cdot \nu_E := \left(\nabla u_\ell|_{T_+} - \nabla u_\ell|_{T_-}\right) \cdot \nu_E$.

The patch-oriented marking strategy employs the edge residual a posteriori error estimator for the eigenvalue problem, see [33, 50],

$$\eta_\ell^2 := \sum_{E\in\mathcal{E}_\ell(\Omega)} \eta_\ell^2(E) \quad \text{with} \quad \eta_\ell^2(E) := |E|\|[\nabla u_\ell] \cdot \nu_E\|_{L^2(E)}^2, \tag{5.3}$$

which is reliable and efficient for sufficiently small mesh-size H_0 [33], in the sense that

$$\|\!|u - u_\ell|\!\| \approx \eta_\ell. \tag{5.4}$$

Based on the local refinement indicators $\eta_\ell(E)$ nodes are marked for refinement. Let $\mathcal{M}_\ell \subseteq N_\ell(\Omega)$ be the minimal set of refinement nodes such that for $0 < \theta \leq 1$ the bulk criterion [48] is fulfilled, i.e.,

$$\theta \sum_{z\in N_\ell(\Omega)} \eta_\ell^2(\mathcal{E}_\ell(z)) \leq \sum_{z\in\mathcal{M}_\ell} \eta_\ell^2(\mathcal{E}_\ell(z)).$$

5.2.4 Refine

For all refinement nodes $z \in \mathcal{M}_\ell \subseteq N_\ell(\Omega)$ mark all edges $\mathcal{E}_\ell(z)$ for refinement. The mesh is then refined by the closure algorithm of Section 2.5.1 and the red-green-blue refinement algorithm of Section 2.5.2. Note that all triangles $T \subseteq \overline{\omega}_z$, $z \in \mathcal{M}_\ell$, are refined either *red* or *blue*.

In the following sections we analyse the properties of this adaptive FEM technique.

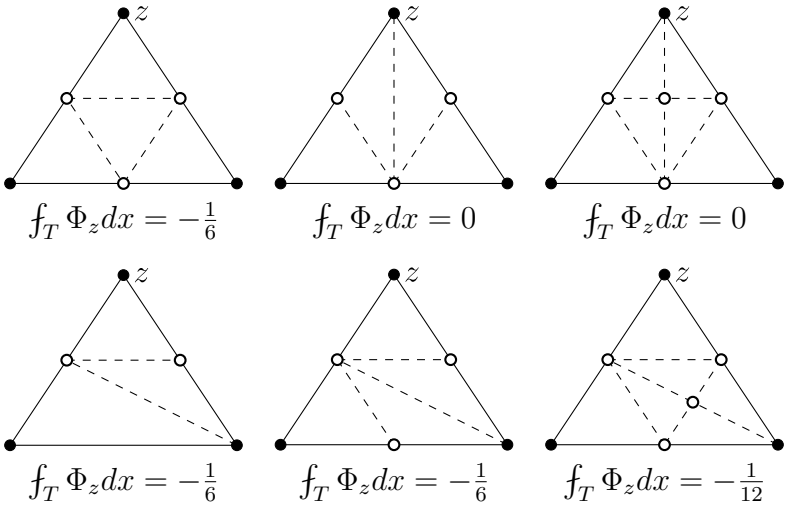

Figure 5.1: All possible sub-triangulations for a triangle $T \subset \overline{\omega}_z$ in the proof of Theorem 5.3.1 with values of $⨍_T \Phi_z dx$.

5.3 Discrete Efficiency

This section introduces the discrete efficiency of η_ℓ as defined in (5.3). A key ingredient for the proof is the following fine-grid function. Let $\varphi_z \in V_\ell$ denote the shape function associated with the node $z \in N_\ell(\Omega)$. Under the assumption that all edges $\mathcal{E}_\ell(z)$ are refined, let ψ_E be the linear shape function of the refined triangulation $\mathcal{T}_{\ell+1}$ associated with the midpoint of the edge $E \in \mathcal{E}_\ell$,

$$\Phi_z := \varphi_z - \sum_{E \in \mathcal{E}_\ell(z)} \psi_E \in H^1_0(\omega_z) \subseteq V.$$

Theorem 5.3.1. *Consider the adaptive FEM of Section 5.2. For some node $z \in N_\ell(\Omega)$ let all edges $\mathcal{E}_\ell(z)$ be bisected in $\mathcal{T}_{\ell+1}$. If z is not opposite to the reference edge $E(T)$ or T is refined by* red*-refinement for at least one triangle T of ω_z, (see Figure 2.3), then*

$$⨍_{\omega_z} \Phi_z \, dx \approx 1 \qquad \text{and} \qquad ⨍_E \Phi_z \, ds = 0 \text{ for all } E \in \mathcal{E}_\ell(\omega_z).$$

Proof. The second assertion, that $⨍_E \Phi_z \, ds = 0$ for all $E \in \mathcal{E}_\ell(\omega_z)$ follows directly from the definition of Φ_z. For the first assertion all possible sub-triangulations together with the values of $⨍_T \Phi_z dx$ are depicted in Figure 5.1. Note that the sub-triangulations for a triangle T of ω_z that result in values $⨍_T \Phi_z dx = 0$ are excluded by assumption and that all other possible sub-triangulations share the same sign for $⨍_T \Phi_z dx$. □

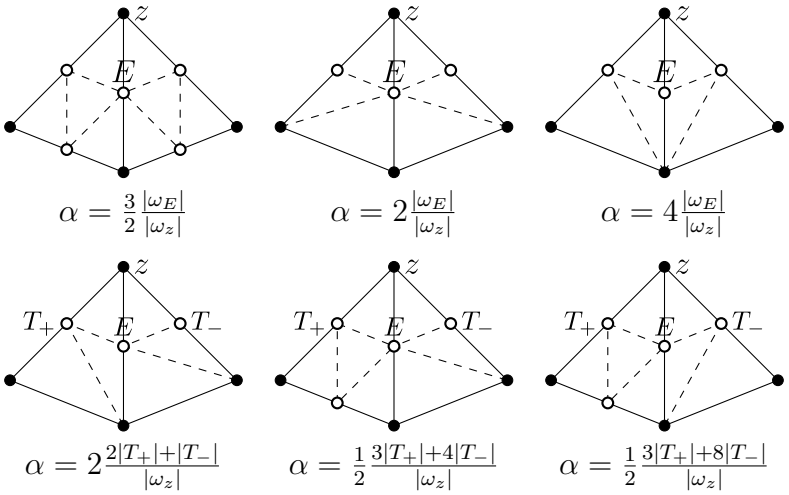

Figure 5.2: All possible sub-triangulations of ω_E in the proof of Theorem 5.3.2 with values of α.

Theorem 5.3.2 (Discrete efficiency)**.** *Consider the adaptive FEM of Section 5.2. Then for any refinement level $\ell \in \mathbb{N}_0$ the following estimate holds*

$$\eta_\ell \lesssim |\!|\!| u_\ell - u_{\ell+1} |\!|\!| + \lambda_{\ell+1}^{3/2} H_\ell^2.$$

Proof. In the *first step* observe that the bulk criterion implies that

$$\eta_\ell^2 \leq \sum_{z \in N_\ell(\Omega)} \eta_\ell^2(\mathcal{E}_\ell(z)) \leq \theta^{-1} \sum_{z \in \mathcal{M}_\ell} \eta_\ell^2(\mathcal{E}_\ell(z)). \tag{5.5}$$

The *second step* is to show that any refinement node $z \in \mathcal{M}_\ell$ and any edge E of $\mathcal{E}_\ell(z)$ satisfy

$$\eta_\ell(E) \lesssim \|\nabla(u_\ell - u_{\ell+1})\|_{L^2(\omega_z)} + \lambda_{\ell+1}\mathrm{diam}(\omega_z)^2 \|\nabla u_{\ell+1}\|_{L^2(\omega_z)}. \tag{5.6}$$

Since $[\nabla u_\ell] \cdot \nu_E$ is constant along the edge E of length $|E|$ with some sign $\pm$ as indicated below, it follows that

$$\pm\eta_\ell(E) = |E|([\nabla u_\ell] \cdot \nu_E).$$

The edge basis function ψ_E from the beginning of this section satisfies $|E| = 2\int_E \psi_E \, ds$. Hence,

$$\pm\eta_\ell(E)/2 = \int_E \psi_E [\nabla u_\ell] \cdot \nu_E \, ds.$$

Let $T_\pm \in T_\ell$ denote the two triangles that share the edge E. Theorem 5.3.1 shows that

$\int_E \Phi_z ds = 0$. With α being the value from Figure 5.2, this implies that

$$\pm\eta_\ell(E)/2 = \int_E (\psi_E + \alpha\Phi_z)\,[\nabla u_\ell]\cdot\nu_E\,ds.$$

Note that $\Delta u_\ell|_{T_\pm} \equiv 0$ and that the function $v_{\ell+1} := \psi_E + \alpha\Phi_z \in V_{\ell+1}$ satisfies $\int_F v_{\ell+1} ds = 0$ on all other edges $F \in \mathcal{E}_\ell(\omega_z)\backslash E$. Therefore, the piecewise Gauss divergence theorem [52] leads to

$$\pm\eta_\ell(E)/2 = \int_{\omega_z} \nabla v_{\ell+1}\cdot\nabla u_\ell dx$$

In fact all the volume contributions and all other edge contributions vanish. Hence,

$$\pm\eta_\ell(E)/2 = \int_{\omega_z} \nabla v_{\ell+1}\cdot\nabla(u_\ell - u_{\ell+1})dx + \int_{\omega_z} \nabla v_{\ell+1}\cdot\nabla u_{\ell+1}dx. \tag{5.7}$$

The first term in (5.7) is estimated via the Cauchy-Schwarz inequality [27] and the discrete estimate $\|\nabla v_{\ell+1}\|_{L^2(\omega_z)} \lesssim 1$, as

$$\int_{\omega_z} \nabla v_{\ell+1}\cdot\nabla(u_\ell - u_{\ell+1})dx \le \|\nabla(u_\ell - u_{\ell+1})\|_{L^2(\omega_z)}.$$

Since $v_{\ell+1}$ is supported on ω_z, the second term in (5.7) can be written as

$$\int_{\omega_z} \nabla v_{\ell+1}\cdot\nabla u_{\ell+1}dx = a(u_{\ell+1}, v_{\ell+1}).$$

Since $v_{\ell+1} \in V_{\ell+1}$, we then have

$$a(u_{\ell+1}, v_{\ell+1}) = \lambda_{\ell+1} b(u_{\ell+1}, v_{\ell+1}).$$

The choice of α as in Figure 5.2 shows that $⨍_{\omega_z} v_{\ell+1}dx = 0$, and hence $c_z := ⨍_{\omega_z} u_{\ell+1}dx$ satisfies

$$a(u_{\ell+1}, v_{\ell+1}) = \lambda_{\ell+1} b(u_{\ell+1} - c_z, v_{\ell+1}).$$

Applying Cauchy-Schwarz, Poincaré-Friedrich's inequality [27] plus the aforementioned discrete estimate

$$\|v_{\ell+1}\|_{L^2(\omega_z)} \lesssim \mathrm{diam}(\omega_z)\|\nabla v_{\ell+1}\|_{L^2(\omega_z)} \lesssim \mathrm{diam}(\omega_z)$$

show that

$$\lambda_{\ell+1} b(u_{\ell+1} - c, v_{\ell+1}) \lesssim \lambda_{\ell+1}\mathrm{diam}(\omega_z)^2\|\nabla u_{\ell+1}\|_{L^2(\omega_z)}.$$

The combination of the previous four estimates shows that

$$\int_{\omega_z} \nabla v_{\ell+1}\cdot\nabla u_{\ell+1}dx \lesssim \lambda_{\ell+1}\mathrm{diam}(\omega_z)^2\|\nabla u_{\ell+1}\|_{L^2(\omega_z)}.$$

Altogether, this second step proves (5.6).

Step three combines (5.5)-(5.6) with the finite overlap of all the patches to conclude that

$$\eta_\ell \lesssim |||u_\ell - u_{\ell+1}||| + \lambda_{\ell+1} H_\ell^2 |||u_{\ell+1}|||.$$

This and the identity $|||u_{\ell+1}||| = \lambda_{\ell+1}^{1/2}$ finish the proof. □

5.4 Saturation Property

This section is devoted to the main result of this chapter, the proof of the saturation property. It is also remarked that the saturation property is equivalent to the reliability of the hierarchical a posteriori error estimator.

Throughout this section, suppose that $(\lambda_\ell, u_\ell) \in \mathbb{R} \times V_\ell$ as well as $(\lambda_{\ell+1}, u_{\ell+1}) \in \mathbb{R} \times V_{\ell+1}$ is some discrete eigenvalue/eigenfunction pair associated with the continuous pair $(\lambda, u) \in \mathbb{R} \times V$ on the level ℓ and $\ell + 1$, respectively, and set $e_\ell := u - u_\ell$ and $e_{\ell+1} := u - u_{\ell+1}$. The eigenvalue error and the errors with respect to the norms $|||\cdot|||$ and $\|\cdot\|$ satisfy [105]

$$|||u - u_\ell|||^2 = \lambda \|u - u_\ell\|^2 + \lambda_\ell - \lambda. \tag{5.8}$$

Furthermore, the following regularity result [33, 50] holds for some constant $0 < C_{\mathrm{reg}} < \infty$,

$$\|u - u_\ell\| \le C_{\mathrm{reg}} H_\ell^s |||u - u_\ell|||, \tag{5.9}$$

where the regularity exponent $0 < s \le 1$ depends on the interior angles of the polygonal domain Ω and $s > 1/2$ holds for the pure Dirichlet boundary conditions of (5.1).

The proof of the saturation assumption requires the following quasi-orthogonality.

Theorem 5.4.1 (Quasi-orthogonality)**.** *Let $\mathcal{T}_{\ell+1}$ be a refinement of the triangulation $\mathcal{T}_\ell$ on some level ℓ in the adaptive FEM of Section 5.2. Then there exists $\varepsilon \lesssim H_0^{2s}$ such that*

$$|||u_{\ell+1} - u_\ell|||^2 \le (1 + \varepsilon) |||e_\ell|||^2 - |||e_{\ell+1}|||^2. \tag{5.10}$$

Proof. The quasi-orthogonality result of Lemma 3.3.1 of Chapter 3 implies that

$$|||u_{\ell+1} - u_\ell|||^2 \le |||e_\ell|||^2 - |||e_{\ell+1}|||^2 + \lambda \|e_{\ell+1}\|^2 + \lambda_{\ell+1} \|u_{\ell+1} - u_\ell\|^2.$$

Let $G_\ell : V \to V_\ell$ denote the Galerkin projection, $a(v - G_\ell v, \cdot)|_{V_\ell} = 0$ for all $v \in V$. The proof of [33, Theorem 3.1] shows that

$$\|u - u_\ell\| \lesssim H_\ell^s |||u - G_\ell u|||.$$

Since $V_\ell \subset V_{\ell+1}$, the best approximation property of the Galerkin projection [27] leads

to

$$\|u - u_\ell\| + \|u - u_{\ell+1}\| \leq 2C_{\mathrm{reg}} H_\ell^s |\!|\!| u - u_\ell |\!|\!|.$$

This and the min-max principle [105] imply (5.10) with $\varepsilon := (\lambda + 4\lambda_0) C_{\mathrm{reg}}^2 H_0^{2s}$. □

Theorem 5.4.2 (Saturation property)**.** *Consider the adaptive FEM of Section 5.2 for some $\mathcal{T}_0$ with sufficiently small maximal mesh-size H_0. Then there exists $0 \leq \varrho < 1$ such that for all $\ell \in \mathbb{N}_0$ the following inequalities hold*

$$|\!|\!| u - u_{\ell+1} |\!|\!|^2 \leq \varrho |\!|\!| u - u_\ell |\!|\!|^2 + \lambda_{\ell+1}^3 H_\ell^4; \tag{5.11}$$

$$|\lambda - \lambda_{\ell+1}| \leq \varrho |\lambda - \lambda_\ell| + \lambda_{\ell+1}^3 H_\ell^4. \tag{5.12}$$

Proof. Theorem 5.3.2 and (5.4) imply for H_0 sufficiently small that

$$|\!|\!| u - u_\ell |\!|\!|^2 \lesssim |\!|\!| u_\ell - u_{\ell+1} |\!|\!|^2 + \lambda_{\ell+1}^3 H_\ell^4.$$

This and the quasi-orthogonality of Theorem 5.4.1 imply the existence of some generic constant $0 < c \leq 1$ such that

$$c |\!|\!| u - u_\ell |\!|\!|^2 \leq (1 + \varepsilon) |\!|\!| u - u_\ell |\!|\!|^2 - |\!|\!| u - u_{\ell+1} |\!|\!|^2 + \lambda_{\ell+1}^3 H_\ell^4.$$

This is equivalent to

$$|\!|\!| u - u_{\ell+1} |\!|\!|^2 \leq (1 + \varepsilon - c) |\!|\!| u - u_\ell |\!|\!|^2 + \lambda_{\ell+1}^3 H_\ell^4.$$

The assertion follows from this with $0 \leq \varrho := (1 + \varepsilon - c) < 1$ for sufficiently small H_0. To prove the second saturation property (5.12), recall the inequalities (5.8) and (5.9) which imply

$$\begin{aligned} |\lambda - \lambda_{\ell+1}| &\leq |\!|\!| u - u_{\ell+1} |\!|\!|^2; \\ |\!|\!| u - u_\ell |\!|\!|^2 &\leq |\lambda - \lambda_\ell| + \lambda C_{\mathrm{reg}}^2 H_\ell^{2s} |\!|\!| u - u_\ell |\!|\!|^2. \end{aligned}$$

For any $H_0 < \lambda^{-1/(2s)} C_{\mathrm{reg}}^{-1/s}$, this shows

$$|\!|\!| u - u_\ell |\!|\!|^2 \leq \frac{|\lambda - \lambda_\ell|}{1 - \lambda C_{\mathrm{reg}}^2 H_0^{2s}}. \tag{5.13}$$

This and (5.11) lead to (5.12) with the constant

$$0 \leq \varrho := (1 + \varepsilon - c)(1 - \lambda C_{\mathrm{reg}}^2 H_0^{2s})^{-1} < 1.$$ □

Note that the saturation property implies (5.2). A surprising consequence of this saturation property is that the higher-order terms $\lambda_{\ell+1}^3 H_\ell^4$ do not depend on the (possibly reduced) convergence rates of the errors $|\!|\!| u - u_\ell |\!|\!|^2 + |\lambda - \lambda_\ell|$ on (non-convex) polygonal domains.

In the subsequent theorem we show that the saturation property is actually equivalent to the reliability of the adaptive method.

Theorem 5.4.3 (Saturation $\Leftrightarrow$ reliability)**.** *Consider the adaptive FEM of Section 5.2 with H_0 sufficiently small. Then for some $0 \leq \varrho < 1$, $0 < c \leq 1$, and all $\ell \in \mathbb{N}_0$, the following inequalities* (5.14) *and* (5.15) *are equivalent.*

$$\|\!|u - u_{\ell+1}|\!\| \leq \varrho \|\!|u - u_\ell|\!\| + \lambda_{\ell+1}^{3/2} H_\ell^2; \tag{5.14}$$

$$c\|\!|u - u_\ell|\!\| \leq \|\!|u_\ell - u_{\ell+1}|\!\| + \lambda_{\ell+1}^{3/2} H_\ell^2. \tag{5.15}$$

Proof. We first show that (5.14) with $0 \leq \varrho < 1$ implies (5.15) with $c := 1 - \varrho$. The triangle inequality plus the saturation property (5.14) yield for any $0 \leq \varrho < 1$ that

$$\begin{aligned} \|\!|u - u_\ell|\!\| &\leq \|\!|u - u_{\ell+1}|\!\| + \|\!|u_\ell - u_{\ell+1}|\!\| \\ &\leq \varrho \|\!|u - u_\ell|\!\| + \|\!|u_\ell - u_{\ell+1}|\!\| + \lambda_{\ell+1}^{3/2} H_\ell^2. \end{aligned}$$

This proves (5.15) with $c := 1 - \varrho$.

For the converse we show that (5.15) with $0 < c \leq 1$ implies (5.14) with $\varrho := (1 + \varepsilon - c^2/2)$. The quasi-orthogonality of Theorem 5.4.1 leads to

$$\|\!|u - u_{\ell+1}|\!\|^2 \leq (1 + \varepsilon) \|\!|u - u_\ell|\!\|^2 - \|\!|u_\ell - u_{\ell+1}|\!\|^2.$$

Inequality (5.15) and Young's inequality [52], results in

$$-\|\!|u_\ell - u_{\ell+1}|\!\|^2 \leq -c^2 \|\!|u - u_\ell|\!\|^2/2 + \lambda_{\ell+1}^3 H_\ell^4.$$

The combination of these inequalities leads to

$$\|\!|u - u_{\ell+1}|\!\|^2 \leq (1 + \varepsilon - c^2/2) \|\!|u - u_\ell|\!\|^2 + \lambda_{\ell+1}^3 H_\ell^4.$$

This proves (5.14) with $0 \leq \varrho := 1 + \varepsilon - c^2/2 < 1$ for sufficiently small H_0. □

Remark 5.4.4. It is shown in [33] that $\|\!|u - u_\ell|\!\| \approx \eta_\ell$ holds for sufficiently small H_0 without any higher-order terms. But this is an estimate for the error $\|\!|u - u_\ell|\!\|$ in contrast to the estimate (5.15) that involves the discrete error $\|\!|u_\ell - u_{\ell+1}|\!\|$. The arguments in the proofs of [33] are global, whereas the present analysis employs the discrete efficiency of Theorem 5.3.2 that does not allow for a global L^2 projection type argument. Hence (5.15) includes the higher-order oscillation terms.

Theorem 5.4.5 (Efficiency)**.** *Consider the adaptive FEM of Section 5.2. Let H_0 be sufficiently small such that the saturation property of Theorem 5.4.2 holds for $0 \leq \varrho < 1$. Then*

$$\|\!|u_\ell - u_{\ell+1}|\!\| \leq 2\|\!|u - u_\ell|\!\| + \lambda_{\ell+1}^{3/2} H_\ell^2 \quad \textit{and} \quad \|\!|u_\ell - u_{\ell+1}|\!\| \lesssim \|\!|u - u_\ell|\!\|.$$

Proof. The triangle inequality reads

$$\|\!|u_\ell - u_{\ell+1}|\!\| \leq \|\!|u - u_{\ell+1}|\!\| + \|\!|u - u_\ell|\!\|.$$

The first assertion then follows from the saturation property of Theorem 5.4.2. For a proof of the second inequality, the min-max principle [105] and (5.8) imply that

$$|\lambda - \lambda_{\ell+1}| \leq |\lambda - \lambda_\ell| \leq \|\!|u - u_\ell|\!\|^2.$$

Together with (5.13) this shows, that for sufficiently small H_0

$$\|\!|u - u_{\ell+1}|\!\|^2 \leq \frac{\|\!|u - u_\ell|\!\|^2}{1 - \lambda C_{\mathrm{reg}}^2 H_0^{2s}}. \qquad \square \tag{5.16}$$

These estimates hold for all *simple* eigenvalues in the spectrum. However, since the constant present in the upper bound depends on the exact eigenvalue λ we require the initial triangulation to be finer in order to obtain *reliable* and *efficient* approximations of higher eigenvalues. On the linear algebra level, due to the use of the Krylov subspace method, we obviously require a larger number of iteration steps for determining higher eigenvalues.

5.5 Numerical Examples

This section is devoted to numerical examples for the solution of the model problem (5.1) on three different domains Ω: the unit square, the L-shaped domain and the isospectral domains.

5.5.1 Preliminary Remarks

The numerical experiments show the performance of the proposed AFEM in comparison to uniform mesh refinement and compare the two a posteriori error estimators

$$\eta_\ell^2 := \sum_{E \in \mathcal{E}_\ell(\Omega)} |E| \|[\nabla u_\ell] \cdot \nu_E\|_{L^2(E)}^2 \qquad \text{and} \qquad \mu_\ell := \|\!|u_\ell - u_{\ell-1}|\!\|.$$

Note that Theorem 5.4.3 shows that for any level ℓ and sufficiently small H_0 that

$$\|\!|u - u_\ell|\!\| \lesssim \mu_{\ell+1} + \lambda_{\ell+1}^{3/2} H_\ell^2.$$

The use of this estimate, however, requires the knowledge of $u_{\ell+1}$. On the other hand, (5.16) shows for sufficiently small initial mesh-size H_0 that $\|\!|u - u_\ell|\!\| \lesssim \|\!|u - u_{\ell-1}|\!\|$. The combination with the aforementioned estimate (employed at level $\ell - 1$) gives

$$\|\!|u - u_\ell|\!\| \lesssim \mu_\ell + \lambda_\ell^{3/2} H_\ell^2.$$

In other words, μ_ℓ is a reliable a posteriori error estimator if H_ℓ is small. Throughout all of our numerical experiments, μ_ℓ is used as a posteriori error estimator on level ℓ.

5.5.2 Unit Square

Consider the model problem (5.1) on the unit square $\Omega = (0,1)^2$. The first eigenvalue/eigenfunction pair reads $(\lambda, u) = (2\pi^2, 2\sin(\pi x)\sin(\pi y))$. Since the solution is smooth, either uniform or adaptive mesh refinement lead to optimal convergence rates of $\mathcal{O}(N_\ell^{-1})$ for $|\lambda - \lambda_\ell|$ in Figure 5.3 and of order $\mathcal{O}(N_\ell^{-1/2})$ for $\|\!|u - u_\ell|\!\|$ in Figure 5.4. Note that for uniform refinement $\mathcal{O}(N_\ell^{-1/2}) = \mathcal{O}(H_\ell)$.

We observe in the experiments that the hierarchical a posteriori error estimators μ_ℓ^2 and μ_ℓ are closer to the eigenvalue and energy errors than the edge residual a posteriori error estimators η_ℓ^2 and η_ℓ. For adaptive refinement μ_ℓ^2 and μ_ℓ are almost exact. This is an empirical observation which is not mathematically justified by our theoretical analysis, because our estimates contain generic constants.

Note that for uniform refinements μ_ℓ is an upper bound while for adaptive refinement μ_ℓ provides a lower bound of the energy error. In contrast to this, η_ℓ is always an upper bound of the energy error. The same observations are made for μ_ℓ^2, η_ℓ^2 and the eigenvalue error.

5.5.3 L-Shaped Domain

Consider the model problem (5.1) on the L-shaped domain $\Omega = (-1,1)^2 \backslash ([0,1] \times [-1,0])$ with the first approximated eigenvalue $\lambda = 9.6397238440219$, see [17]. Since the eigenfunction has a singularity, uniform refinement leads to suboptimal convergence rates of order $\mathcal{O}(N_\ell^{-2/3})$, while adaptive refinement leads to empirical optimal convergence rates of order $\mathcal{O}(N_\ell^{-1})$ as displayed in Figure 5.5.

As in the previous example μ_ℓ^2 is an upper bound for uniform meshes and a lower bound for adaptive meshes, while η_ℓ^2 is always an upper bound. In both cases we observe that μ_ℓ^2 is much closer to the eigenvalue error than η_ℓ^2 and that for adaptive refinement μ_ℓ^2 is almost exact.

Figure 5.6 displays a sequence of refinements towards the corner singularity in the adaptively refined meshes.

5.5.4 Isospectral Domains

Consider the model problem (5.1) on the two isospectral domains of Figure 5.7 with the approximation of the 50-th eigenvalue $\lambda_{50} = 54.187936$, see [17]. Figure 5.8 shows the convergence history for the eigenvalue error.

We observe that adaptive refinement leads to slightly smaller errors for larger numbers of N_ℓ than uniform refinement. For uniform refinement both domains are discretised with the same number of degrees of freedom which results in the same approximated values (up to round-off errors) for the eigenvalue error and the a posteriori error estimators.

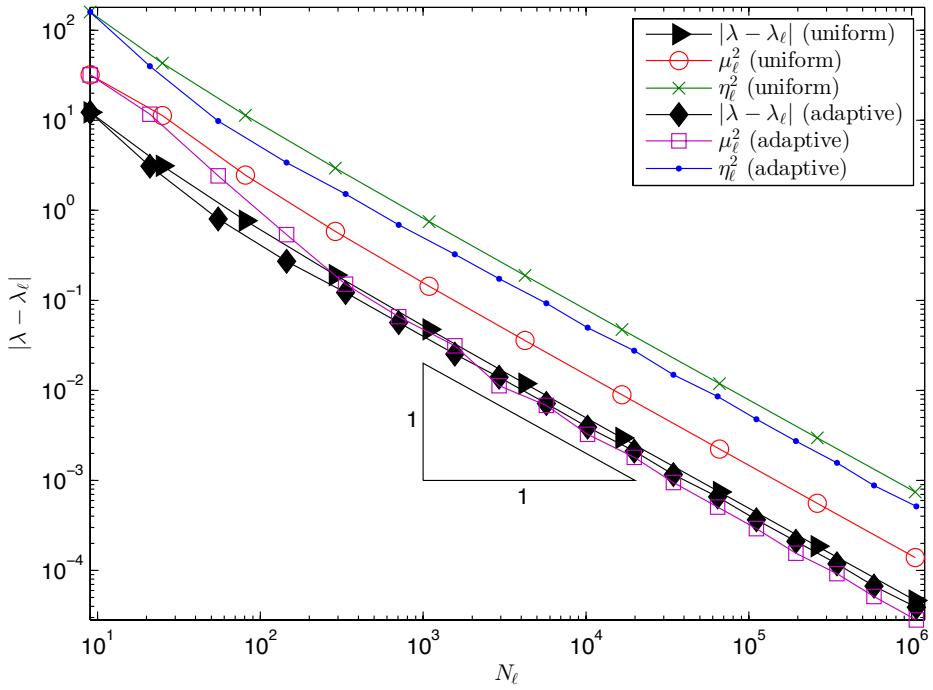

Figure 5.3: Convergence history for $|\lambda - \lambda_\ell|$, η_ℓ^2 and μ_ℓ^2 for uniform and adaptively refined meshes on the unit square.

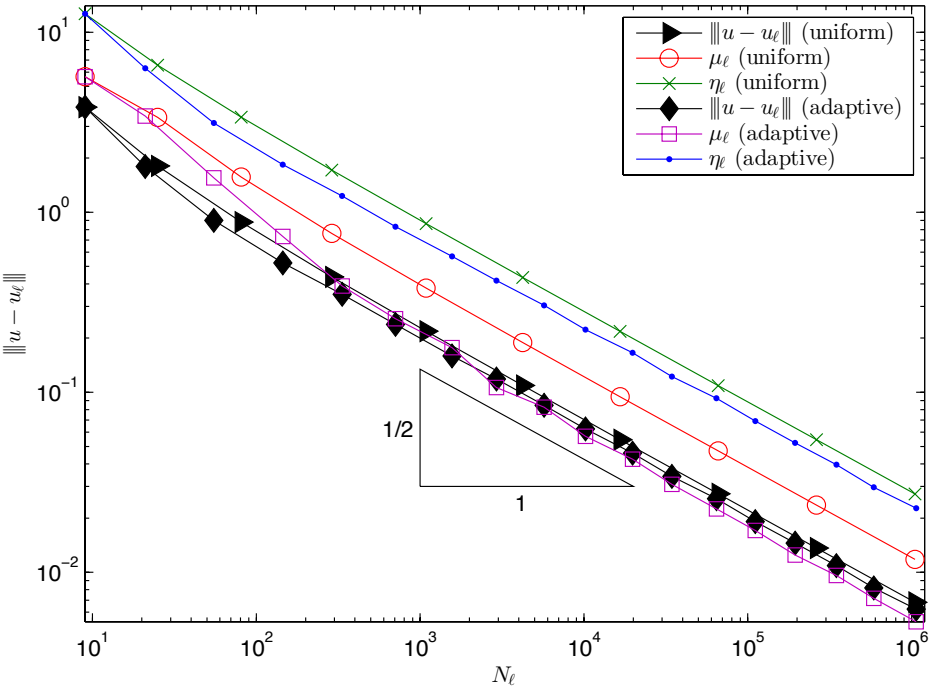

Figure 5.4: Convergence history for $|||u - u_\ell|||$, η_ℓ and μ_ℓ for uniform and adaptively refined meshes on the unit square.

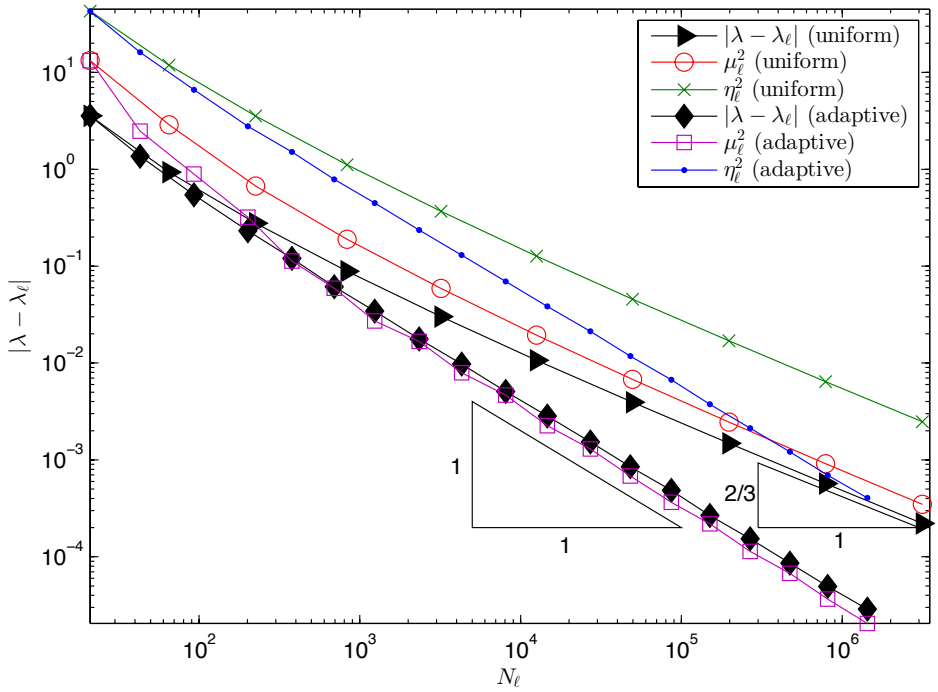

Figure 5.5: Convergence history for $|\lambda - \lambda_\ell|$, η_ℓ^2 and μ_ℓ^2 for uniform and adaptive refined meshes on the L-shaped domain.

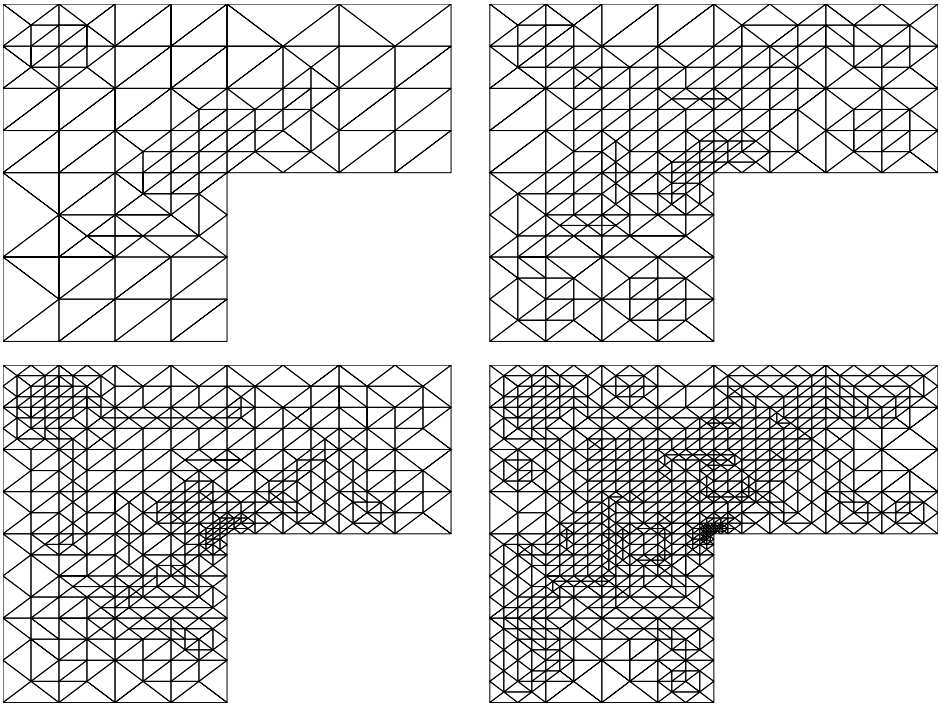

Figure 5.6: Sequence of adaptive refined meshes for the L-shaped domain for μ_ℓ with $N_\ell = 93, 201, 378, 694$.

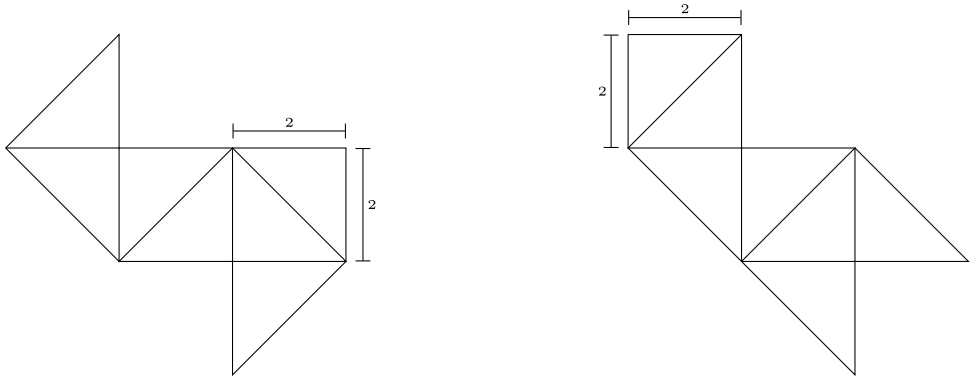

Figure 5.7: Two isospectral domains A (left) and B (right).

For adaptive refinement the values for the two domains lie asymptotically on the same convergence line.

Note that the pre-asymptotic range for μ_ℓ^2 on adaptive meshes is rather long due to the large eigenvalue and that the pre-asymptotic values for μ_ℓ^2 differ for both domains. Again we observe that asymptotically μ_ℓ^2 is almost exact for adaptive refinement.

This experiment provides numerical evidence that the mesh-size restriction due to the contributions $2\lambda_{\ell+1}^3 H_\ell^3$ in (5.2) can be severe. Despite of this, we observe convergence of the AFEM in all experiments. This follows from the analysis of [34].

5.5.5 Three hierarchical adaptive algorithms

The residual-based AFEM is compared to three different versions of hierarchical AFEMs based on the a posteriori error estimators $\mu_{\ell,k}$, $k = 2, 3, 4$. The hierarchical a posteriori error estimators utilize the fine-grid eigenvalue/eigenfunction pairs $(\hat{\lambda}_\ell, \hat{u}_\ell)$ of the uniform *red*-refinement $\hat{\mathcal{T}}_\ell$ of $\mathcal{T}_\ell$. The first version of the hierarchical a posteriori error estimator reads

$$\mu_{\ell,2}^2 := \sum_{T\in\mathcal{T}_\ell} \|\nabla(u_\ell - \hat{u}_\ell)\|_{L^2(T)}.$$

The discrete efficiency of Theorem 5.3.2 leads (for $\theta = 1$) to the a posteriori error estimator

$$\mu_{\ell,3}^2 := \sum_{T\in\mathcal{T}_\ell} \left(\|\nabla(u_\ell - \hat{u}_\ell)\|_{L^2(T)} + \hat{\lambda}_\ell \mathrm{diam}(T)^2 \|\nabla\hat{u}_\ell\|_{L^2(T)}\right).$$

The third version utilizes a separate marking strategy based on

$$\mu_{\ell,4} := |\!|\!| u_\ell - \hat{u}_\ell |\!|\!| + \hat{\lambda}_\ell^{3/2} H^2.$$

If $|\!|\!| u_\ell - \hat{u}_\ell |\!|\!| < \hat{\lambda}_\ell^{3/2} H^2$ then do uniform *red*-refinement, otherwise mark elements accordingly to $\mu_{\ell,2}$. The residual a posteriori error estimator [34, 50] reads

$$\eta_{\ell,2}^2 := \sum_{T\in\mathcal{T}_\ell} |T| \|\lambda_\ell u_\ell\|_{L^2(T)}^2 + \sum_{E\in\mathcal{E}_\ell(\Omega)} |E| \|[\nabla u_\ell]\cdot\nu_E\|_{L^2(E)}^2.$$

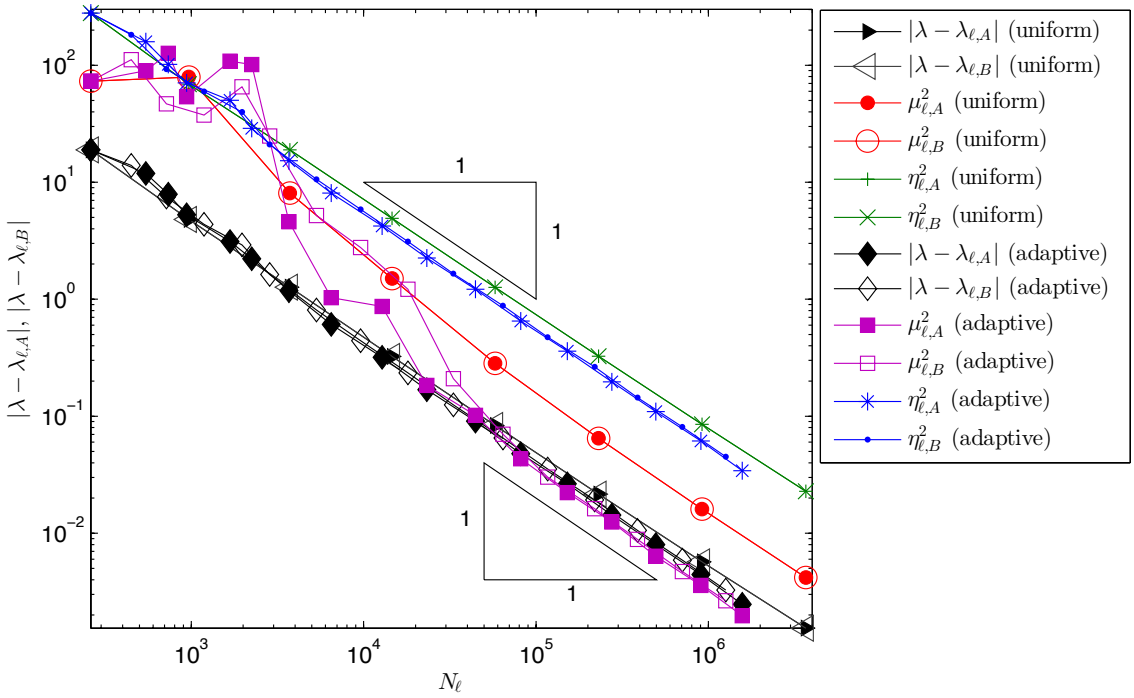

Figure 5.8: Convergence history for $|\lambda - \lambda_\ell|$, η_ℓ^2 and μ_ℓ^2 for uniform and adaptive refined meshes on both isospectral domains A and B.

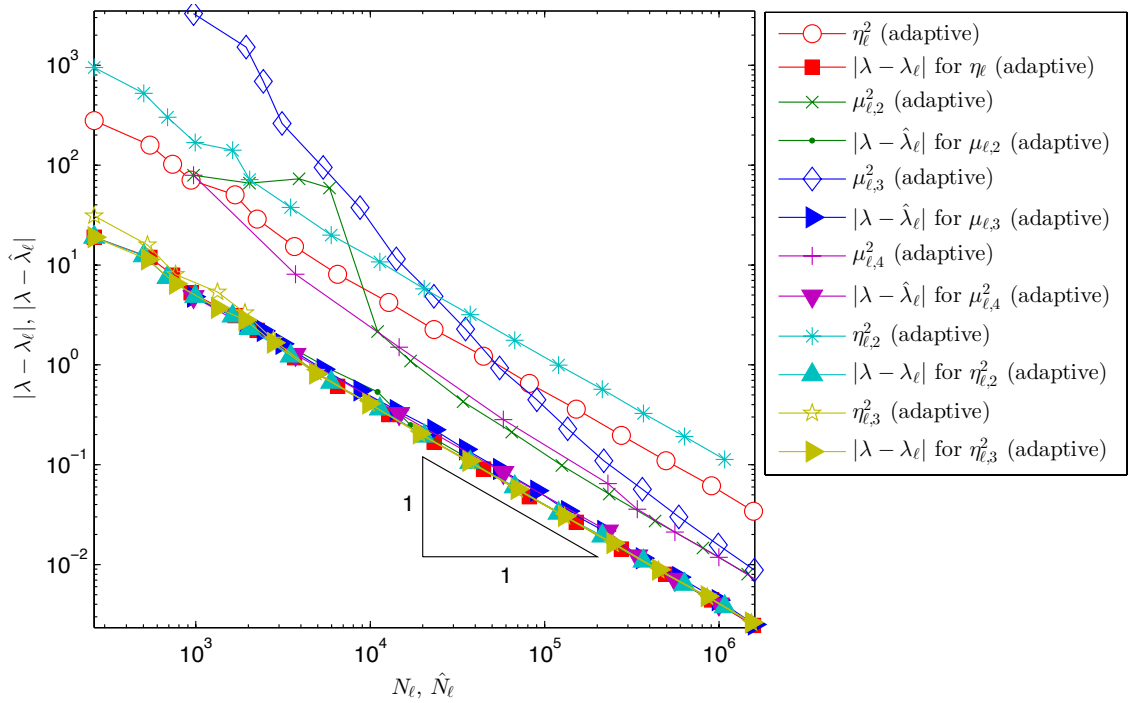

Figure 5.9: Convergence history for different adaptive refinements and the isospectral domain A.

For the averaging operator $A_\ell : P_0(\mathcal{T}_\ell)^2 \to \{V_\ell^2 \cap C(\Omega)^2\}$ for the nodal basis functions φ_z, $z \in N_\ell$,

$$A_\ell(\nabla u_\ell) := \sum_{z \in \mathcal{N}_\ell} \frac{1}{|\omega_z|} \left(\int_{\omega_z} \nabla u_\ell \, dx \right) \varphi_z,$$

the averaging a posteriori error estimator [33] reads

$$\eta_{\ell,3}^2 := \sum_{T \in \mathcal{T}_\ell} \|\nabla u_\ell - A_\ell(\nabla u_\ell)\|_{L^2(T)}^2.$$

Figure 5.9 shows a comparison of the AFEM driven by the a posteriori error estimators η_ℓ, $\eta_{\ell,2}$, $\eta_{\ell,3}$, $\mu_{\ell,2}$, $\mu_{\ell,3}$, and $\mu_{\ell,4}$ for λ_{50} on the isospectral domain A. Note that $\mu_{\ell,k}$, $k = 2, 3, 4$, are plotted versus the degrees of freedom $\hat{N}_\ell$ of the fine-grid solution and compared to the fine-grid eigenvalue errors $|\lambda - \hat{\lambda}_\ell|$. We observe that all AFEM lead to comparable eigenvalue errors but the behaviour of the estimators differs. The averaging estimator $\eta_{\ell,3}^2$ appears to be asymptotically exact. The two residual estimators η_ℓ^2 and $\eta_{\ell,2}^2$ are reliable and efficient from the very beginning and $\eta_{\ell,2}^2$ is larger than η_ℓ^2. The three versions of hierarchical a posteriori error estimators are asymptotically equal but exploit a different pre-asymptotic behaviour. In the pre-asymptotic range, the convergence of the error estimator $\mu_{\ell,2}^2$ is too slow while that of $\mu_{\ell,3}^2$ is too fast. In contrast, the separate marking strategy of the estimator $\mu_{\ell,4}^2$ leads to the best overall convergence.

5.5.6 Conclusions

We have proved the saturation assumption, as well as reliability and efficiency for an adaptive finite element method applied to the model problem of computing eigenvalues of the Laplace operator on Lipschitz domains.

The numerical examples confirm the proved (asymptotic) saturation property of Theorem 5.4.2.

The presented results apply to any simple eigenvalue, but it is clear that for the approximation of a highly oscillating eigenfunction of a larger eigenvalue the initial mesh needs to be sufficiently fine such that the oscillations are resolved.

The (asymptotic) reliability and efficiency of the hierarchical a posteriori error estimator are empirically verified for eigenvalue and energy errors.

The proposed AFEM leads to empirical optimal convergence rates for the eigenvalue and energy errors while uniform refinements leads to suboptimal rates in the presence of corner singularities.

The proposed AFEM is globally convergent in the sense that given any number $k \in \mathbb{N}\backslash\{0\}$ such that the initial problem at level zero is larger than or equal to k and that the step SOLVE computes the discrete eigenvalue λ_ℓ with number k (counted increasingly in multiplicity), then the output of the AFEM is a convergent sequence of real numbers with a limit which is an eigenvalue of (5.1). For a proof note that the bulk criterion in the AFEM of this chapter implies that of [33] and then Theorem 5.1 of that paper implies convergence. The optimality of AFEM is an open question and the recent progress in

```
|-- afemP1EllipticEigenvalueHierarchic.m (main script)
|-- estimatePkEigenvalue.m
|-- Mesh.m
|-- solvePkLaplaceEigenvalue.m
|-- Geometries
|   `-- ... (several geometric data)
|-- Pk
|   |-- Pk.m
|   |-- PkEvaluate.m
|   |-- PkFunctionHandles.m
|   |-- PkInterpolation.m
|   `-- PkMatrix.m
`-- Tools
    |-- integrate.m
    |-- localDoFtoGlobalDoF.m
    |-- matMul.m
    |-- Multigrid.m
    `-- plotConvergence.m
```

Table 5.1: The software directory of Chapter 5.

Chapter 3 does not lead to an immediate result here. The technical point is that in the present analysis no volume contributions are employed and the reliability proof relies upon some global L^2 projection which, seemingly, does not allow a localised version to prove discrete reliability.

The comparison between the hierarchical and the edge residual a posteriori error estimator shows that the hierarchical estimator is much closer to the error than the edge residual estimator. However, the hierarchical a posteriori error estimator does not provide guaranteed error control because it underestimates the error.

5.6 Software Implementation

The software directory with the software files used for the numerical experiments of this chapter is listed in Table 5.1. Since all files, except the main script

`afemP1EllipticEigenvalueHierarchic.m`

which implements the main AFEM loop, are described in the software descriptions of the previous two chapters, here the use of the `PkInterpolation` class object will be described.

For a fast evaluation of the hierarchical a posteriori error estimator

$$\mu_\ell = |||u_\ell - u_{\ell-1}|||$$

the coefficient vector on the previous level $\ell - 1$ is prolongated onto the level ℓ.

```
1  prolong = pk.mesh.pkInterpolation.getProlongation(pk,pkOld);
   xOld = prolong*x;
```

Since the sign of the eigenfunction may have changed from level $\ell - 1$ to level ℓ, μ_ℓ is computed as a minimum.

```
3  eta = min(sqrt((x-xOld)'*A*(x-xOld)),sqrt((x+xOld)'*A*(x+xOld)));
```

The `PkInterpolation` class object is initialised once at the beginning with the polynomial degree `degree`.

```
4  obj = PKInterpolation(degree)
```

Then the object computes once and for all the interpolation weights for the given polynomial degree and all possible refinements: *no*, *red*, *green*, *blue-left*, *blue-right*, and *bisec3* of Section 2.5. The weights at the Lagrange-points are determined in the following function.

```
5  function val = getRefProlongation(newFE,oldFE)
     c4dof = newFE.c4dof;
     val = zeros(newFE.nrBasisFunc,oldFE.nrBasisFunc,newFE.mesh.nrElems);
     for curElem = 1 : newFE.mesh.nrElems
       refPoints = c4dof(newFE.dofU4e(curElem,:),:);
10     val(:,:,curElem) = (oldFE.refBasisCoeff*...
                           oldFE.monomBasis(refPoints(:,1),refPoints(:,2))')';
     end
   end
```

The input is the finite element class for the old level `oldFE` which will be the reference element and the refined level of one of the refinements `newFE`. Line 6 gets all the coordinates of the degrees of freedom for the P_k finite element on the fine level. Line 7 initialised the output. Line 9 gets the coordinates of the fine degrees of freedom on the current fine-grid triangle and in line 10 the values of the coarse basis functions at the coordinates of the fine degrees of freedom are computed.

The `PkInterpolation` object is then attached to the `Mesh` class object and each time a triangle is refined in a certain way, the corresponding pre-computed interpolation matrix is copied to the matrix `localProlongations`. In addition the number of the parent element is stored in `parent4e`.

Then the prolongation matrix is computed in line 1 by a call of the function displayed below.

```
14 function val = getProlongation(newFE,oldFE)
15   S = newFE.mesh.localProlongations;
     parent4e = newFE.mesh.parent4e;
     [I,J] = localDoFtoGlobalDoF(newFE.dofU4e,oldFE.dofU4e(parent4e,:));
     indx = find(S);
     P = sparse(I(indx),J(indx),S(indx));
20   N = sparse(I(indx),J(indx),ones(numel(indx),1));
     N = spfun(@(x)(1./x),N);
     val = P.*N;
   end
```

The input consists of the new finite element `newFE` on the level ℓ and the old one `oldFE` of the previous level $\ell - 1$. The output is the prolongation matrix `val`. In lines 15-16 the stored local prolongations and the number of the parent elements are loaded. In line 17 the fine grid degrees of freedom of each triangle are combined with the coarse degrees of freedom of its parent element. The global assembly is done in line 19 but only for the non-zero entries determined in the previous line 18. Since now the weights for the nodal and edge degrees of freedom are added multiple times to the corresponding matrix entries, this is compensated by the lines 20-22.

6 A Posteriori Error Estimators for Convection-Diffusion Eigenvalue Problems

A posteriori error estimators for convection-diffusion eigenvalue model problems are discussed in [Heuveline and Rannacher, A posteriori error control for finite element approximations of elliptic eigenvalue problems, 2001] in the context of the dual-weighted residual method (DWR). This chapter directly addresses the variational formulation rather than the non-linear ansatz of Becker and Rannacher for some convection-diffusion model problem and presents a posteriori error estimators for the eigenvalue error based on averaging techniques. Two different postprocessing techniques attached to the DWR paradigm plus two new dual-weighted a posteriori error estimators are presented. The first new estimator utilises an auxiliary Raviart-Thomas mixed finite element method [28, 97] and the second exploits an averaging technique in combination with ideas of DWR. The six a posteriori error estimators are compared in three numerical examples and illustrate reliability and efficiency and the dependence of generic constants on the size of the eigenvalue or the convection coefficient.

This chapter is joint work with C. Carstensen and will be published in [59].

6.1 Introduction

While the numerical approximation of eigenvalues of symmetric second-order elliptic partial differential equations (PDEs) with real eigenpairs is relatively well understood, much less is known about non-symmetric problems with possibly complex eigenvalues. A posteriori error estimators for symmetric eigenvalue problems can be found in [50, 80, 89, 93, 108]. The convergence of the adaptive finite element method (AFEM) for the symmetric case is considered in [33, 58, 60, 100]. A posteriori error estimators for some non-symmetric eigenvalue problems can be found in [43, 69, 70]. It is the aim of this chapter to review the results of Heuveline and Rannacher in a direct approach rather than in the non-linear setting of the DWR paradigm following [12, 14, 69]. These results are also applicable to the averaging techniques as for the symmetric eigenvalue problem in [89]. Numerical experiments indicate that the efficiency indices for the residual-type a posteriori error estimators depend strongly on the convection coefficient β. Therefore, this chapter investigates the dual-weighted residual paradigm from Becker and Rannacher [12, 14, 15] and presents two new dual-weighted a posteriori error estimators. The first new estimator is based on the Raviart-Thomas mixed finite element method (MFEM) [28, 97] of first-order and the second one on averaging techniques. Hence, they are named dual-weighted mixed (DWM) and dual-weighted averaging (DWA) a posteriori estimators. This chapter presents numerical evidence that the DWR methodology in combination with the L^2 interpolation scheme of [111] is empirically reliable and efficient

for unstructured triangular meshes while [69] is restricted to structured meshes because of the approximation of the weights by second-order difference quotients.

The convection-diffusion model eigenvalue problem of Subsection 2.4 reads: Seek an eigenpair $(\lambda, u) \in \mathbb{C} \times \{H_0^1(\Omega;\mathbb{C}) \cap H_{loc}^2(\Omega;\mathbb{C})\}$ with

$$-\Delta u + \beta \cdot \nabla u = \lambda u \quad \text{in } \Omega. \tag{6.1}$$

The given data $\beta \in H(div, \Omega; \mathbb{R}^2)$ is assumed to be divergence free in the bounded Lipschitz domain $\Omega \subseteq \mathbb{R}^2$, i.e., $\int_\Omega v \operatorname{div} \beta \, dx = 0$ for all $v \in V := H_0^1(\Omega;\mathbb{C})$.

Consider the weak formulation of the eigenvalue problem given in Section 2.4 for the two complex Hilbert spaces V with energy norm $|||\cdot||| = |\cdot|_{H^1(\Omega;\mathbb{C})}$ (which is a norm on V) and $W := L^2(\Omega;\mathbb{C})$ with norm $\|\cdot\|_{L^2(\Omega;\mathbb{C})}$ and the two bilinear forms $a(\cdot,\cdot)$ and $b(\cdot,\cdot)$ that induce the norms $|||.||| := |.|_{H^1(\Omega)}$ on V and $\|.\| := \|.\|_{L^2(\Omega)}$ on $L^2(\Omega)$. The bilinear form $a(\cdot,\cdot)$ is elliptic and continuous in V and the bilinear form $b(\cdot,\cdot)$ is continuous, symmetric and positive definite, and hence induces a norm $\|\cdot\| := b(\cdot,\cdot)^{1/2}$ on W. For the above model problem, $\|\cdot\| = \|\cdot\|_{L^2(\Omega;\mathbb{C})}$. Since β is assumed to be divergence free, the ellipticity constant of the bilinear form $a(\cdot,\cdot)$ is independent of β, c.f. Section 2.4.

The analysis of the non-symmetric eigenvalue problem requires the dual eigenvalue problem: Seek a (dual) eigenpair $(\lambda^*, u^*) \in \mathbb{C} \times V$ with $\|u^*\| = 1$ such that

$$a(v, u^*) = \overline{\lambda^*} b(v, u^*) \quad \text{for all } v \in V.$$

Throughout this chapter, suppose that λ is a simple eigenvalue in the sense that the algebraic multiplicity and hence the geometric multiplicity is one and that λ is well separated from the remaining part of the spectrum.

Given any finite-dimensional subspace $V_\ell \subset V$, the discrete problems read: Seek primal and dual (discrete) eigenpairs (λ_ℓ, u_ℓ) and $(\lambda_\ell^*, u_\ell^*)$ with $\|u_\ell\| = 1 = \|u_\ell^*\|$ such that

$$\begin{aligned} a(u_\ell, v_\ell) &= \lambda_\ell b(u_\ell, v_\ell) \quad \text{for all } v_\ell \in V_\ell; \\ a(v_\ell, u_\ell^*) &= \overline{\lambda_\ell^*} b(v_\ell, u_\ell^*) \quad \text{for all } v_\ell \in V_\ell. \end{aligned} \tag{6.2}$$

The primal and dual eigenvalues λ_j and λ_j^* as well as the primal and dual discrete eigenvalues $\lambda_{\ell,j}$ and $\lambda_{\ell,j}^*$ are connected by

$$\lambda_j = \overline{\lambda_j^*} \qquad \text{for } j = 1, 2, 3, \ldots \quad \text{and} \quad \lambda_{\ell,j} = \overline{\lambda_{\ell,j}^*} \quad \text{for all } j = 1, \ldots, \dim(V_\ell).$$

The outline of the remaining parts of this chapter is a follows. In Section 6.2 an optimal error estimate for the eigenvalue error is derived. For this, the basic algebraic properties and identities of the non-symmetric eigenvalue problem are reviewed. In contrast to [69], the direct variational formulation is used, rather then the more general non-linear DWR framework of Becker and Rannacher [12, 14]. The weak regularity assumptions and the suboptimal L^2 error estimate of [69] prove the L^2 contribution to the residual identity to be of higher-order. Section 6.3 summarises some old and some new results on several a posteriori error estimators, namely the residual, the averaging, and the dual-weighted

DWR1, DWR2, DWM and DWA a posteriori error estimators. Section 6.4 describes the adaptive finite element method, the interpolation scheme, used for the calculation of the weights, and the computation of the error estimators. In Section 6.5 the error estimators are compared in numerical benchmarks on three different domains for higher eigenvalues and various convection coefficients. Section 6.6 draws some conclusions.

6.2 Algebraic Properties

This section is devoted with the primal and dual residual and the estimation of the eigenvalue and energy error in the primal and dual eigenfunctions.

For the primal and dual discrete eigenpairs (λ_ℓ, u_ℓ) and $(\lambda_\ell^*, u_\ell^*)$, the residuals are defined via

$$\mathrm{Res}_\ell := a(u_\ell, \cdot) - \lambda_\ell b(u_\ell, \cdot) \in V^* \quad \text{and} \quad \mathrm{Res}_\ell^* := a(\cdot, u_\ell^*) - \overline{\lambda}_\ell^* b(\cdot, u_\ell^*) \in V^*,$$

for the dual space V^* of V. Notice that $V_\ell \subset \ker(\mathrm{Res}_\ell)$ and $V_\ell \subset \ker(\mathrm{Res}_\ell^*)$.

It is the goal of this section to derive the following optimal error estimate for the eigenvalue error of simple eigenvalues

$$|\lambda - \lambda_\ell| \lesssim |\!|\!| \mathrm{Res}_\ell |\!|\!|_*^2 + |\!|\!| \mathrm{Res}_\ell^* |\!|\!|_*^2 \tag{6.3}$$

provided that $H_\ell \ll 1$. Throughout this chapter let $e_\ell := u - u_\ell$ and $e_\ell^* := u^* - u_\ell^*$.

Lemma 6.2.1 (Primal-dual error residual identity)**.** *Suppose that (λ_ℓ, u_ℓ) and $(\lambda_\ell^*, u_\ell^*)$ are the discrete primal and discrete dual eigenpairs to the primal and dual eigenpairs (λ, u) and (λ^*, u^*). Then it holds that*

$$(\lambda - \lambda_\ell)\Big(b(u, u^*) + b(u_\ell, u_\ell^*) - b(e_\ell, e_\ell^*)\Big) = \mathit{Res}_\ell(e_\ell^*) + \mathit{Res}_\ell^*(e_\ell).$$

Proof. Direct algebraic manipulations and the definition of the residuals and using that $\lambda = \overline{\lambda^*}$, $\lambda_\ell = \overline{\lambda_\ell^*}$ leads to

$$\begin{aligned} a(u_\ell, u^* - u_\ell^*) - \lambda_\ell b(u_\ell, u^* - u_\ell^*) + a(u - u_\ell, u_\ell^*) - \overline{\lambda_\ell^*} b(u - u_\ell, u_\ell^*) \\ &= a(u_\ell, u^*) - \lambda_\ell b(u_\ell, u^*) + a(u, u_\ell^*) - \overline{\lambda_\ell^*} b(u, u_\ell^*) \\ &= (\overline{\lambda^*} - \lambda_\ell) b(u_\ell, u^*) + (\lambda - \overline{\lambda_\ell^*}) b(u, u_\ell^*) \\ &= (\lambda - \lambda_\ell)(b(u, u^*) + b(u_\ell, u_\ell^*) - b(e_\ell, e_\ell^*)). \end{aligned}$$

□

Lemma 6.2.2. *Suppose that the maximal mesh-size H_ℓ tends to zero as $\ell \to \infty$, then*

$$\lim_{\ell \to \infty} b(e_\ell, e_\ell^*) = 0 \qquad \textit{and} \qquad \lim_{\ell \to \infty} b(u_\ell, u_\ell^*) = b(u, u^*).$$

Proof. The convergence of $|\!|\!| e_\ell |\!|\!|$ and $|\!|\!| e_\ell^* |\!|\!|$ implies the convergence of $\|e_\ell\|$ and $\|e_\ell^*\|$ to zero as $\ell \to \infty$ because of the compact embedding. Hence, the assertions follow from

$|b(e_\ell, e_\ell^*)| \leq \|e_\ell\|\|e_\ell^*\|$ and

$$|b(u, u^*) - b(u_\ell, u_\ell^*)| = |b(u - u_\ell, u^*) + b(u_\ell, u^* - u_\ell^*)| \leq \|e_\ell\| + \|e_\ell^*\|. \qquad \square$$

Remark 6.2.3. Since all eigenvalues converge as $H_\ell \to 0$, λ_ℓ is, as λ, a simple eigenvalue for sufficiently small H_ℓ. For a vector $z \in \mathbb{R}^m$ let z^H denotes its complex conjugate transposed vector. The condition number $1/|y_\ell^H B_\ell x_\ell|$ of the discrete eigenvalue λ_ℓ is defined for right and left eigenvectors x_ℓ and y_ℓ of the algebraic eigenvalue problems

$$A_\ell x_\ell = \lambda_\ell B_\ell x_\ell \quad \text{and} \quad y_\ell^H A_\ell = \overline{\lambda_\ell^*} y_\ell^H B_\ell,$$

with non-symmetric convection-diffusion matrix A_ℓ and symmetric positive definite mass matrix B_ℓ [61, Section 7.2.2]. It is known that $y_\ell^H B_\ell x_\ell \neq 0$ for simple eigenvalues and that $|y_\ell^H B_\ell x_\ell| \gg 0$ if the simple eigenvalue is well separated from the remaining part of the spectrum. Hence, for well separated simple eigenvalues considered in this chapter, it is reasonable to assume $b(u, u^*) \neq 0$. Furthermore, $1/|b(u, u^*)|$ is the condition number of the continuous eigenvalue λ and

$$|b(u, u^*) + b(u_\ell, u_\ell^*) - b(e_\ell, e_\ell^*)| \longrightarrow 2|b(u, u^*)| \quad \text{as } H_\ell \to 0.$$

Suppose that λ is simple such that $b(u, u^*) \neq 0$ and let $\ell \gg 1$ be such that the maximal mesh-size H_ℓ of the triangulation $\mathcal{T}_\ell$ is sufficiently small, i.e.,

$$\max\{\|e_\ell\|, \|e_\ell^*\|\|\} < \min\{1, |b(u, u^*)|/2\}. \tag{6.4}$$

Then $|b(u, u^*)| < |b(u, u^*) + b(u_\ell, u_\ell^*) - b(e_\ell, e_\ell^*)| < 3$, where the lower bound follows from

$$\begin{aligned} |b(u, u^*) + b(u_\ell, u_\ell^*) - b(e_\ell, e_\ell^*)| &= |2b(u, u^*) - b(u, u^* - u_\ell^*) - b(u - u_\ell, u^*)| \\ &\geq 2|b(u, u^*)| - |b(u, u^* - u_\ell^*) + b(u - u_\ell, u^*)| \\ &\geq 2|b(u, u^*)| - \|u\|\|e_\ell^*\| - \|u^*\|\|e_\ell\| \\ &= 2|b(u, u^*)| - \|e_\ell^*\| - \|e_\ell\| \end{aligned}$$

and (6.4). Thus for simple eigenvalues λ it holds that

$$|\lambda - \lambda_\ell| \approx |\mathrm{Res}_\ell(e_\ell^*) + \mathrm{Res}_\ell^*(e_\ell)|. \tag{6.5}$$

This implies the suboptimal eigenvalue error estimate

$$|\lambda - \lambda_\ell| \lesssim |\!|\!|\mathrm{Res}_\ell|\!|\!|_* + |\!|\!|\mathrm{Res}_\ell^*|\!|\!|_*. \tag{6.6}$$

Remark 6.2.4. The proof of the following Lemma 6.2.5 applies a suboptimal L^2 error estimate that is based on the *weak regularity assumption* of the eigenvalue λ with the eigenspace $E(\lambda)$. That is a condition on

$$a_\lambda(\cdot, \cdot) = a(\cdot, \cdot) - \lambda b(\cdot, \cdot)$$

on the quotient space $V/E(\lambda)$ in the sense that

$$|||w||| \leq C_\lambda \sup_{v \in V/E(\lambda)} \frac{|a_\lambda(v,w)|}{|||v|||} \quad \text{for all } w \in V/E(\lambda).$$

The constant C_λ depends on the distance of λ to all other distinct eigenvalues and does not depend on the mesh-size. This weak regularity assumption implies the suboptimal L^2 error estimates [69, (70)-(71)]

$$\|e_\ell\| \lesssim |||\mathrm{Res}_\ell|||_* + |\lambda - \lambda_\ell| \quad \text{and} \quad \|e_\ell^*\| \lesssim |||\mathrm{Res}_\ell^*|||_* + |\lambda - \lambda_\ell|. \tag{6.7}$$

Lemma 6.2.5 (Energy estimate)**.** *Suppose that $b(u,u^*) \neq 0$, the maximal mesh-size H_ℓ is sufficiently small according to* (6.4)*, and (λ_ℓ, u_ℓ) and $(\lambda_\ell^*, u_\ell^*)$ are the discrete primal and discrete dual eigenpairs to the primal and dual eigenpairs (λ, u) and (λ^*, u^*). Then it holds that*

$$|||e_\ell||| + |||e_\ell^*||| \lesssim |||Res_\ell|||_* + |||Res_\ell^*|||_*.$$

Proof. Since $b(u,u) = 1 = b(u_\ell, u_\ell)$, the eigenvalue equations (2.2) and (6.2) imply that

$$a(e_\ell, e_\ell) = \lambda + \lambda_\ell - \lambda b(u, u_\ell) - a(u_\ell, u).$$

The relation $\lambda_\ell b(u_\ell, u) = \lambda_\ell \overline{b(u,u_\ell)} = \lambda_\ell \mathrm{Re}\, b(u,u_\ell) - i\lambda_\ell \mathrm{Im}\, b(u,u_\ell)$ leads to

$$a(e_\ell, e_\ell) = (\lambda + \lambda_\ell)(1 - \mathrm{Re}\, b(u,u_\ell)) + i\,(\lambda_\ell - \lambda)\mathrm{Im}\, b(u,u_\ell) + \lambda_\ell b(u_\ell, u) - a(u_\ell, u).$$

From $0 = \mathrm{Im}\|u_\ell\|^2 = \mathrm{Im}\, b(u_\ell, u_\ell)$ it follows that

$$a(e_\ell, e_\ell) = (\lambda + \lambda_\ell)(1 - \mathrm{Re}\, b(u,u_\ell)) + i\,(\lambda_\ell - \lambda)\mathrm{Im}\, b(u - u_\ell, u_\ell) + \lambda_\ell b(u_\ell, u) - a(u_\ell, u).$$

Since

$$2\mathrm{Re}\, b(u,u_\ell) = \|u\|^2 + \|u_\ell\|^2 - \|e_\ell\|^2 = 2 - \|e_\ell\|^2,$$

this implies

$$|||e_\ell|||^2 = \mathrm{Re}\, a(e_\ell, e_\ell) \leq |\mathrm{Res}_\ell(e_\ell)| + |\lambda - \lambda_\ell|\|e_\ell\| + \frac{|\lambda + \lambda_\ell|}{2}\|e_\ell\|^2. \tag{6.8}$$

The suboptimal estimates (6.6) and (6.7) imply

$$|\lambda - \lambda_\ell| + \|e_\ell\| \lesssim |||\mathrm{Res}_\ell|||_* + |||\mathrm{Res}_\ell^*|||_*. \tag{6.9}$$

Since $\|.\| \lesssim |||.|||$, the aforementioned inequalities (6.8),(6.9) yield

$$|||e_\ell||| \lesssim |||\mathrm{Res}_\ell|||_* + |||\mathrm{Res}_\ell^*|||_*.$$

Similarly it follows that

$$\|\!|e_\ell^*|\!\| \lesssim \|\!|\mathrm{Res}_\ell|\!\|_* + \|\!|\mathrm{Res}_\ell^*|\!\|_*. \qquad \square$$

Theorem 6.2.6 (Eigenvalue error estimate)**.** *Suppose $b(u,u^*) \neq 0$, the maximal mesh-size H_ℓ is sufficiently small such that (6.4) holds and let (λ_ℓ, u_ℓ) and $(\lambda_\ell^*, u_\ell^*)$ be the discrete primal and discrete dual eigenpairs to the primal and dual eigenpairs (λ, u) and (λ^*, u^*) for the simple eigenvalue λ. Then it holds that*

$$|\lambda - \lambda_\ell| \lesssim |\!|\!| Res_\ell |\!|\!|_*^2 + |\!|\!| Res_\ell^* |\!|\!|_*^2.$$

Proof. The aforementioned estimate (6.5), the Cauchy-Schwarz inequality and the previous Lemma 6.2.5 lead to

$$|\lambda - \lambda_\ell| \lesssim |\mathrm{Res}_\ell(e_\ell^*)| + |\mathrm{Res}_\ell^*(e_\ell)| \lesssim |\!|\mathrm{Res}_\ell|\!|_*^2 + |\!|\mathrm{Res}_\ell^*|\!|_*^2. \qquad \square$$

6.3 A Posteriori Error Estimates

This section is devoted to the residual, averaging and dual-weighted residual a posteriori error estimators for the eigenvalue error of simple eigenvalues. The first two residual and averaging based a posteriori error estimators make use of Theorem 6.2.6

$$|\lambda - \lambda_\ell| \lesssim |\!|\mathrm{Res}_\ell|\!|_*^2 + |\!|\mathrm{Res}_\ell^*|\!|_*^2.$$

Here, the dual norms of the primal and dual residuals are bounded separately. The DWR based a posteriori error estimators are derived from the asymptotic estimate (6.5) for simple eigenvalues,

$$|\lambda - \lambda_\ell| \approx |\mathrm{Res}_\ell(e_\ell^*) + \mathrm{Res}_\ell^*(e_\ell)|,$$

where the constant tends to $1/(2|b(u,u^*)|)$ as $H_\ell \to 0$. In general the dual-weighted error estimators avoid any additional inequality, such as approximation properties, with unknown constants. Thus, they are robust with respect to strong convection which is also confirmed by the numerical examples in Section 6.5. One question that arises from the computation of $\mathrm{Res}_\ell(e_\ell^*)$ or $\mathrm{Res}_\ell^*(e_\ell)$ is the calculation of the unknown errors e_ℓ and e_ℓ^*. The rather heuristic approach of [12] states that it is numerically reliable and efficient to approximate these quantities which occur only in the weights. The idea is that one does not need to approximate the weights with higher accuracy than the size of the residual terms. In practice, the unknown primal and dual solutions u, u^* are replaced by solutions of a higher-order method or by higher-order interpolation. In Section 6.4 a higher-order interpolation ansatz for general triangular meshes is described which leads to numerically reliable and efficient dual-weighted a posteriori error estimators.

Throughout this chapter, suppose $(\mathcal{T}_\ell)_\ell$ is a family of shape-regular triangulations of Ω into triangles as in Section 2.5. Let $V_\ell := P_1(\mathcal{T}_\ell) \cap V$ and $h_\ell \in P_0(\mathcal{T}_\ell)$ be such that $h_{\ell|T} := \mathrm{diam}(T)$ for all $T \in \mathcal{T}_\ell$. Given a triangulation $\mathcal{T}_\ell$, define $\mathcal{E}_\ell$ as the set

of inner edges and $\mathcal{N}_\ell$ as the set of inner nodes. Let $h_T := \operatorname{diam}(T)$ for $T \in \mathcal{T}_\ell$ and $h_E := \operatorname{diam}(E)$ for $E \in \mathcal{E}_\ell$. The jump of the discrete gradient $\nabla u_\ell \in P_0(\mathcal{T}_\ell)^2$ in normal direction ν_E along an inner edge $\partial T_+ \cap \partial T_- = E \in \mathcal{E}_\ell$, for $T_+, T_- \in \mathcal{T}_\ell$, is denoted by $[\nabla u_\ell] \cdot \nu_E = \nabla u_\ell|_{T_+} \cdot \nu_E - \nabla u_\ell|_{T_-} \cdot \nu_E$ and $[\nabla u_\ell] \cdot \nu_E = 0$ for boundary edges $E \subset \partial\Omega$.

6.3.1 Residual Estimator

The first a posteriori error estimator is the residual error estimator from [69].

Lemma 6.3.1. *Let (λ_ℓ, u_ℓ) and $(\lambda_\ell^*, u_\ell^*)$ be the discrete primal and discrete dual eigenpairs to the primal and dual eigenpairs (λ, u) and (λ^*, u^*). Then it holds that*

$$\begin{aligned}
|\!|\!| Res_\ell |\!|\!|_*^2 &\lesssim \sum_{T\in\mathcal{T}_\ell} h_T^2 \|\beta\cdot\nabla u_\ell - \lambda_\ell u_\ell\|_{L^2(T)}^2 + \sum_{E\in\mathcal{E}_\ell} h_E \|[\nabla u_\ell]\cdot\nu_E\|_{L^2(E)}^2,\\
|\!|\!| Res_\ell^* |\!|\!|_*^2 &\lesssim \sum_{T\in\mathcal{T}_\ell} h_T^2 \|-\beta\cdot\nabla \overline{u_\ell^*} - \overline{\lambda_\ell^* u_\ell^*}\|_{L^2(T)}^2 + \sum_{E\in\mathcal{E}_\ell} h_E \|[\nabla \overline{u_\ell^*}]\cdot\nu_E\|_{L^2(E)}^2.
\end{aligned}$$

Proof. The proof follows the lines of the proof for the symmetric eigenvalue problem, e.g. [33, 50]. For completeness we give the details of the proof. Let v_ℓ denote the Scott-Zhang interpolation of v onto V_ℓ. Then it holds that

$$\begin{aligned}
\operatorname{Res}_\ell(v) &= \operatorname{Res}_\ell(v - v_\ell) = a(u_\ell, v - v_\ell) - \lambda_\ell b(u_\ell, v - v_\ell)\\
&= \sum_{T\in\mathcal{T}_\ell} \int_T \nabla u_\ell \cdot \nabla(\overline{v - v_\ell}) + (\beta\cdot\nabla u_\ell)(\overline{v - v_\ell})dx - \lambda_\ell \int_T u_\ell(\overline{v - v_\ell})dx\\
&= \sum_{T\in\mathcal{T}_\ell} \int_T (\beta\cdot\nabla u_\ell - \lambda_\ell u_\ell)(\overline{v - v_\ell})dx + \sum_{E\in\mathcal{E}_\ell} \int_E ([\nabla u_\ell]\cdot\nu_E)(\overline{v - v_\ell})ds.
\end{aligned}$$

The approximation property of the interpolation operator [101]

$$\sum_{T\in\mathcal{T}_\ell} \|h_T^{-1}(v - v_\ell)\|_{L^2(T)}^2 + \sum_{E\in\mathcal{E}_\ell} \|h_E^{-1/2}(v - v_\ell)\|_{L^2(E)}^2 \lesssim |\!|\!| v |\!|\!|^2 \tag{6.10}$$

and the Cauchy-Schwarz inequality yield

$$\begin{aligned}
\operatorname{Res}_\ell(v) &\le \sum_{T\in\mathcal{T}_\ell} h_T \|\beta\cdot\nabla u_\ell - \lambda_\ell u_\ell\|_{L^2(T)} \|h_T^{-1}(v - v_\ell)\|_{L^2(T)}\\
&\quad + \sum_{E\in\mathcal{E}_\ell} h_E^{1/2} \|[\nabla u_\ell]\cdot\nu_E\|_{L^2(E)} \|h_E^{-1/2}(v - v_\ell)\|_{L^2(E)}\\
&\lesssim \left(\sum_{T\in\mathcal{T}_\ell} h_T^2 \|\beta\cdot\nabla u_\ell - \lambda_\ell u_\ell\|_{L^2(T)}^2\right)^{1/2} |\!|\!| v |\!|\!| + \left(\sum_{E\in\mathcal{E}_\ell} h_E \|[\nabla u_\ell]\cdot\nu_E\|_{L^2(E)}^2\right)^{1/2} |\!|\!| v |\!|\!|.
\end{aligned}$$

For the second assertion notice that the dual bilinear form $a^*(u^*, \cdot) := a(\cdot, u^*)$ reads in

the model problem

$$a^*(u^*, v) = a(v, u^*) = \int_\Omega (\nabla v \cdot \nabla \overline{u^*} + (\beta \cdot \nabla v)\overline{u^*})\, dx.$$

An integration by parts leads to

$$a^*(u^*, v) = \int_\Omega (\nabla \overline{u^*} \cdot \nabla v - (\beta \cdot \nabla \overline{u^*})v)\, dx \quad \text{for all } v \in V.$$

The same arguments as for the first assertion lead to the assertion for $|||\mathrm{Res}_\ell^*|||$.

□

6.3.2 Averaging Estimator

The averaging technique concerns operators $A : P_0(\mathcal{T}_\ell)^2 \to \{V_\ell^2 \cap \mathcal{C}(\Omega)^2\}$ with the model example

$$A(\nabla u_\ell) := \sum_{z \in \mathcal{N}_\ell} \frac{1}{|\omega_z|} \left(\int_{\omega_z} \nabla u_\ell \, dx \right) \varphi_z.$$

Here and throughout this chapter, φ_z denotes the nodal basis function for an inner node $z \in \mathcal{N}_\ell$. Alternative averaging operators from [29] could be employed as well.

Lemma 6.3.2. *Let (λ_ℓ, u_ℓ) and $(\lambda_\ell^*, u_\ell^*)$ be the discrete primal and discrete dual eigenpairs to the primal and dual eigenpairs (λ, u) and (λ^*, u^*). Then it holds that*

$$\begin{aligned}
|||Res_\ell|||_* &\lesssim \|h_\ell(-div(A(\nabla u_\ell)) + \beta \cdot \nabla u_\ell - \lambda_\ell u_\ell)\|_{L^2(\Omega)} + \|A(\nabla u_\ell) - \nabla u_\ell\|_{L^2(\Omega)}, \\
|||Res_\ell^*|||_* &\lesssim \|h_\ell(-div(A(\nabla \overline{u_\ell^*})) - \beta \cdot \nabla \overline{u_\ell^*} - \overline{\lambda_\ell^* u_\ell^*})\|_{L^2(\Omega)} + \|A(\nabla \overline{u_\ell^*}) - \nabla \overline{u_\ell^*}\|_{L^2(\Omega)}.
\end{aligned}$$

Proof. The proof follows the lines of the proof for the symmetric eigenvalue problem, e.g. [33, 89]. For completeness we give the details of the proof. As in the previous lemma, let v_ℓ denote the Scott-Zhang interpolation of v onto V_ℓ, since $A(\nabla u_\ell)$ is globally continuous the divergence theorem can be applied. This yields

$$\begin{aligned}
\mathrm{Res}_\ell(v) &= \mathrm{Res}_\ell(v - v_\ell) = a(u_\ell, v - v_\ell) - \lambda_\ell b(u_\ell, v - v_\ell) \\
&= \int_\Omega (\nabla u_\ell - A(\nabla u_\ell)) \cdot \nabla(\overline{v - v_\ell}) dx - \int_\Omega \mathrm{div}(A(\nabla u_\ell))(\overline{v - v_\ell}) dx \\
&\quad + \int_\Omega (\beta \cdot \nabla u_\ell - \lambda_\ell u_\ell)(\overline{v - v_\ell}) dx.
\end{aligned}$$

Hölder's inequality leads to

$$\begin{aligned}
\mathrm{Res}_\ell(v) \leq \sum_{T \in \mathcal{T}_\ell} & h_T \| -\mathrm{div}(A(\nabla u_\ell)) + \beta \cdot \nabla u_\ell - \lambda_\ell u_\ell \|_{L^2(T)} \| h_T^{-1}(v - v_\ell) \|_{L^2(T)} \\
&+ \sum_{T \in \mathcal{T}_\ell} \| \nabla u_\ell - A(\nabla u_\ell) \|_{L^2(T)} \| \nabla(v - v_\ell) \|_{L^2(T)}.
\end{aligned}$$

Using the stability and the approximation property (6.10)

$$\sum_{T\in\mathcal{T}_\ell} \|\nabla v_\ell\|^2_{L^2(T)} \lesssim |\!|\!| v |\!|\!|^2 \quad \text{and} \quad \sum_{T\in\mathcal{T}_\ell} \|h_T^{-1}(v-v_\ell)\|^2_{L^2(T)} \lesssim |\!|\!| v |\!|\!|^2,$$

together with the Cauchy-Schwarz inequality yield

$$\mathrm{Res}_\ell(v) \lesssim \Big(\|h_\ell(-\mathrm{div}(A(\nabla u_\ell)) + \beta\cdot\nabla u_\ell - \lambda_\ell u_\ell)\|_{L^2(\Omega)} + \|A(\nabla u_\ell) - \nabla u_\ell\|_{L^2(\Omega)} \Big) |\!|\!| v |\!|\!|.$$

In the same way one proves the assertion for $|\!|\!|\mathrm{Res}^*_\ell|\!|\!|$. □

6.3.3 DWR1 Estimator

The first DWR a posteriori error estimator (DWR1) is derived from the DWR ansatz as in [12] or [69] plus a result from [30].

Lemma 6.3.3. *Let the eigenfunctions $u, u^* \in H^2(\Omega)\cap H^3(\mathcal{T}_\ell)$, $H^3(\mathcal{T}_\ell)$ denote the broken space of piecewise H^3 Sobolev functions, (λ_ℓ, u_ℓ) and $(\lambda^*_\ell, u^*_\ell)$ be the discrete primal and discrete dual eigenpairs to the primal and dual eigenpairs (λ, u) and (λ^*, u^*), and*

$$\begin{aligned} \eta_T &:= \|\beta\cdot\nabla u_\ell - \lambda_\ell u_\ell\|_{L^2(T)} + h_T^{-1/2}\|[\nabla u_\ell]\cdot\nu_E\|_{L^2(\partial T)}, \\ \eta^*_T &:= \|-\beta\cdot\nabla\overline{u^*_\ell} - \overline{\lambda^*_\ell u^*_\ell}\|_{L^2(T)} + h_T^{-1/2}\|[\nabla\overline{u^*_\ell}]\cdot\nu_E\|_{L^2(\partial T)}. \end{aligned} \tag{6.11}$$

Then it holds that

$$\begin{aligned} |Res_\ell(e^*_\ell)| + |Res^*_\ell(e_\ell)| \lesssim &\sum_{T\in\mathcal{T}_\ell} h_T^{3/2}\eta_T \|[\nabla u^*_\ell]\cdot\nu_E\|_{L^2(\bigcup\mathcal{E}_{\Omega_T})} \\ &+ \sum_{T\in\mathcal{T}_\ell} h_T^{3/2}\eta^*_T \|[\nabla u_\ell]\cdot\nu_E\|_{L^2(\bigcup\mathcal{E}_{\Omega_T}))} + HOT \end{aligned}$$

for suitable fixed subsets $\Omega_T \subseteq \Omega$, which contain $T \in \mathcal{T}_\ell$, with skeleton $\bigcup\mathcal{E}_{\Omega_T}$, and a higher-order term

$$HOT := \sum_{T\in\mathcal{T}_\ell} h_T^2\eta_T\|\nabla e^*_\ell\|_{L^2(\Omega_T)} + \sum_{T\in\mathcal{T}_\ell} h_T^2\eta^*_T\|\nabla e_\ell\|_{L^2(\Omega_T)}.$$

Proof. Suppose $u \in H^2(\Omega)$, then integration by parts and Hölder's inequality show that

$$\begin{aligned} &\mathrm{Res}_\ell(v) = \sum_{T\in\mathcal{T}_\ell}\int_T \nabla u_\ell\cdot\nabla(\overline{v-v_\ell}) + (\beta\cdot\nabla u_\ell - \lambda_\ell u_\ell)(\overline{v-v_\ell})dx \\ &\le \sum_{T\in\mathcal{T}_\ell} h_T^{-1/2}\|[\nabla u_\ell]\cdot\nu_E\|_{L^2(\partial T)} h_T^{1/2}\|v-v_\ell\|_{L^2(\partial T)} + \|\beta\cdot\nabla u_\ell - \lambda_\ell u_\ell\|_{L^2(T)}\|v-v_\ell\|_{L^2(T)} \\ &\le \sum_{T\in\mathcal{T}_\ell} \eta_T\omega_T. \end{aligned}$$

Here, η_T is as defined in (6.11) and

$$\omega_T := \|v - v_\ell\|_{L^2(T)} + h_T^{1/2}\|v - v_\ell\|_{L^2(\partial T)}.$$

Let $v_\ell = \mathcal{I}_\ell v \in V_\ell$ be the nodal interpolant of v. The interpolation estimate [27]

$$\|v - \mathcal{I}_\ell v\|^2_{L^2(T)} + h_T\|v - \mathcal{I}_\ell v\|^2_{L^2(\partial T)} \lesssim h_T^4\|D^2 v\|^2_{L^2(T)}$$

leads to

$$\mathrm{Res}_\ell(v) \lesssim \sum_{T\in\mathcal{T}_\ell} h_T^2\eta_T\|D^2 v\|_{L^2(T)}.$$

In [69] $D^2 v$ is locally approximated on each quadrilateral Q by $D^2 v_\ell|_Q$ using finite differences. While this is an appropriate ansatz for structured meshes, for general triangular meshes considered here this is not suited. In [30] it is shown that $v \in H^3(\mathcal{T}_\ell)$ implies

$$\|D^2 v\|_{L^2(T)} \le c_1 h_T^{-1/2}\|[\nabla v_\ell]\cdot\nu_E\|_{L^2(\bigcup\mathcal{E}_{\Omega_T}))} + c_2\|\nabla(v - v_\ell)\|^{1/2}_{L^2(\Omega_T)}.$$

The constant c_1 depends on the shape of elements and c_2 on $\|v\|_{H^3(\Omega_T)}$. This leads to the estimate

$$|\mathrm{Res}_\ell(e_\ell^*)| \lesssim \sum_{T\in\mathcal{T}_\ell} h_T^{3/2}\eta_T\|[\nabla u_\ell^*]\cdot\nu_E\|_{L^2(\bigcup\mathcal{E}_{\Omega_T})} + \mathrm{HOT}$$

with higher-order term

$$\mathrm{HOT} = \sum_{T\in\mathcal{T}_\ell} h_T^2\eta_T\|\nabla e_\ell^*\|_{L^2(\Omega_T)}.$$

Note that the jump term is formally equivalent to the energy norm and that HOT involves an extra factor of $h_T^{1/2}$ compared to the other term of the estimate. Following the argumentation for the primal residual yields the assertion for the dual residual

$$|\mathrm{Res}_\ell^*(e_\ell)| \lesssim \sum_{T\in\mathcal{T}_\ell} h_T^{3/2}\eta_T^*\|[\nabla u_\ell]\cdot\nu_E\|_{L^2(\bigcup\mathcal{E}_{\Omega_T})} + \mathrm{HOT}$$

with the higher-order term

$$\mathrm{HOT} = \sum_{T\in\mathcal{T}_\ell} h_T^2\eta_T^*\|\nabla e_\ell\|_{L^2(\Omega_T)}.$$ □

Remark 6.3.4. From the theory in [30] it remains open to choose the fixed size of the patches Ω_T containing $T \in \mathcal{T}_\ell$. However, the numerical examples of Section 6.5 suggest, that, surprisingly, $\Omega_T = T$ and thus $\bigcup\mathcal{E}_{\Omega_T} = \partial T$ might be sufficient. This seems to be in agreement with [12].

6.3.4 DWR2 Estimator

The second DWR estimator (DWR2) according to [12] reads as follows. Observe that this error estimator involves the unknown exact primal and dual errors e_ℓ and $\overline{e_\ell^*}$. In the numerical examples of Section 6.5, these errors will be approximated by the interpolation described in Section 6.4.

Lemma 6.3.5. *The unknown exact errors e_ℓ and $\overline{e_\ell^*}$ satisfy*

$$|Res_\ell(e_\ell^*) + Res_\ell^*(e_\ell)| = \Bigg| \sum_{T\in\mathcal{T}_\ell} \int_T (\beta\cdot\nabla u_\ell - \lambda_\ell u_\ell)\overline{e_\ell^*}dx + \sum_{E\in\mathcal{E}_\ell}\int_E ([\nabla u_\ell]\cdot\nu_E)\overline{e_\ell^*}ds, \\ + \sum_{T\in\mathcal{T}_\ell}\int_T (-\beta\cdot\nabla\overline{u_\ell^*} - \overline{\lambda_\ell^* u_\ell^*})e_\ell dx + \sum_{E\in\mathcal{E}_\ell}\int_E ([\nabla\overline{u_\ell^*}]\cdot\nu_E)e_\ell ds\Bigg|.$$

Proof. An integration by parts leads to

$$\begin{aligned}\mathrm{Res}_\ell(e_\ell^*) &= a(u_\ell, u^*-u_\ell^*) - \lambda_\ell b(u_\ell, u^*-u_\ell^*)\\ &= \sum_{T\in\mathcal{T}_\ell}\int_T(\beta\cdot\nabla u_\ell - \lambda_\ell u_\ell)\overline{(u^*-u_\ell^*)}dx + \sum_{E\in\mathcal{E}_\ell}\int_E[\nabla u_\ell]\cdot\nu_E\overline{(u^*-u_\ell^*)}ds.\end{aligned}$$

Similarly,

$$\begin{aligned}\mathrm{Res}_\ell^*(e_\ell) &= a(u-u_\ell, u_\ell^*) - \overline{\lambda_\ell^*} b(u-u_\ell, u_\ell^*)\\ &= \sum_{T\in\mathcal{T}_\ell}\int_T(-\beta\cdot\nabla\overline{u_\ell^*} - \overline{\lambda_\ell^* u_\ell^*})(u-u_\ell)dx + \sum_{E\in\mathcal{E}_\ell}\int_E[\nabla\overline{u_\ell^*}]\cdot\nu_E(u-u_\ell)ds.\end{aligned}$$ □

6.3.5 DWM Estimator

Utilising the non standard Raviart-Thomas solution of an auxiliary problem leads to a new approach for a dual-weighted a posteriori error estimator. Note that this error estimator involves the unknown exact primal and dual errors e_ℓ and $\overline{e_\ell^*}$ as well as their unknown gradients ∇e_ℓ and $\nabla\overline{e_\ell^*}$. In practice these errors need to be approximated as described in Section 6.4.

Lemma 6.3.6. *Let $(q_M, u_M) \in RT_0(\mathcal{T}_\ell)\times P_0(\mathcal{T}_\ell)$ and $(q_M^*, u_M^*)\in RT_0(\mathcal{T}_\ell)\times P_0(\mathcal{T}_\ell)$ be the mixed finite element solutions of the equilibrium conditions*

$$\begin{aligned}-div(q_M) + \beta\cdot q_M &= f_\ell \text{ in } \Omega \quad \text{and} \quad q_M - \nabla u_M = 0 \text{ in } \Omega,\\ -div(q_M^*) - \beta\cdot q_M^* &= f_\ell^* \text{ in } \Omega \quad \text{and} \quad q_M^* - \nabla u_M^* = 0 \text{ in } \Omega,\end{aligned}$$

with right-hand sides $f_\ell, f_\ell^*\in P_0(\mathcal{T}_\ell)$ given by $f_{\ell|T} := h_T^{-2}\int_T\lambda_\ell u_\ell$ and $f_{\ell|T}^* := h_T^{-2}\int_T\lambda_\ell^* u_\ell^*$

for $T \in \mathcal{T}_\ell$. Then the unknown exact errors e_ℓ and $\overline{e_\ell^*}$ satisfy

$$|Res_\ell(e_\ell^*) + Res_\ell^*(e_\ell)| \leq \left| \int_\Omega (\nabla u_\ell - q_M) \cdot \nabla \overline{e_\ell^*} dx + \int_\Omega (\overline{\nabla u_\ell^* - q_M^*}) \cdot \nabla e_\ell dx \right.$$
$$\left. + \int_\Omega \beta \cdot (\nabla u_\ell - q_M) \overline{e_\ell^*} dx - \int_\Omega \beta \cdot (\overline{\nabla u_\ell^* - q_M^*}) e_\ell dx \right| + HOT$$

with the higher-order term

$$HOT = \left| \int_\Omega (f_\ell - \lambda_\ell u_\ell) \overline{e_\ell^*} dx + \int_\Omega (\overline{f_\ell^* - \lambda_\ell^* u_\ell^*}) e_\ell dx \right|.$$

Proof. By the definition of the auxiliary problem for q_M and integration by parts it holds that

$$\begin{aligned} \mathrm{Res}_\ell(e_\ell^*) &= \int_\Omega \nabla u_\ell \cdot \nabla \overline{e_\ell^*} dx + \int_\Omega (\beta \cdot \nabla u_\ell - \lambda_\ell u_\ell) \overline{e_\ell^*} dx \\ &= \int_\Omega (\nabla u_\ell - q_M) \cdot \nabla \overline{e_\ell^*} dx + \int_\Omega \beta \cdot (\nabla u_\ell - q_M) \overline{e_\ell^*} dx + \int_\Omega (f_\ell - \lambda_\ell u_\ell) \overline{e_\ell^*} dx. \end{aligned}$$

Element-wise Cauchy-Schwarz and Poincaré [95] inequalities yield

$$\int_\Omega (f_\ell - \lambda_\ell u_\ell) \overline{e_\ell^*} dx \leq \|f_\ell - \lambda_\ell u_\ell\| \|\overline{e_\ell^*}\| \leq \frac{1}{\pi} \left(\sum_{T \in \mathcal{T}_\ell} h_T^2 \|\lambda_\ell \nabla u_\ell\|_{L^2(T)}^2 \right)^{1/2} \|\overline{e_\ell^*}\|.$$

Note that $\|\overline{e_\ell^*}\|$ is of the same convergence order as $|\lambda - \lambda_\ell|$ and that the last term involves an additional term of order $\mathcal{O}(H_\ell)$. Therefore, this term is formally of higher-order compared to $|\lambda - \lambda_\ell|$. The same argumentation leads to

$$\begin{aligned} \mathrm{Res}_\ell^*(e_\ell) &= \int_\Omega \nabla \overline{u_\ell^*} \cdot \nabla e_\ell dx + \int_\Omega (-\beta \cdot \nabla \overline{u_\ell^*} - \overline{\lambda_\ell^* u_\ell^*}) e_\ell dx \\ &= \int_\Omega (\overline{\nabla u_\ell^* - q_M^*}) \cdot \nabla e_\ell dx - \int_\Omega \beta \cdot (\overline{\nabla u_\ell^* - q_M^*}) e_\ell dx + \int_\Omega (\overline{f_\ell^* - \lambda_\ell^* u_\ell^*}) e_\ell dx. \end{aligned}$$

The last term is again a formally higher-order term. □

6.3.6 DWA Estimator

The second new a posteriori error estimator makes use of the ideas of the DWR2 estimator. The new aspect proposed here is not to use integration by parts to obtain a residual term but to involve the averaged gradients $A(\nabla u_\ell)$ and $A(\nabla \overline{u_\ell^*})$ and then to do integration by parts. Again this error estimator involves the unknown exact primal and dual errors e_ℓ and $\overline{e_\ell^*}$ which have to be approximated as described in Section 6.4.

Lemma 6.3.7. *The unknown exact errors e_ℓ and $\overline{e_\ell^*}$ satisfy*

$$\begin{aligned}|Res_\ell(e_\ell^*) + Res_\ell^*(e_\ell)| = \Bigg| &\int_\Omega (\nabla u_\ell - A(\nabla u_\ell)) \cdot \nabla \overline{e_\ell^*} dx + \int_\Omega (\nabla \overline{u_\ell^*} - A(\nabla \overline{u_\ell^*})) \cdot \nabla e_\ell dx \\ &+ \int_\Omega (-div(A(\nabla u_\ell)) + \beta \cdot \nabla u_\ell - \lambda_\ell u_\ell) \overline{e_\ell^*} dx \\ &+ \int_\Omega (-div(A(\nabla \overline{u_\ell^*})) - \beta \cdot \nabla \overline{u_\ell^*} - \overline{\lambda_\ell^* u_\ell^*}) e_\ell dx \Bigg|.\end{aligned}$$

Proof. An addition and subtraction of the averaging term $A(\nabla u_\ell)$ and an integration by parts yields

$$\begin{aligned}\mathrm{Res}_\ell(e_\ell^*) &= a(u_\ell, u^* - u_\ell^*) - \lambda_\ell b(u_\ell, u^* - u_\ell^*) \\ &= \int_\Omega (\nabla u_\ell - A(\nabla u_\ell)) \cdot \nabla \overline{e_\ell^*} dx + \int_\Omega (-\mathrm{div}(A(\nabla u_\ell)) + \beta \cdot \nabla u_\ell - \lambda_\ell u_\ell) \overline{e_\ell^*} dx.\end{aligned}$$

Analogously it follows

$$\begin{aligned}\mathrm{Res}_\ell^*(e_\ell) &= a(u - u_\ell, u_\ell^*) - \overline{\lambda_\ell^*} b(u - u_\ell, u_\ell^*) \\ &= \int_\Omega (\nabla \overline{u_\ell^*} - A(\nabla \overline{u_\ell^*})) \cdot \nabla e_\ell dx + \int_\Omega (-\mathrm{div}(A(\nabla \overline{u_\ell^*})) - \beta \cdot \nabla \overline{u_\ell^*} - \overline{\lambda_\ell^* u_\ell^*}) e_\ell dx. \square\end{aligned}$$

6.4 Adaptive Finite Element Method

The adaptive finite element method (AFEM) generates a sequence of meshes $\mathcal{T}_0, \mathcal{T}_1, \ldots$ and associated discrete subspaces $V_0 \subsetneq V_1 \subsetneq \ldots \subsetneq V$ with discrete primal and discrete dual eigenpairs (λ_ℓ, u_ℓ), $(\lambda_\ell^*, u_\ell^*)$. A typical loop from V_ℓ to $V_{\ell+1}$ consists of the steps

$$\texttt{Solve} \rightarrow \texttt{Estimate} \rightarrow \texttt{Mark} \rightarrow \texttt{Refine}.$$

6.4.1 Solve

The primal and dual generalized algebraic eigenvalue problems

$$A_\ell x_\ell = \lambda_\ell B_\ell x_\ell \quad \text{and} \quad y_\ell^H A_\ell = \overline{\lambda_\ell^*} y_\ell^H B_\ell,$$

are solved with an algebraic eigensolver up to finite precision. Here, the coefficient matrices are the non-symmetric convection-diffusion matrix A_ℓ and the symmetric positive definite mass matrix B_ℓ. The right and left eigenvectors x_ℓ and y_ℓ represent the eigenfunctions

$$u_\ell = \sum_{k=1}^{\dim(V_\ell)} x_{\ell,k} \varphi_k \quad \text{and} \quad u_\ell^* = \sum_{k=1}^{\dim(V_\ell)} y_{\ell,k} \varphi_k$$

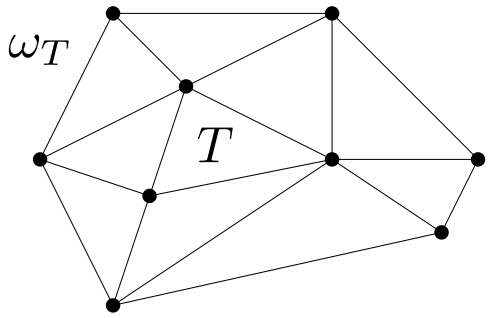

Figure 6.1: Interpolation points for the element patch ω_T to the triangle $T \in \mathcal{T}_\ell$.

with respect to the basis $(\varphi_1, \ldots, \varphi_{\dim(V_\ell)})$ of V_ℓ.

6.4.2 Estimate

Since the weight-terms e_ℓ and $\overline{e_\ell^*}$ in the dual-weighted a posteriori error estimators involve the unknown solutions u and $\overline{u^*}$, they have to be approximated. In the following experiments those functions are approximated by averaging $A(u_\ell) \in P_2(\mathcal{T}_\ell)$ of $u_\ell \in P_1(\mathcal{T}_\ell)$ and $A(\overline{u_\ell^*}) \in P_2(\mathcal{T}_\ell)$ of $\overline{u_\ell^*} \in P_1(\mathcal{T}_\ell)$ on the mesh $\mathcal{T}_\ell$. In contrast to the recovery of a gradient as in [114], the L^2 recovery of [111] is used here which is similar but uses different interpolation points. The post-processing is based on element patches $\omega_T := \cup_{z \subset T} \omega_z$ for $T \in \mathcal{T}_\ell$, where $\omega_z := \cup_{T \in \mathcal{T}_\ell; z \subset T} T$ is the nodal patch. The nodal and edge degrees of freedom for the interpolated $P_2(\mathcal{T}_\ell)$ function are computed for each element separately by a global least square quadratic polynomial fitting. The interpolation points for the least square fitting are the nodal points of ω_T as displayed in Figure 6.1. After all local values are computed, a global $P_2(\mathcal{T}_\ell)$ function is obtained by taking the arithmetic mean values for each node and midpoint of an edge of $\mathcal{T}_\ell$.

In [22] an alternative way of computing the estimator η_{DWR2} based on nodal values is presented. The analysis of this error estimator makes use of a special interpolation operator. This operator assumes that the mesh $\mathcal{T}_\ell$ results from uniform refinement of a coarser mesh and considers the nodal values as values for a higher-order P_2 basis on the coarser grid. The interpolation scheme presented here does not assumes any structure of the mesh.

The step `Estimate` of the AFEM loop involves an appropriate a posteriori error estimator. In the numerical examples of Section 6.5 the following error estimators are compared. Since the residual identity depends on the eigenvalue condition number, the condition number needs to be approximated for efficient a posteriori error control with efficiency indices close to one. In Section 6.5 it is shown empirically that the approximation $1/(2b(u_\ell, u_\ell^*))$ is efficient.

The first a posteriori error estimator is the residual estimator

$$\eta_{\ell,\mathrm{R}} = \frac{1}{2|b(u_\ell,u_\ell^*)|}\sum_{T\in\mathcal{T}}\left(h_T^2\|\beta\cdot\nabla u_\ell-\lambda_\ell u_\ell\|_{L^2(T)}^2+\sum_{E\subset T}h_E\|[\nabla u_\ell]\cdot\nu_E\|_{L^2(E)}^2\right)$$
$$+\frac{1}{2|b(u_\ell,u_\ell^*)|}\sum_{T\in\mathcal{T}}\left(h_T^2\|-\beta\cdot\nabla\overline{u_\ell^*}-\overline{\lambda_\ell^* u_\ell^*}\|_{L^2(T)}^2+\sum_{E\subset T}h_E\|[\nabla\overline{u_\ell^*}]\cdot\nu_E\|_{L^2(E)}^2\right).$$

The second a posteriori error estimator is the averaging estimator

$$\eta_{\ell,\mathrm{A}} = \frac{1}{2|b(u_\ell,u_\ell^*)|}\sum_{T\in\mathcal{T}}\left(\|A(\nabla u_\ell)-\nabla u_\ell\|_{L^2(T)}^2+\|A(\nabla\overline{u_\ell^*})-\nabla\overline{u_\ell^*}\|_{L^2(T)}^2\right)$$
$$+\frac{1}{2|b(u_\ell,u_\ell^*)|}\sum_{T\in\mathcal{T}}h_T^2\|-\mathrm{div}(A(\nabla u_\ell))+\beta\cdot\nabla u_\ell-\lambda_\ell u_\ell\|_{L^2(T)}^2$$
$$+\frac{1}{2|b(u_\ell,u_\ell^*)|}\sum_{T\in\mathcal{T}}h_T^2\|-\mathrm{div}(A(\nabla\overline{u_\ell^*}))-\beta\cdot\nabla\overline{u_\ell^*}-\overline{\lambda_\ell^* u_\ell^*}\|_{L^2(T)}^2.$$

The third a posteriori error estimator is the DWR1 estimator where the higher-order terms are neglected

$$\eta_{\ell,\mathrm{DWR1}} = \frac{1}{2|b(u_\ell,u_\ell^*)|}\left(\sum_{T\in\mathcal{T}_\ell}h_T^{3/2}\eta_T\|[\nabla u_\ell^*]\cdot\nu_E\|_{L^2(\partial T)}+\sum_{T\in\mathcal{T}_\ell}h_T^{3/2}\eta_T^*\|[\nabla u_\ell]\cdot\nu_E\|_{L^2(\partial T)}\right),$$

with η_T and η_T^* from (6.11).

The fourth a posteriori error estimator is the DWR2 estimator where the unknown solutions in the weights, u and u^*, are interpolated by $A(\overline{u_\ell^*})$ and $A(\overline{u_\ell^*})$ as described above

$$\eta_{\ell,\mathrm{DWR2}} = \frac{1}{2|b(u_\ell,u_\ell^*)|}\Bigg|\sum_{E\in\mathcal{E}_\ell}\int_E([\nabla u_\ell]\cdot\nu_E)(A(\overline{u_\ell^*})-\overline{u_\ell^*})ds$$
$$+\sum_{E\in\mathcal{E}_\ell}\int_E([\nabla\overline{u_\ell^*}]\cdot\nu_E)(A(u_\ell)-u_\ell)ds+\sum_{T\in\mathcal{T}_\ell}\int_T(\beta\cdot\nabla u_\ell-\lambda_\ell u_\ell)(A(\overline{u_\ell^*})-\overline{u_\ell^*})dx$$
$$+\sum_{T\in\mathcal{T}_\ell}\int_T(-\beta\cdot\nabla\overline{u_\ell^*}-\overline{\lambda_\ell^* u_\ell^*})(A(u_\ell)-u_\ell)dx\Bigg|.$$

The local refinement indicators read

$$\eta_T := \Bigg|\int_T(\beta\cdot\nabla u_\ell-\lambda_\ell u_\ell)(A(\overline{u_\ell^*})-\overline{u_\ell^*})dx+\sum_{E\in\partial T}\int_E([\nabla u_\ell]\cdot\nu_E)(A(\overline{u_\ell^*})-\overline{u_\ell^*})ds,$$
$$+\int_T(-\beta\cdot\nabla\overline{u_\ell^*}-\overline{\lambda_\ell^* u_\ell^*})(A(u_\ell)-u_\ell)dx+\sum_{E\in\partial T}\int_E([\nabla\overline{u_\ell^*}]\cdot\nu_E)(A(u_\ell)-u_\ell)ds\Bigg|.$$

They are only necessary to determine the set of marked edges for refinement.

The fifth a posteriori error estimator utilised the auxiliary Raviart-Thomas mixed solutions q_M and q_M^* and the averaged gradients $A(\nabla u_\ell)$ and $A(\nabla \overline{u_\ell^*})$

$$\begin{aligned}\eta_{\ell,\mathrm{DWM}} = \frac{1}{2|b(u_\ell, u_\ell^*)|} \Bigg| &\int_\Omega (\nabla u_\ell - q_M) \cdot (A(\nabla \overline{u_\ell^*}) - \nabla \overline{u_\ell^*}) dx \\ &+ \int_\Omega (\overline{\nabla u_\ell^* - q_M^*}) \cdot (A(\nabla u_\ell) - \nabla u_\ell) dx + \int_\Omega \beta \cdot (\nabla u_\ell - q_M)(A(\overline{u_\ell^*}) - \overline{u_\ell^*}) dx \\ &- \int_\Omega \beta \cdot (\overline{\nabla u_\ell^* - q_M^*})(A(u_\ell) - u_\ell) dx \Bigg|,\end{aligned}$$

where the higher-order term is neglected. The local refinement indicators read

$$\begin{aligned}\eta_T := \Bigg| &\int_T (\nabla u_\ell - q_M) \cdot \nabla (A(\nabla \overline{u_\ell^*}) - \nabla \overline{u_\ell^*}) dx + \int_T (\overline{\nabla u_\ell^* - q_M^*}) \cdot (A(\nabla u_\ell) - \nabla u_\ell) dx \\ &+ \int_T \beta \cdot (\nabla u_\ell - q_M)(A(\overline{u_\ell^*}) - \overline{u_\ell^*}) dx - \int_T \beta \cdot (\overline{\nabla u_\ell^* - q_M^*})(A(u_\ell) - u_\ell) dx \Bigg|.\end{aligned}$$

The last error a posteriori error estimator uses both averaged gradients $A(\nabla u_\ell)$ and $A(\nabla \overline{u_\ell^*})$ as well as interpolated L^2 functions $A(u_\ell^*)$ and $A(\overline{u_\ell^*})$ for the weights

$$\begin{aligned}\mu_{\ell,\mathrm{DWA}} = \frac{1}{2|b(u_\ell, u_\ell^*)|} \Bigg| &\int_\Omega (\nabla u_\ell - A(\nabla u_\ell)) \cdot (A(\nabla \overline{u_\ell^*}) - \nabla \overline{u_\ell^*}) dx \\ &+ \int_\Omega (\nabla \overline{u_\ell^*} - A(\nabla \overline{u_\ell^*})) \cdot (A(\nabla u_\ell) - \nabla u_\ell) dx \\ &+ \int_\Omega (-\mathrm{div}(A(\nabla u_\ell)) + \beta \cdot \nabla u_\ell - \lambda_\ell u_\ell)(A(\overline{u_\ell^*}) - \overline{u_\ell^*}) dx \\ &+ \int_\Omega (-\mathrm{div}(A(\nabla \overline{u_\ell^*})) - \beta \cdot \nabla \overline{u_\ell^*} - \overline{\lambda_\ell^* u_\ell^*})(A(u_\ell) - u_\ell) dx \Bigg|.\end{aligned}$$

Here, the local refinement indicators read

$$\begin{aligned}\eta_T := \Bigg| &\int_T (\nabla u_\ell - A(\nabla u_\ell)) \cdot (A(\nabla \overline{u_\ell^*}) - \nabla \overline{u_\ell^*}) dx \\ &+ \int_T (\nabla \overline{u_\ell^*} - A(\nabla \overline{u_\ell^*})) \cdot (A(\nabla u_\ell) - \nabla u_\ell) dx \\ &+ \int_T (-\mathrm{div}(A(\nabla u_\ell)) \beta \cdot \nabla u_\ell - \lambda_\ell u_\ell)(A(\overline{u_\ell^*}) - \overline{u_\ell^*}) dx \\ &+ \int_T (-\mathrm{div}(A(\nabla \overline{u_\ell^*})) - \beta \cdot \nabla \overline{u_\ell^*} - \overline{\lambda_\ell^* u_\ell^*})(A(u_\ell) - u_\ell) dx \Bigg|.\end{aligned}$$

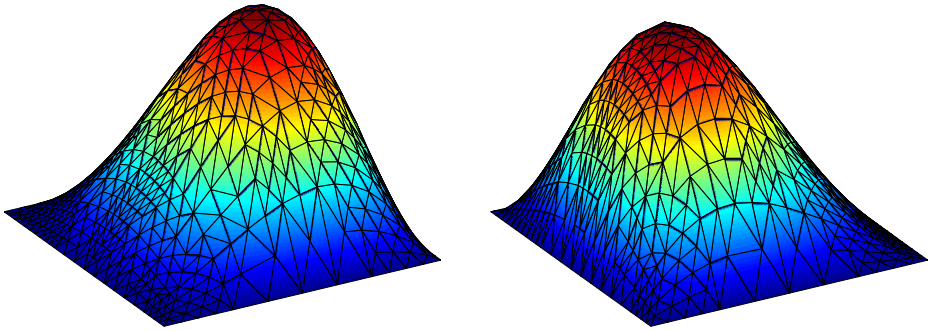

Figure 6.2: Primal (left) and dual (right) discrete solution for $\beta = (3, 0)$ and λ_1 on adaptively refined meshes generated by $\eta_{\ell,\mathrm{R}}$ on the unit square with about 500 nodes.

6.4.3 Mark

Based on the refinement indicators, the set of elements $\mathcal{M}_\ell \subseteq \mathcal{T}_\ell$ that are refined is specified in the algorithm `Mark` . Let $\mathcal{M}_\ell$ be the set of minimal cardinality for which the bulk criterion [48],

$$\theta \sum_{T \in \mathcal{T}_\ell} \eta_T^2 \leq \sum_{T \in \mathcal{M}_\ell} \eta_T^2$$

is satisfied for a given bulk parameter $0 < \theta \leq 1$.

6.4.4 Refine

Given the set $\mathcal{M}_\ell \subseteq \mathcal{T}_\ell$ of marked elements, mark all edges of elements in $\mathcal{M}_\ell$ for refinement. The mesh is then refined by the closure algorithm of Section 2.5.1 and the red-green-blue refinement algorithm of Section 2.5.2.

6.5 Numerical Experiments

This section is devoted to numerical experiments and the empirical evidence of reliability, efficiency and stability for higher eigenvalues and strong convection coefficients. The numerical experiments on the unit square investigate the validity of the residual identity of Lemma 6.2.1 and the efficiency of the proposed eigenvalue condition number approximation. The experiments of the L shaped domain investigate the stability of the a posteriori error estimators for higher eigenvalues and the experiments on the slit domain their robustness in β.

6.5.1 Unit Square

As first example consider the convection-diffusion eigenvalue model problem (6.1) on the unit square $\Omega = (0, 1) \times (0, 1)$. For constant convection coefficient β, the exact eigenvalue

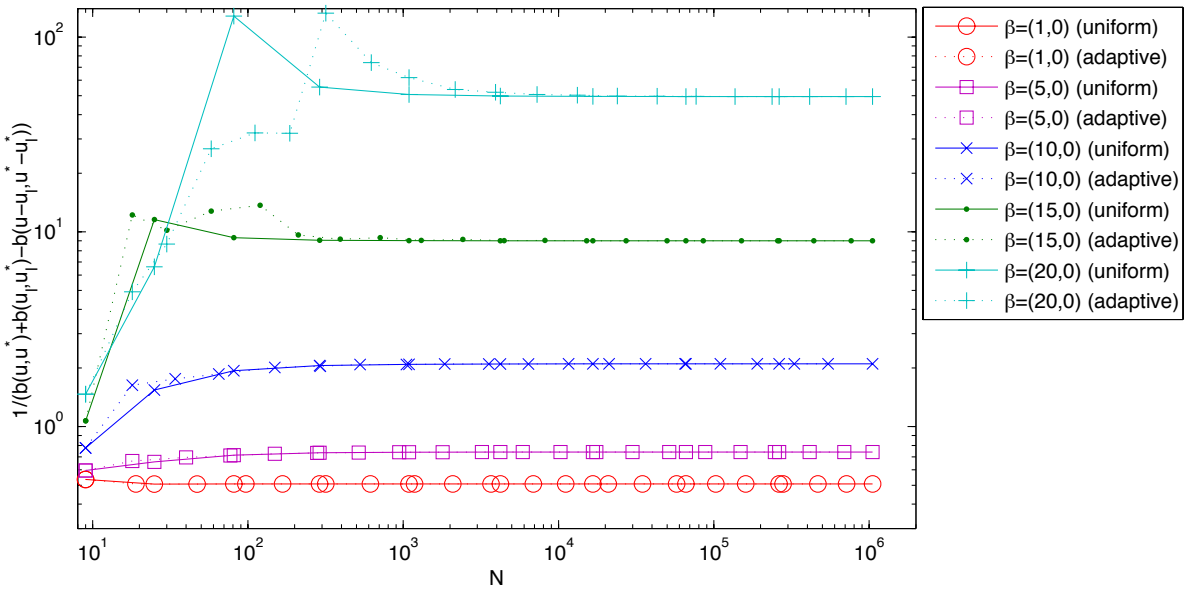

Figure 6.3: Eigenvalue condition numbers for different values of β, λ_1 and sequences of uniform and adaptive meshes generated by $\eta_{\ell,\mathrm{R}}$ on the unit square.

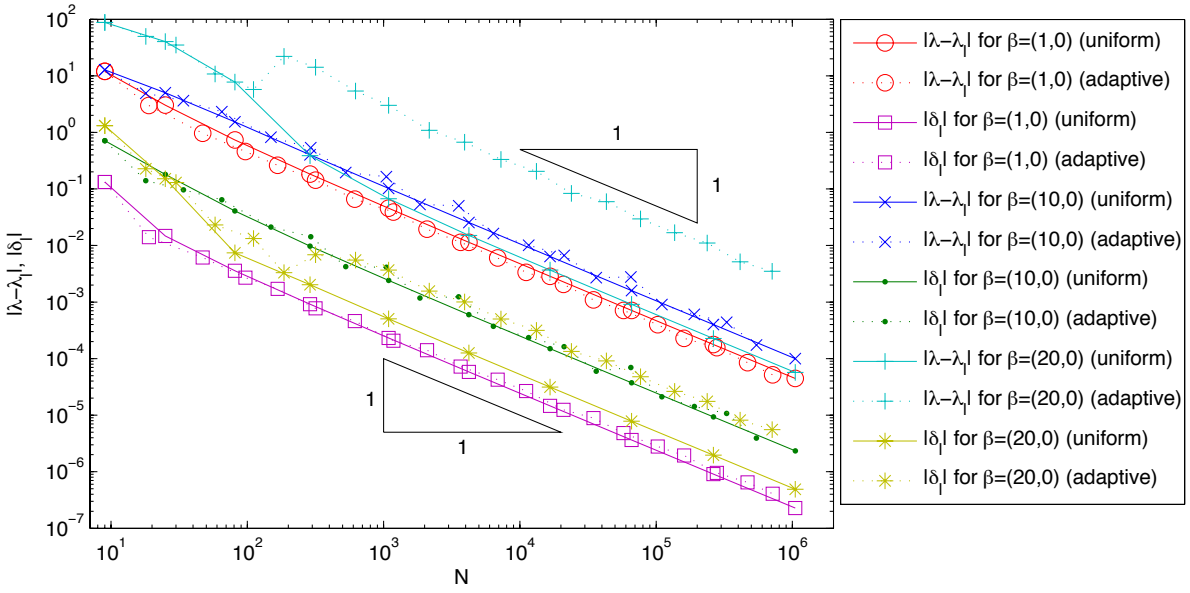

Figure 6.4: Eigenvalue errors and $|\delta_\ell|$ for different values of β, λ_1 and sequences of uniform and adaptive meshes generated by $\eta_{\ell,\mathrm{R}}$ on the unit square.

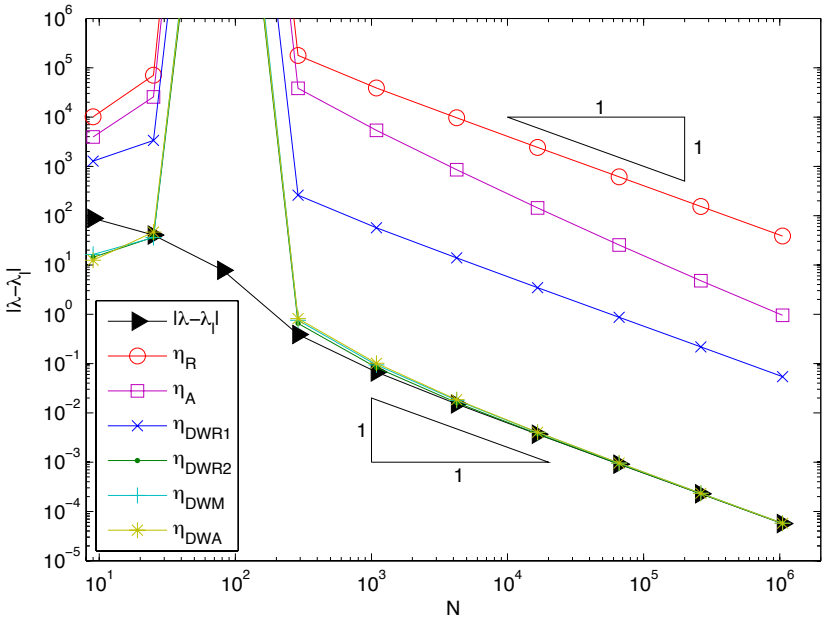

Figure 6.5: Eigenvalue errors and error estimators for $\beta = (20, 0)$, λ_1 and a sequence of uniform meshes on the unit square.

with smallest real part reads $\lambda_1 = |\beta|^2/4 + 2\pi^2$ [96]. The corresponding primal and dual eigenfunctions read

$$u(x,y) = \exp\left(\frac{\beta \cdot (x,y)^t}{2}\right)\sin(\pi x)\sin(\pi y),$$
$$u^*(x,y) = \exp\left(-\frac{\beta \cdot (x,y)^t}{2}\right)\sin(\pi x)\sin(\pi y).$$

Two discrete primal and dual solutions are displayed in Figure 6.2. To investigate the stability of the residual equation of Lemma 6.2.1 which depends on the condition number of the eigenvalue Figure 6.3 shows the factor $(b(u,u^*) + b(u_\ell, u_\ell^*) - b(e_\ell, e_\ell^*))^{-1}$ for different values of β. The values depend strongly on the size of $|\beta|$ and eigenvalue computations beyond $|\beta| \gg 20$ are numerically unstable. Figure 6.4 compares the accuracy of the eigenvalue condition number approximation $(2b(u_\ell, u_\ell^*))^{-1}$ with the error $\delta_\ell := (b(u,u^*) + b(u_\ell, u_\ell^*) - b(e_\ell, e_\ell^*))^{-1} - (2b(u_\ell, u_\ell^*))^{-1}$ compared to the eigenvalue error. Since the error for the eigenvalue condition number is much smaller than the eigenvalue error for different values of β, the proposed approximation $(2b(u_\ell, u_\ell^*))^{-1}$ of the eigenvalue condition number is empirical efficient. In all presented numerical results the sign of $\mathrm{Res}_\ell(e_\ell^*)$ and $\mathrm{Res}_\ell^*(e_\ell)$ turns out to be the same. Thus the triangle inequality $|\mathrm{Res}_\ell(e_\ell^*) + \mathrm{Res}_\ell^*(e_\ell)| \leq |\mathrm{Res}_\ell(e_\ell^*)| + |\mathrm{Res}_\ell^*(e_\ell)|$ in the proof of Theorem 6.2.6 does not destroy the efficiency of the estimate. Let N_ℓ denote the number of unknowns, i.e., the number of inner nodes. Because the domain is convex, even uniform refinement results in optimal convergence rates of $\mathcal{O}(N_\ell^{-1})$ as shown in Figure 6.5. Note that for uniform meshes

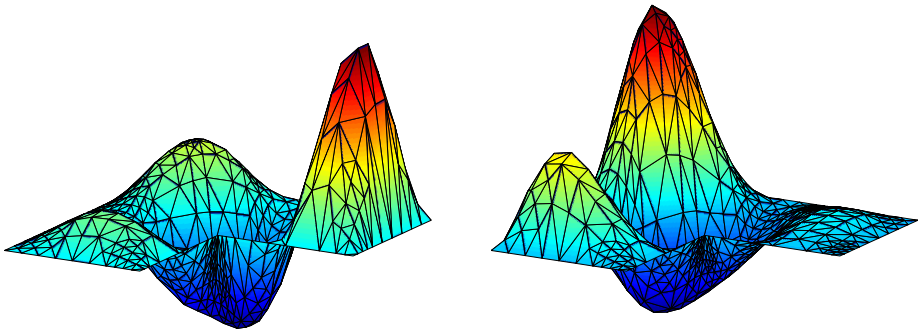

Figure 6.6: Primal (left) and dual (right) discrete solution for $\beta = (3, 0)$, λ_5 on adaptively refined meshes generated by $\eta_{\ell,\mathrm{DWR2}}$ on the L-shaped domain with about 500 nodes.

$N_\ell \approx h_\ell^{-2}$ and that there is some strong pre-asymptotic error due to the eigenvalue condition number estimate. The a posteriori error estimators $\eta_{\ell,\mathrm{DWR2}}$, $\eta_{\ell,\mathrm{DWM}}$, and $\eta_{\ell,\mathrm{DWA}}$ are close to the error while $\eta_{\ell,\mathrm{R}}$, $\eta_{\ell,\mathrm{A}}$, and $\eta_{\ell,\mathrm{DWR1}}$ are by factors $10^4 - 10^6$ larger than the error. Note that the first term of the error estimator $\eta_{\ell,\mathrm{A}}$ is of higher order and $\eta_{\ell,\mathrm{A}}$ is asymptotically reliable.

6.5.2 L-Shaped Domain

The second example is the convection-diffusion eigenvalue model problem (6.1) on the L-shaped domain $\Omega = ((-1, 1) \times (-1, 1))\backslash([0, 1] \times [0, -1])$ with constant convection parameter $\beta = (3, 0)$ and higher eigenvalues. The primal and dual solutions for adaptive meshes generated by the AFEM, based on the a posteriori error estimator $\eta_{\ell,\mathrm{DWR2}}$ for the 5−th eigenvalue with smallest real part, are shown in Figure 6.6. An approximation of the first eigenvalue reads $\lambda = |\beta|^2/4 + 9.6397238$ where 9.6397238 from [17] is an approximation of the first Laplace eigenvalue. In Figure 6.7 it is shown that uniform refinement results in a suboptimal convergence rate of about $\mathcal{O}(N_\ell^{-2/3})$, while adaptive refinement leads to numerically optimal convergence rates of $\mathcal{O}(N_\ell^{-1})$. The experiments show that the a posteriori error estimators are reliable and efficient for adaptive mesh refinement. Notice that the eigenvalues obtained from the AFEM for different estimators lead to similar eigenvalue errors. As before the values of $\eta_{\ell,\mathrm{DWR2}}$, $\eta_{\ell,\mathrm{DWM}}$, and $\eta_{\ell,\mathrm{DWA}}$ are closer to the exact error than those of $\eta_{\ell,\mathrm{R}}$, $\eta_{\ell,\mathrm{A}}$, and $\eta_{\ell,\mathrm{DWR1}}$. In order to study the dependence of the a posteriori error estimators on the size of the eigenvalue, we compare the numerical results for

$$\lambda_1 = |\beta|^2/4 + 9.6397238, \quad \lambda_5 = |\beta|^2/4 + 31.912636,$$
$$\lambda_{20} = |\beta|^2/4 + 101.60529, \quad \lambda_{50} = |\beta|^2/4 + 250.78548$$

with approximations for the corresponding Laplace eigenvalues from [17]. Figure 6.8 shows that the size of the eigenvalue error depends on the eigenvalue and that the

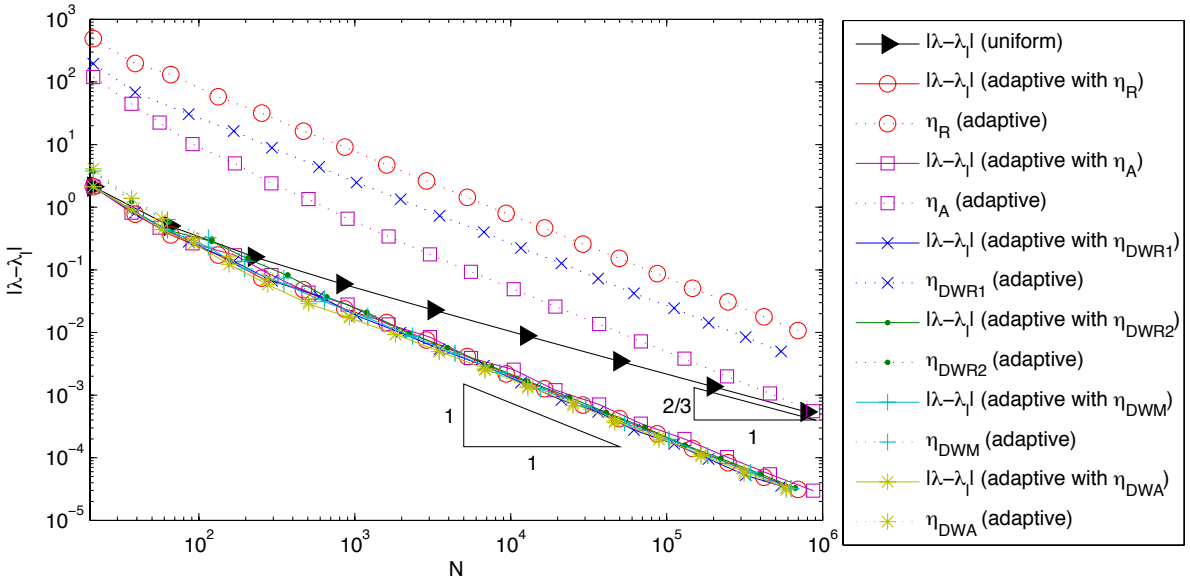

Figure 6.7: Eigenvalue errors and estimators for $\beta = (3, 0)$, λ_1 and sequences of uniform and adaptive meshes on the L-shaped domain.

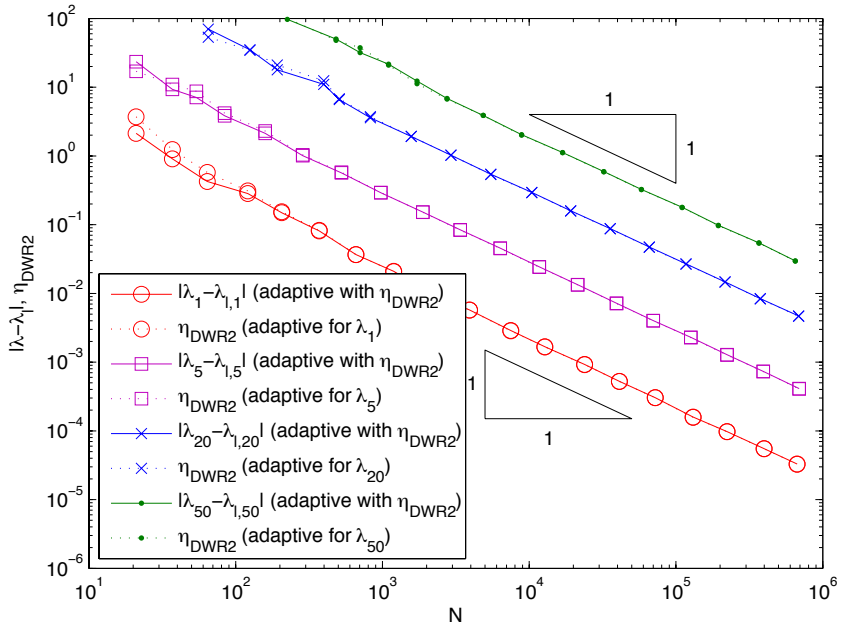

Figure 6.8: Eigenvalue errors for $\beta = (3, 0)$, λ_1, λ_5, λ_{20} and λ_{50} for sequences of uniform and adaptive meshes generated by $\eta_{\ell,\mathrm{DWR2}}$ on the L-shaped domain.

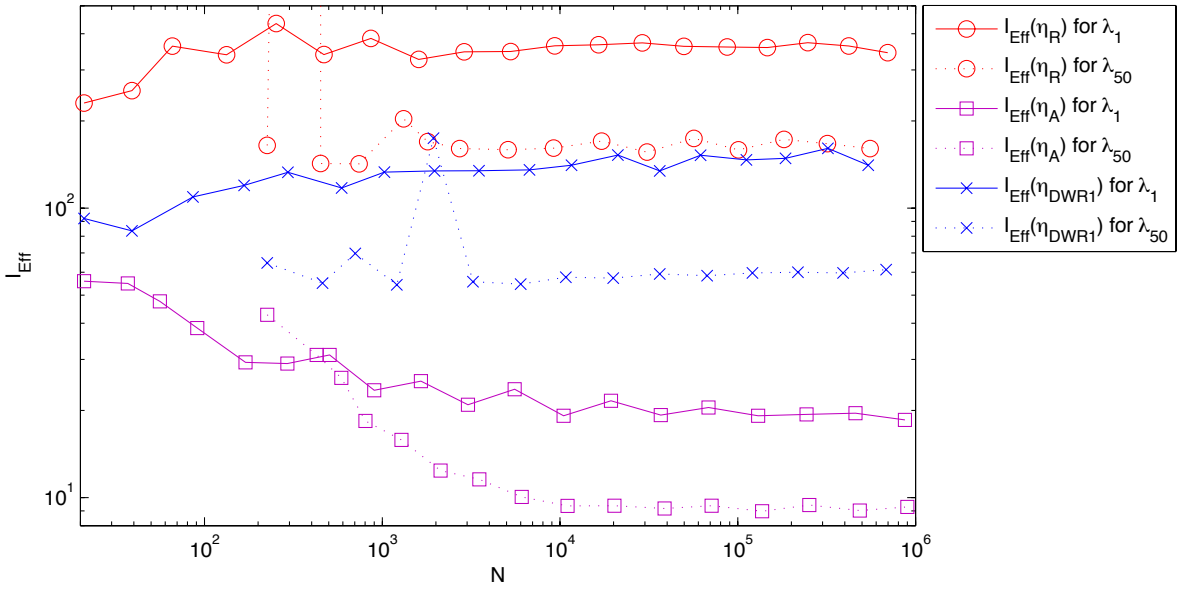

Figure 6.9: Efficiency indices $\mathrm{I}_{\mathrm{Eff}}$ for $\beta = (3, 0)$, λ_1, λ_{50} and adaptive meshes on the L-shaped domain.

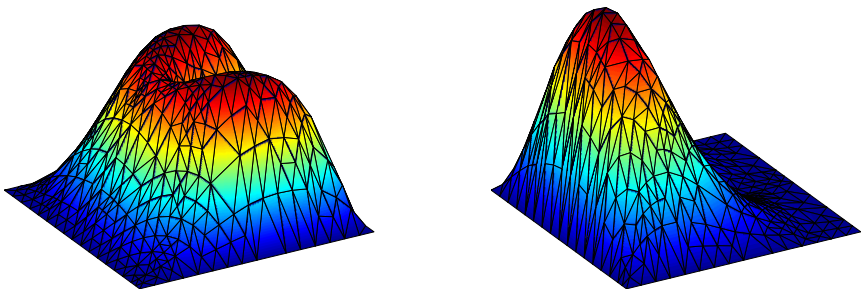

Figure 6.10: Primal (left) and dual (right) discrete solution for $\beta = (3, 0)$ and λ_1 on adaptively refined meshes generated by $\eta_{\ell,\mathrm{DWA}}$ on the slit domain with about 500 nodes.

a posteriori error estimator $\eta_{\ell,\mathrm{DWR2}}$ is asymptotically exact. In order to investigate the dependence on the size of the eigenvalue, the efficiency indices $I_{\mathrm{Eff}} = \eta_\ell/|\lambda - \lambda_\ell|$ for λ_1 and λ_{50} are compared in Figure 6.9. The experiments show that the ratio between the a posteriori error estimators and the eigenvalue error is growing in λ for $\eta_{\ell,\mathrm{R}}$, $\eta_{\ell,\mathrm{A}}$, and $\eta_{\ell,\mathrm{DWR1}}$ while $\eta_{\ell,\mathrm{DWR2}}$, $\eta_{\ell,\mathrm{DWM}}$, and $\eta_{\ell,\mathrm{DWA}}$ are robust in λ. Note that the efficiency indices of $\eta_{\ell,\mathrm{DWR2}}$, $\eta_{\ell,\mathrm{DWM}}$, and $\eta_{\ell,\mathrm{DWA}}$ are close to one.

6.5.3 Slit Domain

As last example consider the convection-diffusion eigenvalue model problem (6.1) on the slit domain $\Omega = ((-1,1) \times (-1,1))\backslash([0,1] \times \{0\})$ with different constant values for β. A computed reference value for the first eigenvalue reads $\lambda_1 = |\beta|^2/4 + 8.3713297112$ with approximation 8.3713297112 of the first Laplace eigenvalue computed on very fine meshes and higher order finite elements. The primal and dual eigenfunctions on adaptive meshes for $\eta_{\ell,\mathrm{DWA}}$ are shown in Figure 6.10. Notice that for the primal eigenfunction the influence of the magnitude of the corner singularity at the origin is much larger than for the dual eigenfunction. This illustrates that it is important to consider both primal and dual residuals. Due to the corner singularity, uniform refinement results in a suboptimal convergence rate $\mathcal{O}(N_\ell^{-1/2})$ while adaptive refinement results in the optimal convergence rate $\mathcal{O}(N_\ell^{-1})$ as shown in Figure 6.11 for $\beta = (15, 0)$. Note that the eigenvalue errors for $\eta_{\ell,\mathrm{R}}$ and $\eta_{\ell,\mathrm{A}}$ are much larger than for $\eta_{\ell,\mathrm{DWR1}}$, $\eta_{\ell,\mathrm{DWR2}}$, $\eta_{\ell,\mathrm{DWM}}$ and $\eta_{\ell,\mathrm{DWA}}$ and even larger than the eigenvalue error for uniform refinement up to $N_\ell = 10^6$. This observation is caused by a much larger pre-asymptotic range for $\eta_{\ell,\mathrm{R}}$ and $\eta_{\ell,\mathrm{A}}$ than for the DWR based a posteriori error estimators. The different adaptive meshes with about $N_\ell = 2500$ are shown in Figure 6.12. The meshes for $\eta_{\ell,\mathrm{R}}$ and $\eta_{\ell,\mathrm{A}}$ show strong refinement towards the two boundary layers on the left and right but almost no refinement towards the corner singularity at the origin which might cause the larger eigenvalue errors. In contrast to that all other refinement indicators show strong refinement toward the corner singularity at the origin which leads to smaller eigenvalue errors. In order to study the dependence of the a posteriori error estimators on the size of the convection coefficient, experiments for $\beta = (1, 0)$ and $\beta = (15, 0)$ are compared in Figure 6.13. The constants of the estimates in Lemma 6.3.1 and Lemma 6.3.2 depend on the size of the convection parameter. Thus, the efficiency indices I_{eff} are expected to depend on the size of $|\beta|$ as well which is confirmed by the numerical experiments. The size of the efficiency indices grows for the a posteriori error estimators $\eta_{\ell,\mathrm{R}}$, $\eta_{\ell,\mathrm{A}}$ and $\eta_{\ell,\mathrm{DWR1}}$ corresponding to the increase of $|\beta|$. In contrast the efficiency indices for $\eta_{\ell,\mathrm{DWR2}}$, $\eta_{\ell,\mathrm{DWM}}$ and $\eta_{\ell,\mathrm{DWA}}$ are robust in β and close to one.

6.6 Conclusions

All the numerical results indicate that the a posteriori error estimators are asymptotically reliable and empirical efficient. The interpolation scheme of Section 6.4 for the weights shows to be empirical stable for unstructured triangular meshes. The approximation of the condition number needs to be included in the a posteriori error estimators in order

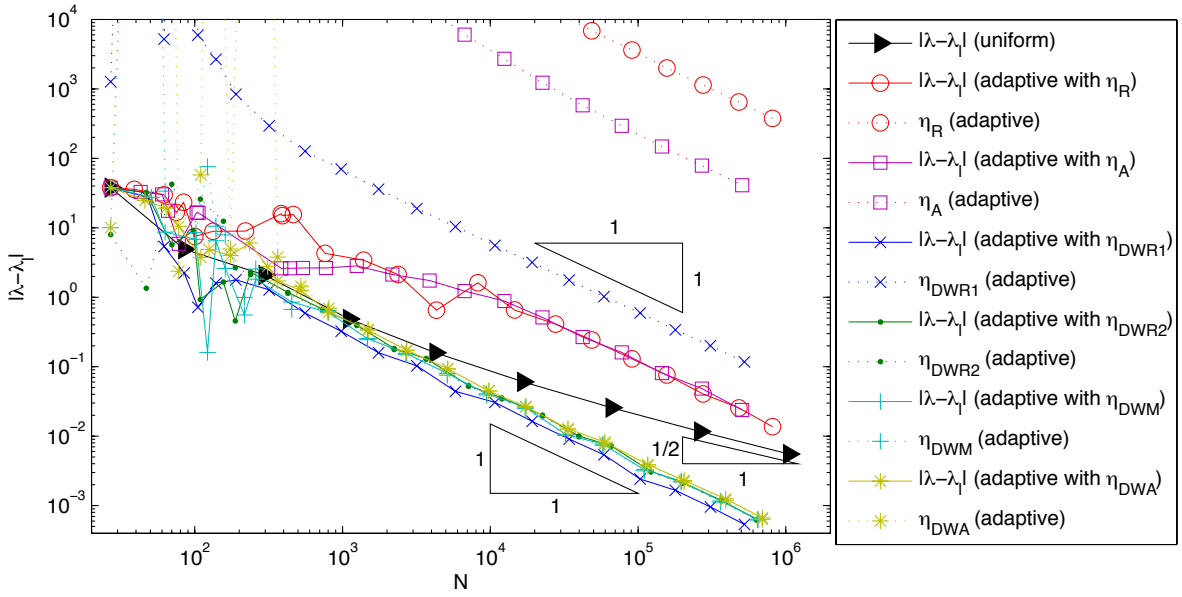

Figure 6.11: Eigenvalue errors and estimators for $\beta = (15, 0)$, λ_1 and sequences of uniform and adaptive meshes on the slit domain.

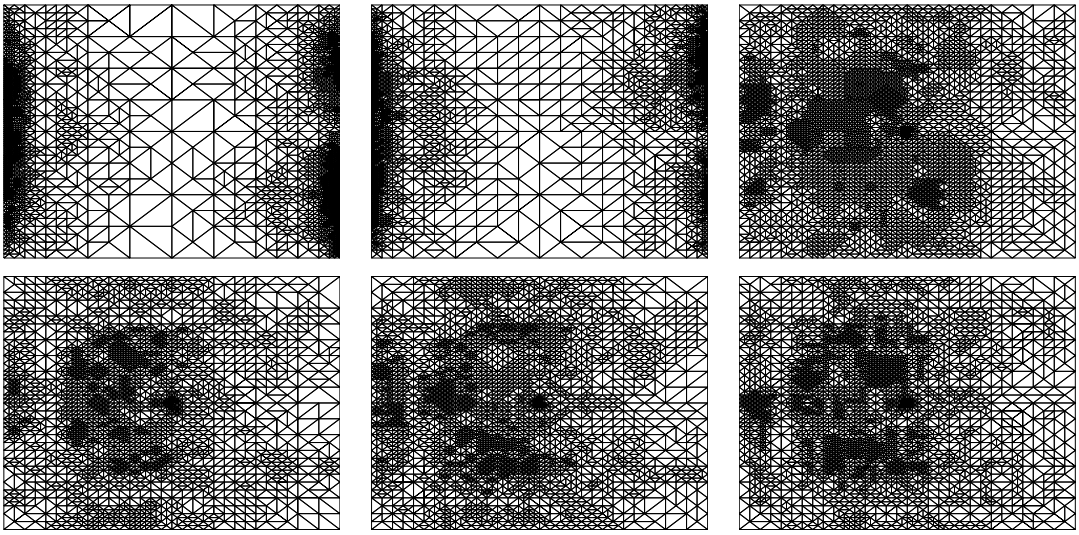

Figure 6.12: Meshes for $\beta = (15, 0)$ and λ_1 generated by the refinement monitored by $\eta_{\ell,R}$, $\eta_{\ell,A}$, $\eta_{\ell,\mathrm{DWR1}}$, $\eta_{\ell,\mathrm{DWR2}}$, $\eta_{\ell,\mathrm{DWM}}$ and $\eta_{\ell,\mathrm{DWA}}$ (from left to right and top to bottom) on the Slit domain with about 2500 nodes.

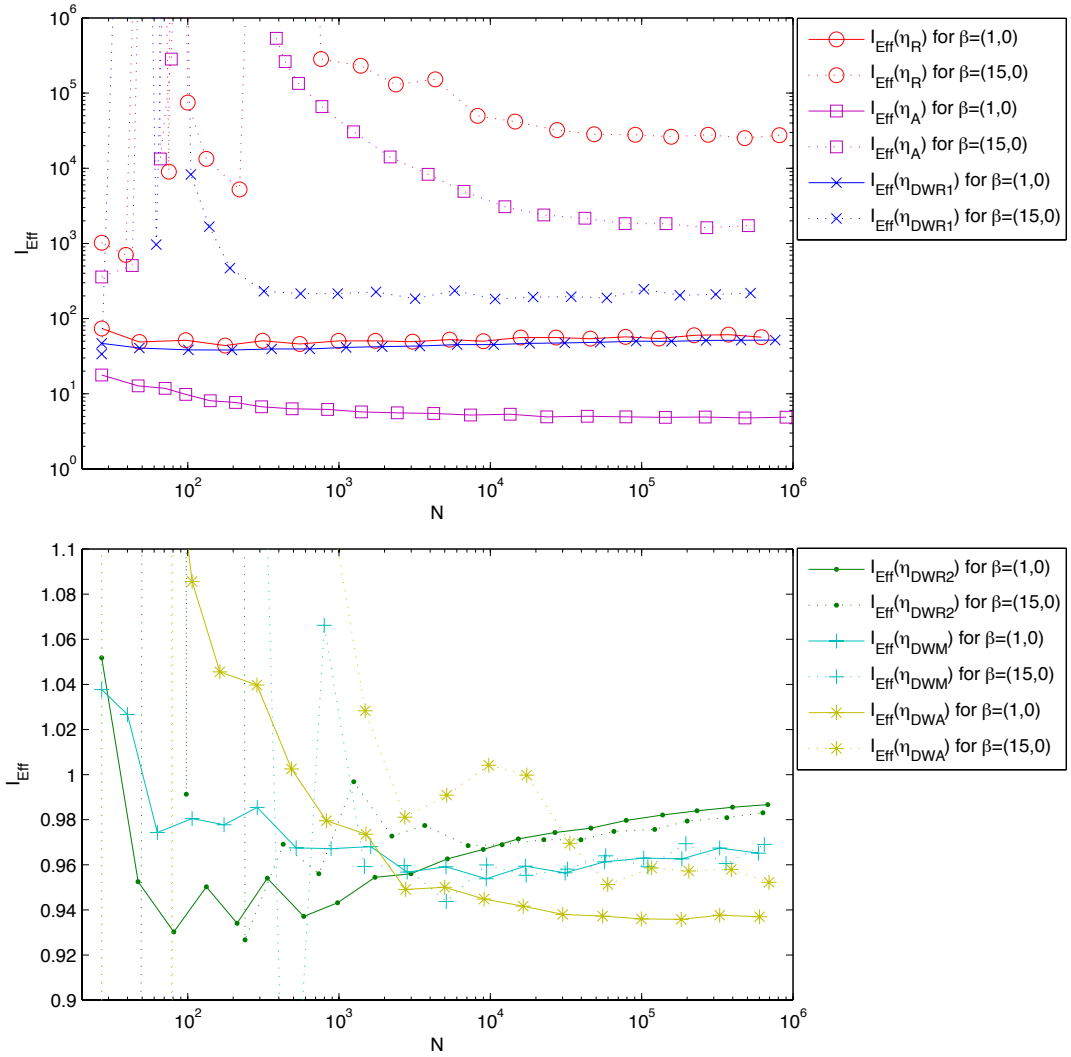

Figure 6.13: Efficiency indices I_{Eff} for $\beta = (1,0)$, $(15,0)$, λ_1 and adaptive sequences of meshes on the slit domain.

to get efficiency indices close to one. The DWR2, DWM and the DWA a posteriori error estimators result in the best asymptotic efficiency indices close to one independently of both, the size of the eigenvalue and the convection parameter. For larger values of $|\beta|$, the DWR-based a posteriori error estimators lead to much smaller eigenvalue errors than the residual and averaging based a posteriori error estimators because of the much smaller pre-asymptotic range. Since the used eigenvalue solver ARPACK [83] shows some instability for convection coefficients larger than $(20,0)$ and coarser meshes those are excluded in this chapter. For highly non-symmetric problems other techniques such as the homotopy methods of Chapter 7 need to be applied in order to compute the same eigenvalue of interest during all steps of the adaptive finite element loop or different finite elements need to be considered such as discontinuous Galerkin finite elements [43].

```
|-- afemPkEllipticNonsymEigenvalue.m (main script)
|-- Mesh.m
|-- solvePkLaplaceEigenvalue.m
|-- Estimate
|   |-- estimatePkEigenvalueNonsymAveraging.m
|   |-- estimatePkEigenvalueNonsymDWA.m
|   |-- estimatePkEigenvalueNonsymDWM.m
|   |-- estimatePkEigenvalueNonsymDWR1.m
|   |-- estimatePkEigenvalueNonsymDWR2.m
|   `-- estimatePkEigenvalueNonsymResidual.m
|-- Geometries
|   `-- ... (several geometric data)
|-- Pk
|   |-- Pk.m
|   |-- PkEvaluate.m
|   |-- PkFunctionHandles.m
|   |-- PkInterpolation.m
|   |-- pkLeastSquareAveraging.m
|   `-- PkMatrix.m
|-- RT
|   |-- RT0.m
|   `-- solveRT0Elliptic.m
`-- Tools
    |-- integrate.m
    |-- localDoFtoGlobalDoF.m
    |-- matMul.m
    |-- Multigrid.m
    |-- P0P1GradientAveraging
    `-- plotConvergence.m
```

Table 6.1: The software directory of Chapter 6.

6.7 Software Implementation

The software directory with the software files used for the numerical experiments of this chapter is listed in Table 6.1. In the following the files that were not used in one of the previous chapters are described.

`afemPkEllipticNonsymEigenvalue.m` implements the AFEM loop for the convection-diffusion eigenvalue problem.

The folder *Estimate* contains the implementations of the error estimators $\eta_{\ell,\mathrm{A}}$, $\eta_{\ell,\mathrm{DWA}}$, $\eta_{\ell,\mathrm{DWM}}$, $\eta_{\ell,\mathrm{DWR1}}$, $\eta_{\ell,\mathrm{DWR2}}$ and $\eta_{\ell,\mathrm{R}}$.

The folder *RT* contains the Raviart-Thomas finite element class object `RT0` and a file to compute the mixed solution `solveRT0Elliptic.m` that are utilised for the DWM a posteriori error estimator.

`P0P1GradientAveraging` implements the averaging operator

$$A(\nabla u_\ell) := \sum_{z \in \mathcal{N}_\ell} \frac{1}{|\omega_z|} \left(\int_{\omega_z} \nabla u_\ell \, dx \right) \varphi_z.$$

```
1  function val = P0P1GradientAveraging(pk,x)
     mesh = pk.mesh;
     grad4e = PkEvaluate.getGradU(1/3,1/3,x,pk,pk.mesh);
     grad4e = grad4e.*[mesh.area4e,mesh.area4e];
5    grad4eX = grad4e(:,1)*ones(1,3);
     grad4eY = grad4e(:,2)*ones(1,3);
     val(:,1) = accumarray(pk.dofU4e(:),grad4eX(:))./mesh.area4n;
     val(:,2) = accumarray(pk.dofU4e(:),grad4eY(:))./mesh.area4n;
   end
```

The input is the P_k finite element object `pk` of degree one and the coefficient vector `x`. The output is the matrix `val` that encodes the values of the averaged gradient at all the vertices. Line 3 evaluates the piecewise constant gradient in the midpoint of each element. In the next line the values are multiplied with $|T|$. In lines 5-6 the x and y values are copied separately. In lines 7-8 the corresponding values for each node z are added together and divided by $|\omega_z|$.

`pkLeastSquareAveraging.m` implements the L^2 averaging scheme of [111] as described in Subsection 6.4.2. The key for-loop over all triangles is displayed below.

```
10 for curElem = 1:mesh.nrElems
     curNodes = mesh.n4e(curElem,:);
     patch = [patch4n(curNodes(1),1:patchSize4n(curNodes(1))),...
              patch4n(curNodes(2),1:patchSize4n(curNodes(2))),...
              patch4n(curNodes(3),1:patchSize4n(curNodes(3)))];
15   curUVal = uVal(patch,:)';
     curX = permute(points4e(patch,1,:),[3 1 2]);
     curY = permute(points4e(patch,2,:),[3 1 2]);
     matrix = pl.monomBasis(curX(:),curY(:));
     c = matrix\curUVal(:);
20   dofs = pl.dofU4e(curElem,:);
     plU4e(curElem,:) = pl.monomBasis(pl.c4dof(dofs,1),pl.c4dof(dofs,2))*c;
   end
```

Lines 11-14 determine the current element patch where the matrix `patch4n` has been precomputed for better performance. The function values for the current patch are extracted in line 15. The lines 16-17 determine the interpolation coordinates. The global least squares fitting in the one degree higher polynomial space is computed in lines 18-19. Lines 20-21 evaluate the least squares solution in the coordinates of the degrees of freedom for the current element.

Up to now the least squares fitting yields a discontinuous approximation. The next function computes a smooth averaged approximation by the arithmetic mean values at node and edge degrees of freedom.

```
23 function val = smooth(pkU4e,pk)
```

```
    dofU4e = pk.dofU4e;
25  weight4dofU4e = ones(size(dofU4e));
    weight4dof = accumarray(dofU4e(:),weight4dofU4e(:),[pk.nrDoF,1]);
    pkU = accumarray(dofU4e(:),pkU4e(:),[pk.nrDoF,1]);
    val = pkU./weight4dof;
end
```

Input are the discontinuous values `pkU4e` for each element and the corresponding finite element `pk`. Output is a coefficient vector `val`. Line 26 computes the weights, i.e., the number of elements attached to any degree of freedom. Line 27 computes the sum of the values for each degree of freedom which is finally divided by the corresponding weight in line 28.

7 An Adaptive Homotopy Approach for Non-Selfadjoint Eigenvalue Problems

This chapter presents adaptive algorithms for eigenvalue problems associated with non-selfadjoint partial differential operators. The basis for the developed algorithms is a homotopy method which departs from a well-understood selfadjoint problem. Apart from the adaptive grid refinement, the progress of the homotopy as well as the solution of the iterative method are adapted to balance the contributions of the different error sources. The first algorithm balances the homotopy, discretisation and approximation errors with respect to a fixed step-size τ in the homotopy. The second algorithm combines the adaptive step-size control for the homotopy with an adaptation in space that ensures an error below a fixed tolerance ε. The outcome of this chapter leads to the third algorithm which allows the complete adaptivity in space, homotopy step-size as well as the iterative algebraic eigenvalue solver. All three algorithms are compared in numerical examples.

This chapter is joint work with C. Carstensen, V. Mehrmann and A. Miedlar and has been published in [37].

7.1 Introduction

Non-selfadjoint eigenvalue problems associated with partial differential operators arise in a large number of applications, such as acoustic field computations [4], structural analysis of buildings or vehicles [67], electric and magnetic field computation [21]. Today, in almost all applications the space is discretised first (typically with a very fine grid) which leads to a large scale linear or non-linear matrix eigenvalue problem. To solve these algebraic eigenvalue problems, classical eigenvalue methods [11, 61, 83, 94] are used.

A priori error estimates for eigenvalues and eigenvectors of elliptic operators and compact operators were developed, e.g., in [9, 10, 42, 75, 81, 98, 105, 113]. All these approaches, although optimal, contain mesh size restrictions, which cannot be verified or quantified, neither a priori nor a posteriori. Verifiable a priori error estimates for symmetric eigenvalue problems were presented in [6, 76, 79].

In order to avoid unnecessarily fine grids, there have been tremendous research activities to design adaptive eigenvalue methods that adapt the grid to the behaviour of the eigenfunctions in recent years. In particular, for selfadjoint elliptic problems the progress in the analysis and computational methods has been substantial. A first approach on a posteriori error analysis for symmetric second order elliptic eigenvalue problems can be found in [108]. A combination of a posteriori and a priori analysis was used in [80] to prove reliable and efficient a posteriori estimates for H^2 regular problems. For non-

smooth solutions a posteriori error estimators were given in [50, 89, 92]. Recent results include [33, 58, 60, 65, 100].

A first a posteriori error analysis for non-selfadjoint elliptic eigenvalue problems was presented in [69]. The difficulty with non-selfadjoint PDE eigenvalue problems is multifold, eigenvalues may be complex, or may have different algebraic and geometric multiplicity. The latter property is a particular difficulty for the discretisation methods because in the finite-dimensional approximation this property may be destroyed. The computed eigenvalues and eigenfunctions may have large errors due to the ill-conditioning of the problem although the approximation error is small. Even when the discretisation retains the multiplicities of the eigenvalues, the algebraic eigensolvers have difficulties with the ill-conditioning of multiple eigenvalues. At this stage the adaptive solution of general non-selfadjoint eigenvalue problems remains a real challenge.

This chapter studies the restricted class of convection-diffusion eigenvalue problems, where for the pure diffusion problem the discussed adaptive methods work nicely. To design an adaptive algorithm for the convection-diffusion problem a homotopy method is used. Homotopy methods are well established for non-symmetric matrix eigenvalue problems [84, 85, 86, 88]. Here, the homotopy approach is used not only on the matrix level but on the level of the differential operator as well. The combination of the adaptive homotopy with mesh adaptivity and iterative matrix eigenvalue solvers involves three different types of errors. These are the *discretisation error* η that arises when the infinite-dimensional variational problems is considered in a finite-dimensional subspace [69] and Chapter 6, the *homotopy error* ν that arises because the diffusion problem is slowly transferred to the convection-diffusion problem [22] and the *approximation error* μ that arises from the iterative matrix eigensolver in finite precision arithmetic [11, 68, 94, 104]. Since the goal is to design methods that are both accurate and efficient, this chapter presents algorithms that are able to provide adaptivity in all three directions by a suitable balancing of all three errors.

As model problem consider the convection-diffusion eigenvalue problem of Section 2.4: *Determine a non-trivial eigenpair* $(\lambda, u) \in \mathbb{C} \times \{H_0^1(\Omega;\mathbb{C}) \cap H_{loc}^2(\Omega;\mathbb{C})\}$ *with* $\|u\|_{L^2(\Omega;\mathbb{C})} = 1$ *such that*

$$-\Delta u + \beta \cdot \nabla u = \lambda u \text{ in } \Omega \qquad \text{and} \qquad u = 0 \text{ on } \partial\Omega \tag{7.1}$$

for some bounded Lipschitz domain $\Omega \subseteq \mathbb{R}^2$ *and a constant coefficient vector* $\beta \in \mathbb{R}^2$.
Its weak formulation reads: *For two complex Hilbert spaces* $V := H_0^1(\Omega;\mathbb{C})$ *with norm* $|||\cdot||| := |\cdot|_{H^1(\Omega;\mathbb{C})}$ *and* $H := L^2(\Omega;\mathbb{C})$ *with norm* $\|\cdot\|_{L^2(\Omega;\mathbb{C})}$ *determine a non-trivial eigenpair* $(\lambda, u) \in \mathbb{C} \times V$ *with* $b(u,u) = 1$ *such that*

$$a(u,v) + c(u,v) = \lambda b(u,v) \quad \text{for all} \quad v \in V, \tag{7.2}$$

where $\overline{(.)}$ *denotes complex conjugation and, for all* $u, v \in V$,

$$a(u,v) := \int_\Omega \nabla u \nabla \overline{v} dx, \quad c(u,v) := \int_\Omega \overline{v}(\beta \cdot \nabla u) dx, \quad b(u,v) := \int_\Omega u\overline{v} dx.$$

For the analysis it is necessary to consider also the dual eigenvalue problem: *Determine a non-trivial dual eigenpair* $(\lambda^*, u^*) \in \mathbb{C} \times V$ *with* $b(u^*, u^*) = 1$ *with*

$$a(w, u^*) + c(w, u^*) = \overline{\lambda^*} b(w, u^*) \quad \textit{for all} \quad w \in V. \tag{7.3}$$

Note that the primal and dual eigenvalues are connected via $\lambda = \overline{\lambda^*}$.

For a finite-dimensional subspace $V_\ell \subseteq V$ the discretised primal and dual problems read: *Determine non-trivial primal and dual eigenpairs* $(\lambda_\ell, u_\ell) \in \mathbb{C} \times V_\ell$ *and* $(\lambda_\ell^*, u_\ell^*) \in \mathbb{C} \times V_\ell$ *such that*

$$a(u_\ell, v_\ell) + c(u_\ell, v_\ell) = \lambda_\ell b(u_\ell, v_\ell) \quad \textit{for all} \quad v_\ell \in V_\ell, \tag{7.4}$$

$$a(w_\ell, u_\ell^*) + c(w_\ell, u_\ell^*) = \overline{\lambda_\ell^*} b(w_\ell, u_\ell^*) \quad \textit{for all} \quad w_\ell \in V_\ell. \tag{7.5}$$

In view of the difficulties for non-selfadjoint problems discussed before, suppose for the remaining part of this chapter that the eigenvalue of interest λ is simple and well-separated from the rest of the spectrum.

To distinguish continuous, discrete and approximated eigenvalues, some further notation is introduced. In the following $\lambda(t)$ will denote the continuous eigenvalue of interest at homotopy step t, $\lambda_\ell(t)$ the corresponding eigenvalue of the discrete problem, while $\tilde{\lambda}_\ell(t)$ denotes its approximation computed by an iterative eigenvalue solver in finite precision arithmetic. The corresponding eigenfunctions are denoted in a similar fashion, i.e., $u(t)$, $u_\ell(t)$, $\tilde{u}_\ell(t)$. In order to distinguish the eigenfunction $u_\ell(t)$ from the corresponding coefficient vector with respect to a given finite element basis, for this eigenvector $\mathbf{u}_\ell(t)$ bold letters will be used. For all these eigenvalues and eigenfunctions or eigenvectors * denotes the solution of the corresponding dual problem, i.e., for the algebraic eigenvalue problem $\mathbf{u}_\ell^*(t)$ denotes the corresponding left eigenvector.

This chapter is organized as follows: Section 7.2 reviews the adaptive finite element method (AFEM) and Section 7.3 discusses the homotopy method. The homotopy error is presented in Section 7.4. In Section 7.5 a complete a posteriori error estimator for all three different error sources is presented. In Section 7.6 several different adaptive homotopy algorithms are developed. Numerical examples compare the performance of the different algorithms in Section 7.7.

7.2 Adaptive Finite Element Methods

In this section we review the basic concept of the adaptive finite element method (AFEM). Starting from an initial coarse triangulation $\mathcal{T}_0$, the AFEM generates a sequence of nested triangulations $\mathcal{T}_0, \mathcal{T}_1, \ldots \mathcal{T}_\ell$ with corresponding nested spaces

$$V_0 \subseteq V_1 \subseteq \ldots \subseteq V_\ell \subset V.$$

A typical AFEM loop consists of the four steps

$$\texttt{Solve} \longrightarrow \texttt{Estimate} \longrightarrow \texttt{Mark} \longrightarrow \texttt{Refine}.$$

7.2.1 Solve

The primal and dual generalized algebraic eigenvalue problems

$$(A_\ell + C_\ell)\mathbf{u}_\ell = \lambda_\ell B_\ell \mathbf{u}_\ell \qquad \text{and} \qquad \mathbf{u}_\ell^*(A_\ell + C_\ell) = \lambda_\ell^* \mathbf{u}_\ell^* B_\ell \tag{7.6}$$

are solved with an algebraic eigensolver. Here the coefficient matrices are the symmetric positive definite stiffness matrix A_ℓ, the non-symmetric convection matrix C_ℓ and the symmetric positive definite mass matrix B_ℓ. The right and left eigenvectors $\mathbf{u}_\ell = [\mathbf{u}_{\ell,k}]$ and $\mathbf{u}_\ell^* = [\mathbf{u}_{\ell,k}^*]$ represent the eigenfunctions

$$u_\ell = \sum_{k=1}^{\dim(V_\ell)} \mathbf{u}_{\ell,k}\varphi_k \quad \text{and} \quad u_\ell^* = \sum_{k=1}^{\dim(V_\ell)} \mathbf{u}_{\ell,k}^*\varphi_k$$

with respect to the basis $(\varphi_1, \ldots, \varphi_{\dim(V_\ell)})$ of V_ℓ.

7.2.2 Estimate

The eigenvalue error is estimated a posteriori with a standard residual type error estimator using the residuals for both, the primal and dual, eigenfunctions. The proof of *reliability*, i.e., that the estimator is an upper bound of the eigenvalue error, can be found in [69] and Chapter 6, where it is shown, that

$$|\lambda - \lambda_\ell| \lesssim \sum_{T\in\mathcal{T}_\ell} \Big(\eta_\ell^2(T) + \eta_\ell^{*2}(T)\Big). \tag{7.7}$$

Here the primal η_ℓ and dual η_ℓ^* refinement indicators for a triangle $T \in \mathcal{T}_\ell$ are defined as

$$\begin{aligned}
\eta_\ell^2(T) &:= h_T^2 \|\beta\cdot\nabla u_\ell - \lambda_\ell u_\ell\|_{L^2(T)}^2 + \sum_{E\in\mathcal{E}_\ell(T)} h_E \|[\nabla u_\ell]\cdot n_E\|_{L^2(E)}^2, \\
\eta_\ell^{*2}(T) &:= h_T^2 \|-\beta\cdot\nabla \overline{u_\ell^*} - \overline{\lambda_\ell^* u_\ell^*}\|_{L^2(T)}^2 + \sum_{E\in\mathcal{E}_\ell(T)} h_E \|[\nabla \overline{u_\ell^*}]\cdot n_E\|_{L^2(E)}^2,
\end{aligned}$$

where $\mathcal{E}_\ell(T)$ denotes the set of all edges for an element $T \in \mathcal{T}_\ell$, h_E is the length of the edge E, h_T is the diameter of the triangle T, n_E denotes an unit normal for the edge E, and $[\cdot]$ denotes the jump across some edge E defined as $[\cdot] := \cdot|_{T_+} - \cdot|_{T_-}$ for two neighbouring triangles $T_\pm \in \mathcal{T}_\ell$ with $E = T_+ \cap T_-$.

Note that the constant in the a posteriori error estimate (7.7) depends on the eigenvalue condition number $1/b(u, u^*)$ as shown in Section 6.2 of Chapter 6.

7.2.3 Mark

Based on the refinement indicators, the set of elements $\mathcal{M}_\ell \subseteq \mathcal{T}_\ell$ that are refined is specified in the algorithm `Mark` . Let $\mathcal{M}_\ell$ be the set of minimal cardinality for which the bulk criterion [48],

$$\theta \sum_{T\in\mathcal{T}_\ell} \left(\eta_\ell^2(T) + \eta_\ell^{*2}(T)\right) \leq \sum_{T\in\mathcal{M}_\ell} \left(\eta_\ell^2(T) + \eta_\ell^{*2}(T)\right)$$

is satisfied for a given bulk parameter $0 < \theta \leq 1$. This minimal set $\mathcal{M}_\ell$ may be computed by a greedy algorithm. Sorting all the values $(\eta_\ell^2(T) + \eta_\ell^{*2}(T))_{T\in\mathcal{T}_\ell}$ in ascending order allows to add elements with largest values successively to the set $\mathcal{M}_\ell$ until the bulk criterion is fulfilled.

7.2.4 Refine

Given the set $\mathcal{M}_\ell \subseteq \mathcal{T}_\ell$ of marked elements, mark all edges of elements in $\mathcal{M}_\ell$ for refinement. The mesh is then refined by the closure algorithm of Section 2.5.1 and the newest-vertex bisection algorithm of Section 2.5.3.

7.3 Homotopy Methods

In this section we will discuss homotopy methods and extend them from the matrix eigenvalue problem to the operator problem. Homotopy methods in the context of non-symmetric matrix eigenvalue problems are discussed in [84, 85, 86, 88]. In [87] an extension to the eigenvalue problem for selfadjoint partial differential operators is presented.

From the eigenvalues and eigenvectors of some known matrix A_0, the eigenvalues and eigenvectors of

$$\mathcal{H}(t) = (1 - f(t))A_0 + f(t)A_1 \quad \text{for} \quad 0 \leq t \leq 1,$$

for a given function $f : [0, 1] \to [0, 1]$ with $f(0) = 0$, $f(1) = 1$, can be computed by following their paths from 0 to 1. In the following we will only discuss the case $f(t) = t$, but in practice, the function f should grow faster towards $t = 1$ to improve the convergence of the homotopy method.

The homotopy concept can be easily extended to the convection-diffusion operator eigenvalue problem. Starting from the spectrum of some known operator, e.g., from $\mathcal{L}_0 u := -\Delta u$, one may use a continuation method to obtain the eigenpairs for the convection-diffusion operator $\mathcal{L}_1 u := -\Delta u + \beta \cdot \nabla u$.

Throughout the chapter the following homotopy equation is considered for the model problem (7.1)

$$\mathcal{H}(t) = (1 - t)\mathcal{L}_0 + t\mathcal{L}_1 \quad \text{for} \quad 0 \leq t \leq 1. \tag{7.8}$$

Since for $t = 0$ we have

$$\mathcal{H}(0) = \mathcal{L}_0,$$

the eigenpairs of $\mathcal{H}(0)$ are the eigenpairs for the Laplace eigenvalue problem. The continuation method uses a 'time'-stepping procedure with nodes $t_0 = 0 < t_1 < \ldots < t_N = 1$ to compute the eigenvalues and eigenvectors of

$$-\Delta u + t_i \beta \cdot \nabla u = \lambda u \quad \text{in} \quad \Omega.$$

When the homotopy reaches its final value 1, the eigenpairs of $\mathcal{H}(1) = \mathcal{L}_1$, are the eigenpairs of the desired problem,

$$-\Delta u + \beta \cdot \nabla u = \lambda u \quad \text{in} \quad \Omega.$$

For each step t_i the corresponding weak finite-dimensional primal and dual problems

$$\begin{aligned} a(u_\ell, v_\ell) + t_i\, c(u_\ell, v_\ell) &= \lambda_\ell b(u_\ell, v_\ell) \quad \text{for all} \quad v_\ell \in V_\ell, \\ a(w_\ell, u_\ell^*) + t_i c(w_\ell, u_\ell^*) &= \overline{\lambda_\ell^*} b(w_\ell, u_\ell^*) \quad \text{for all} \quad w_\ell \in V_\ell, \end{aligned}$$

lead to the generalized primal and dual matrix eigenvalue problems

$$(A_\ell + t_i\, C_\ell)\mathbf{u}_\ell = \lambda_\ell B_\ell \mathbf{u}_\ell, \tag{7.9}$$

$$\mathbf{u}_\ell^*(A_\ell + t_i\, C_\ell) = \lambda_\ell^* \mathbf{u}_\ell^* B_\ell, \tag{7.10}$$

corresponding to the discrete homotopy equation

$$\mathcal{H}_\ell(t) = (1-t)A_\ell + t(A_\ell + C_\ell) = A_\ell + tC_\ell.$$

For simple and well-separated eigenvalues that do not bifurcate during the homotopy process, as considered here, it is known [73] that every eigenvalue $\lambda_\ell(t)$ of the generalized eigenvalue problems (7.9) and (7.10) is an analytic function in t. Choosing appropriate homotopy step-sizes, the eigenvalues can therefore be continued on an analytic path towards the eigenvalues of $(A_\ell + C_\ell, B_\ell)$ [85, 88]. The evolution of an eigenpair as a function of t is called an *eigenpath* and is denoted by $(\lambda_\ell(t), \mathbf{u}_\ell(t))$ and $(\lambda_\ell^*(t), \mathbf{u}_\ell^*(t))$, respectively.

7.4 Homotopy Error

In this section we analyse the homotopy error which in another context is called *modeling error* [22]. As we solve at the beginning of the homotopy process first a selfadjoint problem, we need to understand how the real eigenvalues of the symmetric problem move to the (potentially complex conjugate) eigenvalues of the non-symmetric problem.

Lemma 7.4.1. *For the model problem (7.1), the difference between the exact eigenvalues $\lambda(t)$ of the homotopy $\mathcal{H}(t)$ in (7.8) and $\lambda(1)$ can be estimated via*

$$|\lambda(1) - \lambda(t)| \lesssim \nu(t) := (1-t)|\beta|_\infty \left(|\!|\!| u(t) |\!|\!| + |\!|\!| u^*(t) |\!|\!|\right) \quad \textit{for} \quad 0 \le t \le 1.$$

The constant in the inequality tends to $1/(2b(u(1),u^*(1))$ *as* $t \to 1$.

Proof. For the homotopy parameter $0 \le t \le 1$, the primal and dual weak eigenvalue problems have the form

$$\begin{aligned} a(u(t),v) + tc(u(t),v) &= \lambda(t) b(u(t),v) \qquad \text{for all} \quad v \in V, \\ a(w,u^*(t)) + tc(w,u^*(t)) &= \overline{\lambda^*(t)} b(w,u^*(t)) \quad \text{for all} \quad w \in V. \end{aligned}$$

Algebraic manipulations yield

$$\begin{aligned} &(\lambda(1)-\lambda(t))\Big(b(u(1),u^*(1)) + b(u(t),u^*(t)) - b(u(1)-u(t),u^*(1)-u^*(t))\Big) \\ &\quad = (\lambda(1)-\lambda(t))\Big(b(u(1),u^*(t)) + b(u(t),u^*(1))\Big) \\ &\quad = \lambda(1) b(u(1),u^*(t)) + \overline{\lambda^*(1)} b(u(t),u^*(1)) \\ &\qquad - \overline{\lambda^*(t)} b(u(1),u^*(t)) - \lambda(t) b(u(t),u^*(1)) \\ &\quad = (1-t)c(u(1),u^*(t)) + (1-t)c(u(t),u^*(1)). \end{aligned}$$

Since β is divergence free, it follows that

$$c(u(1),u^*(t)) = -c(u^*(t),u(1)).$$

Then the Hölder inequality implies that

$$\begin{aligned} c(u(t),u^*(1)) - c(u^*(t),u(1)) &\le \|\beta \cdot \nabla u(t)\| \|u^*(1)\| + \|\beta \cdot \nabla u^*(t)\| \|u(1)\| \\ &\le |\beta|_\infty \left(|\!|\!| u(t) |\!|\!| + |\!|\!| u^*(t) |\!|\!| \right). \end{aligned}$$

Since $b(u(t),u^*(t))$ tends to $b(u(1),u^*(1))$ and $b(u(1)-u(t),u^*(1)-u^*(t))$ tends to zero as $t \to 1$, the constant in the eigenvalue error estimate tends to $1/(2b(u(1),u^*(1))$. □

7.5 A Posteriori Error Estimator

In this section we discuss the a posteriori estimation of the eigenvalue error during the homotopy process. For the design of adaptive algorithms, it is of particular interest to bound the difference between the eigenvalue of the original problem at homotopy step $t = 1$ and the iterative approximation for a homotopy step $t \le 1$. Since the exact solution is unknown, this is only based on the computed inexact approximations of right and left eigenvectors and the approximated eigenvalue of $\mathcal{H}_\ell(t)$.

Using the a posteriori error bound for the discretisation error from [69] and Chapter 6, we obtain that for any $0 \le t \le 1$,

$$\begin{aligned} &|\!|\!| u(t) - u_\ell(t) |\!|\!|^2 + |\!|\!| u^*(t) - u_\ell^*(t) |\!|\!|^2 + |\lambda(t) - \lambda_\ell(t)| \\ &\qquad \lesssim \eta^2(\lambda_\ell(t), u_\ell(t), u_\ell^*(t)) := \sum_{T \in \mathcal{T}_\ell} \left(\eta^2(\lambda_\ell(t), u_\ell(t); T) + \eta^{*2}(\lambda_\ell(t), u_\ell^*(t); T) \right). \end{aligned}$$

Here and throughout this chapter,

$$\eta^2(\lambda_\ell(t), u_\ell(t); T) := h_T^2 \|\beta\cdot\nabla u_\ell(t) - \lambda_\ell(t) u_\ell(t)\|^2_{L^2(T)} + \sum_{E\in\mathcal{E}_\ell(T)} h_E \|[\nabla u_\ell(t)]\cdot n_E\|^2_{L^2(E)},$$
$$\eta^{*2}(\lambda_\ell(t), u^*_\ell(t); T) := h_T^2 \|-\beta\cdot\nabla \overline{u^*_\ell(t)} - \lambda_\ell(t)\overline{u^*_\ell(t)}\|^2_{L^2(T)} + \sum_{E\in\mathcal{E}_\ell(T)} h_E \|[\nabla \overline{u^*_\ell(t)}]\cdot n_E\|^2_{L^2(E)}.$$

Following [68, 91, 94], for the algebraic errors we have the estimate

$$\begin{aligned}&\|\!|u_\ell(t)-\tilde{u}_\ell(t)|\!\|^2 + \|\!|u^*_\ell(t) - \tilde{u}^*_\ell(t)|\!\|^2 + |\lambda_\ell(t) - \tilde{\lambda}_\ell(t)| \\ &\qquad \lesssim \mu^2(\tilde{\lambda}_\ell(t), \tilde{u}_\ell(t), \tilde{u}^*_\ell(t)) := \left(\frac{\|\mathbf{r}_\ell\|_{B_\ell^{-1}}}{\|\mathbf{u}_\ell\|_{B_\ell}}\right)^2 + \left(\frac{\|\mathbf{r}^*_\ell\|_{B_\ell^{-1}}}{\|\mathbf{u}^*_\ell\|_{B_\ell}}\right)^2,\end{aligned}$$

with the algebraic residuals

$$\mathbf{r}_\ell := (A_\ell + C_\ell)\mathbf{u}_\ell - \lambda_\ell B_\ell \mathbf{u}_\ell, \quad \mathbf{r}^*_\ell := \mathbf{u}^*_\ell(A_\ell + C_\ell) - \lambda^*_\ell \mathbf{u}^*_\ell B_\ell,$$

and $\|\mathbf{u}_\ell\|_M := \sqrt{\mathbf{u}^*_\ell M \mathbf{u}_\ell}$. The constants for the algebraic error estimators in general depend on the condition number of the considered eigenvalue and the gap in the spectrum, both of which are rather hard to assess in general. However, in the case that the eigenvalue of interest is well-conditioned and well-separated from the remaining part of the spectrum, as considered here, the algebraic residuals present a very good measure for the error in the algebraic solver.

Lemma 7.5.1. *Suppose that $|\lambda_\ell(t) - \tilde{\lambda}_\ell(t)| < 1$. Then, for a fixed $0 \le t \le 1$, the perturbation of the a posteriori error estimator for the discretisation error satisfies*

$$|\eta(\lambda_\ell(t), u_\ell(t), u^*_\ell(t)) - \eta(\tilde{\lambda}_\ell(t), \tilde{u}_\ell(t), \tilde{u}^*_\ell(t))|^2 \lesssim \mu^2(\tilde{\lambda}_\ell(t), \tilde{u}_\ell(t), \tilde{u}^*_\ell(t)).$$

Proof. The triangle inequality leads to

$$\begin{aligned}&|\eta(\lambda_\ell(t), u_\ell(t), u^*_\ell(t)) - \eta(\tilde{\lambda}_\ell(t), \tilde{u}_\ell(t), \tilde{u}^*_\ell(t))|^2 \\ &\quad\le \sum_{T\in\mathcal{T}_\ell} h_T^2 \|\beta\cdot\nabla(u_\ell(t) - \tilde{u}_\ell(t)) - \lambda_\ell(t) u_\ell(t) + \tilde{\lambda}_\ell(t)\tilde{u}_\ell(t)\|^2_{L^2(T)} \\ &\qquad + \sum_{E\in\mathcal{E}_\ell} h_E \|[\nabla(u_\ell(t) - \tilde{u}_\ell(t))]\cdot n_E\|^2_{L^2(E)} \\ &\qquad + \sum_{T\in\mathcal{T}_\ell} h_T^2 \|-\beta\cdot\nabla(\overline{u^*_\ell(t)} - \overline{\tilde{u}^*_\ell(t)}) - \lambda_\ell(t)\overline{u^*_\ell(t)} + \tilde{\lambda}_\ell(t)\overline{\tilde{u}^*_\ell(t)}\|^2_{L^2(T)} \\ &\qquad + \sum_{E\in\mathcal{E}_\ell} h_E \|[\nabla(\overline{u^*_\ell(t)} - \overline{\tilde{u}^*_\ell(t)})]\cdot n_E\|^2_{L^2(E)}.\end{aligned}$$

The local discrete inverse inequality [27] for $v_\ell \in V_\ell$ reads

$$h_T^2 \|D^2 v_\ell\|^2_{L^2(T)} \lesssim \|\nabla v_\ell\|^2_{L^2(T)}.$$

Let $\omega_E := T_+ \cup T_-$ denote the edge patch for two neighbouring triangles $T_\pm \in \mathcal{T}_\ell$ such that $E = T_+ \cap T_-$. This and the trace inequality [27] for $v \in V$

$$\|v\|^2_{L^2(E)} \lesssim h_E^{-1}\|v\|^2_{L^2(\omega_E)} + h_E\|\nabla v\|^2_{L^2(\omega_E)}$$

together with another application of the triangle inequality yield

$$\begin{aligned}
&|\eta(\lambda_\ell(t), u_\ell(t), u_\ell^*(t)) - \eta(\tilde\lambda_\ell(t), \tilde u_\ell(t), \tilde u_\ell^*(t))|^2 \\
&\quad\lesssim \sum_{T\in\mathcal{T}_\ell} h_T^2\|\lambda_\ell(t)u_\ell(t) - \tilde\lambda_\ell(t)\tilde u_\ell(t)\|^2_{L^2(T)} + h_T^2\|\lambda_\ell^*(t)u_\ell^*(t) - \tilde\lambda_\ell^*(t)\tilde u_\ell^*(t)\|^2_{L^2(T)} \\
&\qquad+ \sum_{T\in\mathcal{T}_\ell} h_T^2|\beta|_\infty\left(\|\nabla u_\ell(t) - \nabla\tilde u_\ell(t)\|^2_{L^2(T)} + \|\nabla u_\ell^*(t) - \nabla\tilde u_\ell^*(t)\|^2_{L^2(T)}\right) \\
&\qquad+ \sum_{E\in\mathcal{E}_\ell} \|\nabla u_\ell(t) - \nabla\tilde u_\ell(t)\|^2_{L^2(\omega_E)} + \|\nabla u_\ell^*(t) - \nabla\tilde u_\ell^*(t)\|^2_{L^2(\omega_E)}.
\end{aligned}$$

The finite overlap of the edge patches ω_E and the Poincaré inequality [27] lead to

$$\begin{aligned}
&|\eta(\lambda_\ell(t), u_\ell(t), u_\ell^*(t)) - \eta(\tilde\lambda_\ell(t), \tilde u_\ell(t), \tilde u_\ell^*(t))|^2 \\
&\quad\lesssim |\!|\!| u_\ell(t) - \tilde u_\ell(t)|\!|\!|^2 + |\!|\!| u_\ell^*(t) - \tilde u_\ell^*(t)|\!|\!|^2 \\
&\qquad+ \|\lambda_\ell(t)u_\ell(t) - \tilde\lambda_\ell(t)\tilde u_\ell(t)\|^2 + \|\lambda_\ell^*(t)u_\ell^*(t) - \tilde\lambda_\ell^*(t)\tilde u_\ell^*(t)\|^2 \\
&\quad\lesssim |\!|\!| u_\ell(t) - \tilde u_\ell(t)|\!|\!|^2 + |\!|\!| u_\ell^*(t) - \tilde u_\ell^*(t)|\!|\!|^2 + |\lambda_\ell(t) - \tilde\lambda_\ell(t)|^2.
\end{aligned}$$

The assumption $|\lambda_\ell(t) - \tilde\lambda_\ell(t)| < 1$ completes the proof. □

Lemma 7.5.2. *For the model problem (7.1), the difference between the iterative eigenvalue $\tilde\lambda_\ell(t)$ in the homotopy $\mathcal{H}_\ell(t)$ and the continuous eigenvalue $\lambda(1)$ of the original problem (7.1) can be estimated a posteriori via*

$$|\lambda(1) - \tilde\lambda_\ell(t)| \lesssim \nu(\tilde\lambda_\ell(t), \tilde u_\ell(t), \tilde u_\ell^*(t)) + \eta^2(\tilde\lambda_\ell(t), \tilde u_\ell(t), \tilde u_\ell^*(t)) + \mu^2(\tilde\lambda_\ell(t), \tilde u_\ell(t), \tilde u_\ell^*(t))$$

in terms of

$$\begin{aligned}
\nu(\tilde\lambda_\ell(t), \tilde u_\ell(t), \tilde u_\ell^*(t)) &:= (1-t)|\beta|_\infty\left(|\!|\!|\tilde u_\ell(t)|\!|\!| + |\!|\!|\tilde u_\ell^*(t)|\!|\!|\right) \\
&\quad+ (1-t)|\beta|_\infty\left(\eta(\tilde\lambda_\ell(t), \tilde u_\ell(t), \tilde u_\ell^*(t)) + \mu(\tilde\lambda_\ell(t), \tilde u_\ell(t), \tilde u_\ell^*(t))\right).
\end{aligned}$$

Proof. The triangle inequality gives

$$|\lambda(1) - \tilde\lambda_\ell(t)| \le |\lambda(1) - \lambda(t)| + |\lambda(t) - \lambda_\ell(t)| + |\lambda_\ell(t) - \tilde\lambda_\ell(t)|.$$

The first term is estimated via Lemma 7.4.1 as

$$\begin{aligned}
|\lambda(1) - \lambda(t)| &\lesssim (1-t)|\beta|_\infty\left(|\!|\!| u(t)|\!|\!| + |\!|\!| u^*(t)|\!|\!|\right). \\
&\le (1-t)|\beta|_\infty\left(|\!|\!|\tilde u_\ell(t)|\!|\!| + |\!|\!|\tilde u_\ell^*(t)|\!|\!| + |\!|\!| u(t) - u_\ell(t)|\!|\!|\right. \\
&\quad\left.+ |\!|\!| u_\ell(t) - \tilde u_\ell(t)|\!|\!| + |\!|\!| u^*(t) - u_\ell^*(t)|\!|\!| + |\!|\!| u_\ell^*(t) - \tilde u_\ell^*(t)|\!|\!|\right).
\end{aligned}$$

The a posteriori error bound and Lemma 7.5.1 lead to

$$\begin{aligned}\|\!|u(t) - u_\ell(t)|\!\| &\lesssim \eta(\tilde{\lambda}_\ell(t), \tilde{u}_\ell(t), \tilde{u}^*_\ell(t)) + \mu(\tilde{\lambda}_\ell(t), \tilde{u}_\ell(t), \tilde{u}^*_\ell(t)),\\ \|\!|u^*(t) - u^*_\ell(t)|\!\| &\lesssim \eta(\tilde{\lambda}_\ell(t), \tilde{u}_\ell(t), \tilde{u}^*_\ell(t)) + \mu(\tilde{\lambda}_\ell(t), \tilde{u}_\ell(t), \tilde{u}^*_\ell(t)).\end{aligned}$$

The algebraic error estimates

$$\begin{aligned}\|\!|u_\ell(t) - \tilde{u}_\ell(t)|\!\| &\lesssim \mu(\tilde{\lambda}_\ell(t), \tilde{u}_\ell(t), \tilde{u}^*_\ell(t)),\\ \|\!|u^*_\ell(t) - \tilde{u}^*_\ell(t)|\!\| &\lesssim \mu(\tilde{\lambda}_\ell(t), \tilde{u}_\ell(t), \tilde{u}^*_\ell(t))\end{aligned}$$

then complete the estimate of the first term. The second term is estimated with Lemma 7.5.1 as

$$|\lambda(t) - \lambda_\ell(t)| \lesssim \eta^2(\tilde{\lambda}_\ell(t), \tilde{u}_\ell(t), \tilde{u}^*_\ell(t)) + \mu^2(\tilde{\lambda}_\ell(t), \tilde{u}_\ell(t), \tilde{u}^*_\ell(t))$$

and the third term again with the algebraic error estimate

$$|\lambda_\ell(t) - \tilde{\lambda}_\ell(t)| \lesssim \mu^2(\tilde{\lambda}_\ell(t), \tilde{u}_\ell(t), \tilde{u}^*_\ell(t)).$$ □

7.6 Algorithms

This section combines the homotopy method with the adaptive finite element method and balances the homotopy error, the discretisation error and the approximation error. An important factor in the presented algorithms is the step-size control for the homotopy steps. A very small τ assures that the homotopy method follows the eigenpath of the desired eigenvalue and eigenvector on the expense of large computational costs. If τ is too large, then the method may not capture a crossing or joining of eigenvalues and jump to a different eigenpath. Therefore, the goal is to choose τ in an optimal way, such that it will minimize the computational effort and keep track of the eigenpath. To achieve this, adaptive step-size control techniques that are well established in the numerical solution of ordinary differential equations [66] may be employed, e.g., predictor-corrector procedures as they are commonly used [85]. However, the combination of the homotopy approach with the adaptive finite element method requires a modification of the adaptive step-size control techniques. Future work will also have to include methods that detect multiple eigenvalues, bifurcation in the paths, ill-conditioning, or the treatments of jumps in the eigenpaths.

At this stage, under the given assumptions, the following simple step-size control can be applied. If the number of required refinement steps for the homotopy parameters t_i and $t_i + \tau$ differs significantly, then the homotopy step for $t_i + \tau$ is rejected and $t_i + q\tau$ for some $0 < q < 1$ is used. If the number of refinements is small, then the step-size τ is preserved or even increased by choosing $\tau = q^{-1}\tau$. This simple idea allows to describe the dependence of the step-size not only on the solution but also on the mesh adaptation process.

In the following, to gain understanding about balancing of the different errors, we

`Estimate & Solve`

Input: $\mathcal{T}$, t, ρ, ω, $\tilde{\mathbf{u}}, \tilde{\mathbf{u}}^\star$

1: $[(A + C), B]$ = Create AEVP$(\mathcal{T}, \beta, t)$
2: $[\mu, \tilde{\mathbf{u}}, \tilde{\mathbf{u}}^\star]$ = Solve AEVP$(A + C,\ B,\ \rho,\ \tilde{\mathbf{u}},\ \tilde{\mathbf{u}}^\star)$
3: Compute η
4: $\rho = 2\eta$
5: **while** $\mu > \omega\eta$ **do**
6: $\quad \rho = \frac{\rho}{2}$
7: $\quad [\mu, \tilde{\mathbf{u}}, \tilde{\mathbf{u}}^\star]$ = Solve AEVP$(A + C,\ B,\ \rho,\ \tilde{\mathbf{u}},\ \tilde{\mathbf{u}}^\star)$
8: $\quad$ Compute η
9: **end while**
10: Compute ν

Output: η, ν, μ, λ, $\tilde{\mathbf{u}}, \tilde{\mathbf{u}}^\star$

Figure 7.1: Estimate & Solve

present three different adaptive algorithms for the homotopy driven eigenvalue problem. In Algorithm 1, a fixed step-size τ for the homotopy is considered in order to analyse the influence of the homotopy error ν on the mesh adaptation process. Algorithm 2 considers an adaptive step-size control for the homotopy, based on the number of refinements required to balance the discretisation error η and the desired accuracy ε. Algorithm 3 then finally combines the two concepts from Algorithms 1 and 2. In order to illustrate the differences between the three algorithms their main ideas are depicted in Figure 7.2.

In all three algorithms, ρ denotes the accuracy for the matrix eigensolver, $0 < \omega < 1$ the parameter in the relative accuracy condition for the algebraic approximation error, $0 < \delta < 1$ the parameter balancing the discretisation and homotopy error estimators and $0 < \theta < 1$ the marking parameter for the bulk marking strategy. In Algorithms 2 and 3, γ denotes the maximal number of refinement steps in each homotopy step and τ is the starting step-size for the homotopy, while in Algorithm 1 it is the fixed step-size.

The basic mesh adaptation method is given by the procedures `Estimate & Solve`, `Mark` and `Refine` as described in Section 7.2. In each refinement step, the generalized algebraic eigenvalue problem (AEVP) for $((A+tC), B)$ for a given mesh $\mathcal{T}$ and parameter t is solved and the corresponding error estimators η, ν and μ are computed in the function `Estimate & Solve` in Figure 7.1. The approximation of the eigenpair is considered to be accurate if the estimate for the complete algebraic approximation error μ, (both for the left and right eigenvectors), is smaller then the discretisation error η, up to some fixed constant ω (see line 5). This is achieved by a geometric decrease of the tolerance ρ for the iterative solver starting from $\rho = 2\eta$ (lines 4–6). The algebraic eigenvalue problem is solved using the Arpack [83] implementation of the implicitly restarted Arnoldi method for nonsymmetric eigenvalue problems. The size of the constructed Krylov subspaces is chosen to be as small as possible, see [91], and the approximations of the right and left eigenvectors from the previous iteration are taken as starting values for the new Arnoldi step. Note that here the final accuracy ε of the solution is not required at every step, only the relation between the discretisation error and the algebraic approximation error is used to stop the procedure.

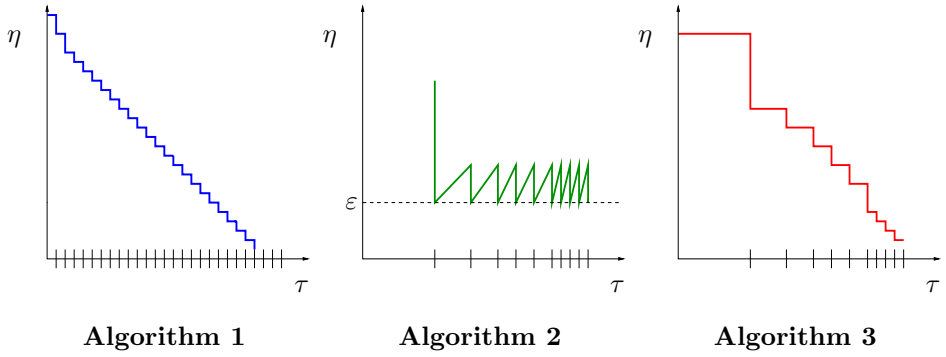

Figure 7.2: Schematic view of three homotopy-based Algorithms.

7.6.1 Algorithm 1

The first algorithm, displayed in Figure 7.3, introduces a homotopy method with fixed step-size τ. For the initial homotopy parameter $t_0 = 0$, the corresponding Laplace eigenvalue problem is solved on the initial mesh $\mathcal{T}_0(t_0)$, where the algebraic eigenvalue problem is solved up to tolerance $\rho(t_0)$, and the corresponding discretisation and homotopy error estimators $\eta_0(t_0)$, $\nu_0(t_0)$ are determined (line 3-6). This initial step is the same for all three algorithms.

In order to balance the discretisation error, the homotopy error, and the desired accuracy ε, the adaptive mesh refinement method is used (lines 9–15). The mesh adaptation process is repeated as long as the discretisation error dominates over the homotopy error multiplied by a balancing factor δ or is larger than the desired accuracy ε (line 9). Throughout the adaptive loop, sequences of meshes $\mathcal{T}_{\ell+j}(t_k)$, error estimators $\eta_j(t_k), \nu_j(t_k), \mu_j(t_k)$ and eigentriple approximations $(\tilde{\lambda}_j(t_k), \tilde{\mathbf{u}}_j(t_k), \tilde{\mathbf{u}}_j^*(t_k))$ are assembled. To avoid unnecessary computational work, the algebraic eigenvalue problem is solved only up to the accuracy $\rho(t_k)$, which depends on the discretisation error $\eta_j(t_k)$ [91] (see line 8 and the `Estimate & Solve` function for details). When the condition in line 9 does not hold, a new homotopy parameter $t_{k+1} = t_k + \tau$ is chosen and the new adaptation process starts with a previously obtained approximation taken as initial guess (line 13). Here $P_{j,j-1}$ denotes the prolongation matrix from the last coarse mesh $\mathcal{T}_{j-1}(t_k)$ to the refined mesh $\mathcal{T}_j(t_k)$ (line 12–13). Note that the final mesh derived for the former homotopy parameter is taken as the initial mesh for the new computations (line 3). After a fixed number of homotopy steps, t_k reaches its final value 1 and the algorithm returns the approximated eigenvalue and eigenvector.

The final number of refinement levels reached up to the parameter t_k is denoted by ℓ, while j is a refinement index for the current parameter t_k. This distinction is made to separate a sequence of meshes for a single homotopy step from the final sequence obtained for the whole algorithm. It has particular importance for the next two algorithms.

Although controlling the homotopy error is beneficial, however, an arbitrary fixed choice of the homotopy step-size, in general, will not work, especially for more complicated problems. In the non-symmetric case the eigenvalues move according to their

Algorithm 1

Input: $t_0 = 0, \tau, \mathcal{T}_0(t_0), \rho, \varepsilon, \omega, \delta,\ \tilde{\mathbf{u}}_0(t_0),\ \tilde{\mathbf{u}}_0^\star(t_0)$

1: $\ell = 1,\ k = 0$
2: **while** $t_k \leq 1$ **do**
3: $\quad \mathcal{T}_0(t_k) = \mathcal{T}_\ell(t_{k-1})$
4: $\quad \rho(t_k) = \rho$
5: $\quad [\tilde{\mathbf{u}}_0(t_k), \tilde{\mathbf{u}}_0^\star(t_k)] = [\tilde{\mathbf{u}}_\ell(t_{k-1}), \tilde{\mathbf{u}}_\ell^\star(t_{k-1})]$
6: $\quad [\eta_0(t_k), \nu_0(t_k), \tilde{\mathbf{u}}_0(t_k), \tilde{\mathbf{u}}_0^\star(t_k)] =$ `Estimate & Solve`$(\mathcal{T}_0(t_k), \rho(t_k), \omega, \tilde{\mathbf{u}}_0(t_k), \tilde{\mathbf{u}}_0^\star(t_k))$
7: $\quad j = 0$
8: $\quad \rho(t_k) = \eta_\ell(t_k)$
9: $\quad$ **while** $\eta_j(t_k) > \max(\delta\nu_j(t), \varepsilon)$ **do**
10: $\quad\quad j = j + 1$
11: $\quad\quad \mathcal{M}_j(t_k) =$ `Mark`$(\eta_j(t_k), \theta)$
12: $\quad\quad \mathcal{T}_j(t_k) =$ `Refine`$(\mathcal{T}_{j-1}(t_k), \mathcal{M}_j(t_k))$
13: $\quad\quad [\tilde{\mathbf{u}}_j(t_k), \tilde{\mathbf{u}}_j^\star(t_k)] = [P_{j,j-1}\tilde{\mathbf{u}}_{j-1}(t_k), P_{j,j-1}\tilde{\mathbf{u}}_{j-1}^\star(t_k)]$
14: $\quad\quad [\eta_j(t_k), \nu_j(t_k), \tilde{\mathbf{u}}_j(t_k), \tilde{\mathbf{u}}_j^\star(t_k)] =$ `Estimate & Solve`$(\mathcal{T}_j(t_k), \rho(t_k), \omega, \tilde{\mathbf{u}}_j(t_k), \tilde{\mathbf{u}}_j^\star(t_k))$
15: $\quad$ **end while**
16: $\quad \ell = \ell + j$
17: $\quad t_{k+1} = t_k + \tau,\ k = k + 1$
18: **end while**

Output: $\tilde{\lambda}(1), \tilde{\mathbf{u}}(1), \tilde{\mathbf{u}}^\star(1)$

Figure 7.3: Algorithm 1

condition number [99]. Ill-conditioned eigenvalues may move very fast as a function of t. The lack of an analogue of the min-max theorem [61] for non-symmetric problems makes the localization of an eigenvalue very hard. In particular, it may be difficult to guarantee fast convergence of the iterative eigensolver to the eigenvalue of interest for the next homotopy parameter $t_k + \tau$ even with the correct starting eigenvalue for a certain parameter t_k if the step-size τ is chosen too large. On the other hand, choosing τ very small leads to a large number of homotopy steps, and since for each step the whole adaptive mesh refinement loop has to be performed, this may lead to large computational effort.

7.6.2 Algorithm 2

In Algorithm 2, displayed in Figure 7.4, an adaptive step-size control for the homotopy is introduced. Starting with an initial step-size τ, the first approximation is computed to assure that the discretisation error $\eta_j(t_k)$ is smaller than the fixed, desired accuracy ε (line 9). No dependence on the homotopy error is considered here. Additionally, for each homotopy parameter only a fixed number of refinement steps γ inside the adaptive loop is allowed (line 10). If the adaptive loop needs more refinement steps than γ, then the eigenvalue problems for parameters t_k and $t_k + \tau$ differ too much and the step-size τ should be decreased to ensure good approximations in the eigenvalue continuation. In that case, the algorithm rejects the current homotopy step (lines 11–13), sets up a new step-size $\tau = q\tau$ (line 12), for some $0 < q < 1$, and starts the adaptation loop for the

Algorithm 2

Input: $t_0 = 0, \tau, \beta, \mathcal{T}_0(t_0), \rho, \varepsilon, \omega, \gamma, \tilde{\mathbf{u}}_0(t_0), \tilde{\mathbf{u}}_0^\star(t_0)$

1: $\ell = 1,\ k = 0$
2: **while** $t_k < 1$ **do**
3: $\quad \mathcal{T}_0(t_k) = \mathcal{T}_{\ell-1}(t_{k-1})$
4: $\quad \rho(t_k) = \rho$
5: $\quad [\tilde{\mathbf{u}}_0(t_k), \tilde{\mathbf{u}}_0^\star(t_k)] = [\tilde{\mathbf{u}}_{\ell-1}(t_{k-1}), \tilde{\mathbf{u}}_{\ell-1}^\star(t_{k-1})]$
6: $\quad [\eta_0(t_k), \nu_0(t_k), \tilde{\mathbf{u}}_0(t_k), \tilde{\mathbf{u}}_0^\star(t_k)] =$ `Estimate & Solve`$(\mathcal{T}_0(t_k), \rho(t_k), \omega, \tilde{\mathbf{u}}_0(t_k), \tilde{\mathbf{u}}_0^\star(t_k))$
7: $\quad \rho(t_k) = \eta_\ell(t_k)$
8: $\quad j = 0$
9: $\quad$ **while** $\eta_j(t_k) > \varepsilon$ **do**
10: $\quad\quad$ **if** $j > \gamma$ **then**
11: $\quad\quad\quad k = k - 1$
12: $\quad\quad\quad \tau = q\tau$
13: $\quad\quad\quad j = 0$
14: $\quad\quad\quad$ **break**
15: $\quad\quad$ **end if**
16: $\quad\quad j = j + 1$
17: $\quad\quad \mathcal{M}_j(t_k) =$ `Mark`$(\eta_j(t_k), \theta)$
18: $\quad\quad \mathcal{T}_j(t_k) =$ `Refine`$(\mathcal{T}_{j-1}(t_k), \mathcal{M}_j(t_k))$
19: $\quad\quad [\tilde{\mathbf{u}}_j(t_k), \tilde{\mathbf{u}}_j^\star(t_k)] = [P_{j,j-1}\tilde{\mathbf{u}}_{j-1}(t_k), P_{j,j-1}\tilde{\mathbf{u}}_{j-1}^\star(t_k)]$
20: $\quad\quad [\eta_j(t_k), \nu_j(t_k), \tilde{\mathbf{u}}_j(t_k), \tilde{\mathbf{u}}_j^\star(t_k)] =$ `Estimate & Solve`$(\mathcal{T}_j(t_k), \rho(t_k), \omega, \tilde{\mathbf{u}}_j(t_k), \tilde{\mathbf{u}}_j^\star(t_k))$
21: $\quad$ **end while**
22: $\quad \ell = \ell + j$
23: $\quad$ **if** $j < \gamma$ **then**
24: $\quad\quad \tau = q^{-1}\tau$
25: $\quad$ **end if**
26: $\quad t_{k+1} = \min(t_k + \tau, 1),\ k = k + 1$
27: **end while**

Output: $\tilde{\lambda}_\ell(1), \tilde{\mathbf{u}}_\ell(1), \tilde{\mathbf{u}}^\star(1)$

Figure 7.4: Algorithm 2

new homotopy parameter $t_k + \tau$. If the number of refinements is smaller than γ, then the algorithm attempts to increase the step-size to $q^{-1}\tau$ (line 24). Otherwise τ is preserved in the next homotopy step. At this point, the previously introduced distinction between global and local refinement indices ℓ and j is used to carry out the rejection step, while keeping the right mesh hierarchy. Meshes obtained for the rejected homotopy parameter will not be considered in the final sequence of meshes.

Note that the initial mesh for the new homotopy parameter is taken as the last but one mesh obtained for the previous homotopy step (line 3). If the step-sizes were chosen optimally and the consecutive problems do not differ too much, then the previous mesh is a good starting mesh for the next step. In this way the continuation of meshes is guaranteed. At the beginning it is reasonable to allow τ to be large and let the algorithm adapt the step-size by itself. However, if the total error is dominated by the homotopy error $\nu_\ell(t_k)$, driving the discretisation error $\eta_\ell(t_k)$ in each homotopy step below ε may lead to large computational effort. Currently, no analysis of the optimal choice of γ is known, that will lead to the minimal number of refinement steps.

Algorithm 3

Input: $t_0 = 0, \tau, q, \mathcal{T}_0(t_0), \varepsilon, \omega, \delta,\ \gamma,\ \tilde{\mathbf{u}}_0(t_0),\ \tilde{\mathbf{u}}_0^\star(t_0)$

$\ell = 1, k = 0$
while $t_k \leq 1$ & $t_{k-1} < 1$ **do**
  $\mathcal{T}_0(t_k) = \mathcal{T}_{\ell-1}(t_{k-1})$
  $\rho(t_k) = \rho$
  $[\tilde{\mathbf{u}}_0(t_k), \tilde{\mathbf{u}}_0^\star(t_k)] = [\tilde{\mathbf{u}}_{\ell-1}(t_{k-1}), \tilde{\mathbf{u}}_{\ell-1}^\star(t_{k-1})]$
  $[\eta_0(t_k), \nu_0(t_k), \tilde{\mathbf{u}}_0(t_k), \tilde{\mathbf{u}}_0^\star(t_k)] =$ `Estimate & Solve`$(\mathcal{T}_0(t_k), \rho(t_k), \omega, \tilde{\mathbf{u}}_0(t_k), \tilde{\mathbf{u}}_0^\star(t_k))$
  $\rho(t_k) = \eta_\ell(t_k)$
  $j = 0$
  while $\eta_j(t_k) > \max(\delta\nu_j(t_k), \varepsilon)$ **do**
    if $j > \gamma$ **then**
      $k = k - 1$
      $\tau = q\tau$
      $j = 0$
      break
    end if
    $j = j + 1$
    $\mathcal{M}_j(t_k) =$ `Mark`$(\eta_j(t_k), \theta)$
    $\mathcal{T}_j(t_k) =$ `Refine`$(\mathcal{T}_{j-1}(t_k), \mathcal{M}_j(t_k))$
    $[\tilde{\mathbf{u}}_j(t_k), \tilde{\mathbf{u}}_j^\star(t_k)] = [P_{j,j-1}\tilde{\mathbf{u}}_{j-1}(t_k), P_{j,j-1}\tilde{\mathbf{u}}_{j-1}^\star(t_k)]$
    $[\eta_j(t_k), \nu_j(t_k), \tilde{\mathbf{u}}_j(t_k), \tilde{\mathbf{u}}_j^\star(t_k)] =$ `Estimate & Solve`$(\mathcal{T}_j(t_k), \rho(t_k), \omega, \tilde{\mathbf{u}}_j(t_k), \tilde{\mathbf{u}}_j^\star(t_k))$
  end while
  $\ell = \ell + j$
  if $j < \gamma$ **then**
    $\tau = q^{-1}\tau$
  end if
  $t_{k+1} = \min(t_k + \tau, 1), k = k + 1$
end while

Output: $\tilde{\lambda}_\ell(1), \tilde{\mathbf{u}}_\ell(1), \tilde{\mathbf{u}}^\star(1)$

Figure 7.5: Algorithm 3

7.6.3 Algorithm 3

The third algorithm, displayed in Figure 7.5, combines both ideas of controlling the homotopy error and using adaptive step-size control. In this way the homotopy method accepts only the approximations which are of a desired accuracy and whose computational cost is reasonable. Simultaneously adaptation in space, in the homotopy and for the iterative solver is applied. During the mesh adaptation the discretisation error $\eta_j(t_k)$ is adapted to be smaller than the homotopy error $\nu_j(t_k)$ as in Algorithm 1. Again the approximation error $\mu_j(t_k)$ is adjusted by the `Estimate & Solve` function, to avoid computing a solution that is too accurate in comparison to the discretisation error $\eta_j(t_k)$. The adaptation of the homotopy parameter t is based on the maximal number of refinement levels γ as in Algorithm 2.

7.7 Numerical Experiments

This section presents some numerical results obtained with the three adaptive homotopy Algorithms 1–3 presented in Section 7.6. As a model problem we consider

$$-\Delta u + \beta \cdot \nabla u = \lambda u \quad \text{in} \quad \Omega \qquad \text{and} \qquad u = 0 \quad \text{on} \quad \partial\Omega$$

with Ω being either the unit square or the L-shaped domain and λ being the eigenvalue with smallest real part, which is known to be simple and well-separated [52] for all $0 \leq t \leq 1$. Thus it will not bifurcate and the evolution of the eigenvalue follows an analytic path. In order to calculate the eigenvalue errors we computed some reference values obtained by Aitken extrapolation on uniform meshes [2].

In order to avoid unnecessary computational work in the algebraic eigensolver Arpack [83], in all experiments the number k of Arnoldi vectors equals 3 and the maximal number `MXITER` of Arnoldi restarts is set to 1 [83]. The experiments were run on a AMD Phenom II X6 2,8 GHz processor with 8GB RAM using the programming environment Matlab R2010a [90].

The homotopy starts with the simple symmetric eigenvalue problem with known smallest eigenvalue $\lambda(t_0) = 2\pi^2$ for the unit square and known approximation $\lambda(t_0) \approx 9.6397238440219$ [107] for the L-shaped domain.

To recall the motivation of the homotopy method, it is important to note that for general non-selfadjoint problems, there is no guarantee that we achieve convergence to an eigenvalue of interest if standard methods are used. Experiments show that with a small number of Arnoldi vectors (i.e., a low dimensional Krylov subspace,) and a random starting vector Arpack does not find any good approximation to an eigenvalue for $t = 1$ even for very fine meshes. Thus, stable adaptive mesh refinement is not possible with a low cost variation of the Arnoldi method in contrast to the situation for selfadjoint problems in [91].

On the other hand, the following numerical experiments show that, starting from the symmetric problem and following the eigenpath lead to accurate approximations of the desired eigenvalue of the original non-selfadjoint problem. In other words, we can view our algorithms as means to provide a starting vector for the non-selfadjoint problem which is sufficiently close to the eigenvector of interest. Therefore, most of the computational work is expected to occur in the last homotopy step $t = 1$ which is confirmed by the numerical experiments.

Note, however, that for large convection parameters β the eigenvalue problem is very ill-conditioned such that the homotopy step-size tends to zero and the Algorithms 2 and 3 fail to converge. In the following, for our experiments we restrict ourselves to some reasonable parameters β. In any case, it is necessary to use a lower bound for the step-size.

t	$\eta_\ell(t)$	$\nu_\ell(t)$	$\mu_\ell(t)$	error estimator
0.0	18.7972	267.9989	0.0025677	286.7986
0.1	21.9037	250.3131	0.0003188	272.2171
0.2	17.6390	224.2302	0.0042579	241.8735
0.3	14.7243	204.8199	0.0066615	219.5508
0.4	12.0933	185.7716	0.0054502	197.8704
0.5	10.1746	167.8197	0.0560768	178.0503
0.6	7.8788	142.9867	0.0189887	150.8845
0.7	11.0907	121.0055	0.0577501	132.1540
0.8	8.4339	85.4466	0.0206147	93.9012
0.9	3.4934	44.0072	0.0025632	47.5031
1.0	0.0854	0.0000	0.0008344	0.0862

Table 7.1: The discretisation $\eta_\ell(t)$, the homotopy $\nu_\ell(t)$, and the iteration $\mu_\ell(t)$ error estimator for all homotopy steps t in Algorithm 1 for Example 1.

t	$\tilde{\lambda}_\ell(t)$	$\frac{\lvert\lambda_\ell(1)-\tilde{\lambda}_\ell(t)\rvert}{\lvert\lambda_\ell(1)\rvert}$	#DOF	CPU time
0.0	20.31171	0.83037	65	0.04
0.1	21.19837	0.82296	65	0.05
0.2	23.76193	0.80155	114	0.09
0.3	28.68327	0.76045	222	0.13
0.4	35.57882	0.70286	436	0.17
0.5	44.58901	0.62762	838	0.24
0.6	55.71845	0.53467	1607	0.35
0.7	68.87482	0.42479	1607	0.41
0.8	83.83805	0.29983	3075	0.66
0.9	100.83461	0.15788	10370	1.86
1.0	119.74434	0.00004	587509	127.34

Table 7.2: The eigenvalue approximation $\tilde{\lambda}_\ell(t)$, relative eigenvalue error $\frac{\lvert\lambda_\ell(1)-\tilde{\lambda}_\ell(t)\rvert}{\lvert\lambda_\ell(1)\rvert}$, number of degrees of freedom (#DOF), and CPU time for all homotopy steps t in Algorithm 1 applied to Example 1.

t	$\eta_\ell(t)$	$\nu_\ell(t)$	$\mu_\ell(t)$	error estimator
0.00	0.0725	183.1140	0.0000000	183.1865
0.25	0.0649	156.7655	0.0000002	156.8303
0.50	0.0740	136.5043	0.0000012	136.5783
0.75	0.0640	88.4754	0.0000598	88.5395
1.00	0.0783	0.0000	0.0004680	0.0788

Table 7.3: The discretisation $\eta_\ell(t)$, the homotopy $\nu_\ell(t)$, and the iteration $\mu_\ell(t)$ error estimator for all homotopy steps t in Algorithm 2 applied to Example 1.

t	$\tilde{\lambda}_\ell(t)$	$\frac{\lvert\lambda_\ell(1)-\tilde{\lambda}_\ell(t)\rvert}{\lvert\lambda_\ell(1)\rvert}$	#DOF	CPU time
0.00	19.74139	0.83513	18420	2.62
0.25	25.98903	0.78295	48506	20.51
0.50	44.73837	0.62637	124817	40.28
0.75	75.98888	0.36538	366519	112.36
1.00	119.74216	0.00002	641569	278.09

Table 7.4: The eigenvalue approximation $\tilde{\lambda}_\ell(t)$, relative eigenvalue error $\frac{\lvert\lambda_\ell(1)-\tilde{\lambda}_\ell(t)\rvert}{\lvert\lambda_\ell(1)\rvert}$, number of degrees of freedom (#DOF), and CPU time for all homotopy steps t in Algorithm 2 applied to Example 1.

t	$\eta_\ell(t)$	$\nu_\ell(t)$	$\mu_\ell(t)$	error estimator
0.0000	18.7972	267.9987	0.0025668	286.7984
0.2500	21.9560	224.1103	0.0070254	246.0733
0.5000	12.7398	173.0761	0.1539409	185.9698
0.7500	6.2305	99.7848	0.0008341	106.0161
0.8750	5.1172	54.7893	0.0003906	59.9069
0.9375	1.8715	27.6650	0.0001211	29.5367
0.9688	1.1430	14.0956	0.0271601	15.2658
0.9844	0.6630	7.0425	0.0141278	7.7196
0.9922	0.2189	3.4744	0.0006248	3.6940
1.0000	0.0745	0.0000	0.0020618	0.0765

Table 7.5: The discretisation $\eta_\ell(t)$, the homotopy $\nu_\ell(t)$, and the iteration $\mu_\ell(t)$ error estimator for all homotopy steps t concerning Algorithm 3 applied to Example 1.

t	$\tilde{\lambda}_\ell(t)$	$\frac{\lvert\lambda_\ell(1)-\tilde{\lambda}_\ell(t)\rvert}{\lvert\lambda_\ell(1)\rvert}$	#DOF	CPU time
0.0000	20.31171	0.83037	65	0.04
0.2500	25.86284	0.78401	112	0.25
0.5000	44.52525	0.62815	661	0.45
0.7500	75.97150	0.36553	3613	0.88
0.8750	96.37374	0.19514	6538	5.20
0.9375	107.66847	0.10081	21936	22.60
0.9688	113.63394	0.05099	40027	53.26
0.9844	116.67842	0.02556	71610	194.81
0.9922	118.19399	0.01290	226196	358.30
1.0000	119.76367	0.00020	685571	587.75

Table 7.6: The eigenvalue approximation $\tilde{\lambda}_\ell(t)$, the relative error $\frac{\lvert\lambda_\ell(1)-\tilde{\lambda}_\ell(t)\rvert}{\lvert\lambda_\ell(1)\rvert}$, the number of degrees of freedom (#DOF), and the CPU time for all homotopy steps t in Algorithm 3 for Example 1.

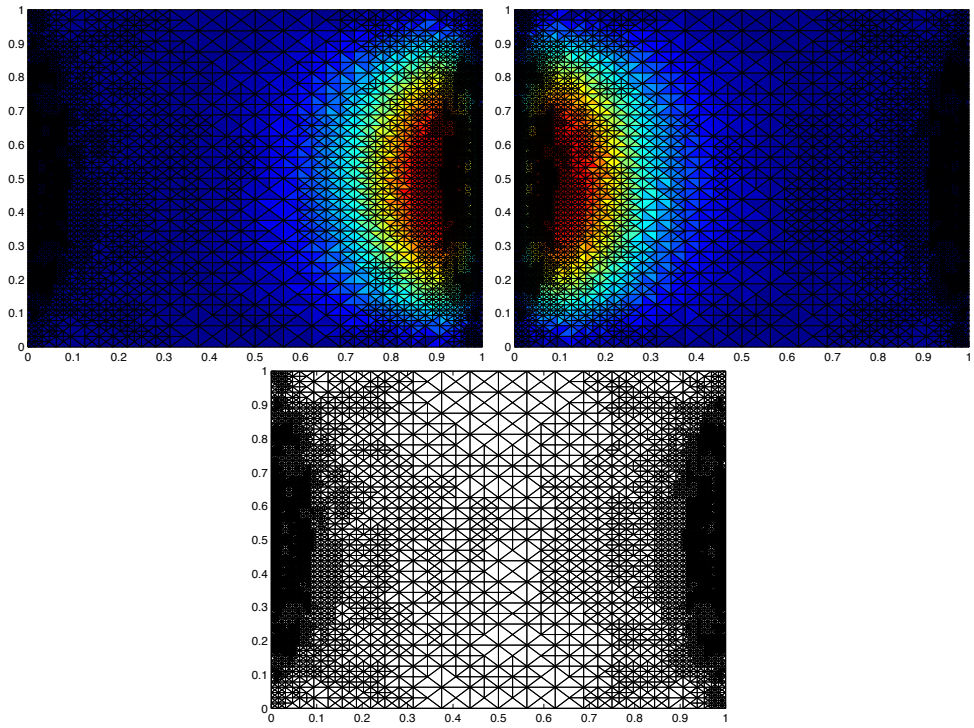

Figure 7.6: Primal (top left) and dual (top right) eigenfunction approximations for the final mesh (bottom) with 6663 nodes for Algorithm 3 applied to Example 1 with $\varepsilon = 10$.

7.7.1 Example 1

For this example let Ω be the (convex) unit square $\Omega = (0,1) \times (0,1)$. We choose the convection parameter $\beta = (20,0)^T$, the starting point of the homotopy $t_0 = 0$, the marking parameter $\theta = 0.3$, the balancing parameter of the discretisation and approximation error estimators $\omega = 0.1$, the step-size update parameter $q = 1/2$, the number of refinement steps $\gamma = 2$, the overall accuracy $\varepsilon = 10^{-1}$, the initial tolerance for the iterative solver $\rho = 1$ and the balancing parameter of the homotopy and discretisation error estimators $\delta = 0.1$. A reference value for the eigenvalue with the smallest real part is given by

$$\lambda \approx 119.7392.$$

In general, one can observe that all three algorithms lead to a finite sequence of homotopy steps and to an adequate approximation of the eigenvalue of interest at the last step $t = 1$. Notice that for all algorithms, more or less, most of the computational work is done at the last step and therefore for the final problem. This can be seen in Tables 7.2, 7.4 and 7.6 when comparing the CPU time after the last step to the previous one. Note that here we only present the data for the best approximation of each homotopy step and not those for the intermediate approximations.

In Algorithm 1 the fixed homotopy step-size $\tau = 0.1$ is chosen. Table 7.1 and 7.2

for Algorithm 1 show that a small homotopy step-size leads to a sequence where the second last homotopy step $t = 0.9$ does involve a small discrete problem, i.e., #DOF = 10370. Therefore, most of the refinement is done only in the last homotopy step $t = 1$, when the final accuracy is reached. Thus, the computational overhead introduced by the homotopy is minor for the right choice of homotopy step-size τ. Since the best choice for τ is not known, it is necessary, and in practice reasonable, to introduce some extra computational overhead by using adaptive step-size control. One may notice that the value obtained in the second last homotopy step has a large relative error and only the final approximation is good. This effect leads to a non-linear convergence rate and results in larger eigenvalue errors for $t < 1$ and accurate values only for $t = 1$.

Algorithm 2 uses an adaptive homotopy step-size control. As initial step-size $\tau = 1$ is chosen. Tables 7.3 and 7.4 show that the first homotopy step is rejected and a smaller step-size τ is taken. In this example Algorithm 2 chooses fewer homotopy steps than the other two algorithms. Due to the fixed control of the discretisation error by ε, the number of degrees of freedom (DOFs) is already high for the simple symmetric problem. This means that for $t < 1$ the error with respect to the DOFs is much larger than for the other algorithms. On the other hand, for the last step $t = 1$ the result is very accurate.

To overcome the drawback of a fixed step-size in Algorithm 1 and a fixed discretisation error control in Algorithm 2, both techniques are combined in Algorithm 3. In Tables 7.5 and 7.6 we observe that the homotopy step-size is decreased very much towards the end of the homotopy process. This effect is due to the fact, that the algorithm increases the number of DOF strongly only for t close to 1. This observation can be interpreted as that the algorithm computes a sufficiently accurate initial approximation to an eigenvector for $t = 1$. Note that most of the computational costs arise for t close to 1 during the last three homotopy steps. Since Algorithm 3 is a combination of the other two algorithms the error for approximations with homotopy steps $t < 1$ is much smaller than for Algorithm 2 but similar to that of Algorithm 1. In contrast to Algorithm 1 the homotopy step-size is adapted, fewer homotopy steps are needed and the steps are more concentrated towards $t = 1$.

For more complicated problems, going beyond this simple model example, it is expected that the adaptive step-size control will lead to faster computation than the method with a fixed step-size. The homotopy procedure in Algorithm 1 only introduces little computational overhead, with the possible drawback of a small (unknown) fixed step-size while Algorithm 2 does adapt the step-size automatically, but for the cost of larger computational overhead. In fact, Table 7.4 shows that the overhead is less than 1/2 of the overall CPU time, which is worthwhile. On the other hand Algorithm 3 needs even more computational time but combines the two advantages of Algorithm 1 and 2. Obviously, Algorithm 2 and 3 need more time than Algorithm 1, since they reject some steps during their automatic step-size control. Nevertheless, this moderate increase of the computational cost seems to be reasonable for more difficult situations, where no convergence to the desired eigenvalues can be guaranteed without path following techniques.

The final approximate primal and dual eigenfunctions for Algorithm 3, together with the corresponding meshes, are depicted in Figure 7.6. The final meshes for the other

algorithms look quite similar. Notice that, due to the adaptive refinement procedure for triangles, the symmetry of the mesh cannot strictly be preserved. In this example, primal and dual solutions of the problem have almost independent supports living on the opposite boundaries of the domain due to the strong convection in x direction. Therefore, all final meshes look quite "symmetric". Note that the meshes are more refined towards the strong boundary layers of both the primal and the dual solution. This observation shows that, in general, it is necessary to adapt the mesh for both the primal and dual eigenfunctions.

7.7.2 Example 2

As in the first example, let Ω be the (convex) unit square $\Omega = (0,1) \times (0,1)$. We choose the parameters the same as in Example 1, except that the homotopy step-size update parameter q has been set to $1/3$ instead of $1/2$. Here we demonstrate how a different choice of q influences the homotopy process for algorithms 2 and 3. Figures 7.7 and 7.8 compare the results obtained for Examples 1 and 2. Comparing the results with those of Example 1 shows that the choice $q = 1/3$ leads to similar relative eigenvalue errors for $t < 1$ but smaller relative eigenvalue error for the final homotopy step $t = 1$. For Algorithm 2, the choice of $q = 1/3$ leads to 10 homotopy steps compared to 5 steps in Example 1. Although this is an increase by a factor of two, the overall computational costs increase only slightly. This can be explained by the fact that in each homotopy step there are fewer refinements and overall fewer rejections of homotopy steps than in Example 1. For Algorithm 3 the choice of $q = 1/3$ leads to one additional homotopy step and the computational costs moderately decrease.

7.7.3 Example 3

For this example let Ω be the (non-convex) L-shaped domain

$$\Omega = (-1,1) \times (-1,1) \backslash ([0,1] \times [-1,1]).$$

We choose the convection parameter $\beta = (10,0)^T$, the starting point of the homotopy $t_0 = 0$, the marking parameter $\theta = 0.3$, the balancing parameter of the discretisation and approximation error estimators $\omega = 0.1$, the step-size update parameter $q = 1/2$, the number of refinement steps $\gamma = 2$, the overall accuracy $\varepsilon = 10^{-1}$, the initial tolerance for the iterative solver $\rho = 1$ and the balancing parameter of the homotopy and discretisation error estimators $\delta = 0.1$. A reference value for the eigenvalue with smallest real part is given by

$$\lambda \approx 34.6397.$$

Again for Algorithm 1 a fixed step-size $\tau = 0.1$ is chosen. The results look similar to those of the Examples 1 and 2. The eigenvalue errors for the homotopy steps $t < 1$ are rather large and only the values for $t = 1$ are accurate. Also most of the CPU time is used on the last level.

Algorithm 2 starts with a step-size $\tau = 1$ which is reduced by the adaptive procedure

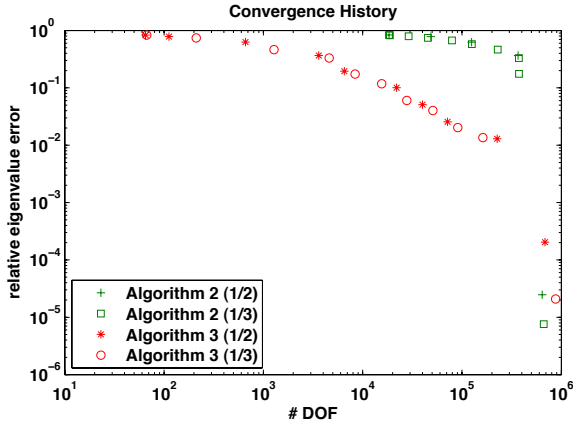

Figure 7.7: Comparison of the convergence history of Algorithms 2, and 3 with respect to #DOF for Example 1 and Example 2.

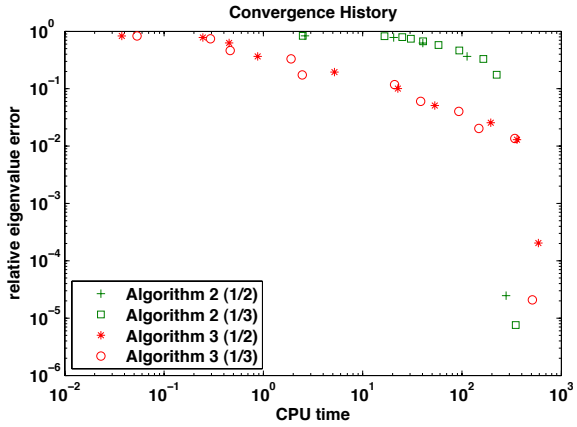

Figure 7.8: Comparison of the convergence history of Algorithms 2, and 3 with respect to CPU time for Example 1 and Example 2.

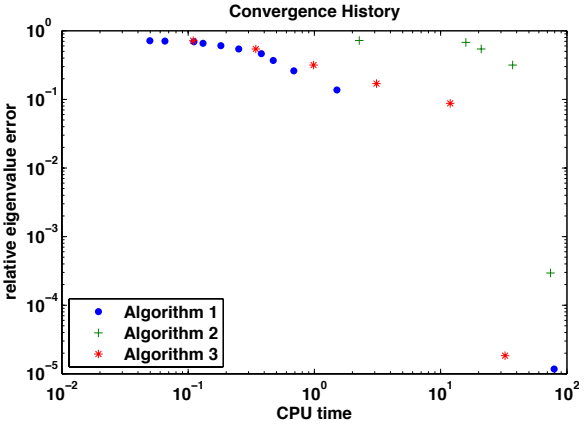

Figure 7.9: Convergence history of Algorithms 1, 2, and 3 with respect to CPU time for Example 3.

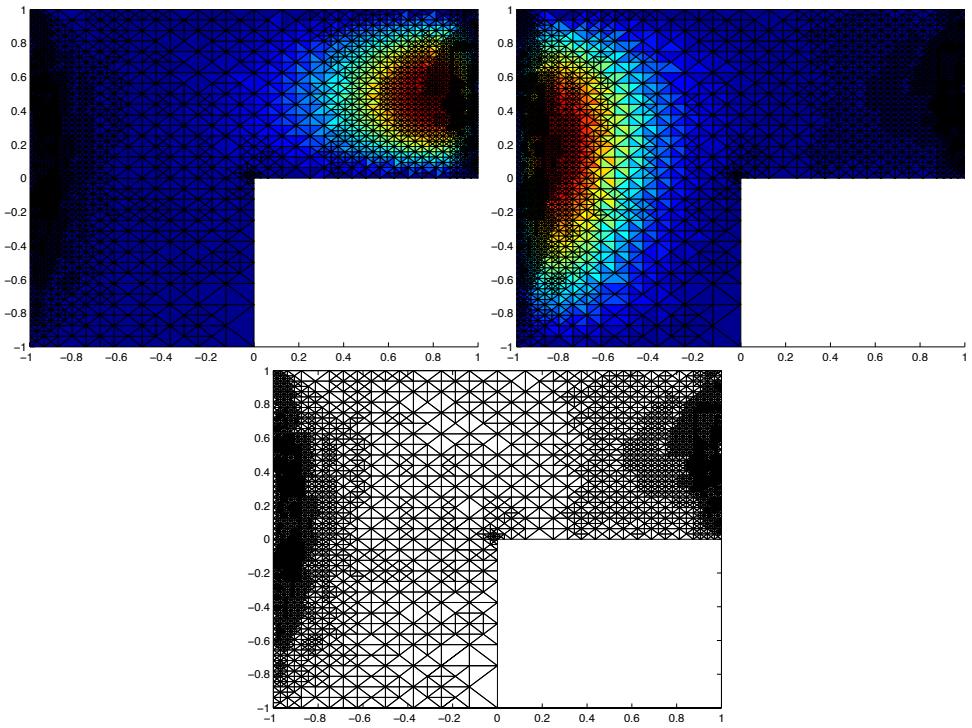

Figure 7.10: Primal (top left) and dual (top right) eigenfunction approximations for the final mesh (bottom) with 3745 nodes for Algorithm 3 for Example 3 with $\varepsilon = 3$.

to $\tau = 0.25$ and afterwards not changed any more. Therefore, Algorithm 2 needs in total only 5 homotopy steps and not 11 as Algorithm 1. Since the discretisation error estimator at each homotopy step is forced to be smaller than the fixed tolerance ε, the number of degrees of freedom is large already for the first homotopy step. Here, in contrast to the previous examples, the approximation for the last step $t = 1$ is less accurate than for the other two algorithms.

The results for Algorithm 3 show the nature of both other algorithms. The step-size is chosen adaptively without loss of accuracy compared to the eigenvalue error of Algorithm 1. Moreover, it needs only one more homotopy step than Algorithm 2 and the meshes for the step $t < 1$ are much coarser than those of Algorithm 2. Again most of the time is spent to compute the final approximation on the last and second last level. It is also interesting to see that the second last approximation of the eigenvalue obtained in Algorithm 3 is much better than the corresponding one for Algorithm 2, despite using four times fewer DOFs.

It is remarkable that for this more complicated example the fastest algorithm, with respect to computational time, is Algorithm 3, see Figure 7.9. Therefore, this experiment strongly underlines the advantages of adaptivity in all three directions, namely the homotopy, the discretisation and the approximation.

Figure 7.10 shows adaptively refined meshes for Algorithm 3 in Example 3. Note that

```
|-- algoritm1.m (main script)
|-- algoritm2.m (main script)
|-- algoritm3.m (main script)
|-- createLinSystem.m
|-- estimate.m
|-- Mesh.m
|-- pdeSolve.m
|-- solve_eigs.m
`-- Geometries
    `-- ... (several geometric data)
```

Table 7.7: The software directory of Chapter 7.

due to the re-entrant corner the meshes show stronger refinement towards the origin. Since the solution for the selfadjoint problem is known to have a strong singularity at the origin, it is not clear whether this extra refinement results from the homotopy process or from the refinement on the last homotopy step $t = 1$. Indeed, looking at the approximated final primal and dual solutions does not suggest extra refinement, since they have function values close to zero at the origin, but this may be misleading. The fact that the convection acts only along the x axis is clearly visible in the shape of the discrete primal and dual solutions. Note that the primal and dual solution are not mirror images as in the previous examples, but again show strong boundary layers on opposite boundary edges.

7.8 Software Implementation

The software directory with the software files used for the numerical experiments of this chapter is listed in Table 7.7. The files `algoritm1.m`, `algoritm2.m`, `algoritm3.m`, `pdeSolve.m` and `solve_eigs.m` where programmed in cooperation with A. Miedlar.

The files `algoritm1.m`, `algoritm2.m`, and `algoritm3.m` implement Algorithm 1, Algorithm 2 and Algorithm 3 as described in Section 7.6.

`createLinSystem.m` assemblies the global matrices A_ℓ, B_ℓ and C_ℓ for the linear finite element. A minimalistic implementation is displayed in the following.

```
function [A,C,B] = createLinSystem(mesh,beta)
  % Create the diffusion matrix A
  area4e = mesh.area4e;
  [z1,z2] = mesh.transformation;
  a = 2*area4e.*sum(z2.^2,2);
  b = -2*area4e.*sum(z1.*z2,2);
  c = 2*area4e.*sum(z1.^2,2);
  Alocal = reshape([a+2*b+c,-a-b,-b-c,-a-b,a,b,-b-c,b,c]'/2, ...
                   [3 3 mesh.nrElems]);
  n4eT = mesh.n4e';
  I = [n4eT;n4eT;n4eT];
```

```
    J = [n4eT(:),n4eT(:),n4eT(:)]';
    A = sparse(I(:),J(:),Alocal(:));
    % Create the convection matrix C
    beta4e = beta(mesh.mid4e);
    a = 2*area4e.*sum(beta4e.*[z2(:,2),-z2(:,1)],2);
    b = 2*area4e.*sum(beta4e.*[-z1(:,2),z1(:,1)],2);
    Alocal = reshape([-a-b,-a-b,-a-b,a,a,a,b,b,b]'/6,[3 3 mesh.nrElems]);
    C = sparse(I(:),J(:),Alocal(:));
    % Create the mass matrix B
    a = area4e/6;
    b = area4e/12;
    Alocal = reshape([a,b,b,b,a,b,b,b,a]',[3 3 mesh.nrElems]);
    B = sparse(I(:),J(:),Alocal(:));
end
```

Line 3 gets the area $|T|$ and line 4 the transformation vectors for the coordinate transformation of the gradients with the three nodes n_1, n_2, n_3 of each triangle

$$z_1 := \frac{1}{2|T|}(n_2 - n_1) \qquad \text{and} \qquad z_2 := \frac{1}{2|T|}(n_3 - n_1).$$

Let $\tilde{T}$ be the reference triangle and $\tilde{\varphi}_1 := 1 - x - y, \tilde{\varphi}_2 := x, \tilde{\varphi}_3 := y$ be the reference nodal basis functions. The local diffusion matrix reads after coordinate transformation onto the reference triangle, $j, k = 1, 2, 3$,

$$a \left(\int_{\tilde{T}} \frac{\partial \tilde{\varphi}_j}{\partial x} \frac{\partial \tilde{\varphi}_k}{\partial x} \, dx \right)_{j,k} + b \left(\int_{\tilde{T}} \frac{\partial \tilde{\varphi}_j}{\partial x} \frac{\partial \tilde{\varphi}_k}{\partial y} \, dx + \int_{\tilde{T}} \frac{\partial \tilde{\varphi}_j}{\partial y} \frac{\partial \tilde{\varphi}_k}{\partial x} \, dx \right)_{j,k} + c \left(\int_{\tilde{T}} \frac{\partial \tilde{\varphi}_j}{\partial y} \frac{\partial \tilde{\varphi}_k}{\partial y} \, dx \right)_{j,k}$$

with

$$a = 2|T|(z_2 \cdot z_2), \qquad b = -2|T|(z_1 \cdot z_2) \qquad \text{and} \qquad c = 2|T|(z_1 \cdot z_1)$$

computed in lines 5-7. The remaining integrals can be computed once and for all on the reference triangle, which has been employed in line 8-9,

$$\left(\int_{\tilde{T}} \frac{\partial \tilde{\varphi}_j}{\partial x} \frac{\partial \tilde{\varphi}_k}{\partial x} \, dx \right)_{j,k} = \frac{1}{2} \begin{pmatrix} 1 & -1 & 0 \\ -1 & 1 & 0 \\ 0 & 0 & 0 \end{pmatrix},$$

$$\left(\int_{\tilde{T}} \frac{\partial \tilde{\varphi}_j}{\partial x} \frac{\partial \tilde{\varphi}_k}{\partial y} \, dx + \int_{\tilde{T}} \frac{\partial \tilde{\varphi}_j}{\partial y} \frac{\partial \tilde{\varphi}_k}{\partial x} \, dx \right)_{j,k} = \frac{1}{2} \begin{pmatrix} 2 & -1 & -1 \\ -1 & 0 & 1 \\ -1 & 1 & 0 \end{pmatrix},$$

$$\left(\int_{\tilde{T}} \frac{\partial \tilde{\varphi}_j}{\partial y} \frac{\partial \tilde{\varphi}_k}{\partial y} \, dx \right)_{j,k} = \frac{1}{2} \begin{pmatrix} 1 & 0 & -1 \\ 0 & 0 & 0 \\ -1 & 0 & 1 \end{pmatrix}.$$

The global assembly of the diffusion matrix A_ℓ is done in Lines 10-13.

The local convection matrix reads after coordinate transformation onto the reference

triangle, $j,k=1,2,3$,

$$a\left(\int_{\tilde{T}}\frac{\partial\tilde{\varphi}_j}{\partial x}\tilde{\varphi}_k\,dx\right)_{j,k}+b\left(\int_{\tilde{T}}\frac{\partial\tilde{\varphi}_j}{\partial y}\tilde{\varphi}_k\,dx\right)_{j,k}$$

with

$$a=2|T|\left(\beta\cdot\begin{pmatrix}z_2^y\\-z_2^x\end{pmatrix}\right)\qquad\text{and}\qquad b=2|T|\left(\beta\cdot\begin{pmatrix}-z_1^y\\z_1^x\end{pmatrix}\right)$$

computed in lines 16-17. The remaining integrals can be computed once and for all on the reference triangle, which has been employed in line 18,

$$\left(\int_{\tilde{T}}\frac{\partial\tilde{\varphi}_j}{\partial x}\tilde{\varphi}_k\,dx\right)_{j,k}=\frac{1}{2}\begin{pmatrix}-1/3&-1/3&-1/3\\1/3&1/3&1/3\\0&0&0\end{pmatrix},$$
$$\left(\int_{\tilde{T}}\frac{\partial\tilde{\varphi}_j}{\partial y}\tilde{\varphi}_k\,dx\right)_{j,k}=\frac{1}{2}\begin{pmatrix}-1/3&-1/3&-1/3\\0&0&0\\1/3&1/3&1/3\end{pmatrix}.$$

The global assembly of the convection matrix C_ℓ is done in Line 19.

Finally, lines 20-24 compute the global mass matrix B_ℓ with the local mass matrices, $j,k=1,2,3$

$$\left(\int_T\varphi_j\varphi_k\,dx\right)_{j,k}=\frac{|T|}{12}\begin{pmatrix}2&1&1\\1&2&1\\1&1&2\end{pmatrix}.$$

`estimate.m` implements the residual a posteriori error estimator $\eta^2(\lambda_\ell(t),u_\ell(t),u_\ell^*(t))$ as described in the following in more detail for the primal residual part of the estimator.

The computation of the primal edge jump

$$\|[\nabla u_\ell(t)]\cdot n_E\|^2_{L^2(E)}=h_E^2|[\nabla u_\ell(t)]\cdot n_E|^2.$$

is displayed below.

```
26 x4e = x(mesh.n4e);
   [z1,z2] = mesh.transformation;
   grad4e = [(z1(:,2)-z2(:,2)).*x4e(:,1)+z2(:,2).*x4e(:,2)-z1(:,2).*x4e(:,3),...
             (z2(:,1)-z1(:,1)).*x4e(:,1)-z2(:,1).*x4e(:,2)+z1(:,1).*x4e(:,3)];
30 normal4ed = mesh.normal4ed;
   grad4sT1 = grad4e(mesh.e4ed(:,1),:);
   grad4sT1(mesh.ed4Db,:) = 0;
   grad4sT2 = zeros(size(mesh.n4ed,1),2);
   indx = find(mesh.e4ed(:,2)>0);
35 grad4sT2(indx,:) = grad4e(mesh.e4ed(indx,2),:);
   jump = (grad4sT1(:,1)-grad4sT2(:,1)).*normal4ed(:,1)...
```

```
      +(grad4sT1(:,2)-grad4sT2(:,2)).*normal4ed(:,2);
jump(mesh.ed4Nb) = 0;
jump = abs(jump);
primaleta4s = jump.^2.*mesh.length4ed.^2;
```

The values of $u_\ell(t)$ at the nodes are extracted in line 26. Lines 27-29 evaluate the piecewise constant gradient. Lines 31-35 extract the values of the gradient for the two triangles T_+, T_- that share an edge E. The jump in normal direction $[\nabla u_\ell(t)] \cdot n_E$ is computed in lines 36-37. The final jump term is obtained in line 40.

The computation of the primal volume term

$$h_T^2 \|\beta \cdot \nabla u_\ell(t) - \lambda_\ell(t) u_\ell(t)\|^2_{L^2(T)}$$

is displayed below.

```
area4e = mesh.area4e;
x4e = lambda*x4e;
beta4e = beta(mesh.mid4e);
b = sum(beta4e.*grad4e,2);
eta4e = (area4e/3).*((b-x4e(:,1)/2-x4e(:,2)/2).^2 ...
                    +(b-x4e(:,2)/2-x4e(:,3)/2).^2 ...
                    +(b-x4e(:,3)/2-x4e(:,1)/2).^2);
primaleta4e = area4e.*eta4e;
```

Here, for the piecewise constant β, a quadrature rule for quadratic polynomials is used

$$\int_T (\beta \cdot \nabla u - \lambda u)^2 = \frac{|T|}{3} \sum_{j=1}^{3} \left(\beta \cdot \nabla u - \lambda u \left(\mathrm{mid}(E_j)\right)\right)^2 .$$

`pdeSolve.m` implements the `estimate & solve` algorithm of Figure 7.1 and the file `solve_eigs.m` solves the algebraic eigenvalue problem via two calls of `eigs`, one for the primal solution and one for the dual solution.

Bibliography

[1] M. Ainsworth and J.T. Oden. *A Posteriori Error Estimation in Finite Element Analysis*. Pure and Applied Mathematics. Wiley, New York, 2000.

[2] A.C. Aitken. On Bernoulli's numerical solution of algebraic equations. *Proceedings Royal Soc. Edinburgh*, 46:289–305, 1926.

[3] J. Alberty, C. Carstensen, and S.A. Funken. Remarks around 50 lines of Matlab: short finite element implementation. *Numer. Algorithms*, 20(2-3):117–137, 1999.

[4] A. Alonso, A. Dello Russo, C. Padra, and R. Rodríguez. A posteriori error estimates and a local refinement strategy for a finite element method to solve structural-acoustic vibration problems. *Adv. Comput. Math.*, 15(1-4):25–59, 2001.

[5] T. Apel. *Anisotropic Finite Elements: Local Estimates and Applications*. Advances in Numerical Mathematics. Teubner, Stuttgart, 1999.

[6] M.E. Argentati, A.V. Knyazev, C.C. Paige, and I. Panayotov. Bounds on changes in Ritz values for a perturbed invariant subspace of a Hermitian matrix. *SIAM J. Matrix Anal. Appl.*, 30(2):548–559, 2008.

[7] M.G. Armentano and R.G. Durán. Asymptotic lower bounds for eigenvalues by nonconforming finite element methods. *Electron. Trans. Numer. Anal.*, 17:93–101, 2004.

[8] D.N. Arnold, A. Mukherjee, and L. Pouly. Locally adapted tetrahedral meshes using bisection. *SIAM J. Sci. Comput.*, 22(2):431–448, 2000.

[9] I. Babuška and J.E. Osborn. Finite element-Galerkin approximation of the eigenvalues and eigenvectors of selfadjoint problems. *Math. Comp.*, 52(186):275–297, 1989.

[10] I. Babuška and J.E. Osborn. Eigenvalue problems. In *Handbook of Numerical Analysis, Vol. II*, pages 641–787. North-Holland, Amsterdam, 1991.

[11] Z. Bai, J. Demmel, J. Dongarra, A. Ruhe, and H. van der Vorst. *Templates for the Solution of Algebraic Eigenvalue Problem. A Practical Guide*. SIAM, Philadelphia, 2000.

[12] W. Bangerth and R. Rannacher. *Adaptive Finite Element Methods for Differential Equations*. Lectures in Mathematics ETH Zürich. Birkhäuser, Basel, 2003.

[13] R.E. Bank and R.K. Smith. A posteriori error estimates based on hierarchical bases. *SIAM J. Numer. Anal.*, 30(4):921–935, 1993.

[14] R. Becker and R. Rannacher. Weighted a posteriori error control in FE methods. In *ENUMATH 97*, pages 621–637. World Scientific, Singapore, 1998.

[15] R. Becker and R. Rannacher. An optimal control approach to a posteriori error estimation in finite element methods. *Acta Numer.*, 10:1–102, 2001.

[16] A. Bermúdez, R. G. Durán, R. Rodríguez, and J. Solomin. Finite element analysis of a quadratic eigenvalue problem arising in dissipative acoustics. *SIAM J. Numer. Anal.*, 38(1):267–291, 2000.

[17] T. Betcke and L.N. Trefethen. Reviving the method of particular solutions. *SIAM Rev.*, 47(3):469–491, 2005.

[18] K.Y. Billah and R. H. Scanlan. Resonance, Tacoma Narrows bridge failure, and undergraduate physics textbooks. *Am. J. Phys.*, 59(2):118, 1991.

[19] P. Binev, W. Dahmen, and R. DeVore. Adaptive finite element methods with convergence rates. *Numer. Math.*, 97(2):219–268, 2004.

[20] D. Boffi. Finite element approximation of eigenvalue problems. *Acta Numer.*, 19:1–120, 2010.

[21] D. Boffi, P. Fernandes, L. Gastaldi, and I. Perugia. Computational models of electromagnetic resonators: analysis of edge element approximation. *SIAM J. Numer. Anal.*, 36(4):1264–1290, 1999.

[22] M. Braack and A. Ern. A posteriori control of modeling errors and discretization errors. *Multiscale Model. Simul.*, 1(2):221–238, 2003.

[23] D. Braess. *Finite Elemente: Theorie, schnelle Löser und Anwendungen in der Elastizitätstheorie*. Springer, Berlin, third edition, 2003.

[24] S.C. Brenner. Convergence of nonconforming multigrid methods without full elliptic regularity. *Math. Comp.*, 68(225):25–53, 1999.

[25] S.C. Brenner. Convergence of the multigrid V-cycle algorithm for second-order boundary value problems without full elliptic regularity. *Math. Comp.*, 71(238):507–525, 2002.

[26] S.C. Brenner. Smoothers, mesh dependent norms, interpolation and multigrid. *Appl. Numer. Math.*, 43(1-2):45–56, 2002.

[27] S.C. Brenner and L.R. Scott. *The Mathematical Theory of Finite Element Methods*, volume 15 of *Texts in Applied Mathematics*. Springer, New York, third edition, 2008.

[28] F. Brezzi and M. Fortin. *Mixed and Hybrid Finite Element Methods*, volume 15 of *Springer Series in Computational Mathematics*. Springer, New York, 1991.

[29] C. Carstensen. All first-order averaging techniques for a posteriori finite element error control on unstructured grids are efficient and reliable. *Math. Comp.*, 73(247):1153–1165, 2004.

[30] C. Carstensen. Estimation of higher Sobolev norm from lower-order approximation. *SIAM J. Numer. Anal.*, 42(5):2136–2147, 2005.

[31] C. Carstensen, M. Eigel, C. Löbhard, and R.H.W. Hoppe. A review of unified a posteriori finite element error control. *Numer. Math. Theor. Meth. Appl.*, 5(4):509–558, 2012.

[32] C. Carstensen and D. Gallistl. Guaranteed lower eigenvalue bounds for the biharmonic equation. *Numer. Math.*, in print, 2013.

[33] C. Carstensen and J. Gedicke. An oscillation-free adaptive FEM for symmetric eigenvalue problems. *Numer. Math.*, 118(3):401–427, 2011.

[34] C. Carstensen and J. Gedicke. An adaptive finite element eigenvalue solver of asymptotic quasi-optimal computational complexity. *SIAM J. Numer. Anal.*, 50(3):1029–1057, 2012.

[35] C. Carstensen and J. Gedicke. Guaranteed lower bounds for eigenvalues. *Math. Comp.*, accepted, 2013.

[36] C. Carstensen, J. Gedicke, L. Kern, J. Neumann, H. Rabus, and M. Rozova. AFEM. Unpublished software manual, 2010.

[37] C. Carstensen, J. Gedicke, V. Mehrmann, and A. Miedlar. An adaptive homotopy approach for non-selfadjoint eigenvalue problems. *Numer. Math.*, 119(3):557–583, 2011.

[38] C. Carstensen, J. Gedicke, V. Mehrmann, and A. Miedlar. An adaptive finite element method with asymptotic saturation for eigenvalue problems. Submitted, 2012.

[39] C. Carstensen, J. Gedicke, and D. Rim. Explicit error estimates for Courant, Crouzeix-Raviart and Raviart-Thomas finite element methods. *J. Comput. Math.*, 30(4):337–353, 2012.

[40] C. Carstensen and C. Merdon. Computational survey on a posteriori error estimators for nonconforming finite element methods for the Poisson problem. *J. Comput. Appl. Math.*, 249:74–94, 2013.

[41] J.M. Cascon, C. Kreuzer, R.H. Nochetto, and K.G. Siebert. Quasi-optimal convergence rate for an adaptive finite element method. *SIAM J. Numer. Anal.*, 46(5):2524–2550, 2008.

[42] F. Chatelin. *Spectral Approximation of Linear Operators*. Academic Press, New York, 1983.

[43] K.A. Cliffe, E.J.C. Hall, and P. Houston. Adaptive discontinuous Galerkin methods for eigenvalue problems arising in incompressible fluid flows. *SIAM J. Sci. Comput.*, 31(6):4607–4632, 2010.

[44] W. Dahmen, T. Rohwedder, R. Schneider, and A. Zeiser. Adaptive eigenvalue computation: complexity estimates. *Numer. Math.*, 110(3):277–312, 2008.

[45] X. Dai, J. Xu, and A. Zhou. Convergence and optimal complexity of adaptive finite element eigenvalue computations. *Numer. Math.*, 110(3):313–355, 2008.

[46] E. Dari, R.G. Durán, C. Padra, and V. Vampa. A posteriori error estimators for nonconforming finite element methods. *RAIRO Modél. Math. Anal. Numér.*, 30(4):385–400, 1996.

[47] E.A. Dari, R.G. Durán, and C. Padra. A posteriori error estimates for nonconforming approximation of eigenvalue problems. *Applied Numerical Mathematics*, 62(5):580–591, 2012.

[48] W. Dörfler. A convergent adaptive algorithm for Poisson's equation. *SIAM J. Numer. Anal.*, 33(3):1106–1124, 1996.

[49] W. Dörfler and R.H. Nochetto. Small data oscillation implies the saturation assumption. *Numer. Math.*, 91(1):1–12, 2002.

[50] R.G. Durán, C. Padra, and R. Rodríguez. A posteriori error estimates for the finite element approximation of eigenvalue problems. *Math. Models Methods Appl. Sci.*, 13(8):1219–1229, 2003.

[51] L. Euler. Elementa doctrinae solidorum.-demonstratio nonnullarum insignium proprietatum, quibus solida hedris planis inclusa sunt praedita. *Novi comment acad. sc. imp. Petropol.*, 4(3):109–140–160, 1752.

[52] L.C. Evans. *Partial differential equations*. American Mathematical Society, Providence, 2000.

[53] S. Ferraz-Leite, C. Ortner, and D. Praetorius. Convergence of simple adaptive Galerkin schemes based on $h - h/2$ error estimators. *Numer. Math.*, 116(2):291–316, 2010.

[54] I.M. Firth and J.M. Buchanan. The wolf in the cello. *J. Acoust. Soc. Am.*, 53(2):457–463, 1973.

[55] G.E. Forsythe. Asymptotic lower bounds for the fundamental frequency of convex membranes. *Pacific J. Math.*, 5:691–702, 1955.

[56] S. Funken, D. Praetorius, and P. Wissgott. Efficient implementation of adaptive P1-FEM in Matlab. *Comput. Methods Appl. Math.*, 11(4):460–490, 2011.

[57] E.M. Garau and P. Morin. Convergence and quasi-optimality of adaptive FEM for Steklov eigenvalue problems. *IMA J. Numer. Anal.*, 31(3):914–946, 2011.

[58] E.M. Garau, P. Morin, and C. Zuppa. Convergence of adaptive finite element methods for eigenvalue problems. *Math. Models Methods Appl. Sci.*, 19(5):721–747, 2009.

[59] J. Gedicke and C. Carstensen. A posteriori error estimators for convection-diffusion eigenvalue problems. *Comput. Methods Appl. Mech. Engrg.*, 268:160–177, 2014.

[60] S. Giani and I.G. Graham. A convergent adaptive method for elliptic eigenvalue problems. *SIAM J. Numer. Anal.*, 47(2):1067–1091, 2009.

[61] G.H. Golub and C.F. Van Loan. *Matrix Computations*. Johns Hopkins University Press, Baltimore, third edition, 1996.

[62] C. Gordon, D. Webb, and S. Wolpert. Isospectral plane domains and surfaces via Riemannian orbifolds. *Invent. Math.*, 110(1):1–22, 1992.

[63] C. Gordon, D. Webb, and S. Wolpert. One cannot hear the shape of a drum. *Bull. Amer. Math. Soc.*, 27(1):134–138, 1992.

[64] P. Grisvard. *Elliptic Problems in Nonsmooth Domains*, volume 24 of *Monographs and Studies in Mathematics*. Pitman, Boston, 1985.

[65] L. Grubišić and J.S. Ovall. On estimators for eigenvalue/eigenvector approximations. *Math. Comp.*, 78(266):739–770, 2009.

[66] E. Hairer, S. P. Nørsett, and G. Wanner. *Solving Ordinary Differential Equations I: Nonstiff Problems*. Springer, Berlin, second edition, 1993.

[67] D. Heiserer, H. Zimmer, M. Schäfer, C. Holzheuer, and R. Kondziella. *Formoptimierung in der frühen Phase der Karosserieentwicklung*. Vdi-Berichte 1846, Würzburg, 2004.

[68] U.L. Hetmaniuk and R.B. Lehoucq. Uniform accuracy of eigenpairs from a shift-invert lanczos method. *SIAM J. Matrix Anal. Appl.*, 28:927–948, 2006.

[69] V. Heuveline and R. Rannacher. A posteriori error control for finite approximations of elliptic eigenvalue problems. *Adv. Comput. Math.*, 15(1-4):107–138, 2001.

[70] V. Heuveline and R. Rannacher. Adaptive FEM for eigenvalue problems. In *Numerical Mathematics and Advanced Applications*, pages 713–722. Springer, Berlin, 2003.

[71] J. Hu, Y. Huang, and Q. Lin. The lower bounds for eigenvalues of elliptic operators by nonconforming finite element methods. Preprint, arXiv: 1112.1145v1, 2011.

[72] M. Kac. Can one hear the shape of a drum? *Amer. Math. Monthly*, 73(4):1–23, 1966.

[73] T. Kato. *A Short Introduction to Perturbation Theory for Linear Operators*. Springer, New York, 1982.

[74] A. Knyazev. lobpcg.m. http://www.mathworks.com/matlabcentral/fileexchange/48-lobpcg-m, 25 May 2000 (Updated 14 Mar 2010).

[75] A.V. Knyazev. New estimates for Ritz vectors. *Math. Comp.*, 66(219):985–995, 1997.

[76] A.V. Knyazev and M.E. Argentati. Rayleigh-Ritz majorization error bounds with applications to FEM. *SIAM. J. Matrix Anal. Appl.*, 31(3):1521–1537, 2010.

[77] A.V. Knyazev and K. Neymeyr. Efficient solution of symmetric eigenvalue problems using multigrid preconditioners in the locally optimal block conjugate gradient method. *Electron. Trans. Numer. Anal.*, 15:38–55, 2003.

[78] A.V. Knyazev and K. Neymeyr. A geometric theory for preconditioned inverse iteration. III. A short and sharp convergence estimate for generalized eigenvalue problems. *Linear Algebra Appl.*, 358:95–114, 2003.

[79] A.V. Knyazev and J.E. Osborn. New a priori FEM error estimates for eigenvalues. *SIAM J. Numer. Anal.*, 43(6):2647–2667, 2006.

[80] M.G. Larson. A posteriori and a priori error analysis for finite element approximations of self-adjoint elliptic eigenvalue problems. *SIAM J. Numer. Anal.*, 38(2):608–625, 2000.

[81] S. Larsson and V. Thomée. *Partial Differential Equations with Numerical Methods*, volume 45 of *Texts in Applied Mathematics*. Springer, Berlin, 2003.

[82] R.S. Laugesen and B.A. Siudeja. Minimizing Neumann fundamental tones of triangles: an optimal Poincaré inequality. *J. Differential Equations*, 249(1):118–135, 2010.

[83] R.B. Lehoucq, D.C. Sorensen, and C. Yang. *ARPACK Users' Guide: Solution of Large-Scale Eigenvalue Problems with Implicitly Restarted Arnoldi Methods*. SIAM, Philadelphia, 1998.

[84] T.Y. Li and Z. Zeng. Homotopy-determinant algorithm for solving non-symmetric eigenvalue problems. *Math. Comp.*, 59:483–502, 1992.

[85] T.Y. Li and Z. Zeng. The homotopy continuation algorithm for the real nonsymmetric eigenproblem: further development and implementation. *SIAM J. Sci. Comp.*, 20:1627–1651, 1999.

[86] T.Y. Li, Z. Zeng, and L. Cong. Solving eigenvalue problems of real nonsymmetric matrices with real homotopies. *SIAM J. Numer. Anal.*, 29:229–248, 1992.

[87] S. H. Lui and G.H. Golub. Homotopy method for the numerical solution of the eigenvalue problem of self-adjoint partial differential operators. *Numer. Algorithms*, 10:363–378, 1995.

[88] S. H. Lui, H. B. Keller, and T. W. C. Kwok. Homotopy method for the large sparse real nonsymmetric eigenvalue problem. *SIAM J. Matrix Anal. Appl.*, 18:312–333, 1997.

[89] D. Mao, L. Shen, and A. Zhou. Adaptive finite element algorithms for eigenvalue problems based on local averaging type a posteriori error estimates. *Adv. Comput. Math.*, 25(1-3):135–160, 2006.

[90] MATLAB, Version 7.10.0.499 (R2010a). The MathWorks, inc., 24 Prime Park Way, Natick, MA 01760-1500, USA, 2010.

[91] V. Mehrmann and A. Miedlar. Adaptive computation of smallest eigenvalues of self-adjoint elliptic partial differential equations. *Numer. Linear Algebra Appl.*, 18(3):387–409, 2011.

[92] K. Neymeyr. A posteriori error estimation for elliptic eigenproblems. *Numer. Linear Algebra Appl.*, 9(4):263–279, 2002.

[93] J.T. Oden, S. Prudhomme, T. Westermann, J. Bass, and M.E. Botkin. Error estimation of eigenfrequencies for elasticity and shell problems. *Math. Models Methods Appl. Sci.*, 13(3):323–344, 2003.

[94] B.N. Parlett. *The Symmetric Eigenvalue Problem*. SIAM, Philadelphia, 1998.

[95] L. E. Payne and H. F. Weinberger. An optimal Poincaré inequality for convex domains. *Arch. Rational Mech. Anal.*, 5:286–292, 1960.

[96] R. Rannacher, A. Westenberger, and W. Wollner. Adaptive finite element solution of eigenvalue problems: balancing of discretization and iteration error. *J. Numer. Math.*, 18(4):303–327, 2010.

[97] P.-A. Raviart and J. M. Thomas. A mixed finite element method for 2nd order elliptic problems. In *Mathematical Aspects of Finite Element Methods*, pages 292–315. Springer, Berlin, 1977.

[98] P.-A. Raviart and J.-M. Thomas. *Introduction à l'Analyse Numérique des Équations aux Dérivées Partielles*. Collection Mathématiques Appliquées pour la Maîtrise. Masson, Paris, 1983.

[99] Y. Saad. *Numerical Methods for Large Eigenvalue Problems*. Manchester University Press, Manchester, 1992.

[100] S. Sauter. *hp*-finite elements for elliptic eigenvalue problems: error estimates which are explicit with respect to λ, h, and p. *SIAM J. Numer. Anal.*, 48(1):95–108, 2010.

[101] L.R. Scott and S. Zhang. Finite element interpolation of nonsmooth functions satisfying boundary conditions. *Math. Comp.*, 54(190):483–493, 1990.

[102] R. Stevenson. Optimality of a standard adaptive finite element method. *Found. Comput. Math.*, 7(2):245–269, 2007.

[103] R. Stevenson. The completion of locally refined simplicial partitions created by bisection. *Math. Comp.*, 77(261):227–241, 2008.

[104] G.W. Stewart and J.G. Sun. *Matrix Perturbation Theory*. Academic Press, Boston, 1990.

[105] G. Strang and G.J. Fix. *An Analysis of the Finite Element Method*. Prentice-Hall, Englewood Cliffs, 1973.

[106] A.H. Stroud. *Approximate Calculations of Multiple Integrals*. Prentice-Hall, Englewood Cliffs, 1971.

[107] L. N. Trefethen and T. Betcke. Computed eigenmodes of planar regions. *Contemp. Math.*, 412:297–314, 2006.

[108] R. Verfürth. *A Review of A Posteriori Error Estimation and Adaptive Mesh-Refinement Techniques*. Wiley and Teubner, Chichester, 1996.

[109] T.F. Walsh, G.M. Reese, and U.L. Hetmaniuk. Explicit a posteriori error estimates for eigenvalue analysis of heterogeneous elastic structures. *Comput. Methods Appl. Mech. Engrg.*, 196(37-40):3614–3623, 2007.

[110] H.F. Weinberger. Upper and lower bounds for eigenvalues by finite difference methods. *Comm. Pure Appl. Math.*, 9:613–623, 1956.

[111] N.-E. Wiberg and X.D. Li. Superconvergent patch recovery of finite-element solution and a posteriori L_2 norm error estimate. *Comm. Numer. Methods Engrg.*, 10(4):313–320, 1994.

[112] H. Wu and Z. Zhang. Enhancing eigenvalue approximation by gradient recovery on adaptive meshes. *IMA J. Numer. Anal.*, 29(4):1008–1022, 2009.

[113] J. Xu and A. Zhou. A two-grid discretization scheme for eigenvalue problems. *Math. Comp.*, 70(233):17–25, 2001.

[114] O.C. Zienkiewicz and J.Z. Zhu. The superconvergent patch recovery and a posteriori error estimates. Part 1: The recovery technique. *Int. J. for Numer. Methods in Engineering*, 33:1331 – 1364, 1992.

List of Figures

List of Tables

Selbständigkeitserklärung

Ich erkläre, dass ich die vorliegende Arbeit selbständig und nur unter Verwendung der angegebenen Literatur und Hilfsmittel angefertigt habe.

Berlin, 19.12.2012 Joscha Micha Gedicke